UNIVERSITY OF SOUTHAMPTON

MODELLING OF MARINE ECOSYSTEMS:
A VIRAL SOLUTION TO THE DOC ENIGMA

By

Rui Quental-Mendes M.Sc.

A Dissertation submitted in candidature for the degree of
Doctor of Philosophy at the University of Southampton
Department of Oceanography

December 1995

"The maturation of the concepts of viral ecology into a picture coherent with the developing puzzle-work of the rest of the microbial food web requires the construction of a more powerful set of experimental tools. The most important lesson learnt so far is maybe that some (many?) of our textbook "truths" in the field of microbial ecology may still be merely professional folklore open to experimental challenge."

Thingstad et al., 1993

- Are Viruses Important Partners in Pelagic Food Webs?

UNIVERSITY OF SOUTHAMPTON

ABSTRACT

FACULTY OF SCIENCE
OCEANOGRAPHY

Doctor of Philosophy

MODELLING OF MARINE ECOSYSTEMS: A VIRAL SOLUTION TO THE DOC ENIGMA

by Rui Quental-Mendes

The role and dynamics of the ocean's pool of dissolved organic carbon (DOC) in both the marine carbon cycle and marine ecosystems is not well known. A large imbalance between net export and measured loss of carbon in the upper 150m of Bermuda remains unexplained. Knowledge of the processes that control the source and rate of production of DOC in the upper ocean, as well as its subsurface remineralisation rate and lifetime are required to explain the ocean's global distribution of nutrients.

May viral lysis yield the carbon required to account for the fluxes into the semi-labile DOC pool of biogeochemical cycles?

The role of marine viruses in ecosystem dynamics is determined and their impact on overall biological production rates and DOC production is analyzed. Viral induced collapse of plankton blooms is investigated. This is achieved through the development of an epidemics model based on a compartmental ecosystem model of the upper ocean. Inter-compartmental flows and fluxes to the deep ocean are plotted daily. A leapfrog integration method with a timestep of two hours is used. The model is run over the period of ten years for the Bermuda Station "S" area. Two thousand simulations are analyzed. Phytoplankton primary production and bacterial production are diverted by viral lysis into the synthesis of new viruses which are inactivated by natural UV radiation and then decay into DOC slowly. The remaining cell debris of lysed hosts flow directly into the detritus and DOC pools respectively. The effect of differing levels of contact rate, inactivation rate, decay time of inactivated viruses and sinking speed of detritus on overall production rates and biomass are investigated.

Results show that marine viruses act as regulators of the size and timing of plankton blooms and are important partners in bacterial trophodynamics. The stability of the ecosystem is extremely sensitive to the contact rate between virus and host cells which provides the underlying mechanism for non linear epidemics. Increased levels of the contact rate determine higher viral infectivity and increase viral lysis which forces phytoplankton and bacterial collapses.

The epidemics result in a considerable growth of bacterial production and hence viral lysis which increase with the shortening in decay time and the slowing of the detritus sinking speed. Variations in the level of the inactivation rate are found to have minor effect on the overall annual production rates but have large effect on the maximum daily flow into lysis during blooms.

The model results on viral production foster support for the viral source of the high-molecular weight fraction of the semi-labile DOC, identify bacterial viruses as its main contributor and show a much improved fit to the observed data in comparison to previous modelling attempts without epidemics.

TABLE OF CONTENTS

LIST OF TABLES

Simulations with a sinking speed of detritus of 1m/day

Version 7 of the model: introduction of variable contact rates in bacterial epidemics.

Table 7.6 Variation in gross bacterial production, bacterial viral lysis, primary production, phytoplankton viral lysis, total viral lysis in mMol N m^{-2} $year^{-1}$ and maximum daily flow into lysis in mMol N m^{-2} d^{-1} for **variable contact rates** in simultaneous epidemics of phytoplankton and bacterial viruses. The decay time of inactivated viruses is **six months** and **fifty years**. The inactivation rate is .792 d^{-1} and sinking speed of detritus is 10m/day. . . . . -285-

LIST OF FIGURES

Chapter 3

Chapter 4

Version 2 of the model : new formulation of zooplankton mortality

Version 3 of the model : Introduction of inactivation rates on viruses.

Version 5 of the model : Introduction of variable contact rates

Version 7 of the model : Introduction of variable contact rates in bacterial epidemics

Acknowledgements

This work was largely funded by an individual research grant of the MAST program of the Commission of the European Communities, reference B/MAST - 900046.

I would like to thank Dr. Kelvin J. Richards of the Oceanography Department at Southampton University for his steering and putting up with my independence but also to his good humour and the remark just before I started writing my upgrading report "I am very curious to see what a biologist can come up with" which scared me and compelled me to give my best. I would also like to thank Dr. Mike J.R. Fasham of the James Rennell Centre, Chilworth, for agreeing to supervise my modelling work and for allowing me to use his open ocean ecosystem model as a platform for the viral epidemics.

I would like also to thank those who motivated and helped me during my time as a research student. These include:

- Dr. Fauzi Mantoura whose enthusiasm on the DOC enigma conquered my attention and imagination during his lectures at the Marine Biogeochemistry course organised by Prof. Disteche in Villefranche-sur-mer in the Summer of 1989;
- Dr. Job Baretta for providing access to the NIOZ library on a weekend where I found the three crucial papers that launched me into this adventure;
- Prof. Bernt Zeitschell for the opportunity of taking part on the Azores-Iceland leg of the METEOR cruise during the JGOFS Spring Bloom Experiment in 1989 during my stay at the Institut für Meereskunde in Kiel. This is where I found information on the molecular weight of viruses which allowed me to make the connection between marine viruses and the DOC enigma;
- Dr. George Jackson for listening to my ideas and incentivating me to publish them during the JGOFS/IGBP meeting on "Modelling the biology, physics and chemistry of the upper ocean and its interaction with the atmosphere" at the Royal Society, London, in March 1990;
- Dr. Carol Turley and Dr. Karen Lochte for their support and advise to back it up with a DOC experiment during the JGOFS Data and Modelling Workshop in Kiel in March 1990;
- Dr. Yoshimi Suzuki for reading the original manuscript during the same workshop and for his invitation on a collaboration experiment that never materialised but nonetheless had me galvanised and made me conceive the details of the experiment;
- Axel Miller for our frequent discussions on DOC;
- Dr. David O'Conner for allowing me to use his ultracentrifuge and swing-out rotor in Boldrewood and for our discussions on viruses and their decay times;
- Chris Inman for his invaluable help in finding the viruses by electron microscopy at the General Hospital

- My parents and my wife for their support at all times and immense logistic help in the final stages of the manuscript.

Chapter 1.

Introduction

One of the major long-term goals of the present oceanography scientific community is to develop models capable of predicting the spatial and temporal variations in the oceanic carbon cycle. One particular component of the carbon cycle that has recently come to attention is the dissolved organic carbon (DOC) enigma.

1.1 The DOC enigma.

It has been assumed that DOC is produced in surface waters by phytoplankton excretion and zooplankton sloppy feeding as well as by dissolution of detritus and faecal pellets (Jumars et al., 1989). Paradoxically, the mean age of DOC in the surface ocean as determined by traditional methods is >1,000 years, implying not only that it consists of very refractory organic compounds but also that their breakdown is extremely slow (Bauer et al., 1992; Williams & Druffel, 1988).

Moreover, the concentration of the traditional DOC is the same both in surface and deep waters (1 ppm = 1 mg l^{-1} ≡ 83 μM l^{-1}) and does not reflect biological processes such as the oxygen minimum and surface primary productivity (Williams & Druffel, 1988).

Historic oceanic DOC amounts of *ca.* 50-100 μmol l^{-1} had put the estimate of global DOC inventory at a level identical to that of carbon in the atmosphere (≈ 750 Gt C) (Sundquist, 1985).

In 1988 Sugimura & Suzuki using an improved technique reported the existence of vertical gradients in the concentrations of DOC and dissolved organic nitrogen (DON) with surface values 2 to 4 times higher and more variable

than those previously measured.

These results were confirmed independently by other researchers thus implying the finding of an extra 1,000 Gt (10^{12} tonnes) carbon pool in the ocean (Martin & Fitzwater, 1992, Peltzer et al., 1992). Though these figures extrapolated from Suzuki's , Martin & Fitzwater's and Peltzer's vertical gradients are now questionable (Suzuki, 1993) additional large DOC horizontal gradients of 100 μMol C l^{-1} have also been found in surface waters between the equator and the equatorial Pacific (Martin & Fitzwater, 1992).

The new pool is concentrated near the surface and appears to be actively involved in the biogeochemical cycling of carbon and nitrogen (Toggweiler, 1990, 1992).

Large changes in DOC concentrations ($\pm$10 to 50 μM C l^{-1} $\equiv$ 1.5 to 7.5 mMol N/m^3 for a C/N ratio = 6.625 or 2.5 to 12.5 mMol N/m^3 for a C/N ratio = 4) were observed *in situ* during the spring bloom in 1989 in the North Atlantic (Kirchman et al., 1991), where daily oscillations of DOC ranging between 1.3 to 6.6 μM C l^{-1} were also measured (Ducklow et al., 1993). The mechanisms of DOC production are not well understood. Nonetheless, the large gradients in DOC concentrations indicate that a large fraction of DOC (20-40%) can turn over in days and that the DOC flux is large relative to primary production. Such large, short-term fluxes cannot be explained with current concepts in plankton ecology (Kirchman et al, 1991).

However they may be relevant to explain the two-thirds (2.2 Mol C m^{-2} for the period of 1 April to 31 December 1992 and 1993) difference in mass balance of dissolved inorganic carbon (DIC) consumption and the production of DOC and suspended particulates (POC) in the upper 150m of Bermuda (Michaels et al., 1994). The explanation offered up to now was that either the sediment traps miss 80% of the sinking

particles or that 70% of the carbon cycling is due to advection.

The breakdown of this organic material and its lifetime in the subsurface layers of the upper ocean has been the subject of two modelling investigations of the ocean's distribution of nutrients (Bacastow & Maier-Reimer, 1991; Najjar, 1990).

1.2 The viral connection.

Until 1989 the concentration of viruses in natural unpolluted waters like the open ocean was believed to be extremely low. However, in that year Bergh et al. and later on Proctor & Fuhrman (1990) using new methods of counting under the electron microscope reported the evidence of an high abundance of free virus found in marine oceanic samples with up to 15 x 10^7 virus particles per ml which was 10^7 times higher than previous abundance estimates.

More recent measurements claim those values to be underestimations - because most of the virus (an average of 60%, and often 90%) are retained on 0.2 μm filters (Paul et al, 1991)-, and have established that marine viruses can be found from the surface to 1500 m depth (Paul et al, 1991; Proctor & Fuhrman, 1991).

Most significantly however, is that the virus production varies rapidly during the year and is closely coupled to plankton blooms (Bratbak et al., 1990, 1993; Borsheim et al., 1990; Heldal & Bratbak, 1991).

A bridging of these two main discoveries is explored. The peculiar biochemistry of viruses and their dynamics make them ideal candidates to explain the "extra" semi-labile DOC.

1.3 Overall aims of study.

The present study focuses on two main overall aims;

1. To determine theoretically and numerically whether there is a viral solution to the DOC enigma,

and,

2. To investigate the dynamics of viral epidemics in a marine ecosystem and its repercussion on biological production.

Therefore, for this second aim an existing one dimensional ecosystem model (Fasham et al, 1990) has been modified to include 3 viral compartments.

In this chapter the general motivation for this project has been outlined.

Chapter 2 starts with a review on the DOC enigma and the methodological problems involved. A connection with marine viruses is suggested and the processes that might control DOC production under the action of viruses are examined. A proposal for a simple experiment testing the virus resistance to breakdown by UV radiation is presented. A review on viruses as community regulators and their biology follows, at the end of which the more specific goals of the project are presented.

Chapter 3 contains a literature review on the SEIR model which is used in standard epidemics modelling. The requisites for a marine epidemics model are enunciated and the structure and functioning of the underlying ecosystem model which is used in this work is described. The model builds upon the upper ocean ecosystem model of Fasham *et al.*, 1990 and Fasham, 1993.

Chapter 4 presents a brief synthesis of the results obtained with Fasham's Model A (1990) and Model B (1993) which are referred to as Control run A and Control run B throughout this study.

Chapter 5 investigates the dynamics of epidemics of phytoplankton viruses in a marine ecosystem. A step by step development of the model introduces differing levels of contact rate, inactivation rate, decay time of inactivated viruses, variable contact rate and sinking speed of detritus into five versions of the model which has a five year runtime. The effect of each modification on overall biological production rates and biomass are investigated.

Chapter 6 presents the analysis of results from epidemics of bacterial viruses. Ten year runs for version six and seven of the model investigate the effect of variation in the epidemics parameters studied in chapter 5 on overall production rates, biomass, interannual variability and host-prey dynamics.

Chapter 7 presents the results from simultaneous epidemics on phytoplankton and bacteria populations. Ten year runs for version 8 of the model investigate the impact of changes in fixed and variable contact rates and decay time on production rates and biomass for detritus sinking speeds of 1m/day and 10m/day.

Finally, in chapter 8 a discussion and conclusions of the study as well as an evaluation of its achievements and limitations are presented. Possible directions for future work in this field are suggested.

Chapter 2.

Connecting Viruses to DOC and Plankton Blooms

2.1 Connecting Virus in Seawater to "Excess" DON and DOC

The last 40 years have witnessed major advances in oceanography triggered by advances in techniques rather than theory. Although theory is invaluable in constructing a coherent picture of the data universe at our disposal, once new methods for data acquisition are invented the data generated often forces us to reconsider our understanding of the processes involved (Wangersky, 1993).

Since 1988, the eve of the start of the JGOFS major sampling program, the oceanographers involved in the study of the global carbon cycle have been excited with the discovery by Yoshimi Suzuki of unsuspected amounts of DOC (Sugimura & Suzuki, 1988) and DON (Suzuki et al, 1985) in oceanic seawater. As a result there was a surge of interest in an area of science that had been dead for 20 years and a revival of active research that in its frenzy has become the most polemic field in oceanography in recent times.

What is DOC ?

According to Wangersky (1993) in his review paper on dissolved organic carbon methods, DOC can be assumed to be that fraction of organic matter found in seawater which is neither excluded nor adsorbed by the 0.2-1.0 μm filter used to remove the POC, and which is not volatile enough to be lost by the acidification and purging technique used to remove the inorganic carbon. As it stands the definition of DOC embraces bacteria, viruses, and much of the colloidal organic material.

Using their method, Suzuki and Sugimura measured concentrations of DON (30-40 μM l^{-1}) and DOC (approximately

300 μM l^{-1}) in surface waters of the western North Pacific that were at least a factor of two higher than those typically obtained for surface ocean water using Wet Chemical Oxidation techniques. Samples from the North Atlantic, although also higher than the values found by wet oxidation methods, were roughly in the range of values found by Sharp (1973), allowing for seasonal differences. Molar DOC and DON concentrations covaried near the value of seven typical of marine plankton and together exhibited a nearly stoichiometric inverse correlation with apparent oxygen utilization (AOU) (Hedges & Farrington, 1993).

These observations were taken to indicate that the consumption of DOC is responsible for oxygen depletion in the deep sea (Martin & Fitzwater, 1992) and that DOM is the predominant substrate for heterotrophic utilization throughout the water column (Hedges & Farrington, 1993).

The relevance of a large proportion of the DOM being labile meant that it could also be exchangeable with atmospheric carbon dioxide on short time-scales (Hedges & Farrington, 1993).

Sugimura and Suzuki's claim that their higher DOC values result from more complete oxidation was later supported by analysis with their instrument of UV-photo-oxidized seawater samples, which indicated large concentrations (50-150 μM l^{-1}) of residual DOC almost exactly equivalent to the difference between one-step analysis of the same waters by the two methods (Sugimura & Suzuki, 1988; Druffel et al., 1989; Suzuki & Tanoue, 1991).

Briefly, Sugimura & Suzuki (1988) and Suzuki et al. (1985) inject 200 μl of filtered, acidified seawater onto Pt-impregnated (3 wt%) alumina catalyst at 680^0 C and measure the resultant CO2 (from DOC) by infra-red absorption or the resultant NO (from DON) by oxidation to NO2 with subsequent spectrophotometric determination (Williams & Druffel, 1988).

Such method is designated High Temperature Catalytic Oxidation (HTCO). This is a close to real time system and the techniques involved are rapid, precise, easily applied aboard ship, and incorporate conditions that should result in rigorous oxidation of DOM components (Hedges, Lee & Wangersky, 1993).

Chen & Wangersky (1993) have confirmed that in productive surface waters, as much as a third to a half of the DOC may be present as labile material, degraded biologically in hours to days in unpreserved samples. Its composition is unknown. They measured decay constants for this organic matter ranging from 0.1-0.5 day^{-1}.

Coming from the same institution - Dalhousie University, Halifax, Canada - a theoretical modelling work by Johnson & Kepkay (1992) on colloid transport and bacteria utilization of oceanic DOC concluded that a substantial fraction of the labile DOC escape degradation in the upper ocean by virtue of its particle size characteristics.

Notwithstanding, a delay of even 1 h in sample processing can result in considerable loss of DOC. At least some of this material can be oxidized by both wet oxidation and HTCO methods. This fraction first detected by Suzuki on his "real time" system had been previously missed because samples were traditionally stored away for months before analysis. Wangersky (1993) suggested that loss may be avoided by the addition of bacteriostatic agents followed by a quick-freezing bath at sub-zero temperatures. A second fraction impervious to wet and photochemical oxidation, but slightly more resistant to biological degradation processes, at least over periods of weeks to a few months, is present in both surface and deep water and can only be measured by HTCO. It is thus semi-labile and its composition is equally unknown. Notice that when both HTCO and wet-chemical methods were applied to nearly axenic plankton cultures of the diatoms

Chaetoceros gracilis and *Phaeodactylum tricornutum* and the flagellate *Isochrysis galbana* the difference in DOC concentration as determined by the two methods increased with increasing age of the culture, from a negligible difference at zero-time to almost 75% after 18 days (Chen & Wangersky, 1993), whereas in sediment porewaters the discrepancy was always less than 10% (Alperin & Martens, 1993). A third fraction is oxidized by both wet chemical techniques and HTCO, but has enough resistance to biological attack to be present also in both surface and deep water. It is thus refractory. Each of the major types of analytical methods measures a different subset of these three DOC fractions (Wangersky, 1993).

Using the HTCO method Martin & Fitzwater (1992) analyzed vertical profiles of young (≈ 100 years old) seawater from 59.5° N south of Iceland in the North Atlantic, middle age (≈ 500 years) water from Drake Passage and old (1,600 years) waters from the equatorial Pacific. Apparent oxygen utilization (AOU) values steadily increase as the subsurface waters age. There was very little change between stations in DOC concentrations in deep water in spite of very large differences in ^{14}C age and in dissolved oxygen levels at the three locations. According to Toggweiller (1992) this result suggests that the consumption of DOC by bacteria in the ocean's deep interior does not explain much of the observed consumption of oxygen. Martin and Fitzwater do, however, find a very strong DOC gradient in surface waters between the equator (130 μM) and 9° N (230 μM) in the equatorial Pacific. They find that the DOC level in water declines as its salinity rises thus representing oceanographic consistency.

Martin and Fitzwater's 100-μM DOC decrease between 9° N and the equator is similar to the vertical DOC decrease in the upper few hundred meters of the North Pacific reported by Sugimura and Suzuki (Toggweiler, 1992).

A major portion of this "new" DOC measurable by the

Suzuki analyzer appeared to be biogeochemically reactive, but resistant to classical wet-chemical oxidants like UV and persulfate (Hedges & Farrington, 1993). However, no standard method has survived the test of continued critical use mined by flaws in the completeness of their oxidation which are a result of poor understanding of the structural characteristics of dissolved organic matter in seawater.

In January 1993 Suzuki retracted his 1985 and 1988 papers because of inconsistencies in data treatment. The reassessment of the original data from his ink chart recorder using the original peak height, the statistical peak height, and the statistical peak area method showed that three different DOC concentrations could be obtained from identical original signals on the chart. As the offsets between the values obtained by the peak height and peak area methods were unacceptably large Suzuki (1993) concluded that the accuracy of the DOC concentrations in the 1988 paper was inadequate to support more recent arguments about DOC inventories in the ocean.

It would be an overinterpretation to say that UV-resistant DOM does not exist. It cannot be ignored that numerous other researchers have now measured elevated concentrations of DOC in seawater using HTCO-based analyzers (Fitzwater & Martin, 1993; Miller et al., 1993; Peltzer & Brewer, 1993; Sharp et al., 1993; Tanoue, 1993; Wangersky, 1993; Chen & Wangersky, 1993; Williams et al., 1993). But says Hedges et al. (1993), those who rejoiced with their higher results closely paralleling those of Suzuki would be better off reconsidering their situation.

The most controversial aspect of the high DOC levels is whether a system blank should be subtracted or not. Catalytic oxidation always recovers more carbon from distilled water than does wet oxidation. Researchers like Suzuki et al. (1992) and Martin & Fitzwater (1992) assume that the carbon in their distilled-water blanks comes from the distilled

water, and do not subtract any blank from their seawater measurements. While Benner et al. (1992) and others conclude that the carbon in distilled-water blanks is actually carbon released from the catalyst itself, and subtract it from their seawater determinations. According to Benner & Strom (1993) blank values range from 10 to 50 μM in different catalysts.

However the intercomparison exercise on DOC and DON measurements by 34 scientists during a Workshop in Seattle in July 1991 has shown that instrument operation is the major determinant of analytical results. Values measured by different operators should be taken with scepticism as these varied by approximately ±40% for the same water sample and in some cases had ranged over an order of magnitude.

Those worried about stoichiometry have an additional cause for concern in that no one, not even Suzuki (1993) himself has been able to reproduce the high DON values (>15 μM l^{-1}) reported by Suzuki in 1985. The accurate determination of DON will always be at a disadvantage because this parameter is usually determined as a small difference between large total nitrogen and inorganic nitrogen measurements.

DON and DOC samples obtained during the JGOFS North Atlantic Bloom Experiment in 1989, which were preserved by slow freezing and analyzed in January 1991 by Fitzwater & Martin (1993) show that the maximum DOC concentration was 160 μM l^{-1} with DOC values increasing towards surface mimicking Suzuki's profiles for the western Pacific.

Another vertical profile of TOC obtained by de Baar et al.(1993) during another JGOFS exercise approximately in the same area at 49°N, 17°W on 5 May 1990 shows an inverse relation with Apparent Oxygen Utilization (AOU) in the upper 1000 m of the water column. An even stronger decrease with depth of TOC was found by Pelzer and Suzuki when intercalibrating with Miller, at nearby station 47°N, 20°W on

the 18 May 1989, although their absolute TOC values were considerable higher at the latter station (de Baar et al, 1993). The difference in measurement values between all these researchers were ascribed to analytical discrepancy due to differences in instrument calibration.

Based on these findings chemical oceanographers reached a consensus and concluded in 1993 that the differences between HTCO and UV methods are real, each technique measuring a different fraction of DOC therefore correcting "old" DOC values would be impossible, as those differences appeared to vary considerably depending on time and location in the ocean. The large difference in high DOC waters such as the oligotrophic Pacific versus freshly upwelled, low DOC water found by Fitzwater & Martin (1993) being such an example.

However, a more recent work by Sharp (1994), the father of the first HTCO system in 1973, concluded that the high DOC measurements with these machines can only be attributed to excessive sensitivity of the infra-red gas analyzer. His evidence comes from the results of yet another new high temperature combustion machine with no catalyst and no infra-red analyzer that burns organic matter to ashes. Measured values are similar to those of a traditional UV-machine.

The conclusions of Sharp (1994) cannot be taken as the final say in the HTCO story. First, there are always pitfalls in the use of new methods. Second, it offers no explanation for the difference in evolution of time series of DOC concentrations between the HTCO and UV measurements of Chen & Wangersky (1993).

So what signal do the traditional methods pick up?

DOC measured by the traditional technique of persulfate-oxidation is largely of low molecular weight (Lee & Henrichs,

1993); ultrafiltration techniques suggest that more than 60% of the material is of molecular weight less than 1000 Da and more than 90% is of less than 30 000 Da (Carlson et al., 1985). A recent work by Ogawa & Ogura (1992) though in near-shore environments south of Tokyo found indeed very little DOC with molecular masses above 10,000.

In contrast, Sugimura & Suzuki (1988) reported that a large portion of the new DOC has very high molecular weight, tens of thousands to millions of daltons. It has been measured by Suzuki that the main substance causing his extra DOC signal seems to be a compound with a very high molecular weight in the range 6,000 to 40,000 (Sugimura & Suzuki, 1988, Williams & Druffel, 1988) and that represents more than 75% of the DOC. However, the nature of such substance is still unknown and has been a source of puzzlement (Jackson, 1988).

A crucial aspect of Suzuki and Sugimura's work is the attempt to break the DOM pool down by size fraction of different relative molecular mass (M_r) using gel filtration. This technique enables the preferential retention of low-M_r material during the passage of a DOC mixture through a column. In their 1988 paper Sugimura & Suzuki show water-column profiles of total dissolved organic carbon (DOC) and total dissolved organic nitrogen (DON) from 2 locations in the western Pacific broken down into six size fractions, where size fraction 6 is the largest molecular weight. Most of the DOM extracted by older methods is composed of smaller molecules, corresponding roughly to size fractions 1 and 2. Most of the gradient in DOC between the upper ocean and the deep ocean is contained in the larger size fractions 3-6. To first order, the larger sizes represent the difference between the old and new material (Toggweiler, 1990).

Fractions 5 and 6 largely disappear in the upper few hundred metres of the ocean. The latter varied between the two locations. Toggweiler (1990) pointed out that the larger pool of smaller compounds that comprise the bulk of Suzuki's

DOM pool (size fractions 3,4 and 5) could conceivably be accounted for by the break-up of the particles in the largest molecular weight fraction (>100,000 daltons) into smaller entities.

A substantial part of the larger compounds can be intact and degraded viruses plus material released by viral lysis of bacteria and phytoplankton. Why?

1- viruses of bacteria have molecular weights of $100*10^6$ daltons [range:18-470] (Laskin & Lechevalier, 1973) and therefore overlap the largest molecular weight fraction ($>10^5$ daltons) of Suzuki's DOC, such that size 6 may indeed be the same material.
2- the DNA protein of these viruses have molecular weights of $69*10^6$ daltons [range:12-490] (Laskin & Lechevalier, 1973) once again falling within size fraction 6.
3- viruses are composed of several polypeptides some of which being large glycoproteins that have a molecular weight range of 10,000 to 82,000 (Hsu et al, 1986, Mari & Bonami, 1988, and VanEtten et al, 1981) therefore falling within the range determined for the unknown compounds that constitute size fractions 3 and 4.
4- their minute size (most viruses have a head size less than 60 nm [range:20-200 nm](Bergh et al, 1989, 1993; Proctor & Fuhrman, 1990; Paul et al, 1991)), makes it impossible for 0.4 μm nucleopore filters to retain them, so they can be considered operationally dissolved.
5- the only way to see them is with a transmission electron microscope using the counting technique developed by Bergh et al, 1989.
6- until very recently the ubiquitous existence of autochthonous marine viruses in concentrations of 10^8 to 10^{11} free viral particles per litre was not acknowledged (Bergh et al, 1989; Proctor & Fuhrman, 1990; Borsheim et al., 1990).

A further point supporting this idea is that Suzuki (personal communication, 1990) was already suggesting, after

the results of a one time experiment, that these compounds might be particles of biological origin with very small size ranging from 0.02 to 0.1 μm.

A virus is a particularly rich source of C, N and P since it is composed of 50% DNA and nearly 50% proteins. These have a low C/N atomic ratio (DNA = 3, proteins = 4 to 5) reflecting their high nitrogen content.

Therefore, the viral hypothesis is very attractive since it easily accounts for the relatively low C/N ratio (5.6 to 6.8 by atoms) in the newly discovered pool of oceanic dissolved organic matter (DOM). Such a low C/N ratio reflects the proteinaceous nature of the "new" DOM as compared to the high C/N ratio of 7-12 of the "old" DOM (Williams & Druffel, 1988).

Furthermore, it would support those who claim that the labile DOM comes directly from the phytoplankton as dissolved organic exudates (Toggweiler, 1990), insofar as a "soup" of cellular components, including proteins, nucleic acids, amino acids, carbohydrates, lipids, cofactors, cell wall components, and assorted complexes, in addition to viruses themselves, is indeed released into the water when the infected phytoplankton or bacteria cell bursts due to viral lysis (Fuhrman, 1992).

Simultaneously, the stability of virus particles (Laskin & Lechevalier, 1981) which have breakdown time scales yet unknown but which one assumes to be in the order of months to years will make them persist long enough in the ocean as to accumulate as high concentrations of DOM. A recent study of degradation of aminoacids and proteins in natural seawater found that the latter took longer than 6 months to breakdown into smaller units. Marine geologists find large concentrations of intact marine viruses in old deep ocean sediments. Biochemical studies of the rate of decomposition of DNA in solution show that under normal conditions, with

typical exposure to air and freshwater, the molecule is seriously degraded if not entirely broken down after 40,000 to 50,000 years (Morell, 1993). Other anedoctal evidence on the resistance of tough protein coatings to degration is provided by the recent revival of sporulated bacteria found in the abdominal contents of a fossilised bee 25 million years old (Cano & Borucki, 1995; Fischman, 1995).

Slow decay times of marine viruses would address the need for the existence of complex unreactive geopolymers that, as many argue, accumulate in the ocean and so explain the hugeness of the oceanic DOM pool (Toggweiler, 1990).

2.1.1 Why have not the previous DOC techniques been able to detect the virus signal?

Viruses have two forms: an active "living" form, the "virion", which thrives in a friendly environment (like the inside of a phytoplankton cell) and an inactive crystal-like form, the "phage", into which the virus reverts when its external environment becomes hostile (i.e. when the phytoplankton cell bursts and the virus is released in free water) ensuring its survival while awaiting for contact with an appropriate host cell.

When in their inactive form viruses have crystal-like structure. Their high molecular weight DNA protein ($69*10^6$ daltons) (Laskin & Lechevalier, 1978), which is in a tightly coiled ball, has a rigid protein coat covering it: the capsid.

This extremely heavy shield (statistical average MW $31*10^6$ daltons but usually as heavy as the DNA itself) is very resistant, is able to withstand high temperatures as well as UV degradation and is thus highly refractory (Laskin & Lechevalier, 1978). This latter form "the phage" is presumably the most abundant form of viruses.

Traditional techniques for DOC measurement like ultraviolet (UV) radiation and persulfate oxidation are not able to breakdown this crystal-like structure for some reason. The inability of the UV methods to oxidize particulate matter efficiently is well known (Wangersky, 1993). UV radiation is routinely used by virologists to inactivate virus, when preparing them for vaccines, precisely because it doesn't destroy their outer structure (Laskin & Lechevalier, 1978). Furthermore, resistance to UV radiation is not unique to viruses. There is evidence that some other organisms contain mechanisms to protect themselves from UV degradation. For instance, some bacteria defend themselves against harmful environmental conditions such as exposure to UV light by encasing themselves in tough protein coatings - they "sporulate" (Lee & Henrichs, 1993). Moreover, some bacteria can produce large quantities of small acid-soluble proteins that act to rearrange slightly the geometry of the DNA inside the bacteria into a much more UV-non reactive form (Lee & Henrichs, 1993).

Suzuki's technique however, does not make use of any UV radiation to breakdown molecules using instead a catalyst assisted high temperature method.

Temperature-recovery curves of DOC in different molecular weight groups in seawater were obtained by Sugimura & Suzuki (1988). The maximum recovery was obtained above 640^{0} C in each group, but the temperature-recovery curve varied with each molecular weight group. Group 6 ($>10^{5}$ daltons) where viruses would be included is the most resistive to oxidation. Lower molecular weight groups were oxidized easily at a lower temperature. Significantly, Suzuki attributed these differences to chemical structure and also molecular weight.

Therefore, it is suggested that Suzuki's technique with its high temperature catalytic oxidation is able to destroy the capsid and release the viral-DNA molecule which

is subsequently burnt. A proposed experiment to test this hypothesis is presented in chapter 8, § 8.5.1.

2.1.2 Implications

Viruses uncouple production and consumption of particulate biomass and they increase the production of DOM (Heldal & Bratbak, 1991). They may thus be a key factor for understanding the transformation between the particulate, colloidal and dissolved fractions of organic material in seawater.

Due to their intrinsic nature viruses sequester into their DNA protein a much elevated and disproportionate concentration of carbon, nitrogen and phosphorus than usual (the P:N:C ratio of DNA and proteins does not conform to the Redfield ratio), and are thus, possibly the main pathway by which biogenic elements are removed from the marine system, whilst in a free floating and "dormant" semi-refractory form (Thingstad et al., 1993).

The bulk of these viruses, both viable and non-viable phages plus virions still inside the host, should be in the euphotic zone where they are produced while infecting phytoplankton cells, bacteria and cyanobacteria. This will occur preferentially during blooms in the upper ocean, because this is the place and the time when the probability of collision with other organisms is higher. This fits with Suzuki's distribution of DOC that is hugely concentrated in the euphotic zone (Williams & Druffel, 1988).

Suzuki has noticed an oscillation on DOC values with the time of day (Williams & Druffel, 1988). This is an evidence that the fraction of biologically extremely labile material that makes up a third to a half of the total DOC is tracking diel cycles in primary productivity (Wangersky, 1993).

Significant diurnal changes in the concentration of viruses (2-5 * 10^7 ml^{-1}) occur in productive waters on a time scale of hours (Heldal & Bratbak, 1991).

The signal of the diurnal variation in the virus density, which is at most 0.65 μM C l^{-1} assuming 0.26 fg C per virus (Fuhrman, 1992), cannot be detected by the DOC machine. The HTCO-DOC machine has a 1 μM resolution but its analytical precision is 3-5%, i.e. 5-8 μM C l^{-1} (Peltzer & Brewer, 1993) falling to 8-16 μM l^{-1} at sea. According to Carlson et al. (1994) the analytical precision has recently been improved to <2% (comparable to $\pm$ 1.1 μM C).

The diurnal variation of viral biomass contributes 10 to 50% to the daily oscillations of DOC. These were measured by Suzuki to range between 1.3 to 6.6 μM C l^{-1} (16-80 mg C m^{-3}) during the JGOFS North Atlantic Bloom Experiment in 1989 (Ducklow et al., 1993).

Furthermore, one suggests that only a small fraction of the considerable amount of carbon, nitrogen and phosphorus actively sequestered from primary producers and incorporated into these viruses will be recorded by sediment traps. By virtue of their small size most will not sink thus remaining free floating in the euphotic zone albeit in the form of UV-inactivated viruses (Suttle & Chen, 1992).

One suggests that such a vertical distribution could explain the imbalance between reduced carbon exported out of the euphotic zone and the higher amounts expected from in situ production inferred from seasonal oxygen signals (Williams & Druffel, 1988).

Accordingly, one should expect DOC and DON to show a seasonal variation where synthesis of DOC and DON have their origin in biological processes as they surely must be. Seasonal variations in DOC associated with changes in primary production were recently reported for the northwestern

Sargasso Sea off Bermuda (Carlson et al., 1994). The contention for a seasonal variation in DON is further supported by the findings of an 11 year study by Butler et al. (1979), in which the seasonal variations of dissolved inorganic and organic N in the waters of the English Channel have been determined. Their N results show that as nitrate (NO_3) is utilized by phytoplankton there is an increase in the concentration of the dissolved organic N fraction and there are always significant amounts of dissolved N in some form in the water.

Some of the free-floating viruses will proliferate by attaching to the right hosts, while the rest of them will become non-viable either by exposure to natural UV radiation (Suttle & Chen, 1992), physical damage to their tails (Heldal & Bratbak, 1991), adsorption to non-host particles (Murray & Jackson, 1992) or other causes thus joining the pool of semi-labile DOC. The fate of these viruses is unknown. Heldal & Bratbak (1991) speculated that decaying viral particles may have their nucleic acid ejected from the capsid in less than four hours thus contributing to the concentration of DNA in water. The very tough and refractory protein coat of the capsid (Laskin & Lechevalier, 1978) would suggest otherwise.

Based on the extremely high molecular weight of these viruses one assumes that they will undergo a slow breakdown by nanoflagellates, bacteria and extracellular enzymes (Bratbak et al., 1990) for a long timescale till their complete remineralization. Long lived substances are common in ocean waters. The old DOC is more than a thousand years old (Williams & Druffel, 1988) and in a recent work its age has been estimated to be 4,100 years for Bermuda waters (Bauer et al., 1992).

Relevant modelling work has been done on the mineralization rate of dissolved organic matter primarily to obtain an estimate of global DOM production, assuming steady state. Toggweiler (1989) was the first to remark that it is

the mineralization of DOM, rather than POM (particulate organic matter), which best explains the phosphate and nitrate distributions in the subsurface ocean. According to Toggweiler the observed nutrient distributions appear to result from the breakdown of a long-lived material which can be transported, via advection and mixing, substantial distances from the locations where it is produced. The subsequent works of Najjar (1990) and Bacastow & Maier-Reimer (1991) support this theory. Using a global circulation model and distributions of dissolved inorganic carbon, alkalinity, phosphate, and oxygen the latter authors have estimated the global average, subsurface mineralization rate of DOC at 15.6 g C m^{-2} $year^{-1}$. This is equivalent to 1.3 Mol C or 325 mMol N m^{-2} $year^{-1}$ for a C/N ratio of 4 and only 196 mMol N m^{-2} $year^{-1}$ for a Redfield ratio of 6.625. Extrapolated to all oceans, this DOC consumption rate is 5.6 x 10^{15} g C $year^{-1}$. Their model required DOC to have a lifetime of 50 years, so that it was refractory enough to be transported beyond the surface layer and labile enough to be largely remineralized in the upper 1000 m.

The subsurface DOC consumption rate of Bacastow and Maier-Reimer (1991) is 12% of the open ocean primary production which was estimated at 130 gC m^{-2} y^{-1} or 10.8 moles C m^{-2} y^{-1} by Martin et al., 1987 during the VERTEX study. This is equivalent to 1635 mMol N m^{-2} y^{-1} which is almost three times larger than primary production estimates for Bermuda.

Seawater DOM continues to be one of the largest and least understood reservoirs of reduced carbon at the earth's surface (Hedges, Lee & Wangersky, 1993).

Relevant modelling work has been done on the mineralization rate of dissolved organic matter primarily to obtain an estimate of global DOM production, assuming steady state. Toggweiler (1989) was the first to remark that it is the mineralization of DOM, rather than POM (particulate organic matter), what best explains the phosphate and nitrate distributions in the subsurface ocean. According to Toggweiler the observed nutrient distributions appear to result from the breakdown of a long-lived material which can be transported, via advection and mixing, substantial distances from the locations where it is produced. The subsequent works of Najjar (1990) and Bacastow & Maier-Reimer (1991) support this theory. Using a global circulation model and distributions of dissolved inorganic carbon, alkalinity, phosphate, and oxygen the latter authors have estimated the global average, subsurface mineralization rate of DOC at 15.6 g C m^{-2} $year^{-1}$. This is equivalent to 1.3 Mol C or 325 mMol N m^{-2} $year^{-1}$ for a C/N ratio of 4 and only 196 mMol N m^{-2} $year^{-1}$ for a Redfield ratio of 6.625. Extrapolated to all oceans, this DOC consumption rate is 5.6 x 10^{15} g C $year^{-1}$. Their model required DOC to have a lifetime of 50 years, so that it was refractory enough to be transported beyond the surface layer and labile enough to be largely remineralized in the upper 1000 m.

The subsurface DOC consumption rate of Bacastow and Maier-Reimer (1991) is 12% of the open ocean primary production which was estimated at 130 gC m^{-2} y^{-1} or 10.8 moles C m^{-2} y^{-1} by Martin et al., 1987 during the VERTEX study. This is equivalent to 1635 mMol N m^{-2} y^{-1} which is almost three times larger than primary production estimates for Bermuda.

Seawater DOM continues to be one of the largest and least understood reservoirs of reduced carbon at the earth's surface (Hedges, Lee & Wangersky, 1993).

2.2 Viruses as regulators of plankton blooms

Predator-prey interaction has traditionally been invoked to explain the mechanism that regulates the densities of both prey and predator populations (Anderson & May, 1979).

The evidence from natural communities, however, suggests that parasites (broadly defined to include viruses, bacteria and protozoa) are likely to play a part analogous, or at least complementary, to that of predators or resource limitation in constraining the growth of plant and animal populations (Anderson & May, 1979).

This holds true in the marine environment too, as several authors suggest that in addition to grazing and limitation of nutrients, infection of phytoplankton and bacteria by marine viruses could be a factor regulating their production. Laboratory evidence provided by Mayer & Taylor's experiments (1979) showed that a marine virus lysed the nanoflagellate *Micromonas pusilli*. Recent studies conducted by Suttle et al. (1991, 1995) succeeded in isolating several viruses that were pathogens to a variety of marine phytoplankton, including a prymnesiophyte (*Chrysochromulina spp.*), a prasinophyte (*Micromonas pusilli*), a pennate diatom (*Navicula sp.*) a centric diatom (of unknown origin), and a chroococcoid cyanobacteriumm (*Synechococcus sp*).

Field studies carried out by Bergh et al. (1989), Bratbak et al. (1990), Borsheim et al. (1990), Proctor & Fuhrman (1990), Yamada et al. (1991), Hara et al. (1991) and Paul et al. (1991) prove not only the ubiquity of marine viruses in seawater and sea ice (Maranger et al. 1994) but also highlight their role in the termination of phytoplankton blooms (Bratbak et al. 1993) and establish them as trophodynamic partners in blooms of bacteria (Bratbak et al. 1990). It is now known that the virus population shows a dynamic behaviour in all bloom events. Viruses are active members of the microbial food web causing lysis in both

bacterial and phytoplankton populations thus diverting part of their production from the predatory food chain. Heterotrophic flagellates are predators that are also submitted to viral infection which regulates their dynamics (Nagasaki et al. 1993).

2.2.1 Virus biology

Viruses are very small particles constituted either by DNA or RNA that are able to take control over the production mechanism of a host cell (Laskin & Lechevalier 1981)

Viruses are host specific, which means that a virus capable of infecting a bacteria is unable to infect a phytoplankton cell. Their infective forms are called phages. Thus they are designated bacteriophages if they attack bacteria, cyanophages if they attack cyanobacteria, etc.

A phage attack starts typically by attaching to the host with their tail and then injecting their viral DNA into the cell. Once inside the viral DNA takes control over the metabolic processes turning them to the synthesis of components of the virus. After about 12 minutes under standard conditions the first of the new brood of virus has made its appearance inside the cell and at 25 minutes the bacterium bursts liberating about 200 new virus particles. The whole process would take about three hours for the phytoplankton nanoflagellate *Micromonas pusilla* (Mayer & Taylor, 1979).

2.2.2 Virus replication and nitrogen cycling.

Because the infected cell (bacteria or phytoplankton) is synthesizing viral DNA at a very fast rate and DNA has a very high nitrogen:phosphorous:carbon ratio this will have a repercussion in the nutrients uptake.

The total protein content of an infected cell will thus increase very fast towards the end of its life. An infected bacterium accumulates 3 times more DNA in the form of phages than a healthy bacterium (Heldal & Bratbak, 1991). Such process could explain the observations of Reinfelder & Fisher (1991) who claim that the total cellular protein in the cytoplasm of cultured diatoms increase markedly when senescence starts.

The nitrogen contained in the virus will be literally locked-up on the free-floating phage and will not be available for the system, unless another infective contact happens or the virus breaks down.

2.2.3 Virus ecology.

Viruses are the most numerically dominant form of life in the oceans with reported concentrations from 10^3 to over 10^8 viruses ml^{-1}. Their abundance decreases from estuarine to offshore environments and from surface to depth, with an occasional subsurface maximum (Boehme et al. 1993, Cochlan et al. 1993, Bird et al. 1993).

It has been argued that if marine viruses are involved in the control of primary or bacterial plankton production, this probably occurs only if a new virulent virus strain emerges, and the effects on primary or bacterial production would most likely only be transient, owing to the rapid evolution and reproduction of resistant phytoplankton or bacteria strains (Waterbury, 1992; Olofsson, 1991).

However, large monospecific phytoplankton blooms are more susceptible to parasites and are known to colapse under the attack of viruses (Bratbak et al. 1993; Nagasaki, 1995). It has been suggested that resistant variants protect the host species from local extinction (Suttle et al, 1991).

In non-bloom situations, viruses continue to divert a

fraction of primary and bacterial production, as most seawater viruses are lytic (Wilcox & Fuhrman, 1994; Jiang & Paul, 1994) and must be produced at the expense of hosts (Suttle et al., 1991).

Some marine viruses are adapted to survive UV radiation and remain infective in the oceanic upper layers for long periods in between plankton blooms of their host (Fuhrman & Suttle, 1993). Further evidence in support of long persistence of viral infectivity for autochtonous marine viruses is given by knowledge that some non-native influenza virus, adapted to transmission in marine waters, are able to remain infective for up to 207 days at temperatures of 17-28°C (Stallknecht et al, 1990).

Viruses may modify community structure and the nature of primary production by forcing species sucession during the bloom season as the predominance of one host is undermined by a rapidly propagating viral infection (Suttle et al. 1991).

It has also been suggested that viruses may stimulate primary and bacterial production by causing cell lysis and enhancing the rates of nutrient recycling (Bratbak et al. 1990; Fuhrman, 1992; Thingstad et al. 1993).

Evidence that populations of genetically related viruses are widely distributed over large geographic areas of the world ocean (Kellogg et al. 1995), that up to 30% of heterotrophic bacteria (Weinbauer & Peduzzi 1994), 3% of cyanobacteria (Suttle 1994) and up to 10% of photosynthetic picoflagellates (Cottrell & Suttle 1995) are lysed daily by viruses, and that the infectivity of viral strains to specific hosts is highly variable (Suttle et al. 1990, 1991) emphasize the dynamic interactions of host-virus systems in the sea (Thingstad et al., 1993).

The diversity of bacterial and phytoplankton populations and their associated viruses in marine communities precludes

the development of generalized host resistance to virus due to the low probability of a virus encountering a suitable host as only a small proportion of the total numbers are made up of any given pathogen or host (Suttle et al. 1991).

Nonetheless as in any dynamic biological system viruses can mutate in response to increased resistance of their host population and develop into new infective strains (Kellogg et al. 1995).

2.2.4 Removal of viruses.

Recent estimates indicate that virus abundances can vary through the spring bloom from 5 x 10^5 in the pre-bloom situation to a maximum of 10^8 viruses ml^{-1} one week after the peak of the diatom bloom (Bratbak et al, 1990, Paul et al, 1991, Fuhrmann, 1992). As during the occurrence of blooms the number of free viruses can vary by a factor of >30 and show large diurnal oscillations, 2-5 * 10^7 ml^{-1} (Heldal & Bratbak, 1991), this implies the existence of a removal mechanism for the viruses.

There are several possible mechanisms: (1) they are ingested by nanoflagellates and ciliates (Gonzalez & Suttle, 1993; Tranvik et al. 1993), choanoflagellates (Marchant & Scott, 1993) and radiolarians (Gowing, 1993), (2) loss of structural integrity because of physical or chemical factors or extracellular enzymatic activity (Fujioka et al. 1980), (3) they form aggregates or adsorb nonspecifically to different living and non-living particles sufficiently large to sediment out of the water column.

The latter is the most likely one as several studies report that coinciding with the collapse in the diatom bloom, a succession of bacteria and viruses are observed in the mucous layer surrounding dead or senescent diatoms, with an estimated maximum of 23% of the total virus population attached to the diatoms (Bratbak et al, 1990). More

significant is the presence of viruses in sinking particles examined in sediment trap material from 30 to 1500 meters collected from the North Pacific Ocean to the subtropical North Atlantic Ocean (Paul et al, 1991, Proctor & Fuhrman, 1990). This suggests that the removal of viruses is mediated by marine snow at rates of 4 percent per day ($1\text{-}3x10^{12}$ m^{-2} d^{-1}) as measured during short term deployments (1 day) of sediment traps in Antarctica at a depth of 60 m (Bird et al., 1993).

Murray & Jackson (1992) tried to develop a theoretical description of the interactions of particle shape, size and speed on viral contact. They derived maximum contact rates from diffusion and fluid motion laws and investigated viral adsorption with target particles. Their conclusion was that bacteria and non-host organisms are a major cause of viral removal in seawater.

However, the most important factor in virus mortality is inactivation by ultra-violet radiation (Suttle & Chen, 1992) which should be highest in the surface waters of the oligotrophic ocean where contact times for virus and host are long (Murray & Jackson, 1993). Inactivation rates in full sunlight were found to range from 0.05 d^{-1} (Fuhrman & Suttle 1993) to 0.999 h^{-1} (Murray & Jackson 1993 and references therein).

Populations of motile spherical organisms of 1, 5, 25 and 125 μm diameter present at 10^{-6} biovolume/water volume have average virus:host contact times of 3 h 3 min, 38 h 35 min, 18 d 9 h and 186 d 16 h, respectively (Murray & Jackson 1993). Viruses with the smallest hosts are the least exposed to mortality by UV irradiance. The inverse of contact time is the average contact rate of $9.1x10^{-5}$, $7.2x10^{-6}$, $6.3x10^{-7}$ and $6.2x10^{-8}$ s^{-1} (Murray & Jackson 1992).

2.3 Conclusions

As Thingstad et al. (1993) put it, viral lysis may play a non-negligible role in the global climate system by interfering with phytoplankton and microbial Carbon cycles of the ocean.

Viruses have all the attributes necessary to explain "the source of the semi-labile fraction of the new DOM, its relative stability to chemical and microbial oxidation, and its molecular composition".

Nonetheless, if the high DOC numbers measured by all the HTCO community are ultimately shifted down, the size of the global new DOC pool will shrink accordingly. Toggweiler (1992) stresses that more than the size of the pool what really matters is its activity and its role in both the marine carbon cycle and marine ecosystems. The intriguing aspects of Sugimura & Suzuki's and of Martin & Fitzwater's data are the large vertical and horizontal DOC gradients they reveal in the upper ocean which cannot survive the tendency of the circulation to reduce them unless large amounts of DOC production and remineralization are taking place (Toggweiler, 1990, 1992). No blank correction, however large, will eliminate these gradients.

The percental distribution of Suzuki's DOC in the surface waters of the western North Pacific at 05° 01' N, 134° 44' E was 11%, 9%, 25%, 16%, 27.5% and 11% for classes 1, 2, 3, 4, 5 and 6, respectively. The focus of the present modelling work is the virus-size fraction of the semi-labile new DOC represented by class 6.

Consequently, in Bermuda surface waters one would expect a DOC-class 6 concentration of 7.3 μM C l^{-1} for a total DOC of 66 μM C l^{-1} (Michaels et al., 1994), assuming the size class distribution of Suzuki's DOC to be representative of ocean waters. This is equivalent to 1.1-2.1 μM N l^{-1} using a

Redfield value of 6.625 or a C/N ratio of 3.5. However a value of 1.8 μM N l^{-1} would also be acceptable as it corresponds to a C/N ratio of 4 typical of bacteria.

Knowing that the occurrence of marine viruses is reported to be 10^8 per ml corresponding to a concentration of 2.167 μM C (Fuhrman, 1992) or 0.619 μM N per litre, assuming a C/N ratio =3.5, it is possible to calculate that the biomass of recognizable viruses in seawater at first sight can only explain 30% of the biomass in fraction 6 or alternatively that fraction 6 has been overestimated by a factor of 3.

However, the challenge is to find a credible source able to produce the semi-labile DOC at a rate equivalent to 12% of primary production into the upper 1 km of the ocean 1to support the subsurface DOC consumption rate of Bacastow and Maier-Reimer (1991) of 325 mMol N m^{-2} y^{-1}.

Therefore, in order to prove that marine viruses are major players in the ocean carbon cycle and are able to easily match a production rate of that magnitude a simulation of an upper ocean ecosystem model to which three virus compartments have been added will be run.

Chapter 3.

The Ecosystem Model.

3.1 Introduction

This chapter discusses the structure and functioning of the epidemics model. It is based on the integrated mixed layer ecosystem model of Fasham et al. (1990), a compartment type model able to simulate seasonal variations in plankton dynamics. Section 3.2 gives a review of recent developments in epidemics modelling. Section 3.3 outlines the requisites for a marine epidemics model. The mathematical formulation of the model will be given in section 3.4. The parameter values used in the model are presented in section 3.5.

3.2 Epidemics modelling (SEIR model).

The study of human epidemics is an ever growing field for model applications. A model capable of predicting the course of a natural epidemic can also estimate the effects of various vaccination programmes. Hence the practical value of epidemiological work. The models that have been developed range from the study of measles, through influenza virus to Aids, embracing all types of infectious diseases.

Nevertheless, they all have in common the same basic structure which is based upon the SEIR equations developed by Kermack & McKendrick from 1927-1939.

The SEIR equations constitute a simple mathematical model of the transmission dynamics of viral and bacterial infectious agents within a population of hosts. It is centred on the notion of a threshold density of susceptible hosts to trigger an epidemic. (Anderson, 1991).

It is computationally demanding to model an epidemic on a person by person basis, so a mean field approximation is adopted where the state variables correspond to quantities averaged over a large population assumed to be homogeneously

mixed. The assumption is that the stochastic fluctuations around these averaged quantities tends to zero as the system size grows.

The SEIR model splits a population into four categories. Individuals enter the population at birth as susceptibles (S) and exit by death or by emigration. Such a person becomes exposed (E) by contact with individuals (called infectives (I)) capable of transmitting the disease. After a latency period these exposed individuals become infectives and later immune or recovered (R). For childhood diseases like measles and chickenpox, immunity is permanent and recovered individuals do not revert to the susceptible class.

The set of four simple nonlinear differential equations of the model relate how the numbers of people in each of these groups change with time, taking into account such things as birth and death rates, the average latency period of the infection, and the average time a person is infectious.

$$\begin{aligned} dS/dt &= m(N - S) - bSI \\ dE/dt &= bSI - (m + a)E \\ dI/dt &= aE - (m + g)I \\ dR/dt &= gI - mR \end{aligned} \qquad (3.1)$$

It is not necessary to keep track of the equation for R because it does not enter the equations for dS/dt, dE/dt or dI/dt except through the relation $R + S + E + I = N$.

The population size N is assumed constant and normalised to 1. The quantity $1/m$ is the average life expectancy of an individual; $1/a$ is the mean latency period and $1/g$ the mean infectious period. The most important parameter in the model, b is the effective contact rate, or the average number/fraction of susceptibles that will catch the disease from a single infective (Pool, 1989, Rand & Wilson, 1991). Values of m, a, and g appropriate for various locales and

diseases can be obtained directly from census data (in the case of m) and the medical literature (in the case of a and g). However, the parameters involved in the contact rate b must be estimated indirectly by using age-specific serological profiles to obtain an average age of infection.

When the parameters m, a, b, and g are held constant, the solution of Equation 1 is a weakly damped oscillation. This is inconsistent with the observation of recurrent epidemics in real world populations for which the time-series possess all the signatures of chaos (Olsen & Schaffer, 1990).

For deterministic systems, the most important characterisation of chaos is sensitive dependence upon initial conditions i.e. the existence of a positive characteristic exponent χ (also known as Lyapunov exponent). Nearby orbits of such a system diverge exponentially fast at a mean rate $\exp(t\chi)$, indicating that small disturbances grow exponentially. This puts obvious limits upon the predictability of the system and determines the characteristic time, $t_p = \chi^{-1}$ giving the prediction horizon. Real-world epidemiological time-series for measles, chickenpox, mumps, poliomyelitis, rubella, etc., show such exponentially decaying predictability (Olsen & Schaffer, 1990; Schaffer et al., 1990). However, for deterministic systems the long-term behaviour of the system is usually determined by its attractors and in several cases the most realistic models for these epidemics only have periodic attractors (limit cycles). These have negative characteristic exponents indicating that small disturbances decay exponentially.

Yet, until 1991 the attempts to obtain chaotic behaviour from the SEIR model for realistic parameter values were unsuccessful. Amongst the modifications tried on the basic SEIR model the first was to perturb the equations with noise, -like changes in birthrate, random movements of infected individuals into or out of the population, or changes in the

weather, such as a severe winter that keeps people inside trading germs. Until recently environmental noise was held responsible for all the irregularities in patterns of epidemics. Researchers in epidemiology restricted themselves to simple solutions of their SEIR models, believing that chaotic solutions were too difficult to deal with and had no application in the real world (Pool, 1989). The practical disadvantage of the noise assumption is that if those fluctuations are shaped by random factors in the host population then it would be very hard to predict the effects of a vaccination program on the course of these infections. Thus, using this year's data to predict next year's outbreak seemed hopeless. Consequently, forecasting would ultimately depend on understanding the source of the noise and learning to predict it (Pool, 1989).

The introduction of seasonal variations in the contact rate was another alternative first pioneered by Yorke & London (1973) and then championed by William Schaffer, Mark Kot, Lars Olsen and Greg Truty from 1985 to 1990. These are the men who teamed-up to analyze several sets of historical data on childhood epidemics and calculated their Lyapunov exponents. Among the factors that may induce seasonally varying transmission rates are changes in the virulence or viability of the pathogen itself due to climatic (temperature and humidity) effects, and more significantly the assembling and dispersion of school children at the beginning and end of term (May & Anderson, 1979).

To model the seasonal component, the constant b in Equation 1 is replaced by a periodic function of time with period one year which is given by

$$b(t) = b_0(1 + b_1 \cos 2\pi t) \qquad (3.2)$$

where b_0 is the average contact rate and b_1 is the seasonal component. If $b_1=0$, the contact rate is constant throughout the year. Large values of b_1 imply high contact rates in the

winter and low ones in the summer (Pool, 1989).

Using the values of m, a, g, and b_0 appropriate for chickenpox from table 1 yields a simple stable annual cycle for all values of b_1 in the interval $0< b_1 \leq 0.3$. Yet, real-world chickenpox epidemics have characteristic exponents which range from $\chi = 0.12$ to $\chi = 0.32$ bits per year (Olsen & Schaffer, 1990). Later work by Rand & Wilson (1991) has confirmed the stability of the annual limit cycle for chickenpox by testing the value of b_0 and found that a large chaotic attractor containing multiple attractors only occurs at higher values in the immediate neighbourhood of the measles contact rate of table 3.1.

By contrast, the measles simulation obtains qualitatively different dynamics for different values of b_1. For $b_1< 0.1$, one observes a simple annual cycle. At values of b_1 around 0.2, the dynamics change to a biennial cycle. Further increases in seasonality induce successive period-doubling bifurcations, until around $b_1 \approx 0.28$ the solutions become chaotic and a pattern of erratic fluctuations emerges, similar to the outbreaks observed in New York City before 1945 (Olsen & Schaffer, 1990). Critics were quick to point that though the SEIR model with seasonal variations in contact rate can generate time series that resemble the measles historical data collected from 1928 to 1963 in major cities around the world, that required an unreasonably high value for b_1 (0.28) as compared to the 0.27 supported by the data (Sidorowich, 1992). However, if the value is reduced below 0.272 the model reverts to periodic behaviour and the only attractor is a limit cycle (Rand & Wilson, 1991).

	Measles	Chickenpox
m	0.02 $year^{-1}$	0.02 $year^{-1}$
a	35.84 $year^{-1}$	36.0 $year^{-1}$
g	100 $year^{-1}$	34.3 $year^{-1}$
b_0	1800 $year^{-1}$	537 $year^{-1}$

b_1	0.28 $year^{-1}$	0.3 $year^{-1}$

Table 3.1: Parameter values for measles and chickenpox taken from Rand & Wilson (1991).

The discrepancy between the SEIR model and the historical data is explained by a new type of process named chaotic stochasticity. Rand & Wilson (1991) have shown that in addition to the periodic attractor, an unstable chaotic repellor also exists for the realistic values of the contact rate. The coexistence of these two invariant sets can generate behaviour displaying chaotic properties when perturbations are added to the system. These perturbations can either be in the form of stochastic fluctuations of the average contact rate (b_0) by a 3% Gaussian noise or stochastic fluctuations corresponding to the import of a few infected individuals when there is a near extinction of the epidemic due to low number of infectives.

To generate this behaviour they proposed an alternative contact rate that fluctuates stochastically

$$b = b_0(1 + \zeta(t))(1 + b_1 \cos 2\pi t) \qquad (3.3)$$

where ζ is white noise with mean 0, amplitude $a = 0.03$ and variance $\sigma = 1$.

Then the SEIR equation is solved for a Poincaré map and the resulting attractor projected onto the I axis with varying b_1. Without noise, the effective chickenpox attractor is a single point (representing a limit cycle) but when b_0 is modulated by only 3% noise it explodes to a size which is two orders of magnitude greater than the noise amplitude. This occurs because of the existence of a chaotic repellor which can be visualized by plotting S against I.

Occasionally the mean field assumptions of the SEIR model fail because the equations allow for the extinction of the infective subpopulation. In systems that possess near extinctions the statistical effects become important.

Therefore Rand & Wilson modified also the description of how dwindling rare individuals interact with the rest of the population by adding a random element of stochastic nature to that process.

The probability that j individuals are infected during this period is approximated by the Poisson distribution

$$p(j) = \frac{(\tau si\delta t)^j}{j!} e^{-\tau si\delta t} \qquad (3.4)$$

where τ is a constant rate of random interactions of each susceptible and infected individual with other members of the population, s = NS(t) and i = NI(t) denote the number of susceptibles and infectives at time t.

Thus the first equation (1) is replaced by

$$dS/dt = m(N - S) - d\mu$$
$$dE/dt = d\mu - (m + a)E$$
$$dI/dt = aE - (m + g)I + I_0 \qquad (3.5)$$

where μ = bSI and the term $d\mu(t)$ is such that its integral on an interval (t,t + δt) has the distribution p(j) given in (3.4). The other terms in the SEIR equation are not stochastically modelled since these are far better controlled and accurately represented by the mean field approximation. The rare events, where i is very small, give extinctions if, as in (1), the term I_0, which represents a very small constant import rate of infectives into the population is zero.
Taking I_0 positive but very small (10^{-6}) avoids the extinction and these stochastic fluctuations launch the system into a chaotic pinball machine. The system is knocked off its periodic limit cycle into the surrounding region of state space which is filled with a chaotic repellor. What should have been a short-lived chaotic transient persists due to the stabilization of the repellor by the background stochastic "noise", and keeps bouncing about the fractal repellor producing a long-term trajectory with positive exponent.

As pointed out by Sidorowich (1992) the novel aspect of the Rand & Wilson proposal is the demonstration that chaotic repellors can act as extremely strong amplifiers for system perturbations, and that these stochastic fluctuations can stabilize the effects of the repellor. The resulting time-series are practically indistinguishable from those of a chaotic attractor.

Furthermore, they claim that chaotic repellors should be more common than chaotic attractors in biological, chemical and some physical dynamical systems because of the simplicity and the ubiquity and the stability of the ingredients in their mechanism.

It is the contact rate (b) parameter in the form of equation (3.2) that constitutes the basis for the viral equations in my ecosystem model.

Ways of determining the value of the contact rate

The easiest way to determine the minimum contact rate in an epidemic of marine viruses is by simple iteration with the model. However such value can be validated against maximum contact rates predicted by diffusion and transport theory for particle-virus contact dynamics (Murray & Jackson, 1992; Johnson & Kepkay, 1992) as well as compared to the values given in the literature of waste water treatment for the removal rate of human enteric viruses in seawater (Carlucci & Pramer, 1960; Fujioka et al, 1980; Metcalfe et al., 1974; Sobsey & Cooper, 1973; Toranzo et al., 1982; Zachary, 1976). See also chapter 2 § 2.2.4.

3.3 Requisites for a Marine Epidemics Model.

It was thought necessary to make use of a model that already incorporates most of the interaction processes (growth and loss terms) required to describe the dynamics of a population and that would work as **a proxy** for the Kermack & McKendrick epidemics model.

A requirement is the selection of a model containing phytoplankton and bacterial populations that could serve as hosts to viral epidemics.

A compartmental ecosystem model containing information about the fluxes between compartments is an ideal choice.

The initial model platform must be simple to minimize the increased dynamic complexity of the final model once the extra compartments needed to describe the viral epidemics are added. Furthermore, a compromise has to be found in the level of complexity incorporated within the new formulations to make the interpretation of results easier.

It is convenient that the model be based on the nitrogen cycle so that it is able to separate the nitrogen pool into ammonium, nitrate and dissolved organic nitrogen, with a microbial loop for recycling ammonium. In this way the impact of the virus epidemic on the regenerated production, DON production and annual primary production rates could be evaluated.

For these reasons, this study and model development build upon the ecosystem model of Fasham et al. (1990). Though other compartmental models have been published since, the Fasham et al. model was the only one available at the beginning of this project. Furthermore it had a successful track record in the coupling to a 3D physical model of the Princeton University general circulation model for the North Atlantic Ocean.

3.4 Description of the Ecosystem Model.

This ecosystem model is based on the upper ocean ecosystem model developed by Fasham et al. (1990) to predict seasonal variations in plankton populations in the oceanic mixed layer. Nonetheless three more compartments describing the growth of the marine virus population have been added to the original seven compartment model which Fasham et al. consider capable enough of representing the essential features of nitrogen cycling in the mixed layer.

Therefore the model comprises now ten compartments or state variables namely; active virus of phytoplankton (Vi_p), active virus of bacteria (Vi_b), inactivated viruses (Ivir), phytoplankton (P), zooplankton (Z), bacteria (B), detritus (D), nitrate (Nn), ammonium (Nr), and dissolved organic nitrogen - DON (Nd); and twenty two intercompartmental flows.

Figure 3.1 shows the diagram of the model depicting the relationship between the state variables and the modelled nitrogen flows between compartments and the deep ocean.

Equations for the ten state variables and some of the underlying assumptions on the ecological processes affecting each compartment are given below. As some of the original equations were modified to include new expressions governing the interaction with the virus compartments, please refer to Fasham et al. (1990), for a full description of the original 7-compartment model and corresponding equations.

The state-variable units are mMol Nitrogen m^{-3}. However flows, such as primary production or particulate flux from the mixed layer, are calculated by the model in areal units of mMol N m^{-2} per day; annual integrated flows are in Mol N m^{-2} per year.

3.4.1 Physical Forcing

Seasonal changes in the mixed layer depth provide dynamical forcing to the model and determine the supply of photosynthetically active radiation (PAR) and nitrate to the phytoplankton compartment.

The mixed layer dynamics are not modelled explicitly, but instead climatic monthly averages compiled by Levitus (1982) are used to specify the annual cycle of mixed layer depth, M, as a function of time, t (days). Interpolated daily values of M(t) are used to calculate b(t) as

$$\frac{dM}{dt} = h(t) \qquad \textbf{(3.1)}$$

When the mixed layer depth changes active swimmers like zooplankton are assumed to maintain themselves within the mixed layer. However, non-motile entities such as phytoplankton, bacteria, or detritus are left behind, or detrained, as the mixed layer shallows. Therefore, when the mixed layer deepens/shallows the volumetric concentration of zooplankton decreases/increases whereas the volumetric concentration for the non-motile entities decreases as the mixed layer deepens but remains the same as the mixed layer shallows.

Following Evans and Parslow (1985) the effect on the concentration of non-motile entities is modelled by defining the variable

$$h^{+}(t) = \max\ (\ h(t)\ ,\ 0\ ) \qquad \textbf{(3.1b)}$$

Diffusive mixing across the thermocline is parameterised as the product of a mixing coefficient and a concentration difference.

The meteorological forcing in the model comes from solar irradiance (calculated as Brock, 1981) and cloud cover (data from Isemer & Hasse, 1985) whose effect on atmospheric transmittance is calculated by the Smith and Dobson (1984) equation. Knowing the light at the surface the light at depth is then calculated using a simple exponential model of the light transmittance through the water column. As phytoplankton itself absorbs light its contribution to the attenuation is parameterised by a self-shading coefficient (equation (3.5c)).

3.4.2 Inclusion of Viruses

3.4.2.1 The Equation for Virus of Phytoplankton

$$\frac{dVi_p}{dt} = \beta_8 P Vi_p . K_8 - \mu_8 Vi_p - \frac{(m + h^+(t))\, Vi_p}{M} \qquad (3.2)$$

where β_8 is the effective contact rate between phytoplankton and virus (ad hoc formulation),
K_8 is a constant for the efficiency of the biomass conversion from host-cell (phytoplankton) into virus,
$\mu 8$ is the specific inactivation rate of phytoplankton virus by natural ultra-violet radiation,
m is a quantity (units m d^{-1}) that parameterizes the diffusive mixing between the mixed layer and the deep ocean,
$h^+(t)$ has been defined above.

The contact rate β_8 is a periodic function of time with period six months given by

$$\beta_8(t) = b_0(1 + b_1 \cos(2\pi \frac{t}{T} - t_0)) \qquad (3.2b)$$

where b_0 is the average contact rate and
b_1 is the seasonal component,
T is the period in days,
t_0 is a non-dimensional number to adjust the phase

of the maximum seasonal contact rate to the peak of the Spring and Autumn phytoplankton blooms.

The term operated by the cosinus is an angle, in radians because of π.

Constant as well as a seasonal varying rate were used in the model simulations. If $b_1=0$, the contact rate is constant throughout the year. Large values of b_1 imply high contact rates in the Spring and Autumn and low ones in the Summer and Winter (Fig. 3.2).

However, the outbreak of diseases may have more to do with the nutritional state of the host rather than with an enhanced transmission for high density populations which is the commonly accepted hypothesis. Whenever host density rises to a level where competition for available food resources is severe, malnourished hosts have their immunological competence lowered and are thus less able to withstand the onslaught of infection. Hence, the effective pathogenicity of a parasite tends to increase (May & Anderson, 1979).

The production of viruses in the model is dependent on the contact rate between virus and phytoplankton and on the efficiency of biomass conversion. A basic assumption is that the disease does not induce immunity (see c. 2.2.3) and all infected cells die and burst releasing new viruses into the water. The cytoplasm and cell debris released by lysis of small phytoplankton cells like picoplankton fuel the DON compartment. However, the phytoplankton in this model is assumed to be composed of larger cells and thus the destination of their lysed cell debris is the detritus compartment. Newly produced viruses enter the pool of inactivated viruses at a rate of approximately 79% day^{-1} due to damaging by natural ultra-violet radiation (Suttle & Chen, 1992). Additional losses in virus concentration are due to diffusive mixing between the mixed-layer and the deep ocean and entrainment of water into the mixed-layer.

3.4.2.2 The Equation for Virus of bacteria

$$\frac{dVi_b}{dt} = \beta_9 B Vi_b . K_8 - \mu_9 Vi_b - \frac{(m+h^+(t))\, Vi_b}{M} \qquad (3.3)$$

where β_9 is the effective contact rate between bacteria and virus,
K_8 is a constant for the efficiency of the biomass conversion from host-cell (bacteria) into virus,
$\mu 9$ is the specific inactivation rate of bacterial virus.

The contact rate β_9 is a periodic function of time with period six months and is given by an equation identical to equation (3.2b).

Due to their small size the lysed cell debris of bacteria can be readily taken up by other bacteria and therefore fuel the pool of labile DON instead of the detritus compartment. Consequently the recycling of this type of nitrogen is extremely fast. Bacteriophages damaged by UV radiation enter the pool of inactivated viruses.

3.4.2.3 The Equation for Inactivated Virus

$$\frac{dI_{vir}}{dt} = \mu_8 Vi_p + \mu_9 Vi_b - \mu_{10} I_{vir} - \frac{(m+h^+(t))\, I_{vir}}{M} \qquad (3.4)$$

where $\mu 10$ is the specific decay rate of inactivated virus into labile DON.

This compartment contains the bacterial and phytoplankton viruses that were inactivated by natural ultra-violet radiation. This type of nitrogen will be made available to bacteria very slowly. Due to their high molecular weight inactivated viruses are harder to breakdown and hence can be considered as semi-labile DON. Thus the concentration levels

and production rates of modelled inactivated viruses will be used to gauge the magnitude of the "new, semi-labile" DON claimed by Suzuki (1985, 1988) and other researchers.

3.4.3 The Phytoplankton Equation

$$\frac{dP}{dt} = (1-\gamma)\,\sigma(t,M,N_n,N_r)\,P - G_1 - \frac{\mu_1 P^2}{k_5+P} - \beta_8 P Vi_p - \frac{(m+h^+(t))\,P}{M} \quad \textbf{(3.5)}$$

where σ(t,M,Nn,Nr) is the average daily phytoplankton specific growth rate,
G1 represents the loss of phytoplankton due to zooplankton grazing,
μ1 is the specific natural mortality rate of phytoplankton,
β8 is the contact rate between virus and phytoplankton,
β8 PVi_p represents the loss of phytoplankton due to viral lysis,
γ is the fraction of total net primary production that is exuded by phytoplankton as DON,

The daily averaged phytoplankton growth rate σ is defined by the equation

$$\sigma = J(t,M)\,.\,Q(N_n,N_r) \quad \textbf{(3.5b)}$$

where J is the light limited growth rate and
Q is a non-dimensional nutrient limiting factor.

The total light limited daily growth rate is averaged over the mixed layer depth,

$$J(t,M) = \frac{2}{M}\int^{\tau}\int^{M} F(I_0(t).\exp[(-k_w - k_c P)Z])\,dzdt \qquad \textbf{(3.5c)}$$

where 2τ is the day-length,
$I_0(t)$ is the PAR immediately below the surface of the water,
K_w is the light attenuation coefficient due to water (assumed to be constant with depth),
K_c is the phytoplankton self-shading parameter,
$F(I)$ is a function describing the phytoplankton photosynthesis-irradiance relationship (the P-I curve) and is defined (Evans & Parslow, 1985),

$$F(I) = \frac{V_p \alpha I}{(V_p^2 + \alpha^2 I^2)^{1/2}} \qquad \textbf{(3.5d)}$$

where V_p is the maximum growth rate and
α is the initial slope of the P-I curve.

The daily variation of $I_0(t)$ with time of day was assumed to be triangular to enable the analytical integration of equation (3.5c).

$I_0(t)$ is defined by

$$I_0(t) = \lambda(1-a).t(c).S(\theta,t) \qquad \textbf{(3.5e)}$$

where λ is the ratio of PAR to total solar irradiance,
a is the air-sea albedo,
t(C) the atmospheric transmittance as a function of cloudiness C,
$S(\theta,t)$ is the solar irradiance at the top of the atmosphere as a function of latitude θ and time t.

There are two possible ways to specify the maximum phytoplankton growth rate V_p; either by using observational data from the area to be modelled or utilizing the

temperature dependent formulation developed by Eppley (1972),

$$V_p = 0.6 \cdot (1.066)^T \qquad \textbf{(3.5f)}$$

The generality of this equation is invaluable when modelling basin-wide biological processes (Sarmiento et al., 1991).

The nutrient limitation factor Q, is calculated using a Michaelis-Menten equation that incorporates an exponential term to allow the preferential uptake of ammonium over nitrate. It was defined as (Wroblewski, 1977),

$$Q(N_n, N_r) = Q_1(N_n, N_r) + Q_2(N_r) = \frac{N_n e^{-\Psi N_r}}{K_1 + N_n} + \frac{N_r}{K_2 + N_r} \qquad \textbf{(3.5g)}$$

where K1, K2 are the half-saturation constants for nitrate and ammonium uptake respectively, and Ψ is a constant that parameterizes the degree of ammonium inhibition of nitrate uptake.

Recently, it was discovered that some phytoplankton have cell-surface enzymes that enable them to utilize DON in larger proportions than previously thought (Palenik & Morel, 1991). Experimental evidence from time series of unicellular algae cultures show that excretion of DON representing 75% of the nitrate uptake, in the early part of the incubation, is followed by DON uptake when the nitrate is exhausted (Collos, 1992). This can be thought of as extracellular storage of organic nitrogen. Furthermore, Collos (1992) has shown that when this process of nitrogen cycling is taken into consideration nitrogen budgets from historical data on plankton cultures can be balanced. Moreover, this process is not unique to laboratory environments. Recent measurements by Bronk et al. (1994) in the Caribbean Sea and Southern California Bight oceanic system have also found that 22 to 74% of the dissolved inorganic nitrogen (NH_4^+ and NO_3^-) taken up by phytoplankton is released as DON. They suggest that release and uptake rates of DON by phytoplankton are particularly important during the development and dissipation of a bloom. In the model the DON release is assumed to be 5%.

Though in the present model DON is not accounted for in the calculation of nutrient limitation, it is my opinion that a new formulation for nitrogen uptake incorporating DON feedback into the phytoplankton compartment ought to be included in future ecosystem models.

Following Fasham et al. (1990), control run A and version 1 of the epidemics model incorporated a constant phytoplankton mortality term $\mu_1 P$, where mortality is assumed to be a constant fraction of the total population. However following Fasham (1993), in control run B and all subsequent versions of the epidemics model the constant phytoplankton mortality term has been replaced by the Michaelis-Menten formulation seen in equation (3.5). The reason for this implementation is to bring the formulation of phytoplankton mortality in line with the Michaelis-Menten formulation for zooplankton mortality introduced in control run B.

The phytoplankton is represented as a single entity lumping together different size classes, such as picoplankton, nanoflagellates and diatoms. These not only have disparate growth rates but also contribute differently for the primary production of the ocean and for the flux of sinking particles. Phytoplankton consumes either nitrate or ammonium but it favours ammonium whenever this is available. Curiously, in nature some eukaryotic phytoplankton are even able to produce ammonium for their own consumption through a special cell surface mechanism that catalyses primary amines that are available in the surrounding water (Palenik & Morel, 1991).

In the original model the phytoplankton concentration is reduced by five mechanisms: entrainment of water into the mixed layer diluting its concentration, diffusive mixing between the mixed layer and the deep ocean, natural mortality, zooplankton grazing and exudation of dissolved organic nitrogen.

In the present model there is an additional cause of phytoplankton mortality due to viral infection.

3.4.4 The Zooplankton Equation

$$\frac{dZ}{dt} = \beta_1 G_1 + \beta_2 G_2 + \beta_3 G_3 - \frac{\mu_2 Z^2}{k_6 + Z} - \frac{h(t) \cdot Z}{M} \qquad (3.6)$$

where G1,G2,G3 are the grazing rates of zooplankton on phytoplankton, bacteria and detritus respectively, $\beta 1, \beta 2, \beta 3$ are the equivalent assimilation efficiencies,
μ_2 is the zooplankton specific loss rate,
k_6 is the half-saturation constant for the loss rate.

The loss rate is assumed to include both excretory losses and losses due to mortality. Fractions ϵ and δ of the total loss are in the form of ammonium and DON respectively. This leaves a fraction $1-\epsilon-\delta$ for the mortality loss, which being mainly due to higher predators that excrete large faecal pellets, is considered to be exported directly from the mixed-layer.

The expression used for the grazing functions G1 was

$$G_1 = \frac{gp1P^2Z}{K3(p_1P + p_2B + p_3D) + p_1P^2 + p_2B^2 + p_3D^2} \qquad (3.6b)$$

where g is the maximum ingestion rate,
p1,p2,p3 are measures of the zooplankton preferences for phytoplankton, bacteria, and detritus respectively, when their concentrations are equal, and
K3 is the half-saturation constant for grazing.

Analogous expressions are used for G2 and G3. This

grazing formulation was designed to ensure that the zooplankton actively switch their grazing to the most abundant resource (Fasham et al., 1990).

The model zooplankton are a highly aggregated entity incorporating organisms from flagellates to euphausiids, and are assumed to be omnivorous grazing phytoplankton, bacteria and detritus. They are able to switch in their consumption patterns according to food availability. Furthermore they are the only compartment which is not affected by detrainment because they are able to actively maintain their position in the mixed layer. The zooplankton losses are parameterized through excretion of ammonium and DON, natural mortality and grazing by higher order predators.

Following Fasham et al. (1990), control run A and version 1 of the epidemics model assumed that both excretion and mortality were linear functions of zooplankton biomass. However following Fasham (1993), in control run B and all subsequent versions of the epidemics model the constant zooplankton loss terms have been replaced by the Michaelis-Menten formulation seen in equation (3.6). For more details see chapter 4.

3.4.5 The Bacteria Equation

$$\frac{dB}{dt} = U_1 + U_2 - G_2 - \mu_3 B - \beta_9 B V i_b - \frac{(m + h^+(t))B}{M} \qquad (3.7)$$

where U1 is the DON uptake,
U2 the ammonium uptake,
$\mu 3$ is the bacterial specific excretion rate, and
$\beta 9$ BVi_b represents the bacterial losses to viral lysis.

U1 is defined,

$$U_1 = \frac{V_b\ B\ N_d}{K_4 + S + N_d} \qquad \textbf{(3.7b)}$$

U2 is defined,

$$U_2 = \frac{V_b\ B\ S}{K_4\ +\ S\ +N_d} \qquad \textbf{(3.7c)}$$

where Vb is the maximum bacterial uptake rate and
K4 is the half-saturation coefficient for uptake.

More than 90% of oceanic bacteria are free-living (Azam et al., 1983). These can take up ammonium and DON and also excrete ammonium. The balance between these two processes determines whether the bacteria act as net utilisers or remineralisers of carbon and nitrogen. Bacteria obtain their carbon from DON and are thought take up ammonium mainly to obtain sufficient nitrogen to synthesize cell protein. A balanced growth model is obtained by defining a total bacterial nitrogenous substrate, S, which when incorporated into a Michaelis-Menten equation for bacterial uptake, ensures that the uptake of ammonium will be η times the DON uptake (see Fasham et al., 1990 for details).

$$S = \min(N_r, \eta N_d) \qquad \textbf{(3.7d)}$$

where η is a function of the bacterial carbon and nitrogen growth efficiencies, and the C/N ratio of bacterial cells and DON (Fasham et al., 1990).

The main problem in modelling bacteria is to determine the character of the substrate they use. It is not known whether bacteria can utilise inactivated viruses nor the timescale for their breakdown.

In the original model bacteria concentrations are reduced by zooplankton grazing, bacterial excretion, diffusive mixing across the thermocline, and entrainment.

In the present model there is an additional cause of bacteria mortality due to viral lysis.

3.4.6 The Detritus Equation

$$\frac{dD}{dt} = (1-\beta_1)G_1 + (1-\beta_2)G_2 - \beta_3 G_3 - \mu_4 D + \frac{\mu_1 P^2}{k_5 + P} + \beta_8 PVi_p . K_7 - \frac{(m + h^+(t) + V)D}{M} \quad (3.8)$$

where $\mu 4$ is the specific rate of breakdown of detritus to DON,
K_7 is a constant determining the detrital fraction of phytoplankton destroyed by viral lysis,
V is the detrital sinking rate.

The sources for the detritus compartment are faecal pellets and dead phytoplankton, plus cell debris resulting from viral lysis of phytoplankton. These detritus can be recycled within the mixed-layer by two mechanisms, reingestion by zooplankton or breakdown into DON and subsequent uptake by bacteria. However, much of the detrital material sinks out of the mixed-layer to the deep ocean. The development of a universal parameterisation of sinking speed for the spectrum of particle sizes in detritus is still forthcoming. Therefore, the sinking rate is assumed to be a constant velocity. Additional losses are caused by diffusive mixing across the thermocline and changes in mixed layer depth.

Notice that the diagram shows a second flux from the phytoplankton into the detritus compartment to determine how much of the debris in sediment traps can be attributed to viral lysis of phytoplankton.

3.4.7 The Nitrate Equation

$$\frac{dN_n}{dt} = -J(t,M)\,Q_1(N_n,N_r)\,P + \frac{(m+H^-(t))}{M}\,.\,(N_0-N_n) \qquad (3.9)$$

where N0 is the constant nitrate concentration below the mixed layer.

The most important nutrients for sustained growth and cell division of phytoplankton are nitrogen, phosphorous and silica. Although nitrogen has been regarded as the limiting factor of primary production in the ocean the importance of iron micronutrients has recently been emphasized (Martin & Fitzwater, 1988). Moreover, the modelling and experimental findings of Riebesell et al. (1993), suggest that diatom growth is CO_2 limited during bloom periods due to a CO_2 requisite by the enzyme mediating carbon fixation in phytoplankton.

Nitrate and ammonium are the two forms of inorganic nitrogen used in the model, thus allowing primary production to be partitioned into "new" production, fuelled by nitrate, and "regenerated" production, fuelled mainly by ammonium.

Nitrate has a sub-thermocline concentration of 2 mMol N m^{-3} in Bermuda Station "S" and enters the mixed-layer by entrainment during the late autumn and winter but also through diffusive mixing across the thermocline throughout the year. It is depleted through new primary production.

3.4.8 The Ammonium Equation

$$\frac{dN_r}{dt} = -J(t,M)\,Q_2(N_r)\,P - U_2 + \mu_3 B + \frac{\epsilon\mu_2 Z^2}{k_6+Z} - \frac{(m+h^+(t))}{M}\,.\,N_r \qquad (3.10)$$

The first two terms represent the uptake of ammonium by phytoplankton (regenerated primary production) and bacteria

respectively, the third represents the excretion by bacteria and the fourth represents the addition from zooplankton excretion. It should be noted that the ammonium concentration below the mixed layer is assumed to be zero.

3.4.9 The DON Equation

$$\frac{dN_d}{dt} = \gamma J(t,M)\, Q(N_n, N_r)\, P + \mu_4 D + \frac{\delta \mu_2 Z^2}{k_6 + Z} + \beta_9 BVi_b . k_7 + \mu_{10} I_{vir} - U_1 - \frac{(m + h^+(t))}{M} . N_d \quad (3.11)$$

where δ is the fraction of DON generated by the zooplankton loss term,
k_9 is the fraction of DON generated by bacterial viral lysis,
$\mu 10$ is the specific decay rate of inactivated virus into labile DON.

About 10% of the traditional DOC pool is made of low-molecular weight compounds like dissolved free amino acids and carbohydrates that are readily taken up by bacteria. Using HTCO methods recent estimates of this "labile pool" put its size at 30 to 50% of the total DOC pool and indicate that it is turned over in hours to days (Wangersky, 1993). These results are a confirmation of the findings of Kirchman *et al.* (1991) which suggested that, in the euphotic zone, up to 25% of the DOC pool is turned over in time scales of 1-10 days. The fast cycling of this material puts in evidence the need for including bacteria in models of the carbon cycle. However, a fraction of the "extra" DOC discovered by Suzuki (1988) is made of high-molecular weight compounds which presumably are more difficult to utilise by the bacteria and is thus refered to as the "semi-labile" pool.
This compartment includes only the labile fraction of DON.

Recently, Bronk & Glibert (1991, 1993) developed methods to isolate DON so that its release and uptake rates could be

quantified. The technique works by measuring the ^{15}N present in the DON pool at the end of $^{15}NH_4^+$ and $^{15}NO_3^-$ uptake experiments by isolating DON with ion retardation resin that removes inorganic nitrogen ions [including NH_4^+ and NO_3^-]. They measured release rates for DON in oceanic systems ranging from 4 to 26 nanogram-atoms of nitrogen per litre per hour, corresponding to total DON turnover times of 10 ± 1 days (10 to 62 days).

The inputs to the DON pool come from exudation of DON by phytoplankton, detrital breakdown into DON, and zooplankton excretion and messy feeding. There are two new additions to the equation; one is the cell debris of lysed bacteria which due to their small size enter the DON pool directly and can be readily utilised by other bacteria; the other is the breakdown of inactivated viruses into labile DON. The DON stocks are depleted through uptake by bacteria, diffusive mixing across the thermocline and changes in the mixed layer depth.

As was the case for ammonium, the labile DON concentration below the mixed layer is assumed to be zero.

3.5 Parameter values

The basic parameter setting for the various versions of this model are those for Bermuda Station "S" as laid by Fasham et al. (1990) in control run A and slightly modified by Fasham (1993) in control run B. The parameters introduced with the virus equations were experimentally subjected to a range of values. Values for all the parameters in the epidemics model are given in appendix A. The summary of experimental characteristics for the simulation runs of versions 1 to 5 of the model can be found in chapter 5 § 5.16 - § 5.20.

3.6 Figures

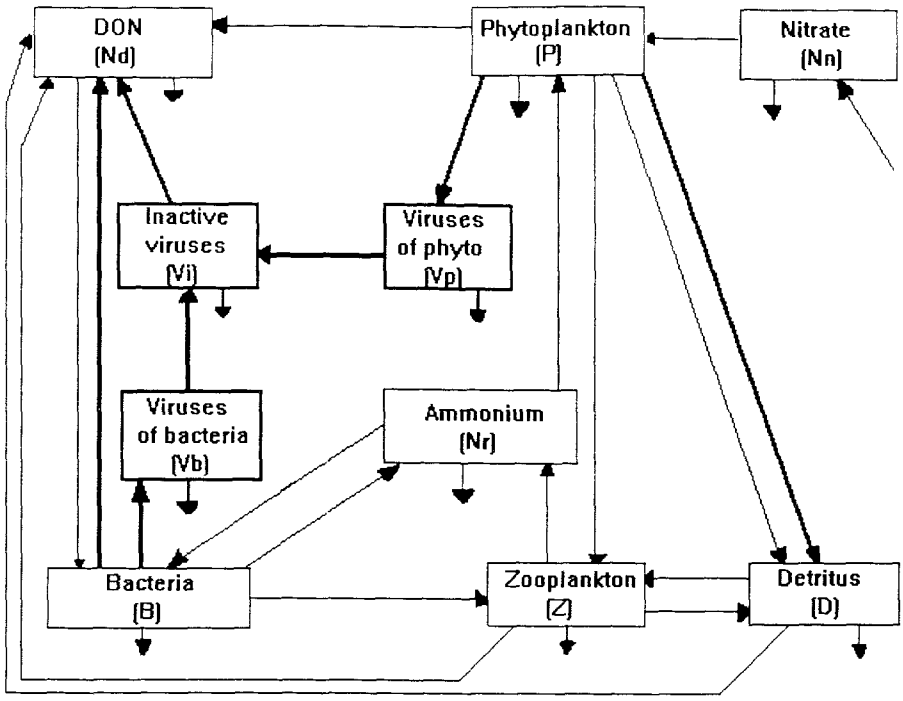

Figure 3.1 Diagram of the ecosystem model. Compartments and flows in heavy solid line are the new additions to the original model (thin solid line) of Fasham et al. (1990).

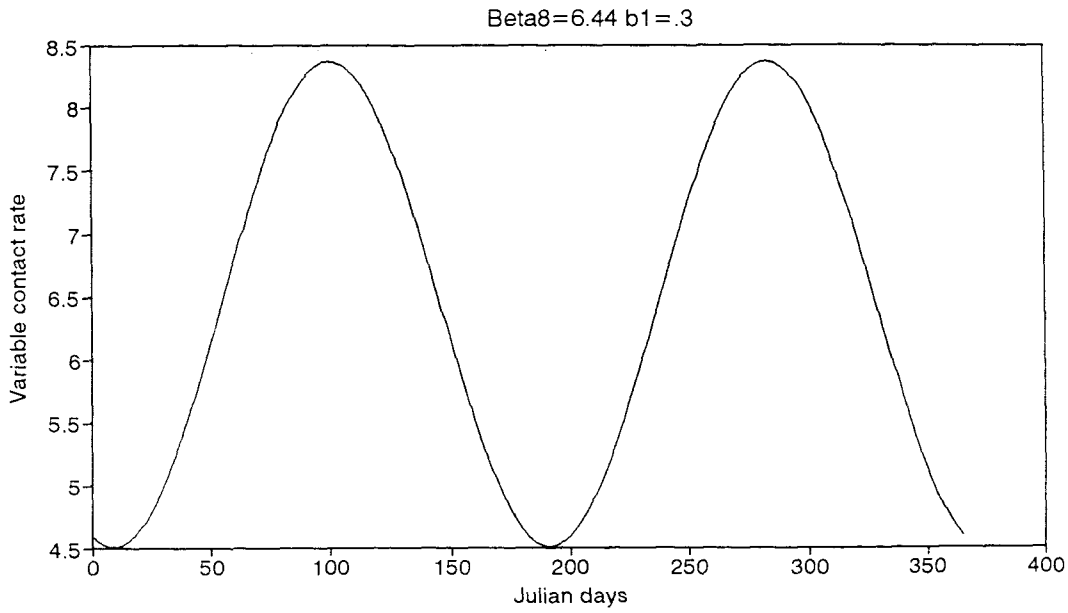

Figure 3.2 Temporal variation of a variable contact rate.

Chapter 4.

Control Runs A + B.

4.1 Introduction

In this chapter, a brief synthesis of Fasham's Model A (1990) and Model B (1993) will be presented as these constitute the basis for the development of the present viral epidemics model. Throughout the rest of this work they will be referred to as control run A and B, respectively. For more detailed information please refer to the relevant papers. The effect of viruses is not included in either of these two control runs.

4.2 Control run A.

In Control run A there is a gradual increase in phytoplankton concentration throughout the late winter with no pronounced bloom, reaching a maximum biomass of 0.4 mMol N m^{-3} in spring (Figs. 4.1.a and 4.13b). A decline in the plankton stock follows after day 100 due to the rapid shoaling of the mixed layer (Fasham et al., 1990; Figs. 4.2 and 4.11a), which leaves behind most of the phytoplankton biomass by detrainment as the mixed layer rises to its summer thermocline level. The phytoplankton remains at a low level of over 0.2 mMol N m^{-3} throughout the summer period. This value is still too high in comparison to the observational data (Fig. 4.13b) which show a phytoplankton biomass less than 0.1 mMol N m^{-3} at this time of the year (Fasham et al., 1990). In the autumn, nitrate is entrained to the system as the mixed layer deepens (Figs. 4.11b and 4.13a) resulting in another phytoplankton bloom. At its height this bloom reaches a biomass over 0.45 mMol N m^{-3} which is even higher than the modelled spring value (Fig. 4.13b). This is not supported by the observational data and hence Fasham et al. (1990) concluded that their simulation greatly overestimated the phytoplankton biomass in the summer and autumn.

In addition the prebloom zooplankton concentrations were so low (Fig. 4.3) that the only significant period showing positive growth was during the spring bloom. However, the growth rate during the event was so high that the model predicted bloom zooplankton concentrations that were much higher than observations (not shown). It will be shown in chapter 5 how the competition with viruses aggravated the zooplankton deficiencies.

Control run A was only partially successful in fitting the phytoplankton, bacteria (Figs. 4.13c,d) and zooplankton observations for Bermuda Station "S".

The equations for phytoplankton and zooplankton were

$$\frac{dP}{dt} = (1-\gamma)\,\sigma(t, M, N_n, N_r)\,P - G_1 - \mu_1 P - \frac{(m+h^+(t))\,P}{M} \qquad (4.1)$$

$$\frac{dZ}{dt} = \beta_1 G_1 + \beta_2 G_2 + \beta_3 G_3 - \mu_2 Z - \mu_5 Z - \frac{h(t)\,.\,Z}{M} \qquad (4.2)$$

4.3 Control run B.

The shortcomings of Model A were addressed by Fasham (1993) in his Model B through the implementation of density-dependent excretion and mortality rates on zooplankton. Such formulation reduces zooplankton loss rates in the winter but allows them to rise during the bloom. According to Fasham this enabled his model to fit much better observations from Bermuda Station "S" and Ocean Weather Station "India". In order to be consistent Fasham also added a Michaelis-Menten mortality for phytoplankton.

These were the modifications,

$$\frac{dP}{dt} = (1-\gamma)\,\sigma(t, M, N_n, N_r)\,P - G_1 - \frac{\mu_1 P^2}{k_5+P} - \frac{(m+h^+(t))\,P}{M} \qquad (4.3)$$

$$\frac{dZ}{dt} = \beta_1 G_1 + \beta_2 G_2 + \beta_3 G_3 - \frac{\mu_2 Z^2}{k_6 + Z} - \frac{h(t) \cdot Z}{M} \qquad (4.4)$$

The values for the new parameter set can be found in table 2 (appendix A). The maximum zooplankton loss rate (μ_2) was set at 0.325 d^{-1} and the maximum specific mortality rate of phytoplankton (μ_1) was set at 0.05 d^{-1}. The half-saturation coefficients k_5 and k_6 were fixed at 0.2 mMol N m^{-3}. Another very important change made by Fasham was to fix the cross-thermocline mixing rate (m) at 0.01 m d^{-1}.

Figures 4.4 a,b show the phytoplankton seasonal cycles obtained for the 10m/day and 1m/day simulations using cross-thermocline mixing rates of 0.1 and 0.01 m d^{-1}.
Control run A was characterised by a clear-cut difference between the 10m/day and 1m/day simulations. That difference has vanished in Model B with both simulations giving now similar results on phytoplankton biomass.

The 10m/day simulation with a cross-thermocline mixing of 0.01 m d^{-1} has been adopted by Fasham (1993) as the new standard for Bermuda Station "S" - Control run B. The reasons for it are two: a lower phytoplankton biomass during summer (Fig. 4.4.a), and a low f-ratio throughout the same period as a result of the lower nitrate flux from below the mixed layer (fig. 4.5 and fig. 4.6).

While the new zooplankton model has certainly made an improvement to the previous model in the prediction of the phytoplankton autumn bloom it cannot reproduce the drop in observed biomass levels to below 0.1 mMol N m^{-3} just after the spring bloom. In that respect Control run A did a better job (Figs. 4.7 and 4.13b).

The new formulation caused the total mixed layer stocks of phytoplankton to decrease by 35% during winter and spring (Fig. 4.8).

A positive result is that the total (areal) mixed layer stock of bacteria during the spring bloom became lower and gave for the first time a perfect fit to the observations (Figs. 4.9 and 4.13d) despite the concentration levels of bacteria (volumetric) remaining similar to Control run A (Fig. 4.13c). However, the bacterial excretion of ammonium droped 19% (Table 4.2). The nitrate cycle was similar, too.

The new formulation of zooplankton mortality and excretion has turned zooplankton into the most dynamic compartment in the model in terms of nitrogen flow and simultaneously made it become the central player for regenerated production (Fig. 4.10). In fact, while the phytoplankton loss to detritus by natural mortality halved, the zooplankton grazing on phytoplankton trebled and so did its excretion of ammonia. Consequently, regenerated production (Table 4.3) is twice that of Control run A for the same annual net primary production, which is 580 mMol N/m^2/year (Table 4.1). This caused the annual f-ratio to drop from 0.71 to 0.55.

The drawback of this approach is that the biomass of zooplankton increased substantially during its seasonal cycle and is now even higher than the zooplankton levels of Control run A by at least a factor of 2 (Fig. 4.3).

Observed data for areal and volumetric primary production over the annual cycle are shown in figures 4.12 a,b.

Figure 4.14 shows DOC measurements in profiles of the upper 260 m for the four seasons of the year in Bermuda.

4.4 Tables

Control Run	Primary production	Gross Bacterial production	Net Bacterial production
A	567.6	251.7	66.5
B	578.2	255.3	104.9

Table 4.1 Estimates of annual totals of phytoplankton primary production, gross bacterial production and net bacterial production in mmol N/m2/yr. Values are calculated for Control Runs A and B. The sinking speed of detritus is 10m/day.

Control Run	DON uptake	Ammonium uptake	Ammonium excretion
A	157.9	93.8	185.2
B	159.6	95.7	150.4

Table 4.2 Estimates of annual totals of DON and Ammonium uptake compared to Ammonium excretion by the model bacteria in mmol N/m2/year. Values are calculated for Control Runs A and B.

Control Run	Regenerated Production	Ammonium excretion by Zooplankton	New Production
A	162.8	77.3	404.8
B	259.4	232.3	318.7

Table 4.3 Estimates of annual totals of Regenerated Production, New Production and Ammonium excretion by zooplankton in mmol N/m2/year. Values are calculated for Control Runs A and B.

4.5 Figures

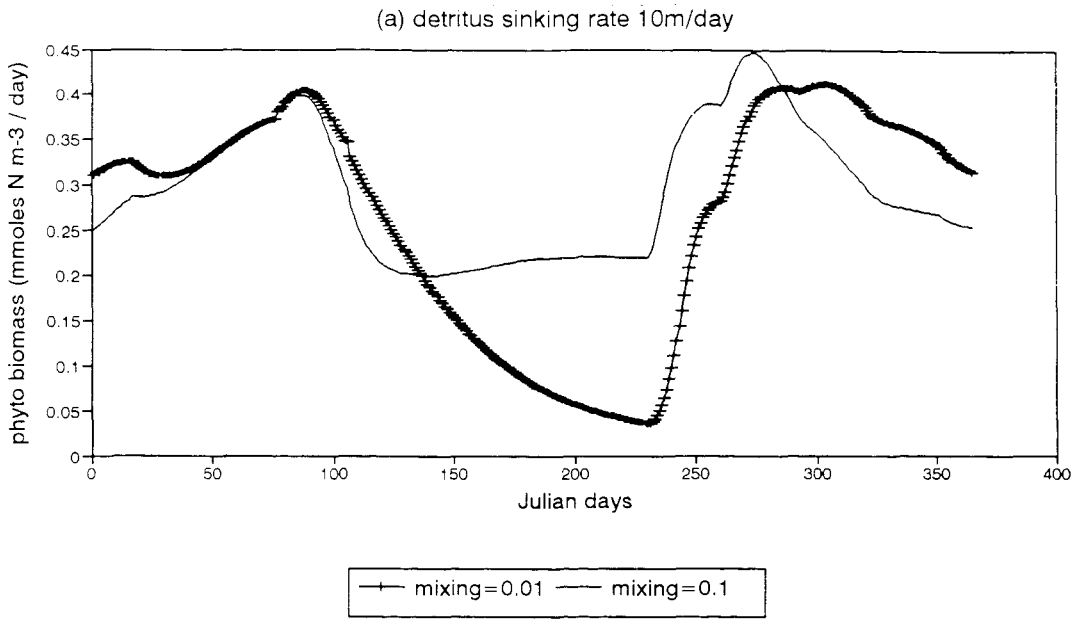

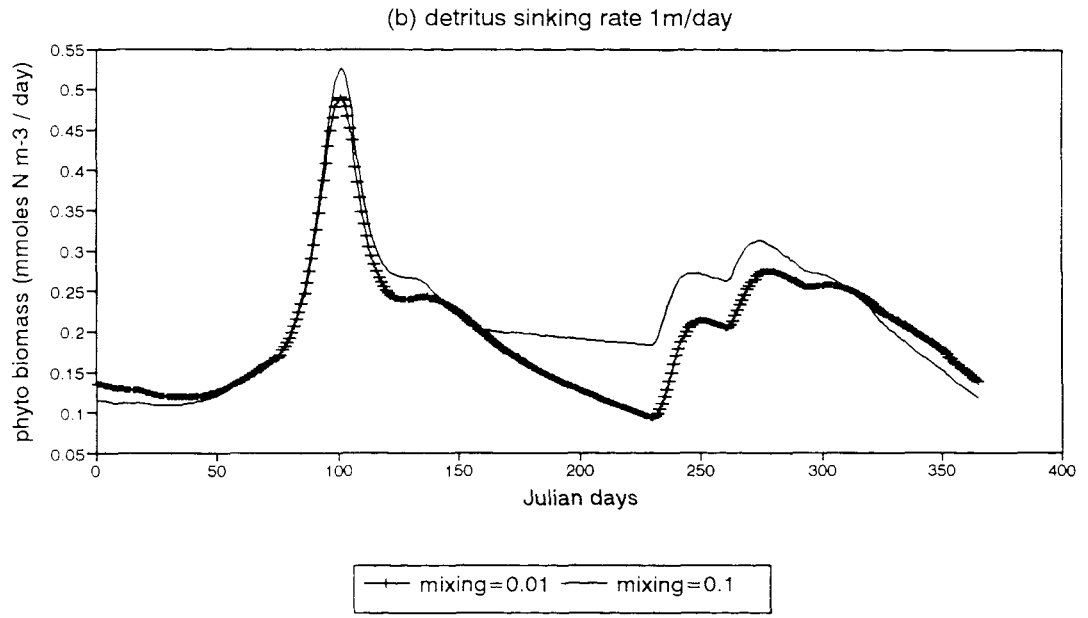

Figure 4.1 Annual cycles of phytoplankton concentration (in mMol N/m^3) plotted against Julian day, for a mixing rate of 0.1m/day (solid line) and 0.01m/day (plus), and a detritus sinking rate of (a) 10m/day and (b) 1m/day, calculated by Fasham's model A.

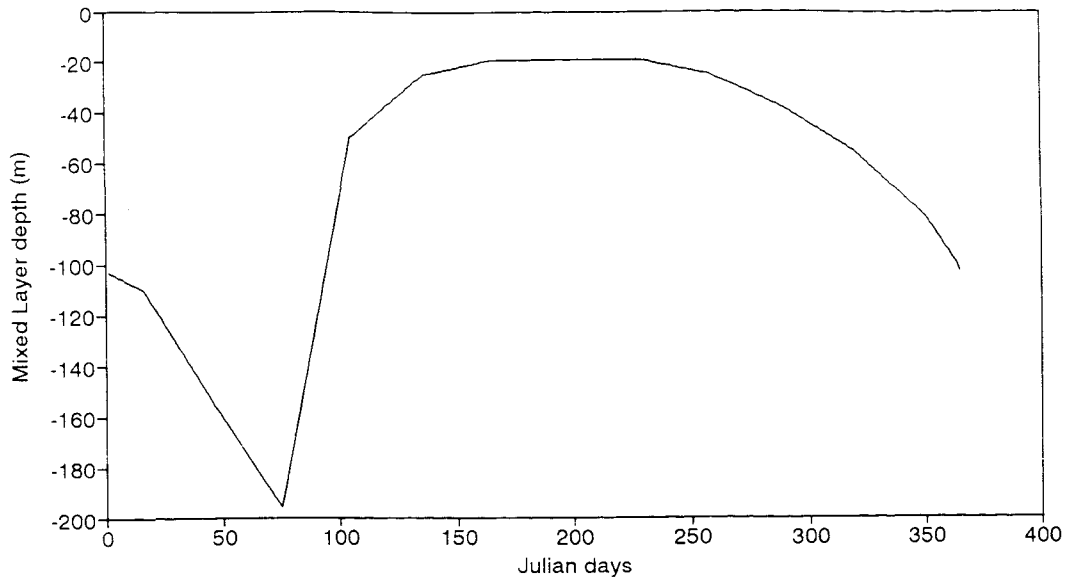

Figure 4.2 Annual cycle of mixed-layer depth in metres from control run A and B, plotted against time (in Julian days).

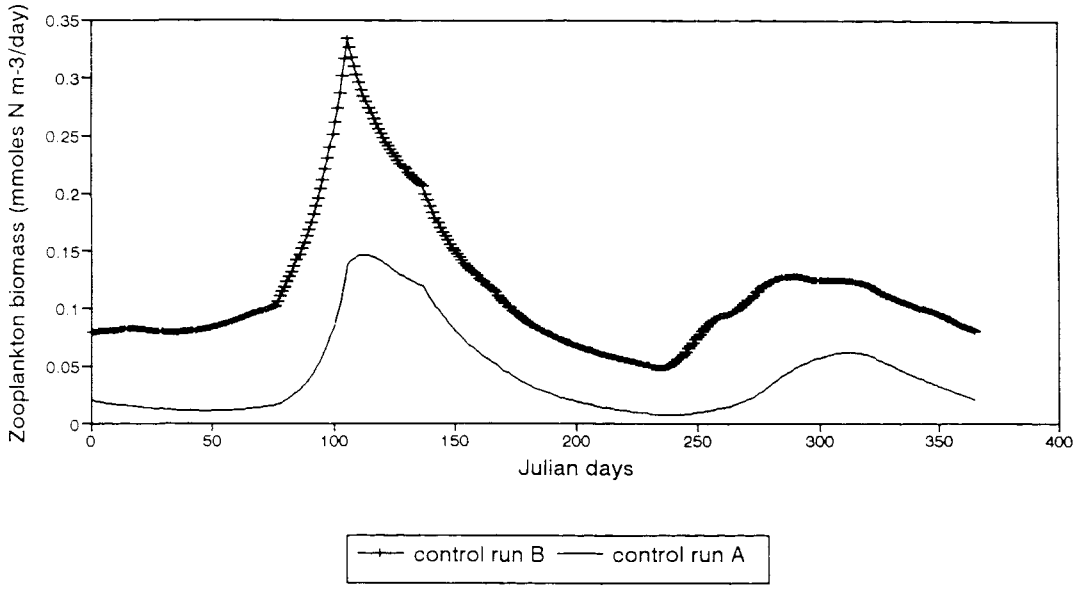

Figure 4.3 Annual cycles of zooplankton concentration (in mMol N/m^3) plotted against Julian day, for control run A (solid line) and control run B (plus) with a detritus sinking rate of 10m/day.

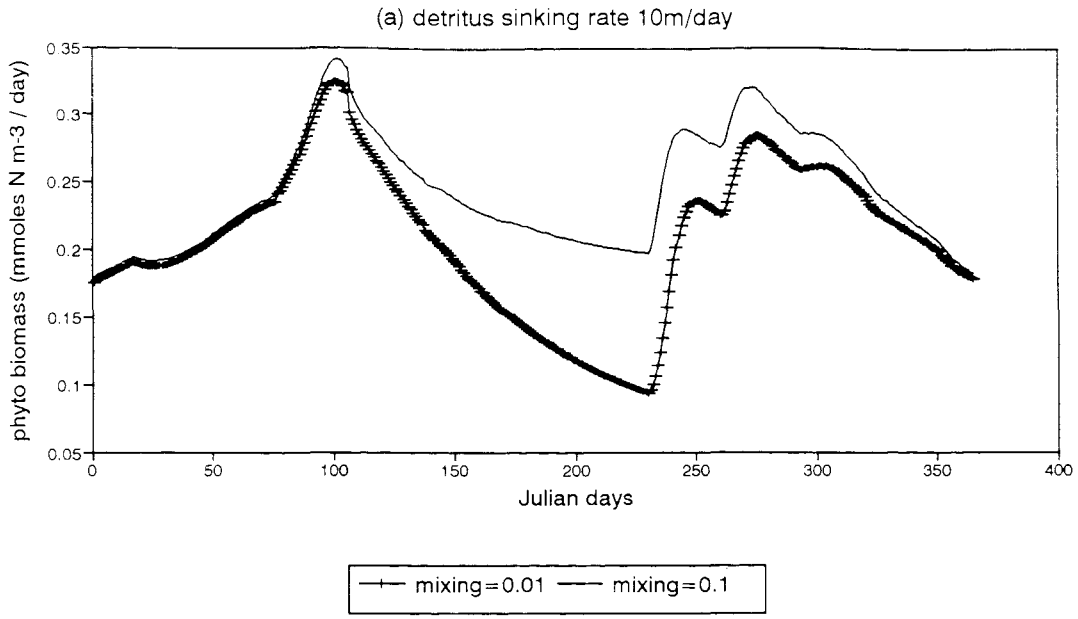

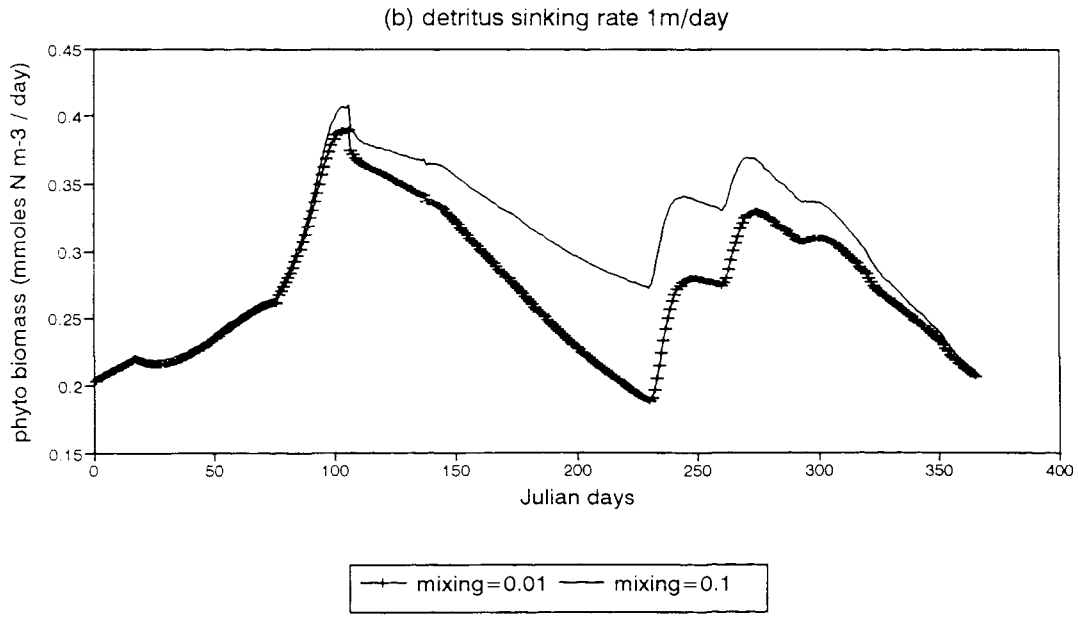

Figure 4.4 Annual cycles of phytoplankton concentration (in mMol N/m^3) plotted against Julian day, for a mixing rate of 0.1m/day (solid line) and 0.01m/day (plus), and a detritus sinking rate of (a) 10m/day and (b) 1m/day, calculated by Fasham's model B.

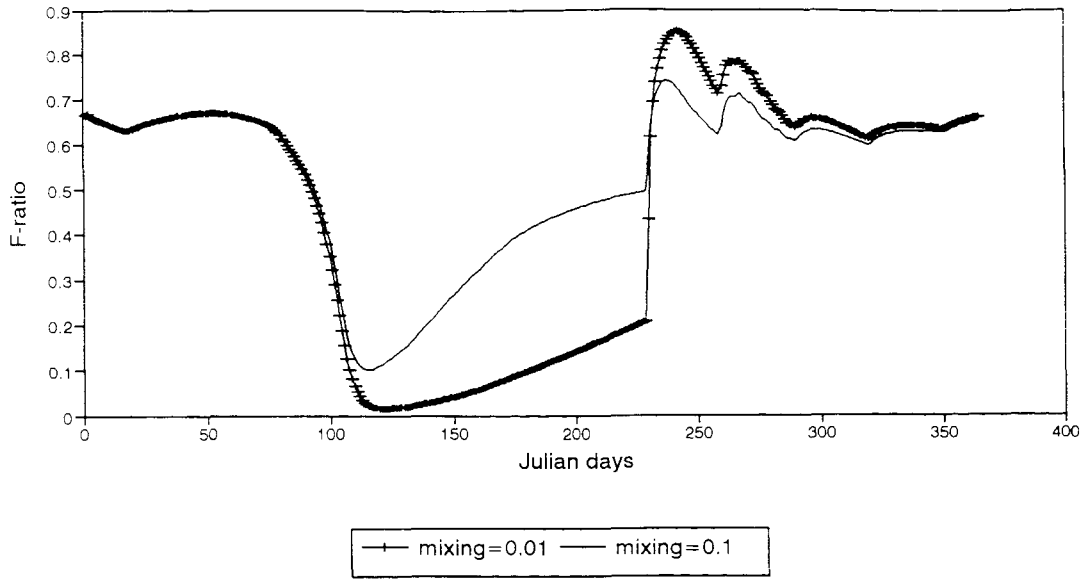

Figure 4.5 Annual cycles of the f-ratios (the ratio of new to total primary production), for a mixing rate of 0.1m/day (solid line) and 0.01m/day (plus), and a detritus sinking rate of 10m/day, calculated by Fasham's model B.

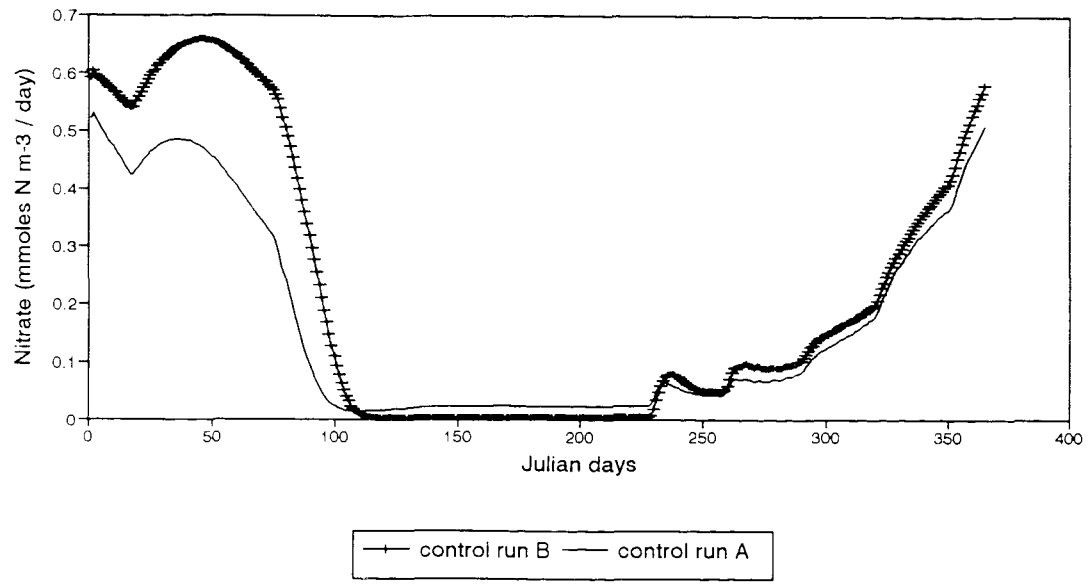

Figure 4.6 Annual cycles of nitrate concentration (in mMol N/m^3) plotted against Julian day, for control run A (solid line) and control run B (plus) with a detritus sinking rate of 10m/day.

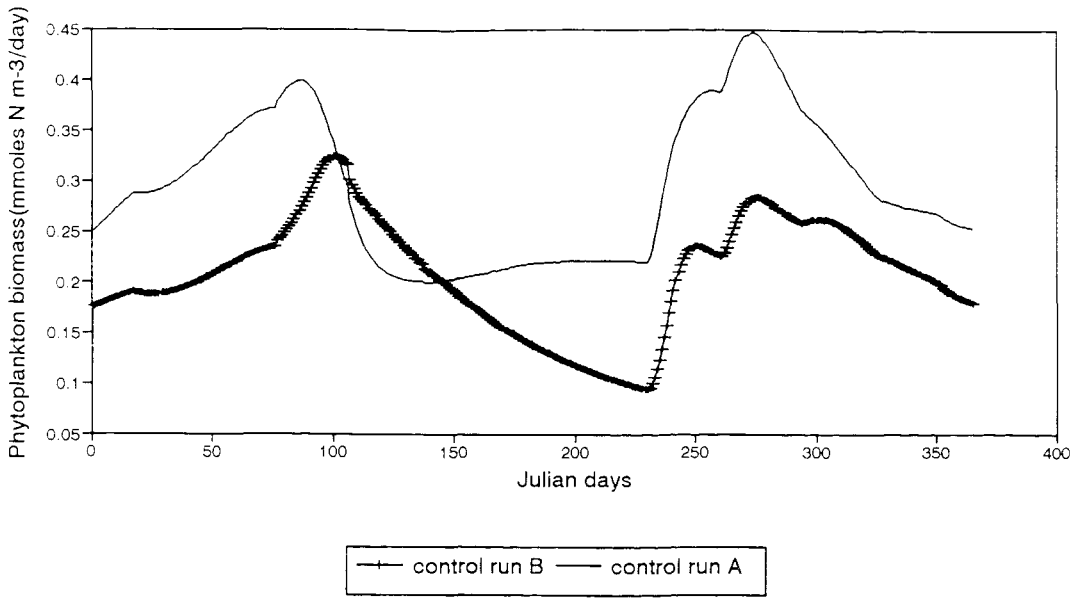

Figure 4.7 Annual cycles of phytoplankton concentration (in mMol N/m^3) plotted against Julian day, for control run A (solid line) and control run B (plus) with a detritus sinking rate of 10m/day.

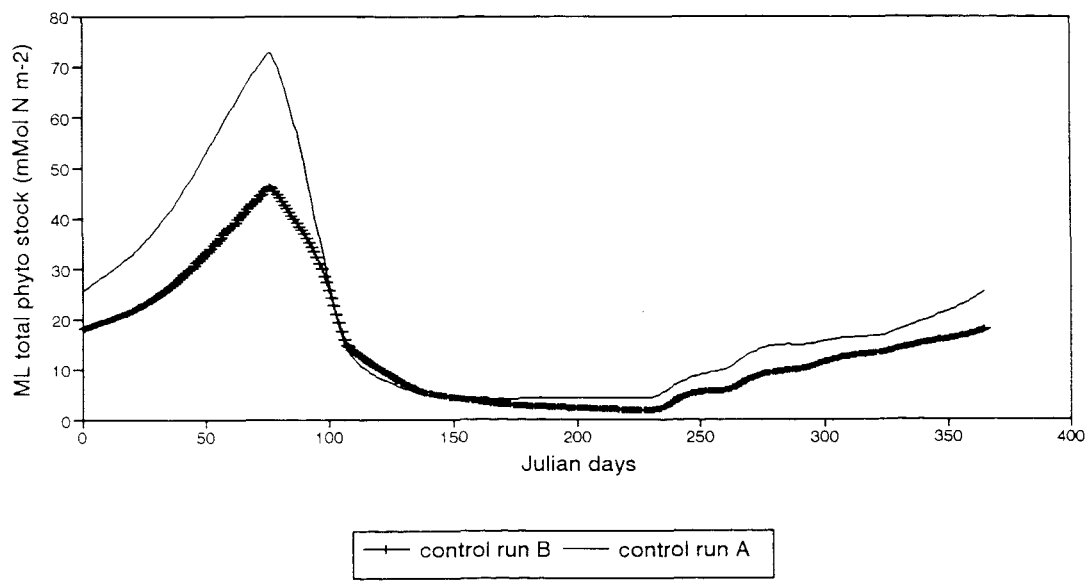

Figure 4.8 Annual cycles of the total biomass stock of phytoplankton in the mixed layer (in mMol N/m^2) plotted against Julian day, for control run A (solid line) and control run B (plus), with a detritus sinking rate of 10m/day.

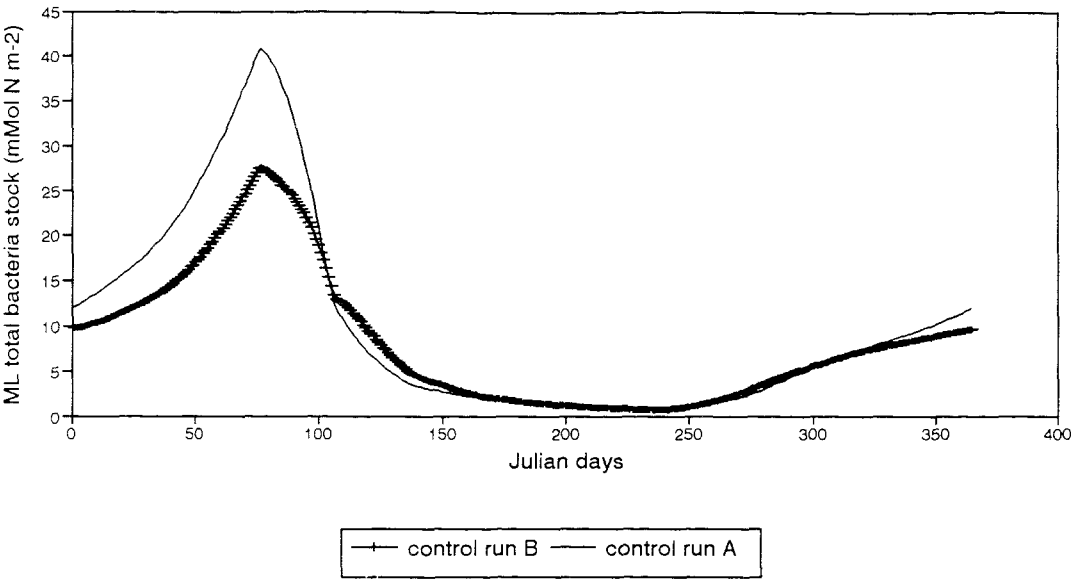

Figure 4.9 Annual cycles of the total biomass stock of bacteria in the mixed layer (in mMol N/m^2) plotted against Julian day, for control run A (solid line) and control run B (plus), with a detritus sinking rate of 10m/day.

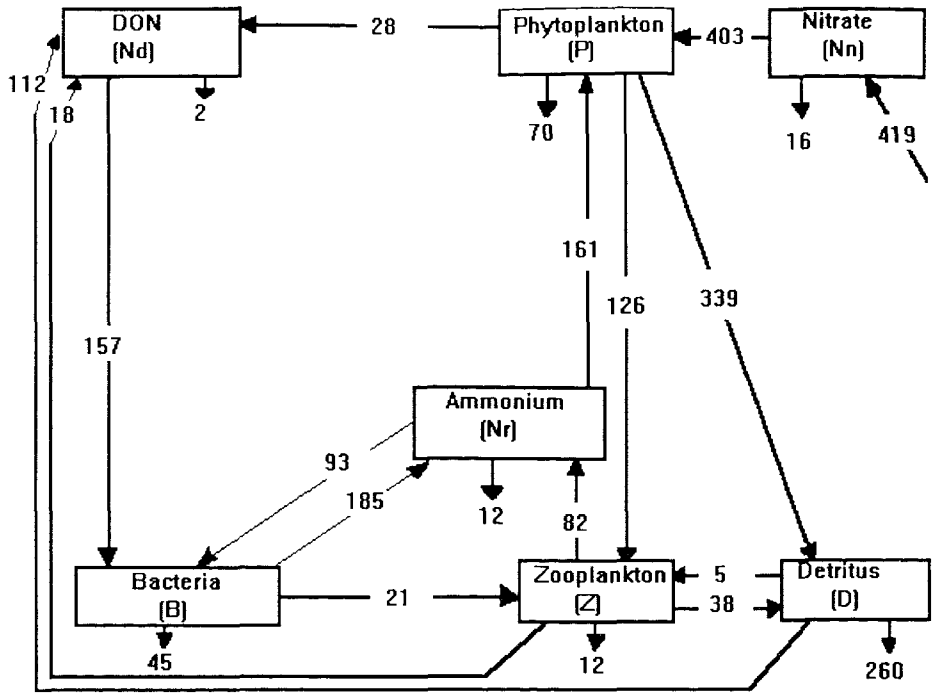

a Control run A sinking rate=10m mixing rate=0.1m/day

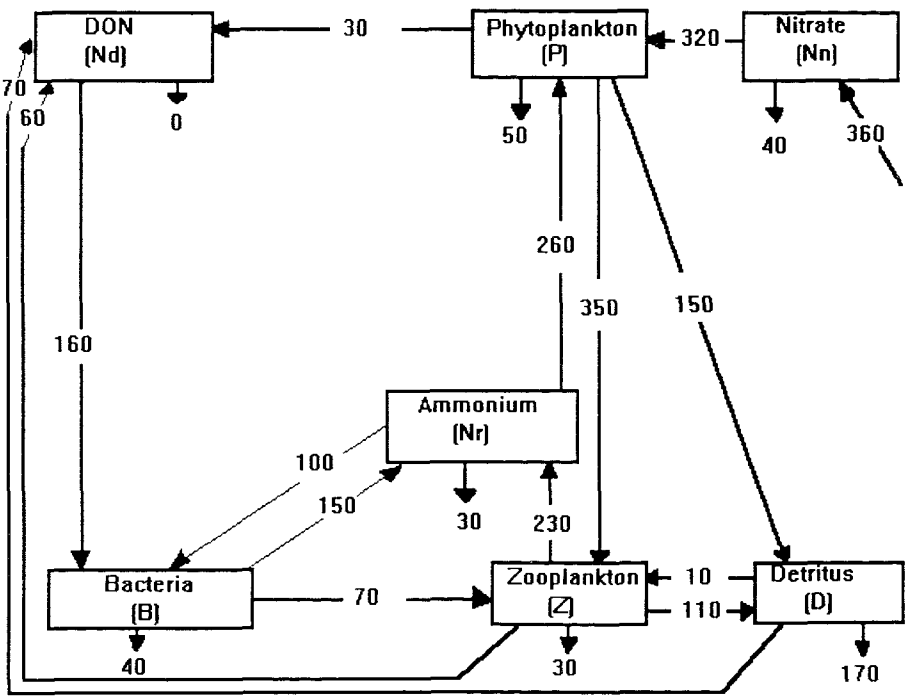

b Control run B sinking rate=10m mixing rate=0.1m/day

Figure 4.10 Annual inter-compartment flows of nitrogen for (a) control run A and (b) control run B.

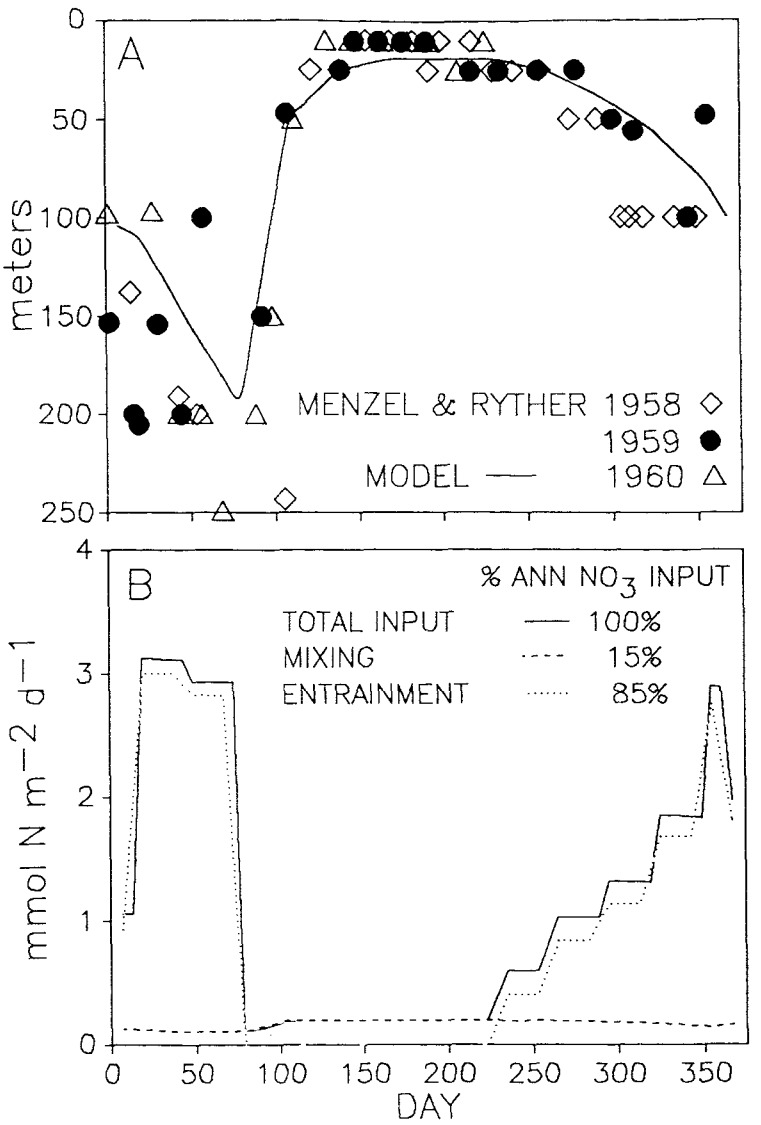

Figure 4.11 Annual cycles of (a) mixed layer depth and (b) NO_3 input for the model, with observed mixed layer depths recalculated from the data of Menzel and Ryther (Bermuda Biological Station, 1960). Taken from Fasham et al. 1990.

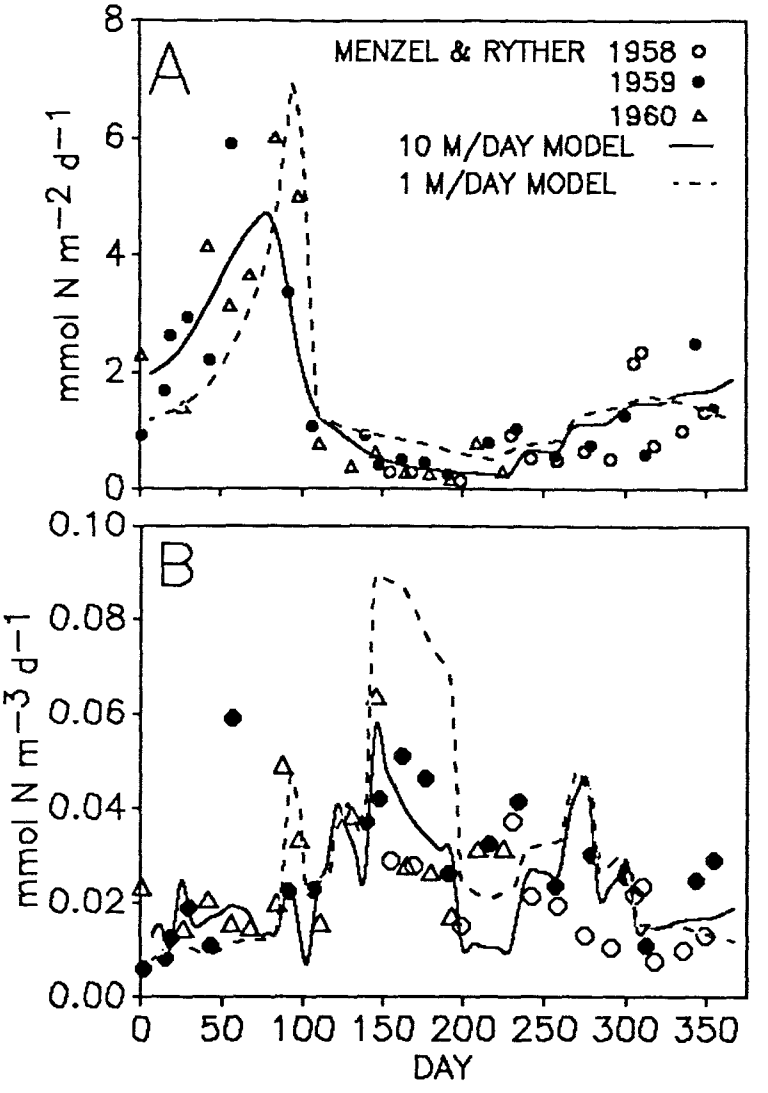

Figure 4.12 Comparison of observed data from Menzel and Ryther (Bermuda Biological Station, 1960) with model output for (a) areal and (b) volumetric primary production (NPP) over the annual cycle (lines and and symbols as in (a)). The Bermuda data were recalculated to reflect mixed layer values only. Taken from Fasham et al. 1990.

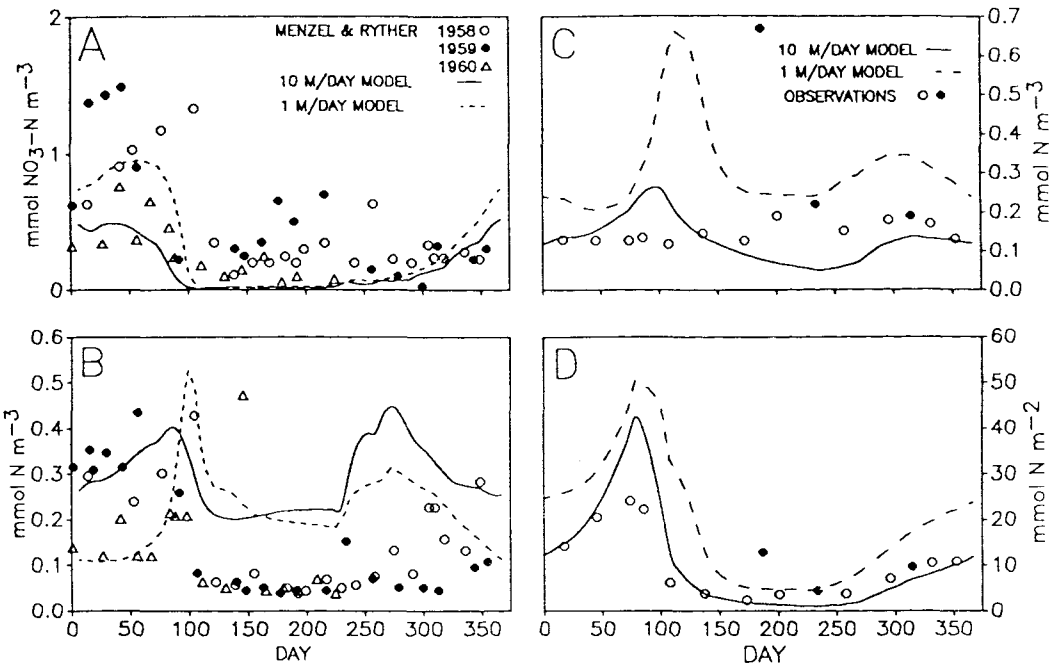

Figure 4.13 Comparison of observed and modelled (A) nitrate (B) phytoplankton nitrogen biomass m^{-3} (recalculated from raw data on chlorophyll) for Model A output. Comparison of observed and modelled bacterial biomass in (C) m^{-3} and (D) m^{-2} Open circles: data collected by Bermuda Biological Station. Solid circles: data from Fuhrman et al. (1989). Data from vertical profiles were averaged over the model mixed layer depth for volumetric data, then multiplied by that depth for areal estimates. (B) and (D) symbols and lines as in (A) and (C), respectively. Taken from Fasham et al. 1990.

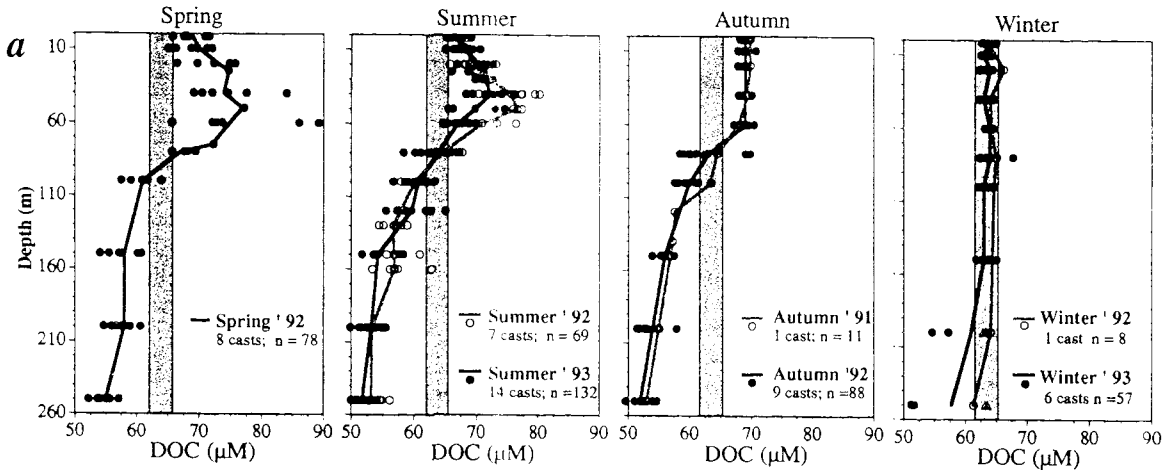

Figure 4.14 Filled and empty circles are DOC measurements made in the western Sargasso Sea in the vicinity of BATS site and Hydrostation S. The lines represent the average profile per season. The general range of DOC during winter mixing is shown by a grey highlighted bar (taken from Carlson et al. 1994).

Chapter 5.

Results I - Epidemics of Phytoplankton viruses.

5.1 Introduction.

Several numerical simulations of the model have been executed with the purpose of investigating the dynamics of viral epidemics in a marine ecosystem and its repercussion in the biological production. This chapter will analyze the results of the dynamics of phytoplankton viruses on five versions of the model, version 1, version 2, version 3, version 4 and version 5, based upon two platforms, model A (Fasham et al., 1990) and model B (Fasham, 1993), respectively. Such results are then to be compared with control runs A and B to unveil how the interaction of the physical and biological processes determines the seasonal behaviour of viral epidemics. The first aim of this chapter is to develop a general relationship between increases in contact rate and the resulting temporal scale of phytoplankton and viral biomass. The second aim is to investigate the dynamics between viral lysis and primary production by varying the parameters most critical to describing the characteristics of the virus epidemic.

The model strategy is presented in section 5.2 (simulation characteristics i.e. initial conditions and model parameters for all runs are presented in tables I and II in appendix A). The response of model version 1 to a wide range of epidemic levels is investigated in section 5.3. This section examines the effects of contact rate increase on the biomass of the biological compartments, with emphasis on phytoplankton, and compares model results with data from Bermuda. Section 5.4 discusses the need for changes in the natural mortality rate of phytoplankton. The influence of new zooplankton dynamics on the course of viral epidemics is presented in section 5.5, thereby introducing version 2 of the model. The control of phytoplankton photosynthesis and

population growth is analyzed in section 5.6. This section investigates viral led changes in limiting factors that modify the growth rate of phytoplankton under bloom conditions, the contribution of viral epidemics to the net change in phytoplankton biomass, how viral lysis compares to zooplankton grazing in the diversion of primary production, and how these translate in terms of population growth rate for viruses and zooplankton. Section 5.7 questions the need for a change in the mixed-layer mixing rate. The parameters most critical to describing the characteristics of the viral epidemic are introduced in sections 5.8 to 5.12. The regulation of viral efficiency in the assimilation of host biomass is presented in the first of these sections. Section 5.9 investigates the impact of virus inactivation rates on the behaviour of the epidemic, thereby introducing version 3 of the model. Section 5.10 justifies the use of tests of maximum daily flow into viral lysis to identify the most interesting contact rates. Changes in the decay rate of inactivated viruses and their repercussion on overall production rates of the version 4 model are examined in detail in section 5.11. The response of the epidemic to seasonally varying contact rates is outlined in section 5.12, thereby introducing version 5 of the model. The chapter ends with a summary and discussion of the conclusions reached from these numerical simulations.

5.2 Solution procedure - Model strategy

The timestep of the model is two hours and the interval between simulation plots is one day. The initial values are given in appendix A. All model runs cover a period of five years and an equilibrium cycle is usually reached on the 4th year. On a IBM PC 386 notebook a run of this length takes 30 minutes of cpu time. Julian day numbers and the corresponding dates are given in appendix B.

The selection of contact rates representative of minimum and maximum production epidemics was initially based on tests

of maximum phytoplankton and virus biomass though later the maximum daily flow of viral lysis was used instead (see § 5.10).

In the model runs the parameters mentioned in 5.1 were successive and independently varied because such a partial sensitivity analysis helps understanding the complexity of the ecosystem model. The contribution of each process and its importance on the ensemble are revealed in this way: it has been noticed that the model is extremely sensitive to the chosen value of the contact rate.

A summary of experimental characteristics for the simulation runs of versions 1 to 5 of the model is presented in § 5.16 - § 5.20. These include the contact rate, the virus assimilation efficiency, the inactivation rate, the decay time of inactivated viruses, the detritus sinking speed, the specific natural mortality rate of phytoplankton and the cross-thermocline mixing rate for each figure presented in this chapter.

Supporting tables and figures in this chapter: version 1 - Table 5.1 and Figures 5.2 to 5.15, version 2 - Figures 5.16 to 5.37, version 3 - Figures 5.38 to 5.41, version 4 - Tables 5.2 to 5.5 and Figures 5.42 to 5.53, version 5 - Tables 5.6 and 5.7 and Figures 5.54 to 5.59.

5.3 Introducing version 1 - Testing the contact rate

The simplest scenario for an epidemics model is basically Fasham's model A (1990) onto which a compartment of phytoplankton viruses is added (Fig. 5.1). This is referred to as version 1 of the model.

A range of values from 0 to 2 have been tested in version 1. Figure 5.2.a,b depicts the annual production of viruses for increasing values of the contact rate ($\beta 8$). When $\beta 8$ is set to 0 the system produces the same results as a

Control run A. With values less than 0.03102 the infection fails to sustain itself in the population and the epidemics will die out in less than 5 years, removing all the viruses from the system. For the maximum annual production of viruses a contact rate of 0.06 is required. Any further increment in its value will yield a lower production.

5.3.1 Effects of $\beta 8$ increase on biomass - Low contact rates

It will be shown that increases in the contact rate value result in a shortening of the spring bloom time span plus a lowering of the summer concentration levels of phytoplankton as well as a drastic reduction of the autumn bloom.

Control run A was only partially successful in fitting the phytoplankton, bacteria and zooplankton observations for Bermuda Station "S". Thus what happens when viruses are explicitly modelled in this pelagic food web?

The minimum contact rate to sustain the viral epidemic in the phytoplankton population is reached when $\beta 8$ is 0.03102 (see Fig. 5.3.a). At first sight the results seem identical to control run A, however, there are some subtle differences. The peak biomasses of both phytoplankton and bacteria (Fig. 5.3.b) are slightly lower during the spring and autumn blooms. After the end of the spring bloom the biomass of phytoplankton adopts a different trajectory to control run A and maintains a slight decreasing trend during all summer reaching its lowest concentration at 0.18 mMol N m^{-3} at the beginning of the autumn bloom. Nonetheless, the most relevant difference is in the zooplankton cycle (Fig. 5.3.c) whose stocks are clearly lower than in control run A and are more in accordance with the observed data for Bermuda Station "S" of 0.009-0.073 mMol N m^{-3} with a mean of 0.018 mMol N m^{-3} obtained by Deevey (1971). However, our main interest is the virus cycle. The Spring phytoplankton bloom is the main event

for the generation of the virus population (Fig. 5.3.d). The biomass of phytoplankton viruses has a sharp increase from day 75 onwards reflecting the onset of stratification of the mixed layer which stops the dilution effect on viruses caused by its previous deepening. When stratification is almost complete by the end of the phytoplankton spring bloom the virus stocks stabilize showing only a very slight increasing trend during the summer period. This trend is negatively correlated with the decreasing phytoplankton biomass. The maximum concentration of viruses is reached at 0.29 mMol N m^{-3} on day 225 just before the deepening of the mixed layer. The deepening of the mixed layer causes a decrease in the concentration of viruses due to dilution of the virus stock.

The behaviour of the system alternated between short and long timescale of adjustment as $\beta 8$ increased. It was noticed that for some intermediate values of the contact rate in-between the minimum and maximum production epidemics the system could not reach an equilibrium cycle within the five year run time as the biomass of viruses was still increasing for some unknown reason. Therefore only those simulations that reach equilibrium during this time were described.

With $\beta 8$ set to 0.045 this epidemic results in a slightly lower phytoplankton biomass at the height of a strong spring bloom (0.35 mMol N m^{-3}), in a slightly shorter time span of the bloom itself (90 days) and on a lower phytoplankton population post-bloom. Over the Summer the phytoplankton biomass remains at a nearly constant 0.12 mMol N m^{-3} and throughout this period the virus population stabilizes at 0.8 mMol N m^{-3} (Fig. 5.3.d). When the Autumn bloom comes the phytoplankton peak value is 30% lower than in control run A at 0.32 mMol N m^{-3} and its decline smoother.

The epidemic yielding the maximum annual viral lysis is reached when $\beta 8$ is increased to 0.06. This simulation produced an even stronger spring bloom between late-March and late-April with a maximum concentration of 0.42 mMol N m^{-3}

(Fig. 5.3.a). There was a sharp decline in the phytoplankton biomass after day 108 and the summer levels were maintained below 0.1 mMol N m^{-3}. The ensuing autumn bloom is smaller with a maximum concentration of 0.26 mMol N m^{-3}. The biomass of viruses reach their maximum concentration at the end of the spring bloom and maintain their level at 1.1 mMol N m^{-3} during the summer (Fig. 5.3.d). The deepening of the mixed layer forces the concentration of viruses to decrease despite a simultaneous phytoplankton autumn bloom whose growth rate is not enough to counterbalance the dilution effect on the viruses. The entrainment of deep water into the system is beneficial to the phytoplankton population since it disperses all cells and doing so also minimises their chance of meeting a virus particle. Therefore, it can be concluded that for low contact rates changes in the mixed layer depth are the external driving force regulating the seasonal concentration of viruses. Notice that on a purely visual assessment this simulation has a much improved fit to the observed phytoplankton data at Bermuda Station "S" (Fig. 4.13.b).

5.3.2 Effect of $\beta 8$ increase on biomass - High contact rates

Figure 5.2.a) shows that any further increase in the value of $\beta 8$ past 0.06 will result in a decrease of the annual production of viruses. However, the investigation of high contact rates may give us an insight on how viruses could control the onset of extremely fast growing blooms, their collapse and their regular or irregular timing. This information may have relevance for seasonal succession of phytoplankton species and coccolithophorid blooms.

A further increase in $\beta 8$ to 0.4 and the phytoplankton bloom starts with a two month delay in relation to the minimum epidemic reaching a much higher peak (1 mMol N m^{-3}) but a much shorter time span (20 days) (Fig. 5.4.a). Thereafter the phytoplankton population goes nearly extinct with a biomass of 2.8E-8 mMol N m^{-3} on day 187. The virus

biomass reaches 1.6 mMol N m^{-3} and decreases steeply during the Summer to a value of 0.6 mMol N m^{-3} until it is pumped up again to 1 mMol N m^{-3} due to a small Autumn phytoplankton bloom. This is followed again by a sharp decline after the end of the phytoplankton bloom, which again gets close to extinction. In simulations with high contact rates diffusive mixing plays an important role in the summer loss of viruses.

5.3.2.1 Collapse of the bloom

The viruses take hold of the phytoplankton bloom when its senescence starts. Figure 5.4.b) depicts the annual cycle of phytoplankton versus virus biomass for the simulation outlined above. It shows that the increase in the concentration of viruses is negligible during the first sixty days of the spring bloom. However, once the peak of the phytoplankton bloom is reached then the virus concentration starts increasing markedly. For example, between days 133-134 while the phytoplankton is close to 1 mMol N m^{-3} the virus biomass jumps from 0.5 to 0.7 mMol N m^{-3} Nonetheless, it is during the collapse of the phytoplankton bloom which is precipitated by the increase in the concentration of viruses that their presence begins to be felt. Thus, three days after the peak of the spring bloom the biomass of viruses has increased to 1.4 mMol N m^{-3} while the phytoplankton biomass has declined to 0.3 mMol N m^{-3}. From day 137 the build-up on the virus concentration slows-down and it takes 3 to 5 more days to reach the maximum concentration of 1.6 mMol N m^{-3}.

5.3.2.2 Timing of blooms

There is a change in the behaviour of the system occurring when the contact rate is gradually increased up to two. First the Autumn bloom will enter a two year cycle when $\beta 8=0.5$ then it will be suppressed when $\beta 8= 0.6$ (not shown). Meanwhile there is a regular shifting forward on the timing of the spring bloom itself whose peak biomass originally on day 87 is gradually displaced into late summer (Fig. 5.5.a).

When $\beta 8$ reaches 0.8 this single annual bloom takes place on day 198 and it keeps shifting towards day 224 which is reached when $\beta 8$ is 1.1. Finally, with increasing $\beta 8$ values the bloom begins receding into the first half of the year and blooms on day 109 when $\beta 8$ is 1.6. Between $\beta 8$=1.8 and 1.9 there is a considerable inter annual variation on the timing of the bloom such that a sole irregular annual bloom can occur anytime between day 100 and 350. Further increasing $\beta 8$ to 2.0 and over results in the system entering a steady domain where a series of solutions with two and three year cycles will occur for the Spring bloom, even though the physical forcing has an annual cycle. All these results stem from the non-linearities of the biological equations. The sequence of regular-random-regular patterns that were produced draws a parallel with the period-doubling sequence to chaotic behaviour under increasing contact rate values found on the SEIR equations (Pool, 1989; Olsen & Schaffer, 1990, Rand & Wilson, 1991).

5.3.2.3 Peak concentration of phytoplankton and virus

In simulations with $\beta 8 \geq 0.4$ there is a sudden growth of phytoplankton blooms that spring up from negligible biomass to blooms of 0.7 mMol N m^{-3} and over in just 2 or 3 days and then collapse equally fast. Provided these contact rates and the parameterisation being realistic this result may be relevant to explain short lived blooms sometimes observed in the ocean. Most of them would pass undetected though they may be spotted by satellite.

Figures 5.6.a) and 5.6.b) depict the Spring and Autumn maximum biomass of phytoplankton and virus versus the contact rate. These results show a drastic rise in both the phytoplankton and virus biomass during the spring bloom between contact rates 0 and 0.6. The maximum phytoplankton biomass is reached in spring at 1.2 mMol N m^{-3} when $\beta 8$ is 0.6. Likewise, the maximum viral biomass reaches over 1.6

mMol N m^{-3} for $\beta 8$ values between 0.4 and 0.9. Between contact rates 0.8 and 1.2 there is a gradual decrease in the maximum biomass of phytoplankton which is now reached in the second half of the year and corresponds to a single annual bloom. From $\beta 8$ of 1.3 onwards the bloom shows up again in the first half of the year but the biomass of phytoplankton continues its decreasing trend being the lowest concentration 0.18 mMol N m^{-3} reached when $\beta 8$ is 1.5. However, the maximum biomass of phytoplankton increases gradually between contact rates 1.5 and 2.0 reaching 1.1 mMol N m^{-3} for the latter value. Nonetheless, the recurrence of the spring bloom will meanwhile change to a two year cycle. It can be concluded that for contact rates 0.09 - 2.1 the maximum concentration of phytoplankton is well over 0.6 mMol N m^{-3} with the exceptions $\beta 8$= 1.1 -1.5.

From figure 5.6.b) one can also conclude that for contact rates 0.08 - 2.1 the maximum concentration of viruses is always over 1.2 mMol N m^{-3} with the only exceptions $\beta 8$= 1.4 and 1.5.

5.3.3 Comparison of model results with data from Bermuda Station "S"

Two contact rates were selected for this comparison: $\beta 8$ 0.03102 which is as previously shown the minimum $\beta 8$ to keep the viral epidemic alive in the phytoplankton population and $\beta 8$ 0.06 which is the one yielding the maximum annual production of viruses.

Figure 5.7 shows the simulated seasonal cycles of vertically integrated (areal) mixed layer Net Primary Production (NPP), for two selected $\beta 8$ values, compared with control run A 10m/day run. Both $\beta 8$ simulations give a slightly better fit to the observed data than does control run A's simulation be it spring, summer or autumn (Fig. 4.12.a).

However, the β8 0.06 simulation bears some resemblance to Model A's 1m/day run (Quental-Mendes, 1992), especially during the early part of the year although that one reached a much higher NPP of 7 mMol N m^{-2} on day 100.

The modelled volumetric primary production is similar to the data published by Fasham et al. (1990) only during autumn and maybe late spring but is disparately different during summer.

Figure 5.8 shows a comparison of the seasonal cycle of nitrate for the 3 simulations. The β8 0.06 simulation gives the best fit to the data in the early part of the year just like Model A's 1m/day did. However, none of the simulations reproduced the observed high summer nitrate values. Fasham et al. (1990) attribute the discrepancy between model results and nitrate observations to deficient techniques for measuring low concentrations of this nutrient in the late fifties. Moreover, they point out that more recent data obtained by Altabet (1989) suggest that summer nitrate levels are usually less than 0.1 mMol m^{-3}, which would support the model results.

The most striking result of this exercise, lies in the comparison of the simulated seasonal cycles of phytoplankton biomass. The β8 0.03102 simulation gave an overall lower concentration of phytoplankton during the build-up phase of the spring and autumn blooms in comparison to Control run A's 10m/day simulation. However, both blooms lasted longer. The spring bloom was extended for 10 more days and the autumn bloom was extended for 22 more days. Although the summer levels were lower than control run A this simulation still overestimated the phytoplankton biomass in the summer and autumn twofold.

Nonetheless, a much improved simulation was to be obtained with β8 0.06. This simulation yielded a classic spring bloom that reached a maximum concentration of 0.42

mMol N m^{-3} and once again its shape was reminiscent of Model A's 1m/day simulation (Fig. 5.9). Moreover, in contrast to Model A's 1m/day and Control run A 10m/day simulations this simulation of the viral epidemic gave a perfect fit to the observed low levels of phytoplankton biomass in the summer and autumn. Other modellers have achieved this by altering the carbon/chlorophyll ratio (Fasham, 1995, personal communication).

All the previous simulations would have produced a lower summer concentration of phytoplankton had a cross-thermocline mixing rate of 0.01 m/day been used instead of the standard 0.1 m/day (Fig. 5.10 a,b).

There are no significant improvements in the seasonal cycle of bacteria in these simulations. The concentrations of bacteria are lower than control run A (Fig. 5.3.b) but they do not fit the observed data which show an almost level concentration all year round. However, Ducklow et al. (1993) have reported that time-series observations show that bacteria concentrations increase up to fivefold in response to phytoplankton blooms in other areas of the Atlantic Ocean. Nonetheless, the total mixed layer (areal) biomass stock of bacteria (Fig. 5.11) can be reduced in spring from control run A levels of 40 mMol N m^{-2} to the 15 mMol N m^{-2} of the β8 0.06 simulation. This suggests that the 25 mMol N m^{-2} of the observation data is reachable with an intermediate value for the contact rate.

The β8 0.03102 simulation produced a more reasonable seasonal cycle of zooplankton than the control run A simulation did. However, any further increase in the contact rate causes the extinction of zooplankton. Such an extreme sensitivity to increased levels of competition for phytoplankton food confirms that the ability of zooplankton to switch between resources is being hampered due to high losses in zooplankton mortality outside the bloom period (Fasham, 1993).

The field of marine viruses is still in its infancy and as yet there are no observations available on their seasonal cycle in Bermuda. However, it is known that in many different places the highest observed number of viruses is usually 10^{11} l^{-1} one week after the bloom (Fuhrman, 1992). This is equivalent to 0.7 mMol N m^{-3} assuming 0.26fg C per virus (Fuhrman, 1992) and a C/N ratio of 3. That concentration is approximately the same as the model shows for this period of the year in the β8 0.06 simulation (Fig. 5.3.d). Nonetheless, as there are not yet time-series on viruses covering the whole year we do not know if they would indeed accumulate till 1 mMol N m^{-3} as shown in the model results.

One would predict that DOM analysis performed during summer will show a lower C/N ratio than during other periods of the year reflecting the increased proteinaceous nature of the living biomass present at the time. The biomass of viruses and its mixed layer stocks are always higher than the phytoplankton biomass during summer. They are also higher that those of bacteria with the exception of the run for the epidemics minimum where bacteria stocks were slightly higher between day 75 and 108 (Figures 5.12 a,b).

In order to fully understand the dynamics of the model it is important to analyze the annual inter-compartment flows of nitrogen. Figures 5.13 a,b) and figure 4.10.a) show the flow networks for the three simulations.

The total annual net primary production for the control run A, β8 0.03102 and β8 0.06 simulations were 580, 495 and 380 mMol N m^{-2} y^{-1}, respectively. The corresponding f-ratios (Fig. 5.14) were 0.71, 0.82 and 0.91, respectively.

The flow diagrams show that the only significant difference between control run A and the β8 0.03102 simulation is in the inputs and outputs of the zooplankton compartment. The viral epidemics on phytoplankton has not affected new production but it has caused the direct flow of

nitrogen from phytoplankton into zooplankton (grazing) to decrease by a factor of 6. The zooplankton could not compensate this loss with its alternative food sources, bacteria and detritus, as these flows too show a reduction by a factor of 10. Consequently, the ammonia excretion by zooplankton decreased by a factor of 6 and this then became reflected in a halving of regenerated production.

The contact rate that produces the maximum output of lysed material is only twice the minimum contact rate necessary to keep the viral infection in the system. Thus, the $\beta 8$ 0.03102 simulation yielded 44.6 mMol N m^{-2} y^{-1} of viruses which was 9% of the annual net primary production and represented only 11.2% of the total mortality of phytoplankton. The $\beta 8$ 0.06 simulation yielded 148 mMol N m^{-2} y^{-1} of viruses which was 38.9% of the ANPP and represented 48.1% of the total mortality of phytoplankton.

The increase in the contact rate value from its epidemics minimum to that required for the maximum annual output of viruses resulted not only on a 23% decline on primary production but also on a halving of most flows in the food web model. Obvious exceptions were the phytoplankton into virus flow which has trebled, plus all those related to zooplankton which stopped due to its extinction. The latter caused regenerated production to decline by a factor of 3. Notice that the 14% decrease in new production although light is the first tell-tale sign of the growing impact of increased contact rates on the core of primary production.

Regenerated production decreases with increased contact rates because increased phytoplankton mortality due to viral lysis results in more primary production flowing into virus, rather than zooplankton. Moreover, this virus flow is not being recycled back to phytoplankton because no decay has been allowed for in the virus compartment and therefore the nitrogen is being locked-up in it.

5.3.4 Summary

The results obtained so far look very good for $\beta 8$ = 0.06. The simulation fits extremely well to the observation data of phytoplankton biomass at Bermuda Station "S", outperforming Control run A. Nevertheless, the primary production is 34% lower than control run A which is low in comparison to the general estimate of 0.58 Mol N m^{-3} $year^{-1}$, reported by Fasham et al. (1990). In addition the phytoplankton biomass during late winter and early spring is on the lower limits of the observational data. Moreover, the zooplankton population does not survive for long because of the competition of the viruses. It becomes extinct after the first 183 days. Therefore, the evidence points to the need of improving the formulation of zooplankton mortality as well as decreasing the natural mortality rate of phytoplankton in order to balance the losses by viral lysis. It also points to the need of including a mechanism to decrease the efficiency of the virus growth rate. This can best be done through the use of a biomass conversion constant regulating the conversion rate of the biomass of the lysed cell into the biomass of the virus. Additional mechanisms that will be used for the removal of viruses and their recycling in the ecosystem are a virus inactivation rate and decay rate of inactivated viruses into DON.

5.4 Modifying the natural mortality rate of phytoplankton

In Control run A the rate of natural mortality already parameterizes the death of phytoplankton cells caused by viral lysis, or by photosynthesis being insufficient to meet respiratory needs. As the former is being explicitly modelled in our version of the model it makes sense to adjust the natural mortality accordingly. However, one has to keep in mind that Fasham treated phytoplankton natural mortality as a free parameter to tune the model so that an annual primary production of 0.58 Mol N m^{-2} y^{-1} could be obtained at Bermuda.

Four different values for the natural mortality were tried in the β8 0.06 simulation to evaluate their effect on primary production. They were 0, 0.025, 0.045 and 0.09 d^{-1}, respectively.

Table 5.1 shows that increasing natural mortality leads to an increase in regenerated production but a decline in new production. These are then reflected in lower f-ratios. However, the net result is a slight decline in annual primary production. Notice that the increase in natural mortality has resulted in a drastic reduction of viral lysis of phytoplankton by a factor of 13.

Consequently the seasonal biomass of viruses declines for each increment in the natural mortality of phytoplankton (Fig. 5.15.b). The maximum concentration of viruses is 1.9 mMol N m^{-3} day^{-1} when the natural mortality is 0 but only 0.2 mMol when the natural mortality is 0.09 day^{-1}.

Changes in the natural mortality rate affect the seasonal biomass of phytoplankton (Fig. 5.15.a). Its increase causes the onset of the spring bloom to be delayed. ie. the lower the natural mortality rate the earlier the spring bloom starts and the earlier it is completed. The higher the natural mortality rate is, the higher the maximum concentration of phytoplankton in the spring bloom will be and the later its peak is reached. It is 0.3 mMol N m^{-3} on day 95 when natural mortality is 0 but grows to 0.56 mMol N m^{-3} on day 106 when the natural mortality is 0.09 day^{-1}.

Nonetheless increases in the natural mortality rate have no effect on the biomass of the autumn phytoplankton bloom.

Despite all the changes in phytoplankton natural mortality the zooplankton did not recover. Therefore, the original value of 0.045 day^{-1} has been retained.

Fasham et al. (1990) had found that natural mortality

was the most sensitive parameter in control run A. Judging by the variation in annual net primary production alone one would have to conclude that this is not the case in the epidemics model for maximum viral production since its normalized sensitivity was low ranging from - 0.004 to - 0.104. If however, the variation in annual viral lysis is taken for reference instead then the normalized sensitivity of natural mortality was found to be high, ranging from - 1.124 to - 0.838, thus demonstrating its importance.

As all the previous implementations including a modification of the initial conditions (not shown), as well as of the virus efficiency (not shown) and a virus inactivation rate (not shown) were unsuccessful in reviving the zooplankton seasonal cycle it was decided to implement the modifications in the zooplankton mortality term described in Fasham (1993). Thus, from here on the results of version 2 of the epidemics model will be compared to control run B.

5.5 Impact of new mortality term of zooplankton on viral epidemics (version 2)

The new model - version 2 - was submitted to the whole range of progressively higher contact rates tested in version 1 (Fig. 5.5.b). Some differences in model behaviour were found for high contact rates. For $\beta 8=1.0$ a single annual bloom comes every consecutive year but its height is higher every other year. The phytoplankton blooms in mid-summer (day 199) are *ca.* 11.6% higher than those that take place the following year at the beginning of autumn (day 256). Consequently the peak concentration of viruses is 23% higher in summer blooms (day 207) than in autumn blooms (day 261).
For $\beta 8=1.3$ there is a single annual bloom every year but its timing and size vary significantly.
For $\beta 8=1.5$ the single bloom enters a biennial cycle but its timing and size continue varying significantly. For example the peak concentration of viruses ranged from 0.6-1.7 mMol N/m^3. For $\beta 8=2.1$ the single bloom continues its biennial

cycle but becomes regular on time (2nd, 4th, 6th, 8th, 10th year on day 207) and also on size (the phytoplankton concentration is 0.8 mMol N/m^3).
All these were examples of inter annual variability forced by high constant contact rates.

The peak phytoplankton biomass during the spring bloom is reached later in version 2 than in version 1. This is a reflection of the existing differences in peak concentration and timing of the phytoplankton bloom in the base models A and B which is a direct result of the new phytoplankton and zooplankton mortality formulations. The peak biomass during spring bloom is reached at day 87 in control run A and at day 101 in control run B.

For lower contact rates the same patterns of annual primary production decline and changes in the seasonal cycle of phytoplankton emerged. However, the main difference is that zooplankton are now able to compete successfully with viruses at any contact rate.

Furthermore, slightly higher contact rates are now needed for the epidemics minimum and the maximum annual output of virus to be reached (Fig. 5.16 a,b). In a total biomass conversion situation (k_8=1) the new values are β8 0.0355 and 0.08, respectively.

Figures 5.17 a,b,c) and figures 5.18 a,b,c) show the model results of phytoplankton, bacteria and zooplankton for the two β8 simulations compared to Control run B. The lower β8 produces annual cycles that are very similar to control run B albeit of slightly lower concentration values. The higher β8 simulation once again yielded a classic spring bloom with a maximum concentration that is very close to the other two simulations. This simulation offers a better rendition of the post-bloom drop of biomass levels observed in Bermuda though the 0.05 mMol N m^{-2} of summer phytoplankton biomass from the observational data are slightly

underestimated. By comparison, the curbing effect on the autumn bloom is not as drastic as in version 1 because control run B already gives a very good prediction of its actual size. The most noticeable difference is that the maximum concentration of phytoplankton (0.16 mMol N m^{-3}) is reached early in the autumn bloom with a slow decline afterwards.

Although the seasonal cycle of zooplankton was not disrupted by the viral epidemic its concentration levels decreased by a factor of two in the higher $\beta 8$ simulation. This results in an almost perfect match to the zooplankton levels of the original cycle in control run A (Fig. 5.17.c). The exception being a period of 16 days during the height of the spring bloom when zooplankton reached a maximum concentration of 0.2 mMol N m^{-3} compared to the 0.14 mMol N m^{-3} of control run A. As the zooplankton levels in control run B are overestimated (Fasham, 1993) this can be seen as an improvement over that model.

Likewise the bacteria concentration levels decreased by a factor of two in the $\beta 8$ 0.08 simulation (Fig. 5.17.b). This reduction becomes even more drastic when the total mixed layer bacterial stocks are compared for the three simulations (Fig. 5.18.b). The higher $\beta 8$ simulation underestimates the mixed layer stock of bacteria in spring while the other two simulations give a good fit to the observations. However, as none of the simulations showed any resemblance to the pattern of bacteria concentrations of the observational data, which remain almost constant all year round, it is concluded that deficiencies still exist in the bacteria model.

The seasonal cycle of phytoplankton viruses showed the same pattern displayed for version 1. However, this time the concentration levels of virus in the $\beta 8$ 0.08 simulation were consistently higher than in their version 1 analogue already reaching 1 mMol N m^{-3} at the height of the spring phytoplankton bloom increasing to 1.6 mMol N m^{-3} at the end

of summer (Fig. 5.19.a). By comparison, the lower $\beta 8$ simulation produced a virus biomass of 0.21 mMol N m^{-3} at the height of the bloom and reached its maximum concentration at 0.4 mMol N m^{-3}. In version 1 a target of 0.7 mMol N m^{-3} was set for the concentration of viruses a week after the bloom. The high $\beta 8$ simulation overestimated the target while the low $\beta 8$ underestimated it.

Consequently, the total mixed-layer stock of marine viruses is also higher than in version 1 for both $\beta 8$ simulations (Fig. 5.19.b). The difference is especially noticeable between the simulations that produce their respective maximum annual output of viruses.
The maximum stock of viruses in version 2 is 120 mMol N m^{-2} at the onset of stratification declining to 30 mMol N m^{-2} during summer while the equivalent data for version 1 is 98 mMol and 20 mMol N m^{-2}, respectively.

In version 2, there is an increase by a factor of 4 in the total virus stock produced, between simulations for the epidemics minimum and those for the maximum annual output.

Mixed-layer marine viruses were the dominant live biomass all year round in the two epidemic simulations of version 2. The only exception being the period between days 38-115 in the lower $\beta 8$ simulation when first the biomass of phytoplankton and then later on (days 98-115) the biomass of zooplankton and bacteria became higher than that of viruses.

The flow networks for control run B and the two $\beta 8$ simulations are shown in Figure 4.10.b) and figures 5.20 a,b.

The total annual primary production for control run B, $\beta 8$ 0.0355 and $\beta 8$ 0.08 simulations were 578, 532 and 312 nMol N m^{-2} y^{-1}, respectively. The corresponding f-ratios (Fig. 5.21) were 0.55, 0.59 and 0.83, respectively.

The new epidemics minimum simulation (β8 0.0355) is a vast improvement over its version 1 counterpart because it yields a higher ANPP that is not only very close to the measurement values obtained for Bermuda Station "S" but is also reached with a much lower annual f-ratio. The flow diagrams show that the introduction of viruses in the system has caused a 10-20% generalised reduction in the inter-compartmental flows compared to control run B.

The β8 0.0355 simulation yielded 36.8 mMol N m^{-2} y^{-1} of viruses which was 6.9% of the ANPP and represented only 8.1% of the total mortality of phytoplankton. In comparison to version 1 those values portray a reduction of the impact of viruses on the ecosystem. The variable loss rate of zooplankton has enabled it to sustain with ease the competition of viruses for the same food source. As the 15% decrease of nitrogen uptake by grazing was relatively small the production of ammonia suffered only a 17% reduction and therefore the regenerated production remained still high at 216 mMol N m^{-2} y^{-1}.

The β8 0.08 simulation yielded 150.3 mMol N m^{-2} y^{-1} of viruses which was 48.1% of the ANPP and represented 57.3% of the total mortality of phytoplankton. In comparison to version 1 these values portray an increase of the impact of the viruses on the ecosystem thus not validating any possible claim on the softening effect on the virus epidemics created by the new zooplankton formulation.

The increase in the contact rate value from its epidemics minimum to that required for the maximum annual output of viruses resulted not only on a 41% decline on primary production but also on a generalised reduction of most flows in the model by a factor of 3 or 4. However, the flow into virus has increased four-fold while new production declined by only 17.8%. Regenerated production was the casualty in this new epidemic of viruses and consequently the annual f-ratio is too high. Nonetheless, it is remarkable how

zooplankton could survive the fierce competition of viruses and still thrive in it!

Although the total viral production was barely an increase to its version 1 predecessor its relative weight on the diversion of primary production was higher because the ANPP is actually lower. Consequently, compared to the other causes of phytoplankton mortality, zooplankton grazing (27.8%) and natural mortality (14.9%), the relative weight of viruses increased and viral lysis became the most important contributor for the phytoplankton mortality.

However, in the next section the seasonal cycle of specific rates will show that zooplankton grazing and detrainment rates can rise more steeply than that of viral lysis and also reach higher values at certain periods.

5.6 Control of Phytoplankton Photosynthesis and Population Growth under viral epidemics

Biomass specific rates are invaluable to understand the controlling factors in the rise and fall of phytoplankton populations.

Following Fasham et al. (1993) the model equation for phytoplankton was recasted by normalising all the terms by the phytoplankton biomass P. This gives the following equation for the net population growth rate of phytoplankton:

$$1/P.(dP/dt) = (1-\gamma_1)\mu_p - \mu_m - \mu_g - \mu_v - \mu_{mix} - \mu_{detr} \qquad (1)$$

where 1/P.(dP/dt) is the specific rate of change of phytoplankton biomass (we will refer to this quantity as the biomass growth rate),
μ_p the specific phytoplankton growth rate,
γ_1 the fraction of phytoplankton growth exuded as DON,
μ_m the specific natural mortality rate,

μ_g the specific loss rate due to grazing,
μ_v the specific loss rate due to viral lysis,
μ_{mix} the specific loss rate due to diffusive mixing, and
μ_{detr} the specific loss rate due to detrainment.

Thus, if the right-hand side of equation (3.6) is positive then the phytoplankton concentration will increase and vice versa.

Still following Fasham et al. (1993) the specific phytoplankton growth rate μ_p can be written as follows

$$\mu_p = V_p(T) \cdot L(I) \cdot (Q_1(N_n, N_r) + Q_2(N_n)),$$

where $V_p(T)$ is the maximum phytoplankton growth rate, which is a function of temperature T (equation (12) in chapter 3), and L, Q_1, and Q_2 are nondimensional factors representing the limiting effect of irradiance (I), nitrate and ammonium concentrations (N_n and N_r), respectively on phytoplankton growth rate. As formulated in the ecosystem model, the phytoplankton growth rate is averaged over the diel light-dark cycle and so the maximum possible value of the function L, assuming that light is saturating for photosynthesis throughout the whole daylight period τ, would be $\tau/24$. The factors Q_1 and Q_2 can individually take values between 0 (complete limitation) and 1 (no limitation) but their sum should be ≤ 1. The mortality rate μ_m is variable and depends on the concentration of phytoplankton (equation (7) in chapter 3). The grazing rate μ_g is mainly determined by the zooplankton biomass concentration but, because a Michaelis-Menten formulation was used to represent the effect of prey density on ingestion rate (equation (16) in chapter 3), it will also be a function of P.

The plot of μ_p - the specific phytoplankton growth rate (Fig. 5.22) shows that the viral epidemic in the $\beta 8$=0.08 simulation caused a generalized increase on the phytoplankton

growth rate especially during summer and autumn.

5.6.1 Limiting factors of phytoplankton growth compared to control run B

To understand the factors controlling phytoplankton growth rate one needs to plot the seasonal cycles of $V_p.L$, Q_1, and Q_2 for the $\beta 8$=0.08 and control run B simulations (Figs 5.23 a,b). The light limited growth rate of phytoplankton $V_p.L$ reflects the seasonal change of solar insolation at Bermuda and was identical in both simulations. However there were some remarkable differences between the two simulations in the nitrate factor Q_1. In control run B the nitrate factor Q_1 was high during late winter at 0.458 but when the height of the spring bloom growth rate (0.178 d^{-1}) was reached on day 107 the Q_1 factor had already dropped to a negligible 0.035. Nonetheless, the ammonium factor Q_2 scored 0.243 meaning that from day 93 onwards ammonium had become the predominant form of nitrogen fuelling the spring bloom. There had been a sizeable Q_2 factor at around 0.25 during late winter associated with bacteria and zooplankton excretion of ammonia but as this ammonium was rapidly utilized the phytoplankton growth became highly nutrient limited throughout the summer (Fig. 5.22) and never realized its maximum possible nutrient-saturated value of $\approx$1.2 d^{-1}. In autumn the entrainment of nitrate rich waters into the mixed layer was reflected on a sudden but modest rise of the Q_1 factor to 0.134 on day 237. The availability of nutrients caused the phytoplankton growth rate to rise fast and although the rates reached ($\approx$0.158 d^{-1} on day 236) were not as high as at the spring bloom they marked the onset of the autumn bloom.

The $\beta 8$ 0.08 simulation could not have been more contrasting. The nitrate factor Q_1 at 0.657 is at least 43% higher than control run B's during late winter and only dropped much later in the spring bloom. On day 100 when the height of the spring growth rate was reached (0.202 d^{-1}) Q_1

was 0.412 and Q_2 was 0.08 meaning that nitrate was the main fuel driving the bloom and it thus remained until day 108. The second burst in growth rate that followed was fuelled by ammonium excreted by zooplankton and its height was reached on day 129 (0.155 d^{-1}) when Q_2 was 0.158 and Q_1 negligible at 0.009.
Unlike control run B the phytoplankton growth rate remained constant throughout the summer ($\approx$ 0.13 d^{-1}) at a level even higher than during late-winter in spite of a declining Q_2 and due to a rising Q_1 that reflected an upwardly diffusive mixing of nitrate into the mixed-layer. However it was the exceptionally quick and high rise in the nitrate factor Q_1 to 0.321 on day 245 that caused the phytoplankton growth rate in the autumn bloom to reach a record height of $\approx$0.33 d^{-1} on day 243, which is a remarkable twofold increase on control run B.

Nonetheless, figure 5.17.a) shows that these high growth rates are not translated into phytoplankton concentrations higher than control run B.

5.6.2 Factors controlling net change in phytoplankton biomass

This can be investigated by plotting the seasonal changes of the specific biomass growth rate (1/P.(dP/dt)), phytoplankton growth rate (μ_p), natural mortality rate (μ_m, plotted as a negative value), grazing rate (μ_g, plotted as a negative value), viral lysis rate (μ_v, plotted as a negative value), diffusive mixing rate (μ_{mix}), and detrainment rate (μ_{detr}).

The plot (Fig. 5.24) shows that the lowest phytoplankton growth rates occurred during the first 75 days of the year. However, as the rates of viral lysis were not exceedingly high the phytoplankton population had a moderate positive growth (shaded area in Fig. 5.24). When convective mixing began to decline with the onset of stratification the biomass growth rate dropped due to detrainment. For three quarters of the rising phase of the spring bloom (day 79-95) the biomass growth rate maintained just a slightly positive growth

against the combined effect of zooplankton grazing, viral lysis and detrainment. Although being apparently at odds with the ever increasing ML volumetric biomass of phytoplankton (Fig. 5.17.a) that slight positive growth is easily discernible in the ML areal biomass of phytoplankton (Fig. 5.18.a).

Nevertheless, one wonders how the bloom could have developed and reach a biomass of 0.29 mMol N m^{-3} on day 103 (Fig. 5.17.a). From day 95 onwards the population growth rate suffered a sharp decline and became significantly negative. Note however that there was no nutrient limitation and the down-turn in phytoplankton growth rate had not yet occurred. It can therefore be argued that the initial limiting factor on the phytoplankton spring bloom was the combined effect of zooplankton grazing, detrainment and viral lysis. The phytoplankton spring growth rate became eventually nutrient limited and thereafter a secondary burst in growth rate occurred due to an increase in the availability of ammonium but none gave rise to a positive growth rate of the phytoplankton biomass. Already on day 115 at the beginning of the secondary burst the growth of phytoplankton biomass had been controlled by viral lysis and this situation continued until day 230. Thereafter convective mixing began eroding the mixed-layer resulting in the entrainment of nutrient rich waters. The combined effect of plentiful supply of nutrients and increased light levels gave extremely high growth rates during the autumn bloom resulting in a net population growth that at 0.19 d^{-1} was twenty-five times higher than the spring bloom. The decline in the autumn bloom was initiated by a decline in phytoplankton growth rate in day 244 for reasons yet unclear but probably caused by a slow down in the nitrate factor Q_1 whose down-turn occurred two days later. This decline was accentuated at first by natural mortality and subsequently by viral lysis. After the autumn bloom the phytoplankton population was mainly controlled by viral lysis although, as the phytoplankton growth rate remained high, the viruses were not always able to keep up with the phytoplankton growth resulting in a sequence of predator-prey

cycles continuing until day 313.

The period of positive biomass growth is longer-lasting during the spring bloom and the growth rate of the phytoplankton population during the autumn bloom is twice that of control run B (Fig. 5.25).

5.6.3 A comparison of viral lysis and zooplankton grazing in the diversion of primary production

To focus on this we need a plot of the seasonal changes in the specific loss rates of primary production (defined as the loss terms of the phytoplankton equation divided by the primary production).

During winter viral lysis was the major consumer of phytoplankton (Fig.5.26) being responsible for over 60% of the diversion of primary production while zooplankton grazing removed between 10-20%. However, as convective mixing further deepened the mixed-layer losses to viral lysis declined to about 40% of primary production on day 75 while losses to zooplankton grazing remained constant. Nonetheless, when the phytoplankton growth rate started rising signalling the onset of the spring bloom in response to the shoaling of mixed-layer depth the decline in viral lysis resumed and reached a bottom 30% of primary production on day 97. It is shown in the next section that this decline was due to viral losses to detrainment. Throughout this period the primary production losses to zooplankton grazing had been rising at an ever increasing rate closely following the phytoplankton bloom. Consequently, in the immediate week preceding the height of phytoplankton biomass at the spring bloom (day 98-103) and coinciding with a declining phytoplankton growth rate (from day 100 onwards) viral lysis became second to zooplankton grazing as the main cause for phytoplankton mortality. The maximum loss to zooplankton grazing was reached at 69% of primary production on day 110.
This situation of dominance lasted up to day 114 when the

phytoplankton bloom was already 10 days into its declining phase and a still rising rate of viral lysis surpassed a declining rate of zooplankton grazing diverting 64% of primary production. Similarly, for the brief period between days 102-105 phytoplankton losses to detrainment were also higher than those due to viral lysis. Detrainment removed 45% of primary production on the latter day.
Thereafter in sharp contrast to the other loss factors the losses to viral lysis became ever more important as the phytoplankton biomass declined. By the end of summer viral lysis was diverting over 90% of primary production and zooplankton grazing less than 7%. However, there was a drastic drop in viral lysis at the onset of the autumn bloom in spite of a twofold increase in phytoplankton growth rate. This was due to the dilution effect on viruses caused by the entrainment of deep waters into the mixed-layer. The losses to viral lysis reached a bottom 33% of primary production at the peak of the bloom on day 243. Nonetheless, as the bloom's declining phase started losses to viral lysis rose rapidly and soon reached 80%. Afterwards in late autumn there was a limit cycle behaviour typical of predator-prey interaction and the losses to viral lysis oscillated between 60-70%. Notice that while zooplankton grazing was being affected by dilution the losses to natural mortality increased and surpassed those of zooplankton grazing during the declining phase of the bloom. Thereafter the losses to zooplankton grazing and natural mortality stabilized at 20% and 10% of primary production, respectively.

5.6.4 Seasonal variations in the population growth rate of viruses and zooplankton

A plot of the seasonal cycle of net specific growth of virus biomass (defined as the rate of lysed hosts converted less losses by mixing and detrainment divided by the biomass of viruses) in the mixed-layer (Fig. 5.27) shows that though modest the only significant periods showing positive growth for the virus population were before the spring bloom and

after the autumn bloom. However, the shoaling of the mixed-layer was a period of significant negative growth for the virus population. Once the physical process was completed the virus population returned to a barely positive growth rate which lasted all summer well into the autumn bloom. By contrast, the significant positive growth rates of the zooplankton population occurred during blooms and were many times higher than those of viruses (Fig. 5.28). The autumn bloom was the period when their highest growth rate was reached. In comparison to control run B (Fig. 5.29) the period of positive growth lasts longer during the spring bloom and the growth rates of the zooplankton population are significantly higher in both the spring and autumn blooms. Nonetheless, the phytoplankton population displayed the widest range of negative and positive growth rates.

To summarise, up to here the most important controlling factor of virus populations is detrainment and in all our simulations at least 98.5% of the virus annual production was removed from the mixed layer by this physical process.

5.7 Changing the Mixed-Layer mixing rate

Let us question on the suitability of the low mixing rate of control run B to fit the summer phytoplankton biomass to the observations and for lowering the f-ratio in the epidemics model.

A simulation run for $\beta 8$ 0.08 using a higher cross-thermocline mixing rate of 0.1 m d^{-1} yielded not only a higher virus production of 174 mMol N m^{-2} y^{-1} but also a higher primary production of 386.5 mMol N m^{-2} y^{-1} as well as a lower annual f-ratio of 0.81 (Fig. 5.30). Unfortunately, the latter is still too high and was achieved at the cost of a higher summer value of the f-ratio (Fig. 5.31.a). Nonetheless, the summer values of the phytoplankton biomass though they were higher than 0.05 mMol N m^{-3} d^{-1} fitted the observations better (Fig. 5.31.b). Despite the higher

production of viruses their maximum concentration was slightly lower at 1.4 mMol N m^{-3} d^{-1} (Fig.5.31.c). The reason is that viral lysis has dropped slightly to 45% of ANPP representing a lower 53.3% of total phytoplankton mortality. By contrast zooplankton grazing increased to 26.5% of ANPP from the 23.3% of the previous simulation and represents now 31.3% of the phytoplankton total mortality. Consequently, that has lead to a modest increase in regenerated production from 17% to 19% of total primary production.

One concludes that lowering the mixing rate is not a universal panacea for obtaining lower annual f-ratios nor lower summer concentrations of phytoplankton. Those can also be achieved by selecting an appropriate contact rate.

5.8 Regulating the virus efficiency

Bratbak et al. (1990) and Bo rsheim et al. (1990) suggested that 62% of the total host-cell production is diverted into the viral synthesis. When the phytoplankton or bacterial cell is eventually lysed about 150 new virus are released in the water together with some cytoplasm and cell debris (the cell walls). Consequently, not all the biomass of the host-cell is converted into new viruses. Therefore, the efficiency of biomass conversion was adjusted from 100% to 62% in the equation governing the virus growth rate and the new value of K_8 is .62, down from its original value of 1. The remaining 38% is allocated to cell debris and enters the detritus compartment with a biomass conversion constant K_7=.38, up from its original value of 0 (see equations 3.3 and 3.21, in chapter 3).

A simulation for these values against a progressively higher contact rate showed a gradual decline in the primary production in all aspects similar to our past simulations (Fig. 5.32). The main difference is that an higher contact rate is required to achieve equivalent loss by viral lysis. For example, while in the k_8=1 simulation the maximum annual

output of viruses was reached at $\beta 8$ 0.08 in the present k_8=.62 simulation it is reached at $\beta 8$ 0.13. Similarly the minimum contact rate needed for a viral epidemic had to be increased to 0.061 in the k_8=.62 simulation.

The concentration of viruses and their mixed layer stocks are 33% lower in the new $\beta 8$ 0.13 simulation due to the fact that the biomass conversion of lysed cells into virus is now only partial (Figs. 5.33 b,c). In the k_8=1 simulation the maximum concentration of viruses was 1.57 mMol N m^{-3} d^{-1} while in the k_8=.62 simulation it is 1.06 mMol N m^{-3} d^{-1} in effect a 32% drop. These differences in the seasonal cycle of viruses are also reflected in their mixed layer stocks. At the onset of stratification the former had reached 120 mMol N m^{-2} declining to 30 mMol N m^{-2} when stratification had been completed. By contrast the same values for the latter are 80 mMol N m^{-2} and 20 mMol N m^{-2}, respectively.

In the new $\beta 8$ 0.13 k_8=.62 simulation the phytoplankton growth rate was higher showing a 6% increase during the second burst of the spring bloom, 9% during summer and 3% at the autumn bloom (Fig. 5.34). This agrees with what was found in the previous section on the effect of increased contact rates on the phytoplankton growth rate. However, the concentration of phytoplankton remained identical to that in the previous k_8=1 simulation (Fig. 5.33.a) in spite of higher losses to viral lysis imposed by the increase in contact rate value (Fig. 5.35).

Neither changes in biomass concentration nor on mixed-layer stock of viruses are noticeable in the simulation for the minimum epidemic ($\beta 8$ 0.061) when compared to its k8=1 counterpart though a slightly lower biomass concentration of phytoplankton did occur.

However, the seasonal cycle of biomass specific rates of phytoplankton (Fig. 5.35) showed for the minimum epidemic a rate 50% higher in viral lysis for the k8=.62 simulation.

This resulted on a 64% increase in the phytoplankton losses to lysis from 36.8 to 60.2 mMol N m^{-2} yr^{-1} concurrently with a 11.3% drop in phytoplankton grazing. The 10.3% decrease in ammonium excretion by zooplankton which ensued caused a 8.9% drop in regenerated production to 197.1 mMol N m^{-2} yr^{-1} (Fig. 5.36a). Consequently, the annual f-ratio increased from 0.59 to 0.61. The extra flow into detritus of lysed cell debris (22.9 mMol N m^{-2}) is not enough to compensate the generalized repercussions in the system of a diminished intake of food (phytoplankton) by zooplankton.

Nonetheless, for slightly higher $\beta 8$ values a small but significant result of the lowering of the conversion efficiency is the increase in regenerated production. For example in the $\beta 8$ 0.13 simulation regenerated production has risen 9% from 52.9 to 57.6 mMol N m^{-2} yr^{-1} thus increasing to 316.2 mMol m^{-2} yr^{-1} the annual primary production. Though modest this resulted on a small lowering of the f-ratio from 0.83 to 0.82 which was most noticeable at the end of summer (Fig. 5.37). That is all the more remarkable as the loss to viral lysis has actually increased 7% from 150.3 to 161.4 mMol N m^{-2} while the new production had a negligible decline from 259.2 to 258.6 mMol N m^{-2}. The explanation for the higher regenerated production is that the flow of lysed cell debris to the detritus compartment is fuelling the production of ammonium by bacteria (Fig.5.36.b).

5.9 Inclusion of a virus inactivation rate (version 3)

The main cause for inactivation in the open ocean of freshly produced viruses has been identified as being natural ultra-violet β radiation which is able to penetrate the mixed-layer of the surface ocean. The estimated inactivation rate has been calculated at 0.033 h^{-1}, when averaged over 24h and integrated over the upper 30 m of the water column (Suttle & Chen, 1992). Therefore, this inactivation rate was implemented in the model with a standard value of 0.792 d^{-1}

although some runs with an inactivation rate of 0.5 and 1.0 d^{-1} were also made for comparison (Fig. 5.58 a,b).

The most obvious consequence of a viral inactivation rate is to raise, in this particular case by a factor of 107, the contact rate values needed to sustain an epidemics minimum and to reach a maximum output of viruses (Fig. 5.38). However it has also served to expose that the response surface of the model is close to a discontinuity located only 3-5% above the contact rate value for the minimum epidemics. That is manifested by a sharp 57% increase in viral lysis of phytoplankton that can be best detected by analysis of the maximum daily flows (Fig. 5.39) though its impact on phytoplankton biomass is mostly evident on the earlier collapse of the spring bloom by a week. Past the discontinuity interval there is a sharp 25% drop in the maximum daily flow into viral lysis and the curve regains its gradual increasing trend towards a new maximum set at 2.2 mMol N m^{-2} d^{-1} at the same level of the discontinuity value and which is reached at $\beta 8=10$, 54% above the contact rate value for the minimum epidemic. When the maximum annual output of viruses is attained at $\beta 8= 14$ the maximum daily flow of viral lysis of the spring bloom has declined 9.5% and been surpassed by a new maximum set 6% higher by the autumn bloom.

In the simulation for the minimum epidemic $\beta 8$ was 6.5 and the most apparent impact of the viruses was a sharp drop on the phytoplankton biomass between days 107 and 113 (Fig. 5.40). That contrasts to the smoother decline in control run B. But because the time-window of the viruses from day 102 to 133 was just 31 days of significant flow into lysis, which varied from 0.1 to 0.9 mMol N m^{-2} d^{-1}, their impact did not last long and a small secondary phytoplankton bloom took place on day 128. Once the virus effect became negligible the trend of the phytoplankton biomass was to quickly approach the biomass levels of control run B which were reached at the end of the summer (5.40 and 5.17.a). The viruses did not

come for the Autumn bloom. Under these circumstances the loss of 37% of primary production to viral lysis in the seven days of the spring bloom collapse may be considered high though it was second to zooplankton grazing which was 70% for the same period of time. In spite of a significant 25% share during their main time-window overall viral lysis represented only 2.4% of the annual primary production compared to 60% of zooplankton grazing.

Increasing the contact rate 3% to $\beta 8$ 6.7 resulted in 43.9% of primary production being lysed during the collapse of the bloom between days 94 and 107. More significantly there was a clear predominance of lysis over zooplankton grazing with 63.6% of phytoplankton production being lost to viral lysis between days 99 and 105. However during the more extended period of significant flow into lysis from day 89 to 130 their impact was only slightly higher at 30.2%. Nonetheless the annual primary production losses to viral lysis have more than doubled to 5.5%.

The overall effect of the inactivation rate has been to circumscribe the existence of active viruses almost exclusively to bloom events ensuing thereafter a sharp decline of the active viral biomass. Consequently, the main viral biomass becomes inactivated and its maximum concentration is reached at the end of the spring bloom/early summer as opposed to end of summer.

A remarkable consequence of the introduction of an inactivation rate on viruses is the creation of a resilient Autumn bloom which cannot be suppressed even by extremely high contact rates. Therefore the behaviour of the ecosystem is reversed in relation to the previous version of the model with no inactivation. Small increases in the contact rate up to 8% higher than the value of the minimum epidemic have a visible effect on the Spring bloom depredating its biomass to two thirds of its original level but have no impact on the Autumn bloom due to the residual level of virus being too low

at the beginning of the latter bloom. Contact rates above 9% of the value for the minimum epidemic cause discernible drops in the late declining phase of the Autumn bloom. Slight increases in its value result in drops in the autumn phytoplankton biomass being initiated earlier. Above 15% the contact rate will give rise to a small secondary bloom after one such drop. Further increasing the contact rate results in more secondary blooms being formed in Autumn. The contact rate for the maximum annual output of viruses is 2.15 times that of the minimum epidemic and results in the lowering of the spring phytoplankton biomass to one third of its original level as well as in the creation of an additional series of four secondary blooms in autumn.

5.9.1 Summary

Summarising, as the output of viruses approaches its maximum with increasingly higher contact rates a "paradox of enrichment" (Rosenzweig, 1971) in phytoplankton biomass begins to manifest itself first during the autumn bloom and at a later stage during the spring bloom as well. This variation in biomass values is typical of a limit cycle oscillation of predator-prey interaction. As the inactivation rate removes a hefty part of the spring bloom viruses the active viruses left have not enough biomass to crop down the autumn bloom from its very beginning. This results in a delay between the phytoplankton bloom and the build-up of a critical biomass of viruses. Once the bloom collapses the viruses are quickly inactivated and phytoplankton can bloom again provided the limiting factors allow for it. Increasing the contact rate shortens this delay thus arising a situation of multiple blooms. However, this oscillation problem can be avoided if the constant inactivation rate is replaced by a Michaelis-Menten type formulation (Fasham, personal communication). The mortality of the highest predator in a model can be thought of as a closure term and Steele & Henderson (1992) pointed out that if a constant form was chosen then limit cycle behaviour would occur at high levels

of nutrient supply.

This reversal in behaviour extends also to the seasonal cycle of phytoplankton growth rates which show that spring growth rates are up to two times higher than in the previous implementation where inactivation is zero (Fig. 5.41.a). More significantly however is that they are also 21-47% higher than the following autumn growth rates in tune with the original 13% difference in control run B.

Perhaps the most significant result of the inactivation of viruses is that the dynamic of the specific rates of viral lysis has increased by a factor of 3 to 6 (Fig. 5.41.b).

Finally, halving the inactivation rate results in a halving of the contact rate needed to produce the same level of viral lysis, primary production or minimum epidemics. Thus initiating the epidemic at a lower $\beta 8$.

5.10 Justification for the selection of contact rates based on tests of maximum daily flow of viral lysis

The reason why half-way through this chapter I started sampling and monitoring the maximum daily flow into viral lysis instead of maximum phytoplankton biomass as previously done is because when the inactivation rate was introduced in the virus equation the phytoplankton biomass in the autumn bloom remained unaffected for a large range of contact rates. And thus the test was picking up the constant maximum value of the autumn bloom and not the declining Spring bloom for which it had been conceived.

On the other end sampling the active virus biomass was inadequate because the values were so small has to be difficult to determine small differences in amplitude. Sampling the inactivated virus biomass was not appropriate either because the maximum value is always reached outside the Spring bloom. The ideal sampling is therefore the maximum

daily flow into viral lysis because it is closely coupled to the spring bloom itself.

5.11 Inclusion of a decay rate on inactivated viruses (version 4)

There is no evidence in the literature up to now on the timescale of the breakdown of authochtonous marine viruses. However, the breakdown rates of dead organic matter were reviewed by Jones and Henderson (1986) and found to lie between 0.004 and 0.18 d^{-1}. In the model decay times of 0.0054794, 0.0109589 and 0.0328767 d^{-1} corresponding to six months, three months and one month respectively have been used to breakdown inactivated viruses into labile DON. The justification for this breakdown time is that the molecular weight of viruses is too high for bacteria or any other agent to successfully break it down in a shorter period. This makes it in fact a semi-labile DON. However some runs of one day decay time and no decay were also made for comparison.

Simulations of differing inactivation rates yield identical annual production rates (primary production, viral lysis and bacterial production) for the minimum (Table 5.2) and maximum (Table 5.3) production epidemics provided they all use the same rate of decay on inactivated viruses. Obviously, the contact rates can not be identical because they are proportional to the inactivation rate.

Nevertheless it was noticed that the relative value of the minimum contact rate got marginally smaller ($\leq$2.5%) with increases in the inactivation rate. One caveat is that the contact rate for each minimum epidemic was determined by trial runs and not by extrapolation from other minimum values.

Note however that in spite of all the care put into it for operational reasons it is sometimes difficult to determine with identical level of accuracy the contact rate

value for minimum epidemics and that may result in a small degree of variability being introduced in the annual production rates.

In simulations of minimum epidemics differences in inactivation rate can tilt the balance in favour of viral lysis or zooplankton grazing. That may cause a small secondary effect on regenerated production but hardly any disturbance to the other flows in the model (see flow networks Fig. 5.42.a). Lower inactivation rates benefit viruses while higher inactivation rates benefit the zooplankton.
However, in simulations of maximum annual viral lysis (Fig. 5.42.b) none of the flows are affected by changes in inactivation rate.

An example of the sensitivity of the model response in simulations of minimum epidemics is demonstrated when inactivation rates 1.0, .792 and .5 d^{-1} with a decay time of one month produced results of annual viral lysis of 21, 30 and 37 mMol N m^{-2} $year^{-1}$, respectively (Table 5.2). The contact rates used were 8.0, 6.4 and 4.1, respectively. Their flow networks are very similar. The main difference being that the excess 8 mMol N m^{-2} $year^{-1}$ into viral lysis of the .5 inactivation simulation are diverted into zooplankton grazing in the .792 simulation. In comparison, the results for the maximum annual viral lysis (Table 5.3) were much narrower at 204.8 mMol N m^{-2} $year^{-1}$ for contact rates 18.0, 14.0 and 9.0 respectively. Their flow networks are so similar that it is impossible to tell them apart.

Simulations of identical inactivation rate but differing decay rate on inactivated viruses do not yield the same annual production rates though they require an identical set of contact rates for the minimum (Table 5.4) and maximum (Table 5.5) production epidemics.

Nonetheless, it was noticed that faster decay times

require a slight reduction in contact rate to sustain the virus at a level of minimum epidemic. For example decay times of fifty, ten and one year, six months, one month and one day required $\beta 8$ values of 6.74, 6.69, 6.6, 6.5, 6.44, 6.4, 6.3 in simulations where the inactivation rate was .792 (Table 5.4). These minor adjustments are difficult to explain but they may be needed due to an increasingly higher phytoplankton growth rate during the spring bloom which results from the faster recycling of nitrogen. But also one cannot rule out the caveats mentioned for the inactivation rate.

In comparison the maximum annual viral lysis is reached at a steady $\beta 8=14.0$ for all decay simulations. However there is only a 9-13% (around 20 mMol N m^{-2} y^{-1}) marginal increase in the annual viral output from $\beta 8=10.0$ upwards.

Figure 5.43 a,b,c) and Table 5.5 show a generalized increase in primary production, viral lysis and bacterial production when the decay time of inactivated viruses is progressively shortened from fifty years to one month and eventually to one day, up from the production levels of decay zero simulations. One remark is that the same production levels can be obtained for different contact rates under various inactivation rate scenarios (Fig. 5.44).

When the decay time is shortened from six to one month primary production and viral lysis rise by around 25 mMol N m^{-2} y^{-1} and 20 mMol N m^{-2} y^{-1} representing an average increase of 7 and 10% respectively, for most contact rates. For the minimum epidemic a 44.6% increase of 9.3 mMol N m^{-2} y^{-1} in viral lysis contrasts to a more modest 5.3% increase of 5.5 mMol N m^{-2} y^{-1} in bacterial production. Nonetheless the main beneficiary of shorter decay times is bacterial production which showed a very significant increase exceeding by around 55 mMol N m^{-2} y^{-1} their counterparts for contact rates above 9. Depending on the bacterial production under consideration this represented a 77 to 93% difference.

Notice that only decay times of one month or less can induce the DON and ammonium uptake by bacteria as well as losses to ammonium excretion and zooplankton grazing to increase with the contact rate (Fig. 5.45). This results in a bacterial production of 126.9 mMol N m^{-2} y^{-1} a 21% increase on control run B when $\beta 8$ reaches 9.0 for the one month decay simulation. Though declining slowly thereafter when the maximum annual viral lysis is eventually reached at $\beta 8$=14.0 the bacterial production remains yet 12% above the value for control run B. All these results were confirmed by the production levels yielded by simulations with a inactivation rate of .5 (Fig. 5.46).

The maximum bacterial production is reached at a contact rate 33.3% to 35.7% below the one for the maximum annual viral lysis and within ±10% of the one for maximum daily flow of viral lysis.

The maximum daily flow into viral lysis is reached either at the beginning or halfway the course between minimum and maximum production epidemics (Fig. 5.47). Its highest value is up to 2.4 mMol N m^{-2} d^{-1} in some simulations regardless of inactivation or decay rates (Table 5.4).

In the minimum epidemics the maximum daily flow into viral lysis increased with faster decay rates from 0.9 to 1.4 to 1.8 mMol N m^{-2} d^{-1} when decay times of zero, six months and one month were used but dropped to 0.4 mMol N m^{-2} d^{-1} when the decay time was shortened to one day.

In the discontinuity above the minimum contact rate the values were 2.255, 2.06, 1.9 and 2.0 mMol N m^{-2} d^{-1} respectively. In the whole range of contact rates tested for these decay rates the highest maximum daily flows were 2.255, 2.23, 2.33 and 2.32 mMol N m^{-2} d^{-1}, respectively.

In simulations of minimum epidemics viral lysis becomes significantly important when the phytoplankton growth rate

approaches and reaches its maximum (Fig. 5.48). As described before this corresponds to the collapsing phase of the bloom when the phytoplankton biomass is half its peak value.

An earlier collapse of the phytoplankton spring bloom occurs for each increase in decay rate (Fig 5.49 a,b). Consequently there is also a lowering of the maximum concentration of phytoplankton at the height of the bloom. The lowest biomass maximum is reached in the one month decay simulation at 11% below control run B. However once again the odd result here is for the one day decay simulation which not only collapses later than the others but also reaches the height of control run B.

Therefore, faster decay rates also result in earlier and lower maximum concentration of inactivated viruses and hasten the rate of their decline during Summer (Fig. 5.50.a). In the minimum epidemic the maximum concentration of inactivated viruses for the decay zero simulation is 0.227 mMol N m^{-3} on day 156. Although the concentration in the six months decay simulation is 3.8% higher it is reached 19 days earlier. However, the one month decay simulation is 28.5% lower and is reached 34 days earlier. Those differences increase to a value 96.8% lower reached 35 days earlier in the one day decay simulation.

Nonetheless by the end of Summer on day 228 the decline on the concentration of inactivated viruses has widened those differences to 35%, 96.5% and 99.99% below the 0.2189 mMol N m^{-3} of the zero decay simulation in the six month, one month and one day simulations, respectively.

The effect a decay rate increase has on the biomass of inactivated viruses is especially noticeable in simulations for the maximum annual output of viruses which show a drastic decline in maximum concentration from 1.1 to 0.8, 0.4 and 0.023 mMol N m^{-3}, in the zero decay, six month, one month and one day decay simulations, respectively (Fig. 5.50.b).

In the minimum epidemic a breakdown of inactivated viruses in the six month decay simulation increases the supply of DON by up to 20% in late Summer and that is repercuted in an up to 60% higher concentration of bacteria during this period.

Faster decay rates mean also that a DON surplus will be available progressively earlier during the Summer season (Fig. 5.51.a). In the simulation for one month decay a 16% DON increase during mid-Summer fuels a 40% higher bacterial biomass. A quick release of viral nitrogen in the one day decay simulation increases by 30% the DON supply during the collapsing phase of the spring bloom giving rise to a 20% higher bacterial biomass (Fig. 5.51.b).

In spite of an effective reduction in contact rate for the minimum epidemic the annual viral lysis increased from 13.2 to 21.3 and 30.3 mMol N m^{-2} y^{-1} when the decay time was shortened from zero to six months and one month, respectively. The corresponding increase in percental viral lysis from 2.4% to 3.7% and 5.4% of primary production was accompanied by an increase in regenerated production during Summer which still was not enough to lower the annual f-ratio.

The seasonal f-ratios of the minimum epidemics are so similar that can only be differentiated from each other in late Summer. The zero decay simulation has an f-ratio of 0.2332 which is 13.2% higher than Control run B signalling a 14.7% lower regenerated production at this time of year. However both the six month and one month decay simulations have lower f-ratios than control run B by 10.7% and 19.4%, respectively signalling a 16.6% and 31.1% higher regenerated production at the end of Summer. These results were to be expected from the patterns of DON release and associated rises in bacterial biomass in these simulations. Nonetheless even the one day decay simulation has shown an f-ratio 1.3% lower than Control run B which reflects a 1.5% higher

regenerated production.

Faster decay rates bring down the seasonal f-ratio of maximum production epidemics (fig. 5.52). During autumn, winter and spring the seasonal f-ratios for the maximum production epidemic in the six and one month decay simulations are respectively 8.6% and 15.3% lower on average than in the zero decay simulation.

Nevertheless, the difference between these simulations in Summer is considerable. The regenerated production remains very high during the course of the Summer in the six and one month decay simulations and at the end of this period the f-ratios at 0.16 and 0.125 are half and third that of zero decay, respectively. That signals that the regenerated production is three and four times higher. Furthermore not only are these f-ratios 13.6% and 24.8% lower than in the epidemics minimum but also 22.4% and 39.4% lower than control run B for the same period. Those values reflect a regenerated production at the end of summer that at 0.102 and 0.137 mMol N m^{-2} d^{-1} is 21.4% and 43.2% higher than in the epidemics minimum simulation but also 39.8% and 87.7% higher than control run B.

A comparison of flow networks for the one month and six months decay simulations (Fig 5.53 c,d) shows that the amount of nitrogen diverted into viral synthesis is roughly the same (138.8 versus 127.0 mMol N m^{-2} y^{-1}) in maximum production epidemics. However, in the one month decay simulation 75% of that nitrogen reenters the system via DON and 25% is lost by detrainment versus 40% and 60%, respectively in the six months decay simulation. The amount that reenters the system through DON at 104.5 mMol N m^{-2} y^{-1} is twice that of six months and therefore 2.3 times less nitrogen is lost to detrainment in the form of inactivated virus. DON flow to bacteria is up by 66 mMol a 57% increase and so is the uptake of ammonium by 57% too. A 40% increase in bacterial excretion of ammonium takes only 9.2 mMol of the extra DON while a

significant 47.5 mMol of these is diverted by zooplankton grazing which is up by 2.25 times. Consequently the excretion of ammonium by zooplankton is 56% higher and leads to a 36% increase in regenerated production by 30.9 mMol N m^{-2} y^{-1}. Thus the annual f-ratio drops from 0.74 to 0.67.

5.11.1 Effect of a fast decay time on production rates

In the simulation for minimum epidemic a comparison between one day and one month viral decay shows a difference of 8.1 mMol N m^{-2} y^{-1} (+1.4%) in primary production, -10 mMol N m^{-2} y^{-1} (-32.9%) in viral lysis and 7.6 mMol N m^{-2} y^{-1} (+7%) in bacterial production (Fig. 5.43 a,b,c).

The same comparison for a simulation of the maximum annual viral lysis showed a difference of 12.4 mMol N m^{-2} y^{-1} (+3.5%) in primary production, 9.4 mMol N m^{-2} y^{-1} (+4.2%) in viral lysis and 48.9 mMol N m^{-2} y^{-1} (+41.5%) in bacterial production.

Thus the model results for a viral decay of one day show but for one exception that primary production and viral lysis are only slightly higher than in the one month viral decay simulation. This means that an instantaneous recycling of virus cannot reverse the decline in primary production caused by lysis in spite of a considerable boost to bacterial production. That gives support to the need for a DON feedback into phytoplankton as an alternative source of nitrogen as suggested by Collos (1993). Further work outside the realms of this thesis would be needed to investigate whether a DON feedback would increase primary production to the observations level of 578 mMol N m^{-2} y^{-1} in Bermuda Station "S" while absorbing the losses to lysis imposed by its coexistence with a viral epidemic.

The results for a viral decay of one day show also that though the concentration of active virus is 53% smaller (in

minimum but not maximum production epidemic) their impact on the phytoplankton biomass remains identical. The biomass of active virus increases threefold between minimum and maximum production epidemic simulations.

However the most relevant result of the one day viral decay is the drastic reduction in the concentration of inactivated virus which becomes on average 22% lower than active virus and follows exactly the same seasonal cycle.

5.11.2 Summary

Bacteria start profiting from the viral epidemic on phytoplankton if decay times last one month or less.

A faster decay time on inactivated viruses counters their tendency to accumulate during the Summer season and may lower their concentration to a level below that of active virus.

The seasonal cycle of phytoplankton biomass in all simulations of minimum epidemic are similar to control run B and differ only in the post-height collapse of concentration levels in spring and summer (Fig. 5.49.a,b). However, the result of epidemics for the maximum annual output of viruses are more interesting in that there are no marked blooms of phytoplankton during the year only some oscillations of *ca.* 20 to 40% in spring and autumn around the low 0.09 mMol N/m^3/day average concentration level (Fig. 5.49.c).

The present structure of the model forces a deficit of 13-17 to 214-276 mMol N m-2 y^{-1} in the annual primary production compared to control run B, in order to accommodate viral lysis according to minimum or maximum viral epidemic scenarios.

The decline of primary production with increasing contact rates is initially very steep but then becomes very

gradual. A $\beta 8=100$ would be required to push the primary production below 100 mMol N m-2 y-1 and yet no extinction of phytoplankton occurs for even higher contact rates.

The highest net transfer of nitrogen to viral lysis is reached at $\beta 8=14.0$ regardless of decay rate for a .792 inactivation rate.

5.12 Inclusion of a variable contact rate (version 5)

Seasonally varying contact rates have recently been shown to be fundamental for the rendition of credible behaviour in models of human epidemics (Rand & Wilson, 1992). In this model of marine viruses the seasonal contact rate increases at the spring and autumn blooms when phytoplankton reach higher concentrations and decreases during summer and winter (Fig. 3.2). The seasonal component of the contact rate b_1 was given a value of 0.30 taken from Rand & Wilson (1992) which results in a oscillation of 30% around the average contact rate. Results from these simulations are compared below to fixed contact rate equivalents of identical inactivation and decay at .792 d^{-1} and six months, respectively.

With a variable contact rate the peak flow into lysis during the spring bloom is 2.6 times larger and occurs 3 days earlier at 3.7 mMol N/m^2 on day 101 when the peak value of the variable contact rate reaches 8.37, for the minimum epidemic (Fig. 5.54 a,b). From day 101 to 104 viral lysis diverts more than 100% of the daily primary production (up to 1.5 times) meaning it is reducing the standing stock of phytoplankton (Fig. 5.55). That is unique to variable contact rates and has never occurred for fixed contact rates during spring blooms. Though it occurred only during autumn blooms with much higher contact rates, close to maximum epidemics.

The biomass of inactivated viruses from a pre-bloom concentration of 0.016 mMol N/m^3 (Fig. 5.50.a) increases

twenty-twofold between day 97-135 and reaches 0.35 mMol N/m^3/day at the end of this period. This is a 45% increase on the levels obtained with a fixed contact rate and is achieved in two steps: one during the declining phase of the spring bloom and another increase during the subsequent secondary blooms. That pattern results from the dynamics of active viruses (Fig. 5.56) whose winter biomass from a low 10^{-10} mMol N/m^3 on day 51 increases during the spring bloom to a peak 0.04 mMol N/m^3 on day 103 and then drops to a very low 10^{-19} mMol N/m^3 during summer but shows a remarkable recovery during the autumn bloom to 0.006 mMol N/m^3 due in part to the rise in contact rate during this event. This recovery is significantly larger than for the fixed contact rate simulation in which the minimum summer value was 10^{-15} mMol N/m^3 and could only rise to 10^{-6} mMol N/m^3 during the autumn bloom. Although the height of the phytoplankton spring bloom is identically reached on day 97 at 0.31 mMol N/m^3 its collapse to 0.1 mMol N/m^3 on day 107 occurs four days earlier and at a 39% lower biomass than with a fixed contact rate (Fig. 5.49.a). However, the supply of nutrients is still plentiful to fuel two secondary blooms of phytoplankton, which is one more than with a fixed $\beta 8$. Likewise, in the autumn bloom (Fig. 5.49.b) there is a unique collapse of the phytoplankton biomass between days 315 - 330 from a concentration of 0.24 to 0.17 mMol N/m^3 which then rises during the subsequent secondary bloom to 0.195 mMol on day 352, thus rejoining the level values of fixed contact rate simulations.

The largest depth integrated flows during the spring bloom tend to occur when the mixed-layer depth is *ca.* 100m. However, the flow into viral lysis (3.7 mMol N/m^2) on day 101-102 is the largest of the phytoplankton loss terms in the whole annual cycle in spite of a shallower mixed-layer depth of 70-65m. The flow into lysis is even larger than the peak flow into zooplankton grazing (*ca.* 3.0-3.2 mMol N/m^2 from day 87-97) that occurred when the mixed-layer was almost twice as deep. The relative magnitude of these processes is depicted

in Fig. 5.55. Overall losses to viral lysis increased twofold diverting 7% of the annual primary production which at 552 mMol N/m^2/year (Table 5.6) is 2% lower than with a fixed contact rate due to a 5% decline in regenerated production (Table 5.7) because of lower ammonium excretion by zooplankton (Fig. 5.57.a).

Summarising, seasonally varying contact rates within the annual cycle yield larger rates of viral lysis and higher concentration of viruses during bloom events and also increase the overall rate of the annual primary production diverted by lysis (Table 5.6). The higher values in virus biomass and lysis fluxes are distributed towards the higher contact rates above the average value of minimum epidemic, partly because peak contact rates (Fig. 3.2) were made to coincide with periods of higher phytoplankton productivity. These turn out to occur when the mixed-layer depth is between 60-70m on days 102 and 323 (Fig. 4.2).

In maximum epidemics viral lysis takes place during all seasons of the year (Fig. 5.54.c). Therefore the largest flows into lysis occur during the highest primary production times in winter and spring when the mixed-layer is 50-200m deep in spite of the highest biomass of active viruses being reached only when the mixed-layer shoals to 20-60m. The variable contact rate causes the phytoplankton biomass to oscillate 30-50% around the biomass levels of the fixed rate simulation, being higher in winter and summer, and lower during spring and autumn (Fig. 5.49.c). Consequently with a variable contact rate peak flows into lysis are 25% larger during winter than with a fixed contact rate but are 15% smaller during the spring bloom and similar in summer and autumn (Fig. 5.54.c). That results in a 3% lower annual viral lysis though the total annual primary production remains identical (Fig. 5.57.b and Table 5.6).

5.13 Changing the sinking speed of detritus

The model results for a sinking rate of 1m d^{-1} are similar in nature to those presented in the previous sections and the minor differences found do not justify a detailed presentation in this work. A synthesis of the variation in annual primary production, viral lysis and bacterial production for increasing levels of the contact rate under three different inactivation rates is depicted in Figure 5.58 a,b).

Simulations for a detrital sinking speed of 1m d^{-1} had a 18% higher maximum annual output of viruses than those for 10m d^{-1} (Fig. 5.59). The annual primary production is also up to 13% higher. However, the bacterial production is the most benefited by a slower sinking rate of detritus with a 70-87% increase over 10m/day simulations.

5.14 Summary and discussion

The main concerns of this project are to introduce epidemics dynamics into a model of an upper ocean ecosystem developed by Fasham et al.(1990) and Fasham (1993), and determine whether its levels of viral production can account for the subsurface consumption rate of semi-labile DOC suggested by Bacastow & Mayer Reimer (1991).

In this chapter, results from progressive changes to the structure of the basic model have been presented and analyzed using tools of flow analysis and by visual assessment. Of particular interest was the exploration of how the newly implemented inactivation and decay rates on marine viruses affected the response of the model. The effect of a range of contact rates from minimum to maximum production epidemics and beyond on rates of viral lysis and primary productivity were examined.

Increasing/reducing the natural mortality rate of phytoplankton does not significantly affect the annual primary production though it influences considerably the losses to viral lysis in two ways: delaying/hastening the start of the spring bloom and increasing/reducing the diversion of resources to detritus, both of which regulate the availability of phytoplankton biomass to viruses.

The Michaelis-Menten formulation for the zooplankton mortality enabled the coexistence of zooplankton with viruses at all levels of competition throughout the range of viral epidemics examined.

Simulations with zero inactivation rate on viruses resulted in the build-up of active viruses during summer which allowed an easy control of the biomass of the phytoplankton autumn bloom or the forcing of a biennial cycle just by regulating the contact rate. This made it possible to give a remarkably good fit to the observational data of phytoplankton biomass at Bermuda Station "S". The best fit was given by the contact rate yielding the maximum annual output of viruses in version 1.

Small values for the inactivation rate of *ca.* 0.01 d^{-1} (Quental-Mendes, 1992) produced very interesting results and suggested the potential of a virus inactivation rate as a fine-tuning tool of the model. Briefly, low inactivation rates had three main consequences: first was a sharp decline of the active viral biomass after blooms, second it allowed for a series of small outbreaks of phytoplankton blooms to happen during the summer, and third it contributed to an even lower concentration of viruses over winter thus allowing the following spring bloom to start earlier.

However, increases in inactivation rate to values more in line with those reported in the literature restricted the existence of the bulk of active viruses to bloom events, introduced a delay in the build-up of a critical biomass of

viruses during blooms, raised phytoplankton growth and specific loss rates and gave origin to a limit cycle behaviour of predator-prey interaction when higher contact rates where used thus frustrating the attempt of forcing the autumn biomass levels of phytoplankton to be lower than those of the spring bloom.

In minimum epidemics the short term benefit of an increase in inactivation rate is the higher maximum daily flow of nitrogen into viral lysis at the height of a more intense and prolonged spring bloom of phytoplankton which has had more time to develop and build-up extra biomass due to a 35 day delay in the start of viral lysis; the long term disadvantage is a lower annual total viral lysis due to the shorter lysing period.

Although overall rates of production and viral lysis in maximum production epidemics are unaffected by changes in inactivation rate these are extremely important in the creation of limit cycle behaviour between viruses and phytoplankton.

Simulations with different inactivation rates and identical decay rate yield similar production rates, however the dynamics of their phytoplankton and virus biomass are not identical. For example, in the one month decay simulation for the maximum production epidemic, the amplitude in the oscillations of phytoplankton biomass in the autumn bloom are damped noticeably faster with a inactivation rate of .5 d^{-1} than for .792 d^{-1}. That happens because in the former the growth rate of the viruses is 61% higher than the phytoplankton growth rate at some occasions during the autumn bloom. Consequently viral lysis is removing up to 1.6 times more nitrogen than is being produced by primary production thus reducing the standing stock of phytoplankton.

There is a generalized increase in primary production, viral lysis and bacterial production when the decay time of

inactivated viruses is shortened from six to one month and eventually to one day, up from the production levels of decay zero simulations. Fast decay rates on inactivated viruses increase slightly the supply of DON and raise bacterial biomass which increases zooplankton grazing on bacteria and phytoplankton. The reduction in phytoplankton biomass due to grazing and lysis in combination with a rise in the zooplankton excretion of ammonium increase the time span and peak value of the ammonium limiting factor Q2 which boosts the phytoplankton growth rate by up to 20% during the spring bloom resulting in an increase of the rate of viral lysis. Those phytoplankton growth rates are 30% to 2.5 times higher than control run B for minimum and maximum production epidemics, respectively.

It was found that the concentration of active and inactivated viruses starts increasing at the end of the phytoplankton bloom. Field observations during blooms of *Emiliania huxleyi* in Norwegian coastal waters (Bratbak, 1993) corroborate the timing of the model results. The maximum concentration of inactivated viruses is reached between days 120-140 for the various inactivation and decay simulations in minimum and maximum production epidemics.

One would therefore predict that HTCO-DOM analysis performed in April-May will show a lower C/N ratio than during other periods of the year reflecting the increased proteinaceous nature of the "living" biomass present at the time.

It was also found that the concentration of active phytoplankton viruses varies by several orders of magnitude during the annual cycle from $3.6*10^{-16}$ to 0.02 mmol N m^{-3} which is more than the change in its host concentration and represents only one virus particle per every 20 m^3 to a maximum $2.8*10^6$ virus particles per ml. Their peak concentration is reached during the decay phase of the phytoplankton spring bloom and their numbers decline

drastically during summer. Their bottom concentration is reached when the mixed-layer starts deepening at the onset of the autumn bloom. Therefore, for most of the annual cycle active viruses are below the detection limit of electron microscopy which is 10^4 virus/ml, the equivalent of 1.8-$7.2*10^{-5}$ mMol N/m^3.

Contact rates for maximum production epidemics are roughly twice that for minimum epidemics. Moreover, the minimum epidemic is located next to a discontinuity in maximum daily viral lysis which yields larger flows with increases in contact rate.

In minimum epidemics, peak specific rates of viral lysis of *ca.* .12 d^{-1} diverted at times up to 60% of the daily primary production and were comparable to those of zooplankton grazing on phytoplankton. However, the overall areal maximum daily flows into viral lysis are one third or more lower than those into grazing because the mixed-layer depth is shallower when the peak values of lysis are reached. Therefore zooplankton diverted considerable more nitrogen annually because it is not restricted to bloom events and grazes during the whole year. The first phase of the spring bloom is controlled by zooplankton and the second by viruses.

Nevertheless, in maximum production epidemics viruses control the whole annual cycle with higher peak specific rates of lysis of *ca.* .4 d^{-1} that divert up to 80% of the daily primary production. However, its maximum daily flow of 2 mMol N m^{-2} is only 11% to two times larger than the minimum epidemic value. Nonetheless, the highest maximum daily flows into lysis occur within a range of contact rates 1-40% larger than the value for minimum epidemics and encompassing the discontinuity located above the minimum epidemic.

Zooplankton loses its predominance over lysis as the main cause of phytoplankton mortality and diversion of primary production when the contact rate is 32% higher than

the value for minimum epidemics.

Phytoplankton mortality caused by viral infection was found to range between 4-8% to 70-71% of the total mortality in minimum and maximum production epidemics. In contrast, the corresponding phytoplankton mortality attributed to zooplankton grazing ranged between 65-67% to 18%, respectively.

It was shown that inactivation and decay play a more important role than detrainment in the regulation of the biomass of active and inactivated viruses. Detrainment removes less than 5% of the annual viral production. However the autumn-winter entrainment of waters in the mixed-layer has the effect of diluting the concentration of active and inactivated viruses. Its importance increases with longer decay rates when the concentration of inactivated viruses is higher. Losses to diffusive mixing during the summer period lost their importance since its rate was reduced from 0.1 to 0.01 m d^{-1}.

The model results show that the overall rate of viral lysis is 21-37 mmol N/m^2/year in minimum epidemics corresponding to a diversion of 2.4% to 6.7% of the annual phytoplankton primary production. However, the results for epidemics that yield the maximum annual viral lysis are ten times higher at 205-224 mMol N/m^2/year, representing on average 64% of the total annual primary production.

The reduction of modelled annual primary production values below the 580 mMol N / m^2/ year original estimate of Fasham et al. (1990) as a result of viral epidemics should not be a matter of concern in view of recent developments in the understanding of the system dynamics at Bermuda Station "S" unveiled by the BATS programme of the JGOFS Time Series at this site. The annual primary production at this station was found to vary significantly from one year to another (Michaels, 1994 and Michaels et al. 1994).

Overview on flows into viral lysis

Three parameters were found to affect the timing and size patterns of flows into viral lysis:

- Increases in contact rate lead to an earlier start and late ending of lysis for each bloom event. The response of the maximum daily flow into lysis to increases in $\beta 8$ is not uniform, there were peaks of identical value 1-40% above the minimum contact rate which decline slightly thereafter. These are 57% higher than the maximum daily flow into lysis yielded by the minimum epidemic.
- Increases in inactivation rate lead to a later start and earlier end of lysis for each bloom event. They also lead to higher levels (peaks) of the maximum daily flow into lysis.
- Increases in decay rate lead to an earlier start and identical end time of lysis. They also lead to higher maximum daily flow into lysis in spring and autumn blooms in both minimum and maximum epidemics. There were two exceptions: the one day decay simulations which produced atypical results in minimum epidemics starting later and producing very small daily flows into lysis. And the decay=0 simulation whose flow oscillations at the autumn bloom in maximum epidemics were 4 times higher than others.

In contrast, variable contact rates do not change the start nor end time of lysis but change their pattern during bloom events by hastening an earlier reach of the peak of viral lysis by up to 3 days and boosting the peak flow into lysis during the spring bloom up to 2.6 times.

5.15 Tables

	$\mu 1$= 0 d^{-1}	$\mu 1$= 0.025 d^{-1}	$\mu 1$= 0.045 d^{-1}	$\mu 1$= 0.09 d^{-1}
Total Primary production	381.5	385.1	380.1	340.7
Regenerated production	10.6	25.32	34.36	43.87
New production	370.85	359.83	435.75	296.84
f-ratio	0.97	0.93	0.91	0.87
Natural mortality	0	95.01	159.5	254.3
Viral lysis	314.3	218.4	148.0	24.0

Table 5.1 Modelled annually integrated Total, New, and Regenerated primary production and f-ratio plus natural mortality and viral lysis in mMol N m^{-2} yr^{-1} for Bermuda obtained using phytoplankton mortality rates ($\mu 1$) of 0, 0.025, 0.045 and 0.09 d^{-1}.

Inactivation rate	Beta8	Primary production	Net Bacterial production	Viral lysis	Maximum daily flow into lysis
0 d^{-1}	0.0611	509.6	81.9	60.7 (12%)	0.43 (76)
.5 d^{-1}	4.1	557.1	109.7	37.3 (7%)	1.40 (100)
.792 d^{-1}	6.4	560.9	108.9	30.4 (5%)	1.87 (100)
1 d^{-1}	8.0	566.8	108.3	21.2 (4%)	1.69 (103)

Table 5.2 Estimates of annual viral lysis, and corresponding percentage to net uptake of nitrogen by phytoplankton (in brackets) compared with the resulting primary production and net bacterial production, in mMol N/m^2/year, for minimum epidemics with inactivation rates of 0, .5, .792 and 1 d^{-1}. Also shown, the maximum daily flow into viral lysis in mMol N/m^2 and day when achieved (in brackets). The lysed phytoplankton debris flows into the detritus compartment. The decay time of inactivated viruses was **one** month. Sinking speed of detritus 10m/day.

Inactivation rate	Beta8	Primary production	Net Bacterial production	Viral lysis	Maximum daily flow into lysis
.5 d^{-1}	9	326.0	60.5	204.8 (63%)	1.953 (90)
.792 d^{-1}	14	327.3	61.0	204.8 (63%)	2.006 (92)
1 d^{-1}	18	323.1	60.2	204.8 (63%)	1.968 (88)

Table 5.3 Estimates of annual viral lysis, and corresponding percentage to net uptake of nitrogen by phytoplankton (in brackets) compared with the resulting primary production and net bacterial production, in mMol N/m^2/year, for epidemics for the maximum annual output of phytoplankton viruses with inactivation rates of .5, .792 and 1 d^{-1}. Also shown, the maximum daily flow into viral lysis in mMol N/m^2 and day when achieved (in brackets). The lysed phytoplankton debris flows into the detritus compartment. The decay time of inactivated viruses was **six** months. Sinking speed of detritus 10m/day.

Decay time	Beta8	Primary production	Net Bacterial production	Viral lysis	Maximum daily flow into lysis
50 years	6.74	546.3	94.3	34.4 (6%)	2.30 (98)
10 years	6.69	550.5	96.0	30.7 (6%)	2.17 (100)
1 year	6.6	551.7	98.7	35.1 (6%)	2.14 (97)
6 months	6.44	565.0	103.4	21.1 (4%)	1.40 (104)
3 months	6.43	560.3	104.0	29.7 (5%)	1.83 (100)
1 month	6.4	560.9	108.9	30.4 (5%)	1.87 (100)
1 day	6.3	574.4	109.9	9.0 (2%)	0.47 (118)

Table 5.4 Estimates of annual viral lysis, and corresponding percentage to net uptake of nitrogen by phytoplankton (in brackets) compared with the resulting primary production and net bacterial production, in mMol N/m^2/year, for minimum epidemics of phytoplankton viruses with decay times of inactivated viruses of fifty, ten and one year, plus six, three and one month plus one day. Also shown, the maximum daily flow into viral lysis in mMol N/m^2 and day when achieved (in brackets). The lysed phytoplankton debris flows into the detritus compartment. The inactivation rate was .792 d^{-1}. Sinking speed of detritus 10m/day.

Decay time	Beta8	Primary production	Net Bacterial production	Viral lysis	Maximum daily flow into lysis
50 years	14	302.8	26.8	179.0 (59%)	2.04 (271)or 96
10 years	14	304.1	28.4	181.1 (60%)	1.86 (269)or 94
1 year	14	317.3	45.4	196.2 (62%)	1.90 (92)
6 months	14	327.3	61.0	204.8 (63%)	2.00 (92)
3 months	14	338.4	82.3	213.6 (63%)	2.11 (92)
1 month	14	352.0	117.8	223.9 (64%)	2.16 (91)
1 day	14	364.4	166.7	233.3 (64%)	2.14 (91)

Table 5.5 Estimates of maximum annual viral lysis of phytoplankton, and corresponding percentage to the net uptake of nitrogen by phytoplankton (in brackets) compared with the resulting primary production and net bacterial production, in mMol N/m^2/year, for epidemics of phytoplankton viruses with decay times of inactivated viruses of fifty, ten and one year, plus six, three and one month plus one day. Also shown, the maximum daily flow into viral lysis in mMol N/m^2 and day when achieved (in brackets). The lysed phytoplankton debris flows into the detritus compartment. The inactivation rate was .792 d^{-1}. Sinking speed of detritus 10m/day.

Beta8	Primary production	Net Bacterial production	Viral lysis of phytoplankton	Maximum daily flow into lysis
6.44	551.7	102.9 (255.5)	39.6 (7%)	3.668 (101)
6.9	522.8	99.0 (251.6)	72.3 (14%)	5.001 (92)
14	326.8	60.7 (186.9)	198.0 (61%)	1.716 (93)

Table 5.6 Estimates of annual totals of viral lysis of phytoplankton and corresponding percentage to the net uptake of nitrogen by phytoplankton (in brackets) compared with the resulting phytoplankton primary production and net and gross (in brackets) bacterial production in mmol N/m2/yr. Also shown is the maximum daily flow into lysis in mmol N/m2/day and day when achieved (in brackets). Values are calculated for the minimum epidemic (Beta8=6.44), for the epidemic with the maximum daily flow into lysis (Beta8=6.9), and for the epidemic with the maximum annual output of viruses (Beta8=14). The lysed phytoplankton debris flows directly into the detritus compartment and the decay time of inactivated viruses is **six months**. Sinking speed of detritus is 10 m/day. Variable contact rate.

Beta8	New production	Regenerated production	Zooplankton grazing	Natural mortality of phytopl.
6.44	317.9	233.9	310.6	129.2
6.9	312.7	210.1	270.0	118.9
14	238.8	88.0	59.1	38.7

Table 5.7 Estimates of annual totals of new and regenerated production, zooplankton grazing and natural mortality of the model phytoplankton in mmol N/m2/year. Values are calculated for the minimum epidemic (Beta8=6.44), for the epidemic with the maximum daily flow into lysis (Beta8=6.9), and for the epidemic with the maximum annual output of viruses (Beta8=14). The lysed phytoplankton debris flows directly into the detritus compartment and the decay time of inactivated viruses is **six months**. Sinking speed of detritus 10m/day. Variable contact rate.

5.16 Summary of experimental characteristics for the simulations represented in each figure of version 1

In all these simulations the Assimilation efficiency (k8) is 1, the viruses are not inactivated and there is no decay time.

Figure number	Contact rate (Beta8)	Sinking rate of detritus (m/day)	Cross-thermocline mixing rate	Natural mortality rate (d^{-1})
5.2. a b	0 - 2.1 0 - 0.5	10m	0.1	0.045
5.3. a,b,c,d 5.7 5.8 5.11 5.12. a,b 5.13. a,b 5.14	minimum 0.03102 maximum 0.06	10	0.1	0.045
5.4. a,b	0.4	10	0.1	0.045
5.5 5.6. a,b	0 - 2 0 - 2.5	10	0.1	0.045
5.9 Model A	maximum 0	10 1	0.1	0.045
5.10. a b	minimum maximum	10	0.01 and 0.1 0.01 and 0.1	0.045
5.15. a,b	maximum	10	0.1	0 0.025 0.045 0.09

5.17 Summary of experimental characteristics for the simulations represented in each figure of version 2

In all these simulations the sinking rate of detritus is 10 md^{-1}, the viruses are not inactivated and decay time is zero.

Figure number	Contact rate-$\beta 8$	Virus assimilation- k8	Cross-thermocline mixing rate	Natural mortality rate-d^{-1}
5.16 a b	0 - 2.1 0 - 0.3	1	0.01	0.05
5.17a,b,c 5.18a,b,c 5.20 5.21 5.22 5.23. a,b	minimum 0.0355 maximum 0.08	1	0.01	0.05
5.19. a,b version 1 version 2	minimum 0.03102 maximum 0.06 minimum 0.0355 maximum 0.08	1	0.1 0.01	0.045 0.05
5.24 5.25 5.26 5.27 5.28 5.29	maximum 0.08	1	0.01	0.05
5.30	maximum 0.08	1	0.1	0.05
5.31a,b,c	maximum 0.08	1	0.01 and 0.1	0.05
5.32	0 - 0.3	.62 1	0.01	0.05
5.33a,b,c 5.34 5.35 5.37	minimum 0.061 maximum 0.13 minimum 0.0355 maximum 0.08	.62 1	0.01	0.05
5.36 a b	minimum 0.061 maximum 0.13	.62	0.01	0.05

5.18 Summary of experimental characteristics for the simulations represented in each figure of version 3

In all these simulations the virus assimilation is .62, the natural mortality is 0.05 d^{-1} and the cross-thermocline mixing rate is 0.01 m/day. The decay time of viruses is zero.

Figure number	Contact rate (Beta8)	Inactivation rate of viruses	Sinking rate (m/day)
5.38	0 - 100	.792	10 and 1
5.39	6 - 25	.792	10
5.40a,b,c	minimum = 6.5 intermediates 7.3 and 7.5 maximum= 14.0	.792	10
5.41a,b,c	minimum=0.061 maximum= 0.13	0	10
	minimum = 6.5 intermed= 6.7 maximum= 14.0	.792	

5.19 Summary of experimental characteristics for the simulations represented in each figure of version 4

In all these simulations the virus assimilation is .62, the natural mortality is 0.05 d^{-1} and the cross-thermocline mixing rate is 0.01 m/day. The sinking speed of detritus is 10m/day.

Figure number	Contact rate (Beta8)	Inactivation rate of viruses	Decay time
5.42 a,b c,d	min=4.1; 8.0 max=9.0; 18.0	.5 and 1	1 month
5.43a,b,c	0 - 16	.792	1 day 1 month 6 months
5.44	0 - 100	1, .792, .5	6 months
5.45	3 - 7	.5	1 month
5.46	1 - 11	.5	0 1 month 3 months 6 months
5.47	6 - 16	.792	0 1 day 1 month 6 months
5.48	6.44	.792	6 months
5.49a,b,c 5.50 a,b	minimum 6.5 6.3 6.4 6.44 6.44-variable maximum 14.0	.792	 0 1 day 1 month 6 months 6 months
5.51 a,b	minimum 6.5 6.3 6.4 6.44	.792	 0 1 day 1 month 6 months
5.52	maximum 14.0	.792	0 1 day 1 month 6 months
5.53 a b c,d	min = 6.4 min = 6.44 max = 14.0	.792	1 month 6 months

5.20 Summary of experimental characteristics for the simulations represented in each figure of version 5

In all these simulations the virus assimilation is .62, the natural mortality is 0.05 d^{-1} and the cross-thermocline mixing rate is 0.01 m/day.

Figure number	Contact rate (Beta8)	Inactivation rate of viruses	Decay time	Sinking speed of detritus (m/day)
5.54 a,b c,d	minimum 6.5 6.3 6.4 6.44 6.44- variable maximum = 14.0	.792	0 1 day 1 month 6 months 6 months	10
5.55	minimum 6.44 (variable)	.792	6 months	10
5.56	minimum 6.5 6.3 6.4 6.44 6.44- variable	.792	0 1 day 1 month 6 months 6 months	10
5.57 a b	6.44- variable 14.0- variable	.792	6 months	10
5.58 a b	0 - 100	1 .792 .5	6 months	10 1
5.59	0 - 18	.792	6 months	10 and 1

5.21 Figures

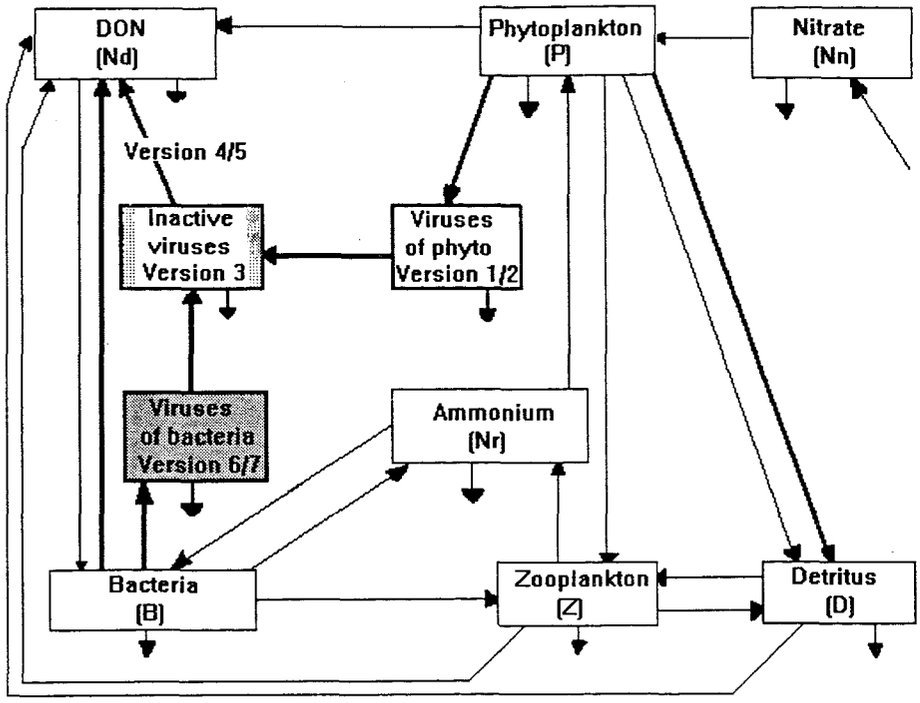

Figure 5.1 Overview of the model development: version 1 and 2 (white); version 3 (vertical stripes); version 4 and 5 (arrow); version 6 and 7 (shaded).

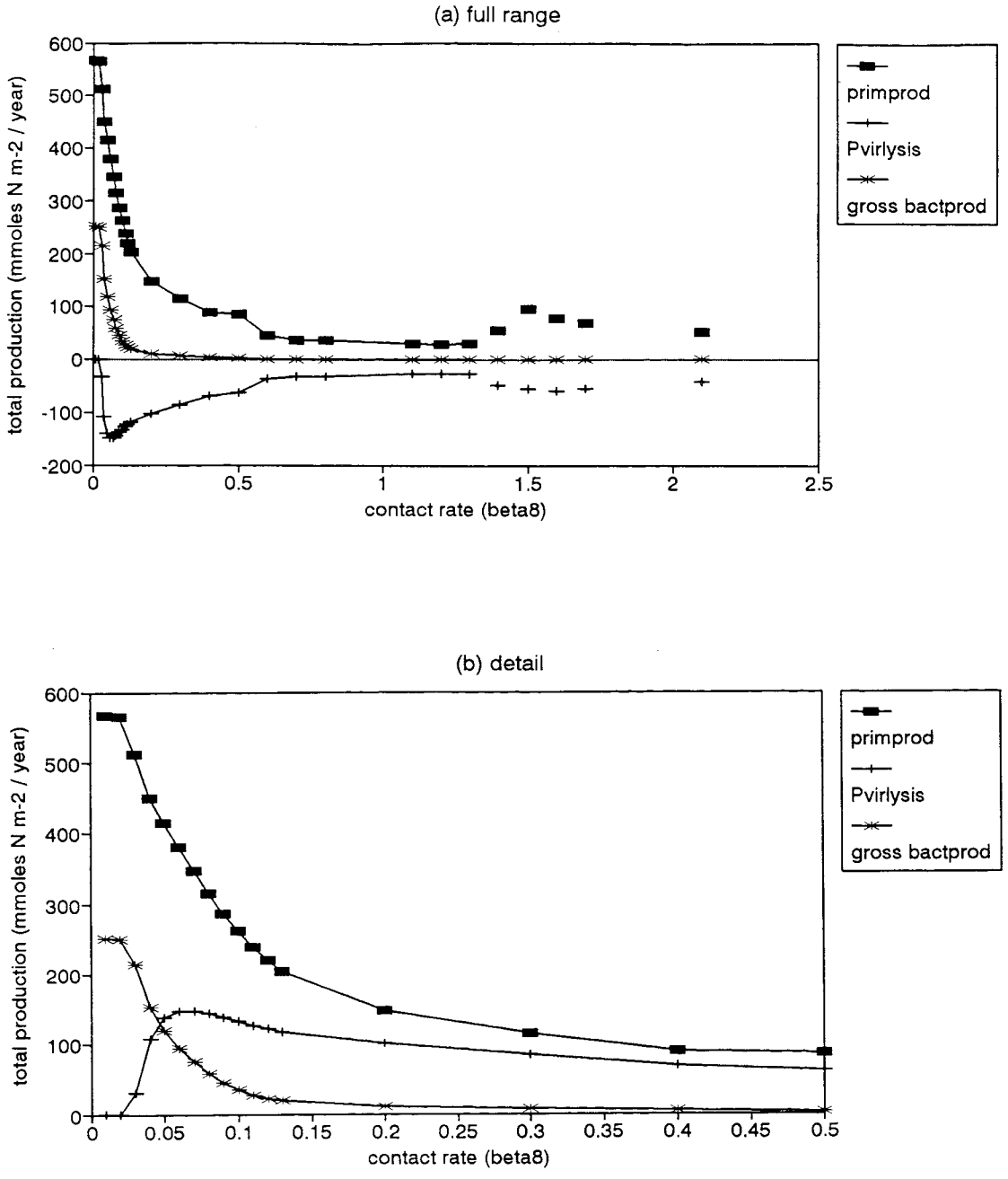

Figure 5.2 Variation in annual primary production (filled square), bacterial production (star) and corresponding losses by phytoplankton
viral lysis (cross) in mMol N/m^2/year, plotted against increasing levels of the contact rate (beta8) in single epidemics of phytoplankton viruses. The inactivation rate of viruses is 0 d^{-1} and the sinking rate of detritus is 10m/day. This version of the model uses a 100% conversion of host biomass into virus.
(a) - Full range of beta8 values (0 - 2.1).
(b) - Detail of beta8 values between 0 - 0.5. Viral lysis shown as positive.

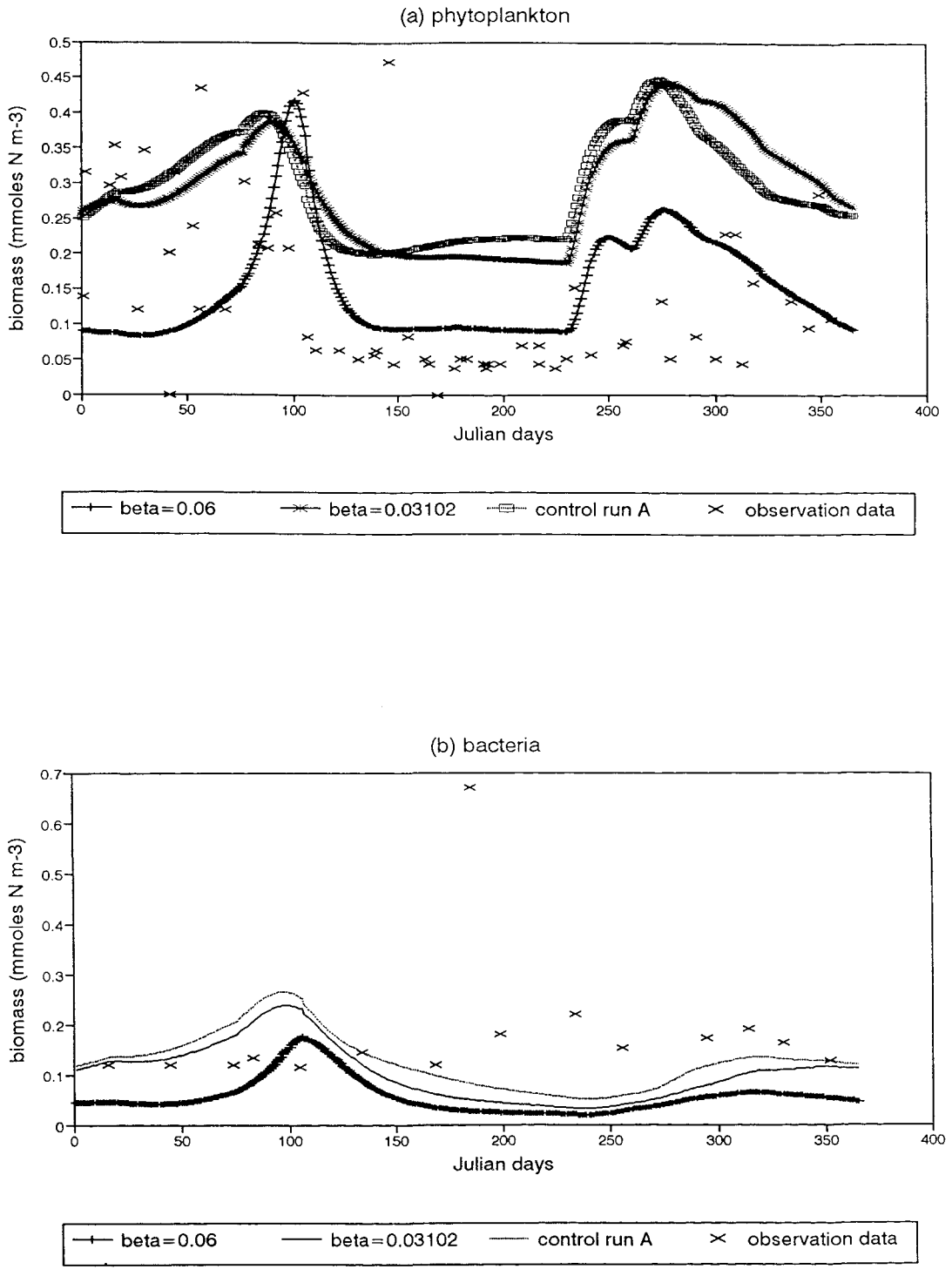

Figure 5.3 Seasonal variation of (a) phytoplankton, (b) bacteria, (c) zooplankton and (d) virus in minimum (star or fine solid line) and maximum (plus) epidemics versus control run A (empty square or dotted).

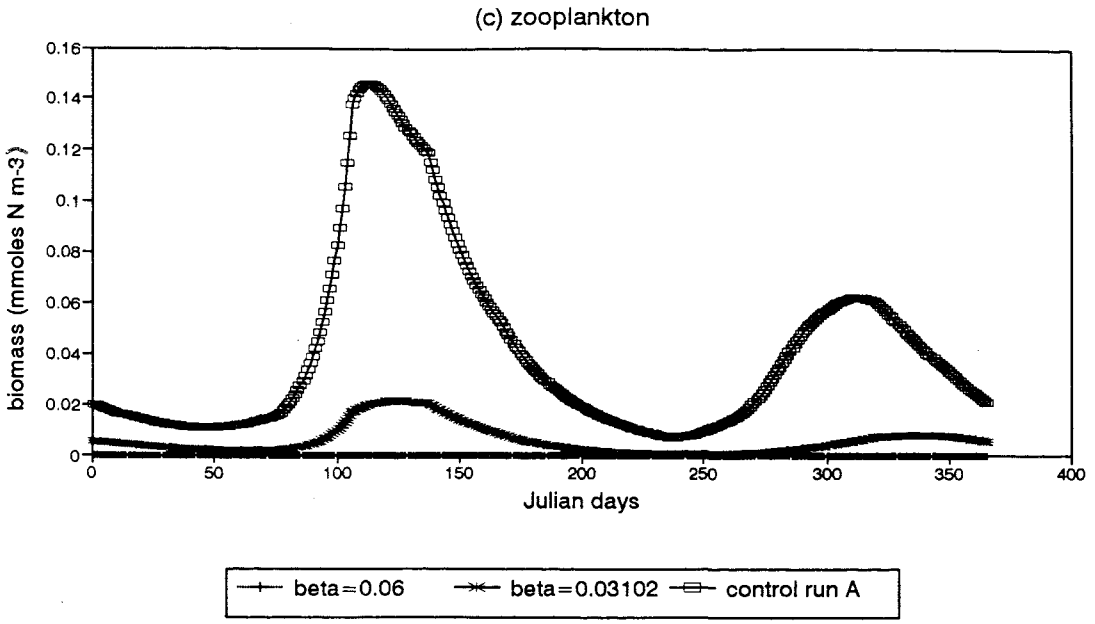

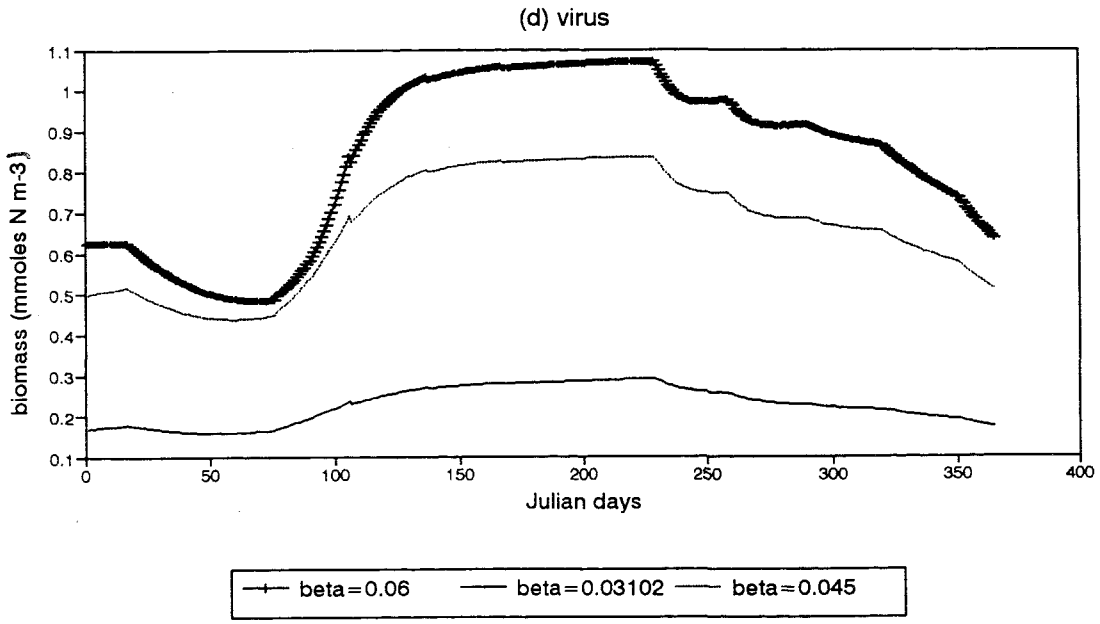

Figure 5.3 - continued

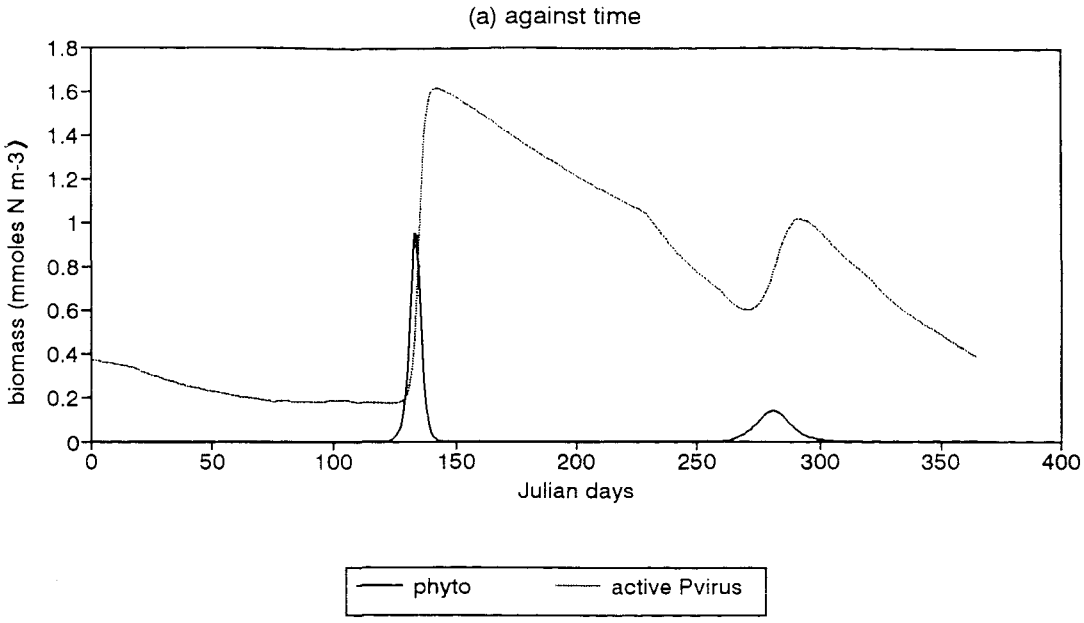

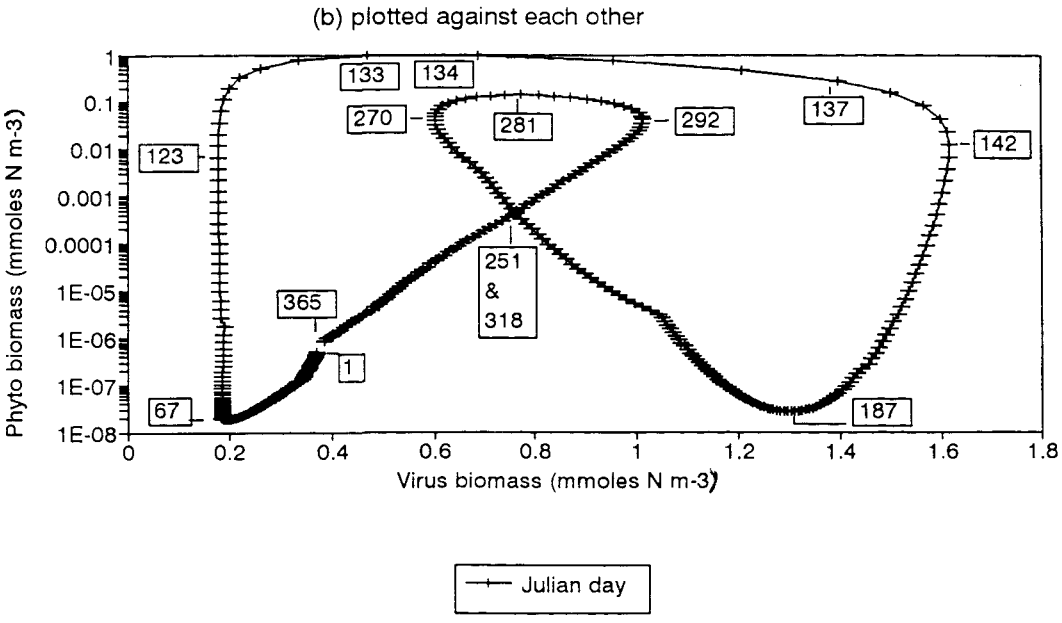

Figure 5.4 Seasonal variation of phytoplankton and virus for a contact rate beta8= 0.4, plotted (a) against time and (b) against each other.

(a) version 1

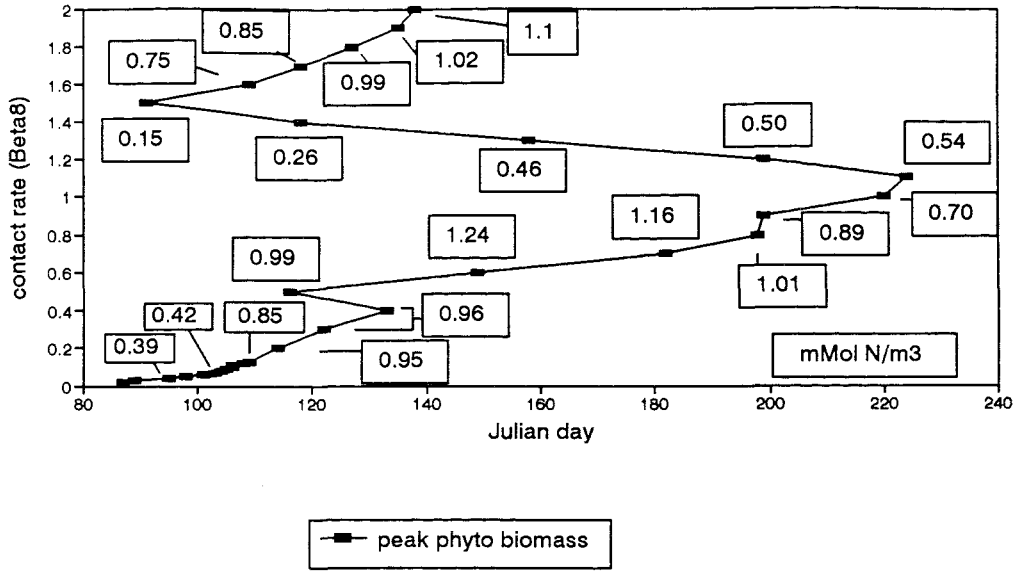

(b) version 2

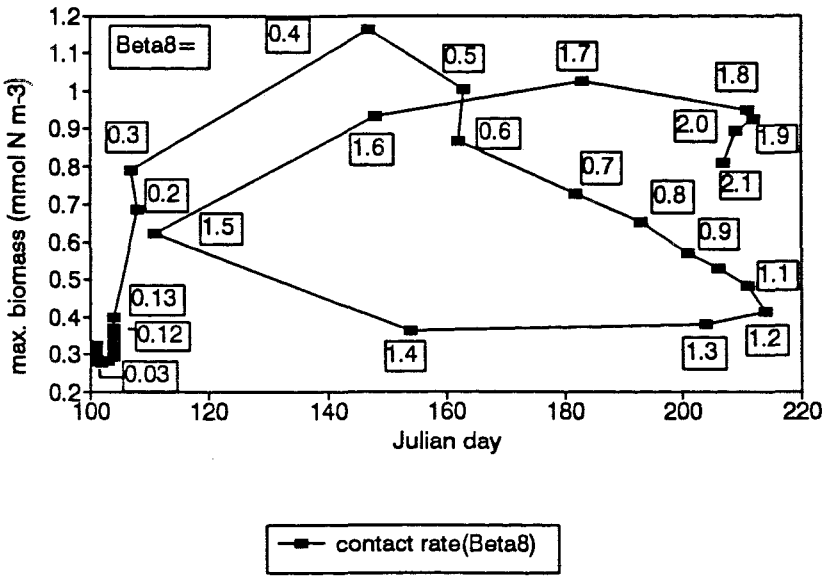

Figure 5.5 Shifting in time of phytoplankton bloom for increasing values of the contact rate (beta8) in (a) version 1 and (b) version 2 of the model.

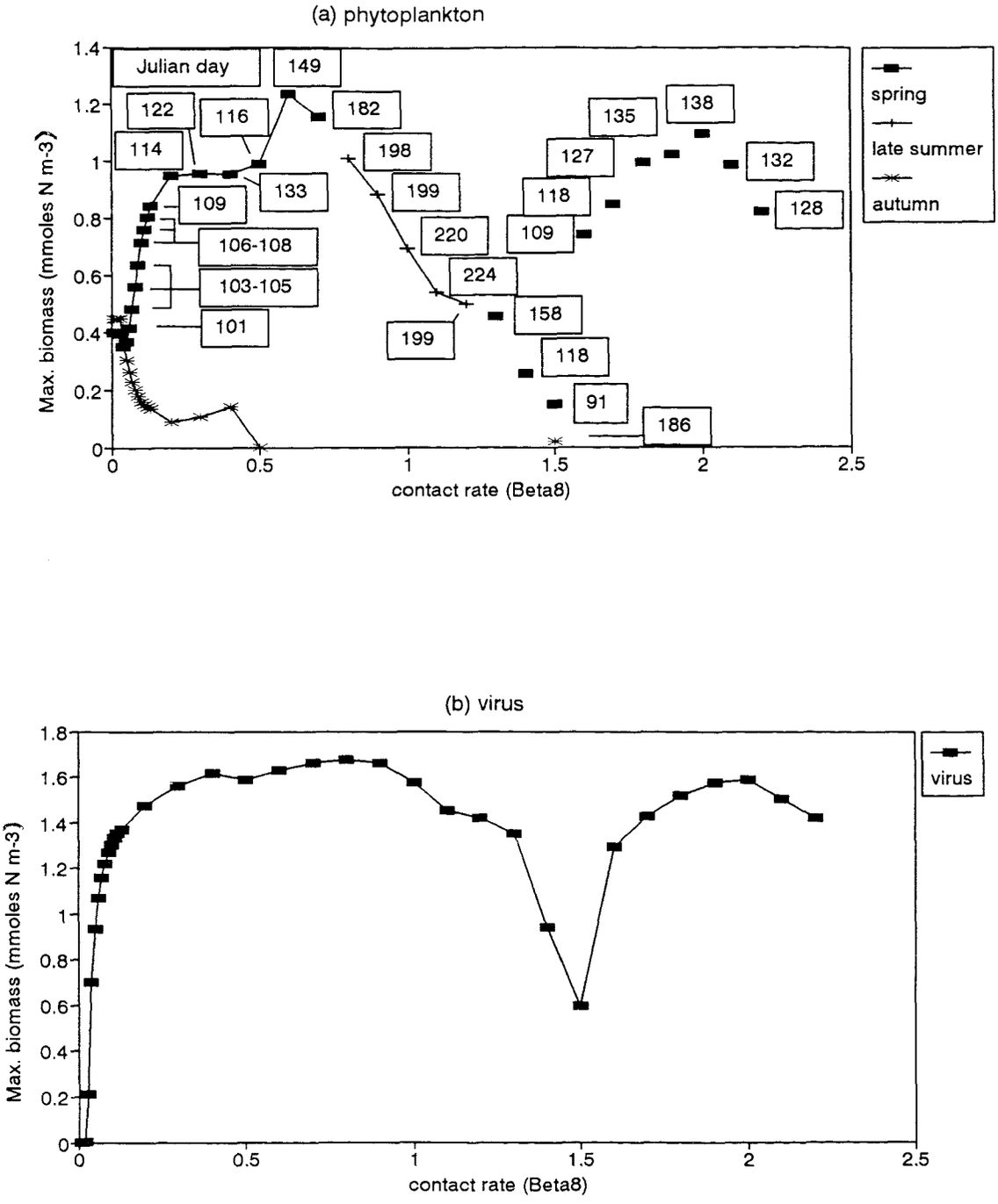

Figure 5.6 Variation of peak biomass values of (a) phytoplankton and (b) virus for increasing values of the contact rate (beta8).

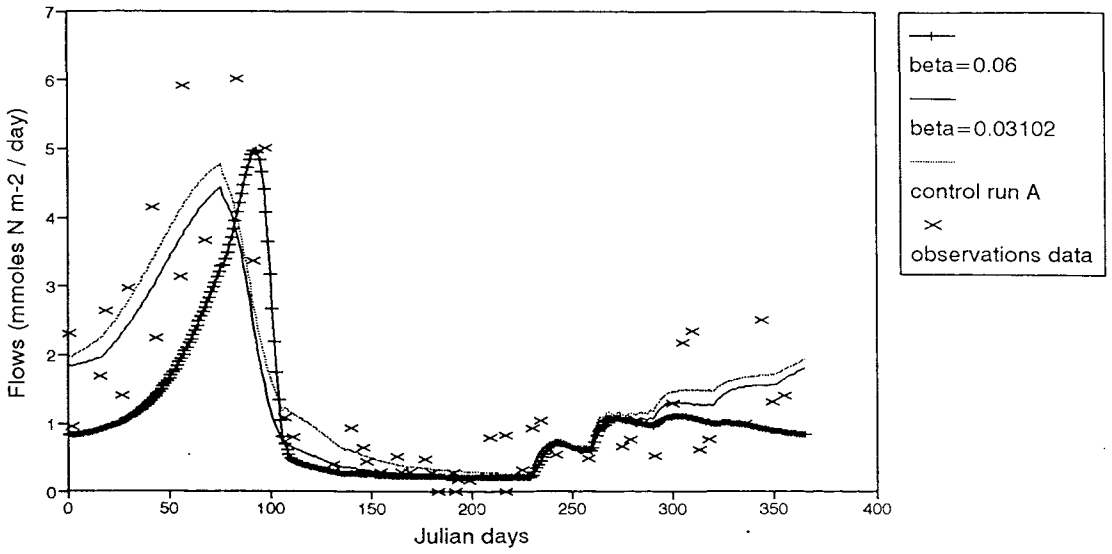

Figure 5.7 Seasonal variation of areal primary production for minimum (solid) and maximum (plus) epidemics versus control run A (dotted).

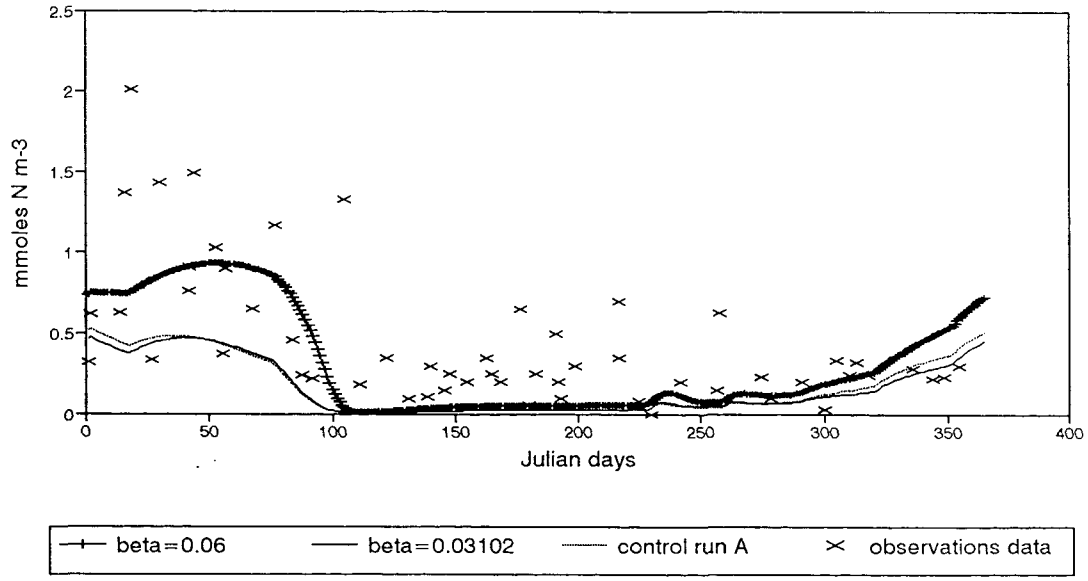

Figure 5.8 Seasonal variation of nitrate concentrations for minimum (fine solid line) and maximum (plus) epidemics versus control run A (dotted).

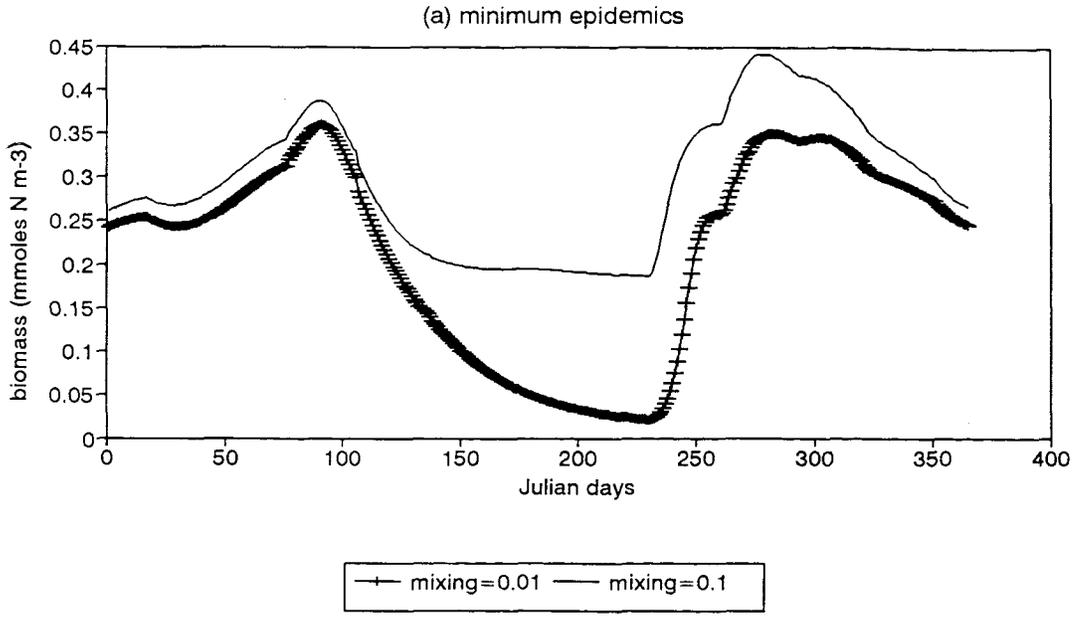

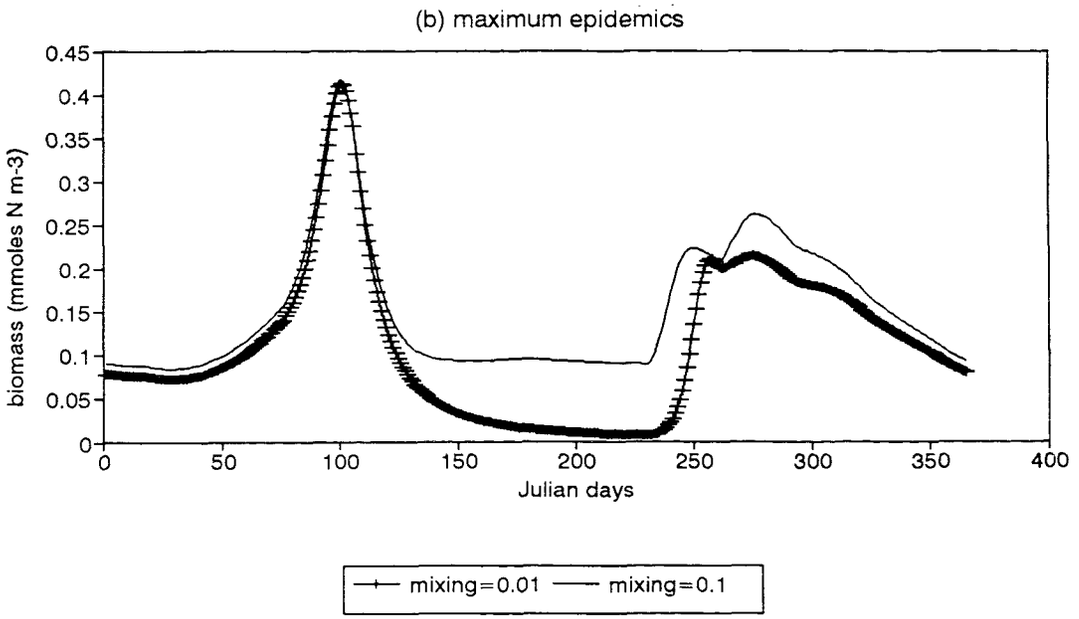

Figure 5.10 Seasonal variation of phytoplankton in (a) minimum and (b) maximum epidemics for cross-thermocline mixing rates of 0.01 (plus) and 0.1 (solid line) m/day.

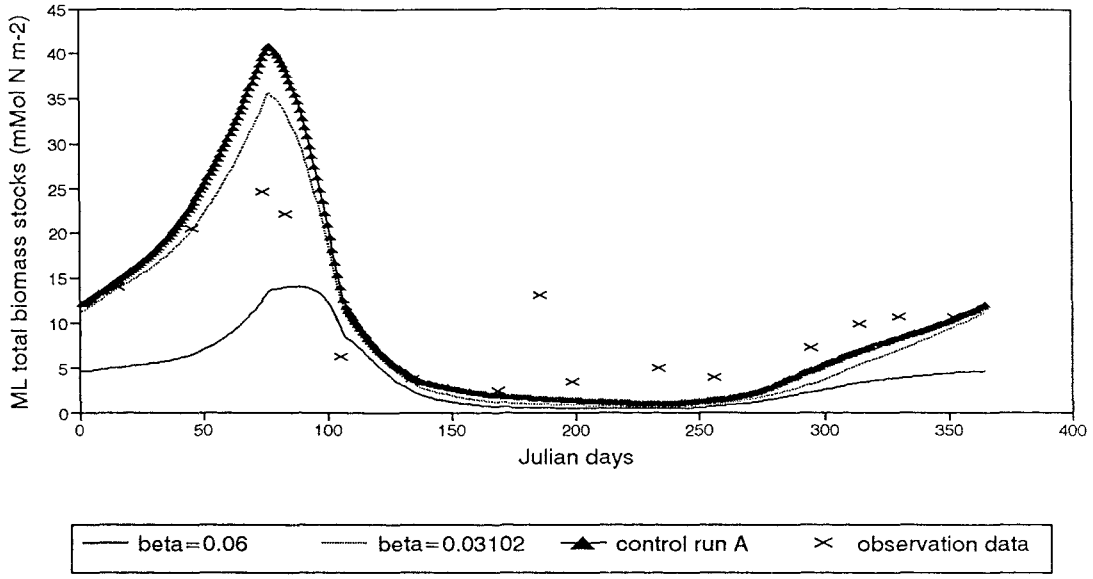

Figure 5.11 Seasonal variation of the areal biomass stock of bacteria for minimum (dotted) and maximum (solid line) epidemics versus control run A (triangle).

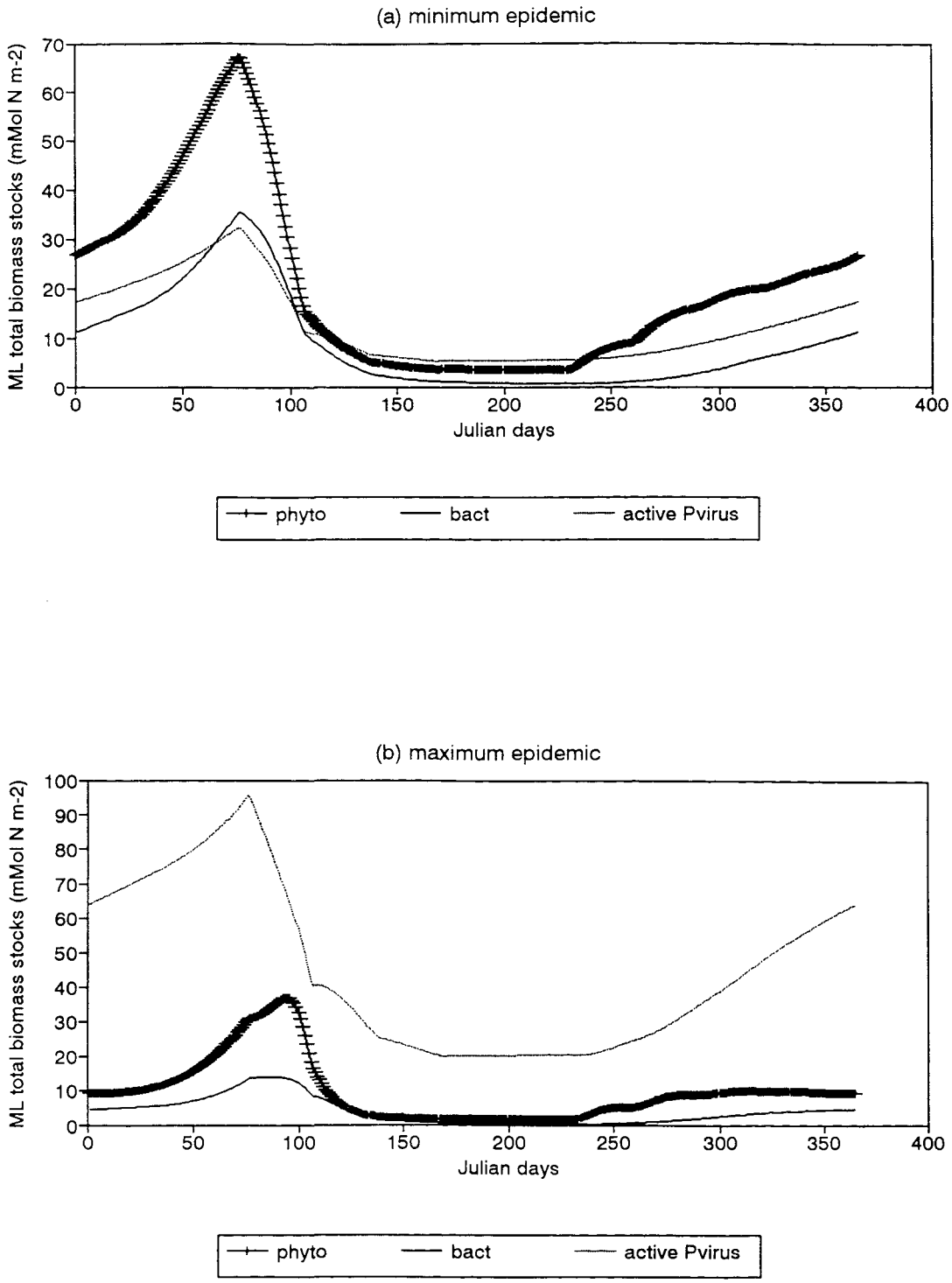

Figure 5.12 Seasonal variation of areal biomass stocks of phytoplankton (plus), bacteria (solid line) and virus (dotted) in (a) minimum and (b) maximum epidemic.

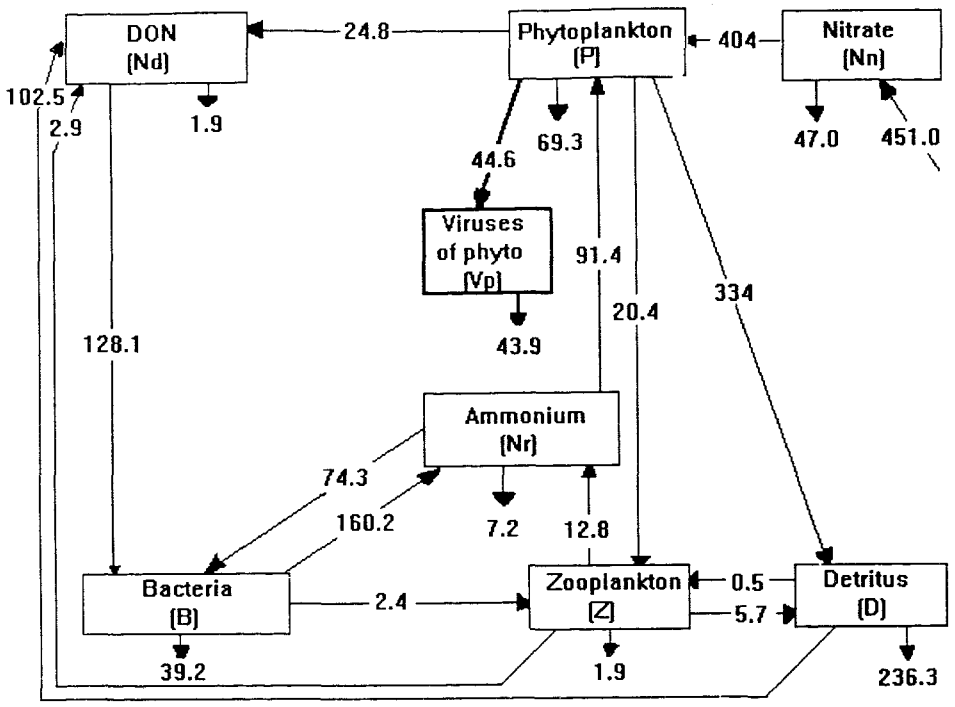

a Minimum epidemics Beta 8=0.03102 k8 = 1 sink=10 mixing=0.1

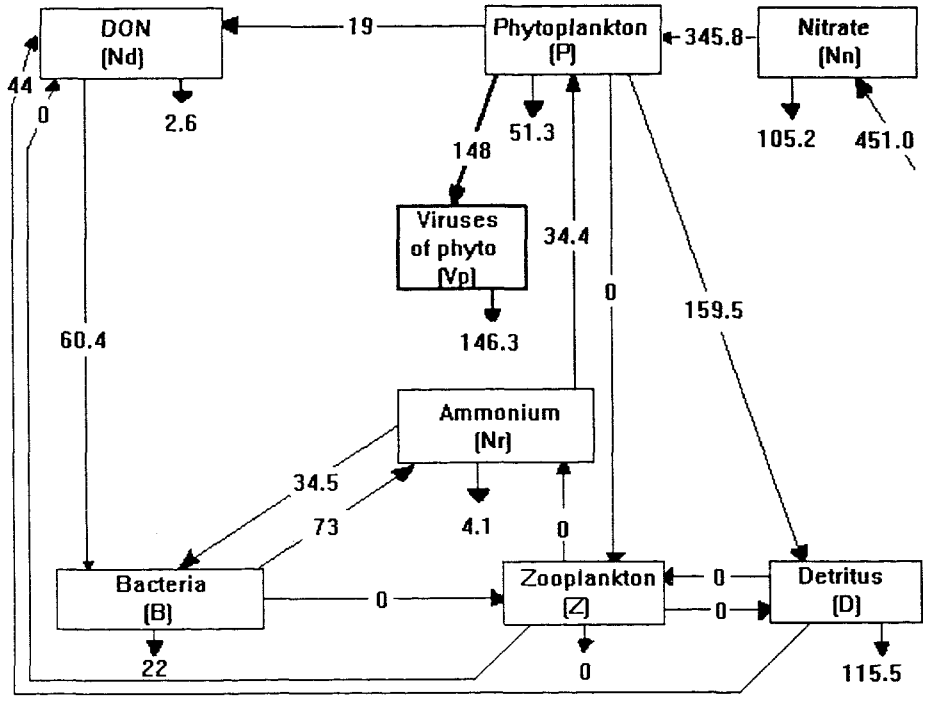

b Maximum epidemics Beta 8=0.06 k8=1 sink rate=10 mixing=0.1

Figure 5.13 Annual inter-compartment flows of nitrogen for (a) minimum and (b) maximum epidemic simulations in version 1 with a mixing rate of 0.1m d^{-1}.

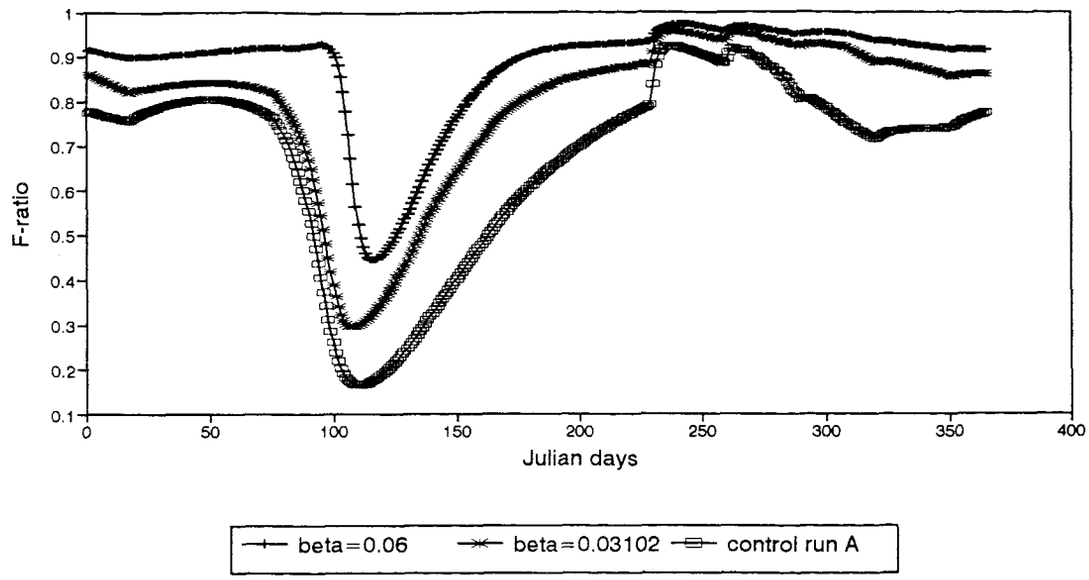

Figure 5.14 Comparison of f-ratios for minimum (star) and maximum (plus) epidemics and control run A (empty square).

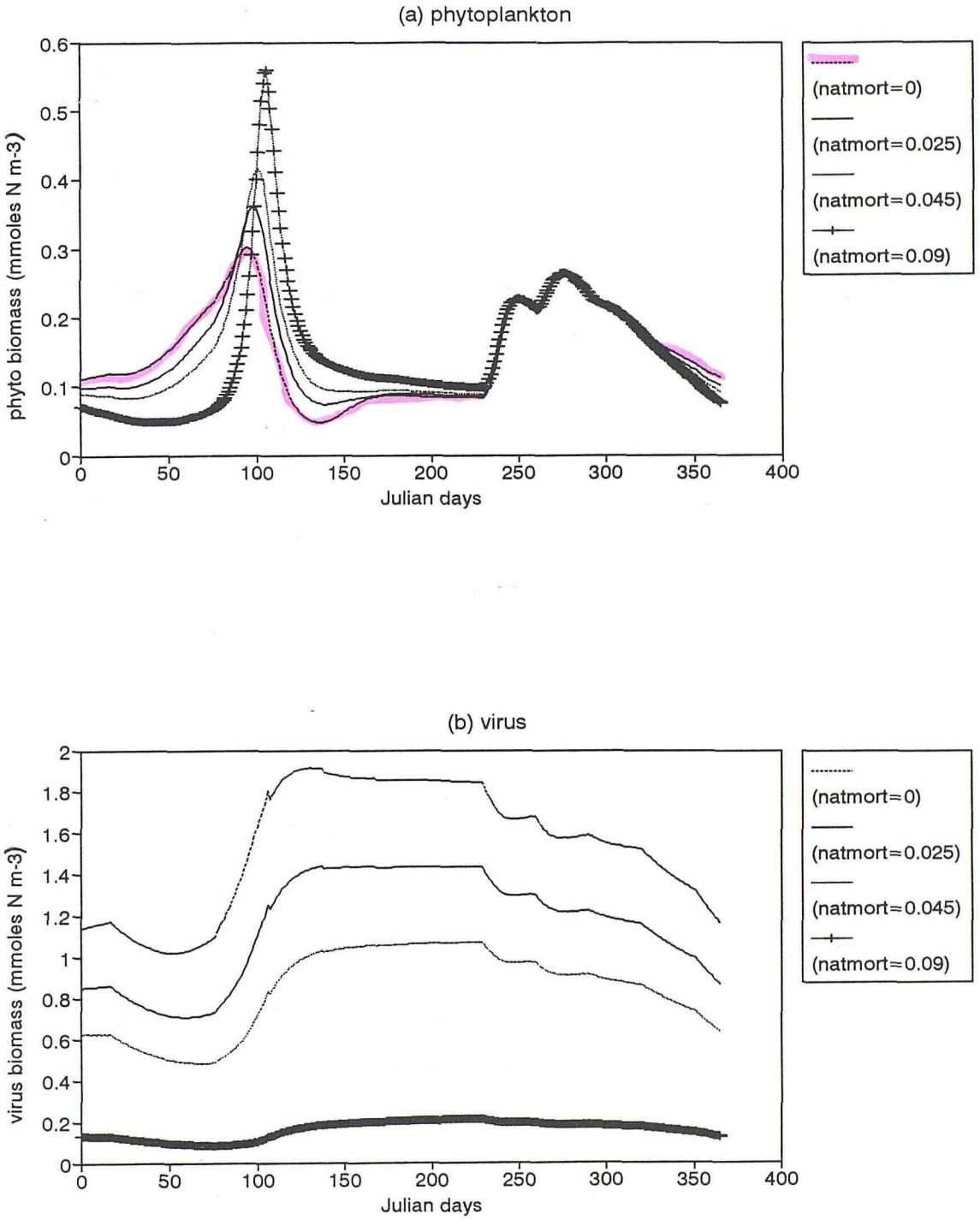

Figure 5.15 Annual cycles of (a) phytoplankton and (b) virus biomass for different levels of phytoplankton natural mortality.

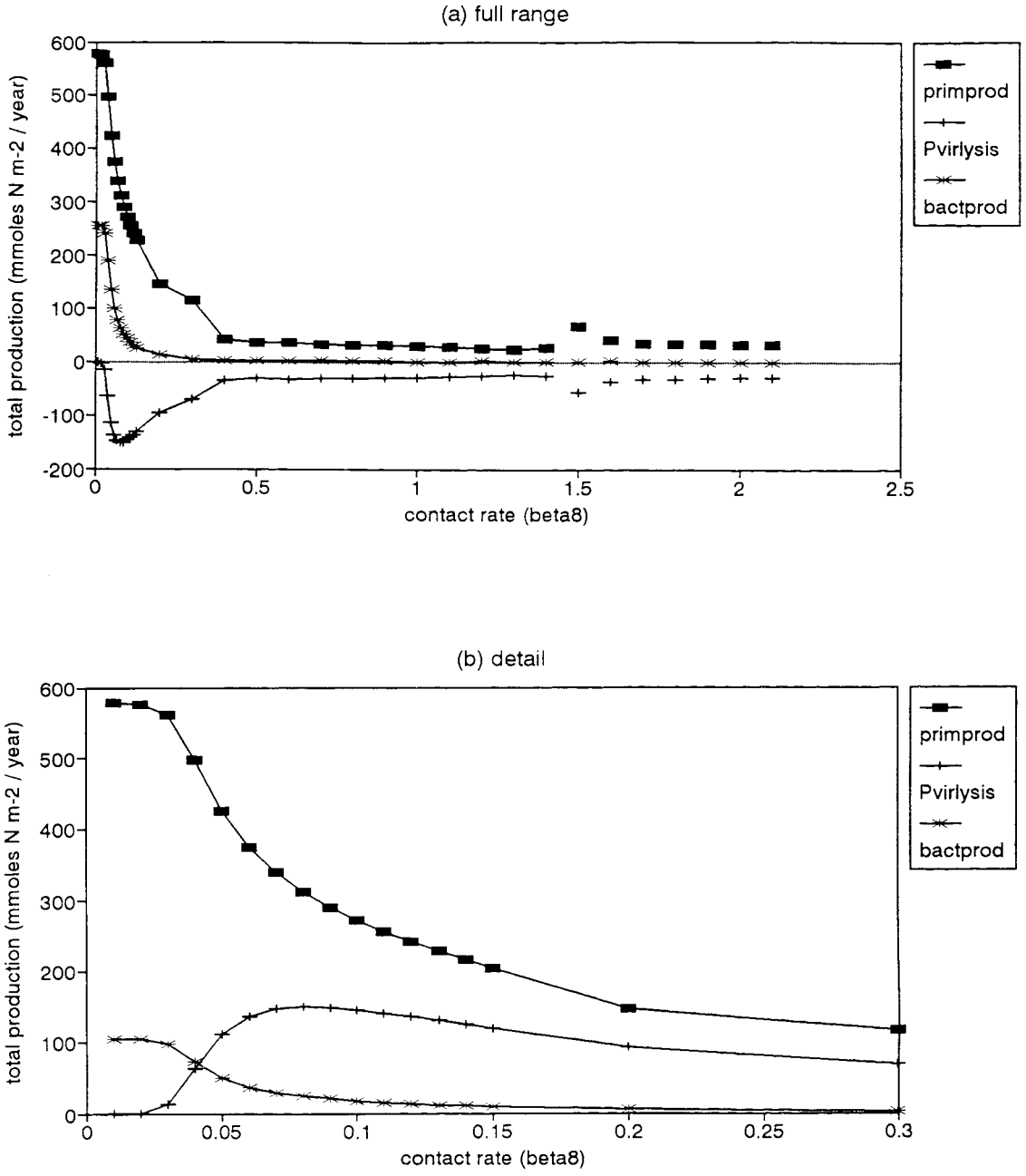

Figure 5.16 Variation in annual primary production (filled square), bacterial production (star) and corresponding losses by phytoplankton viral lysis (plus) in mMol N/m^2/year, plotted against increasing levels of the contact rate (beta8) in single epidemics of phytoplankton viruses. The inactivation rate of viruses is 0 d^{-1} and the sinking rate of detritus is 10m/day. This version of the model uses a 100% conversion of host biomass into virus.
(a) - Full range of beta8 values (0 - 2.1)
(b) - Detail of beta8 values between 0 - 0.3.

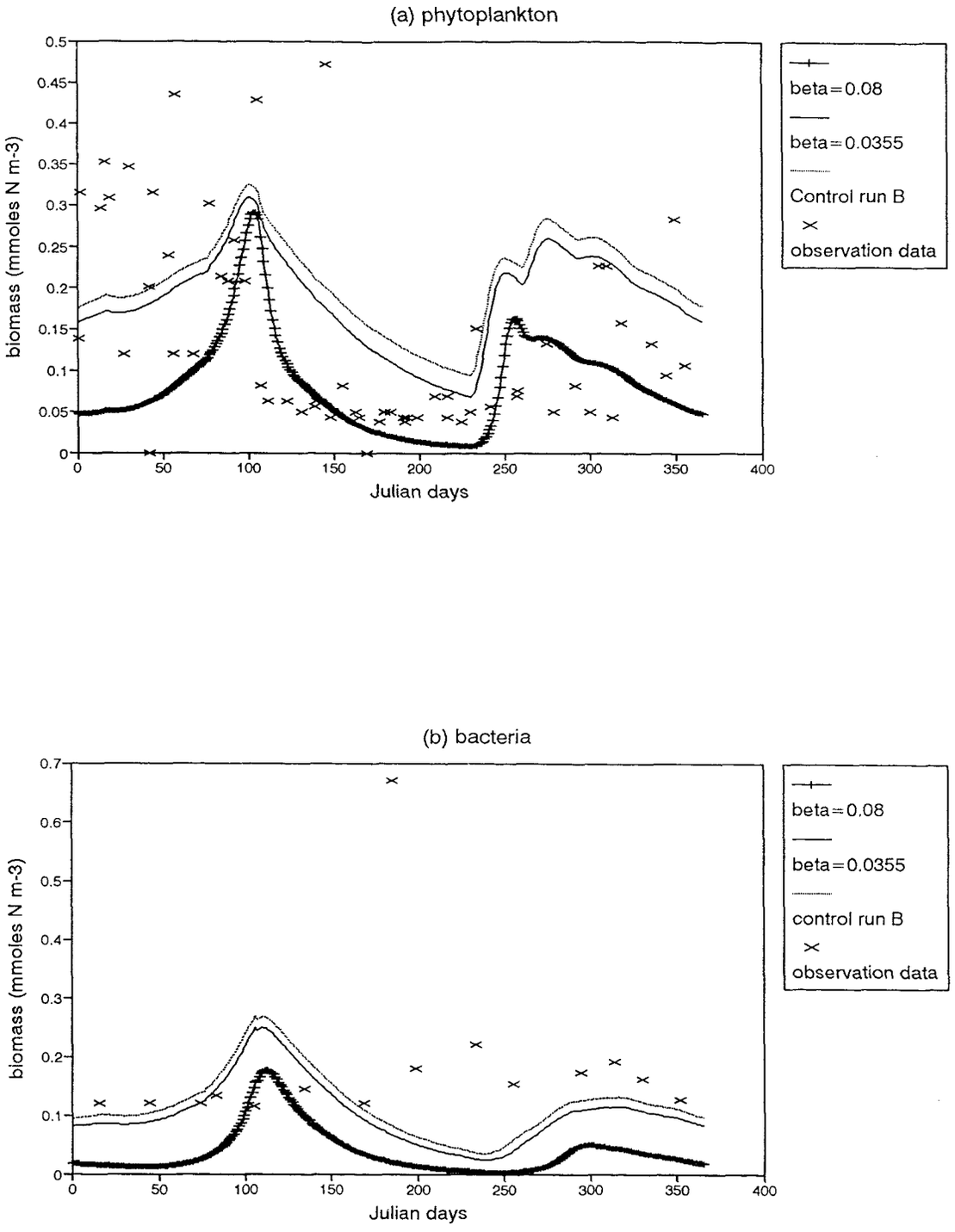

Figure 5.17 Seasonal variation of (a) phytoplankton, (b) bacteria and (c) zooplankton biomass in minimum (solid line) and maximum (plus) epidemics versus control run B (dotted) and control run A (heavy dotted).

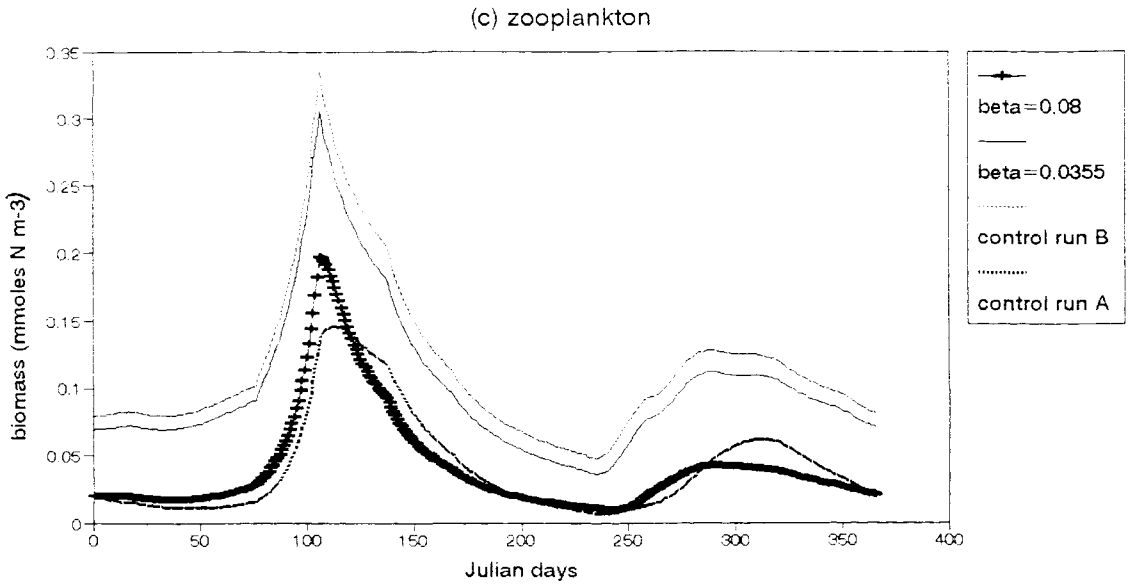

Figure 5.17 -continued

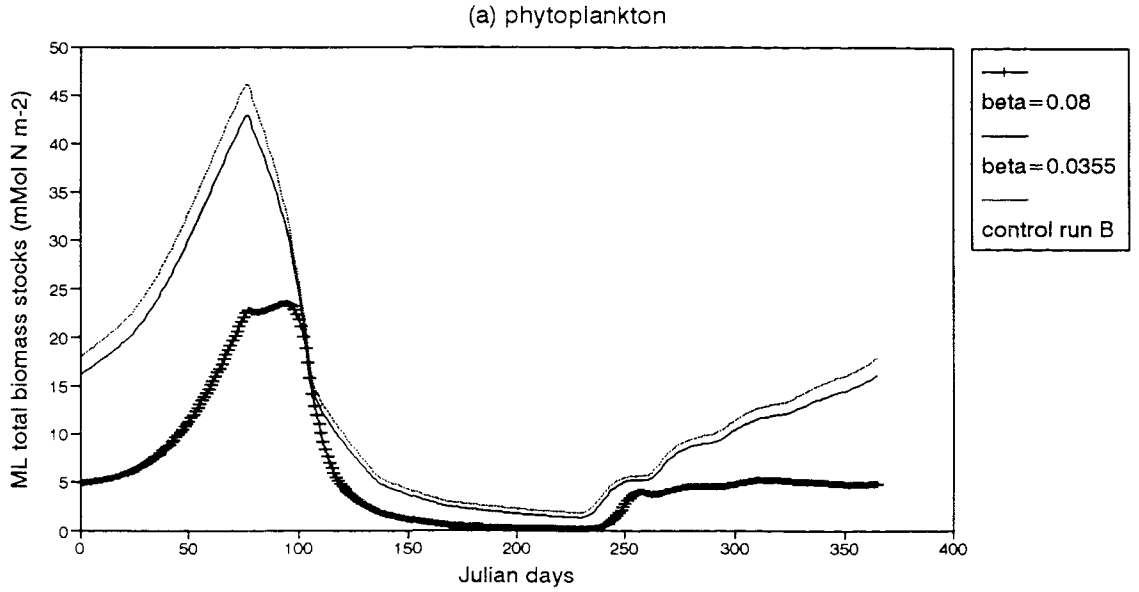

Figure 5.18 Seasonal variation of (a) phytoplankton, (b) bacteria and (c) zooplankton total mixed-layer stocks in minimum (solid line) and maximum (plus) epidemics versus control run B (dotted).

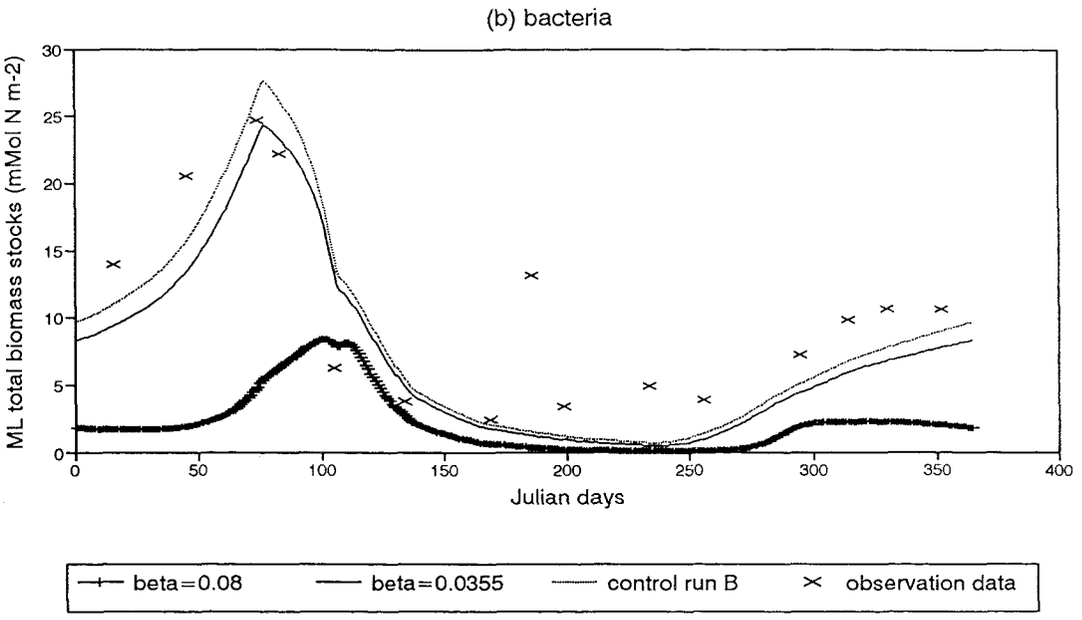

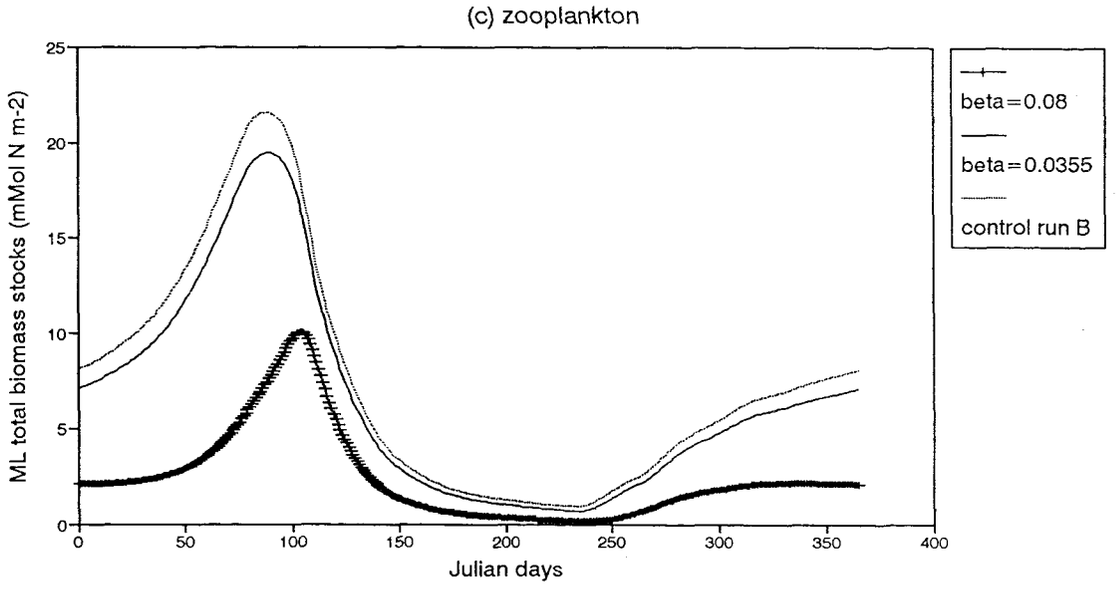

Figure 18 - continued

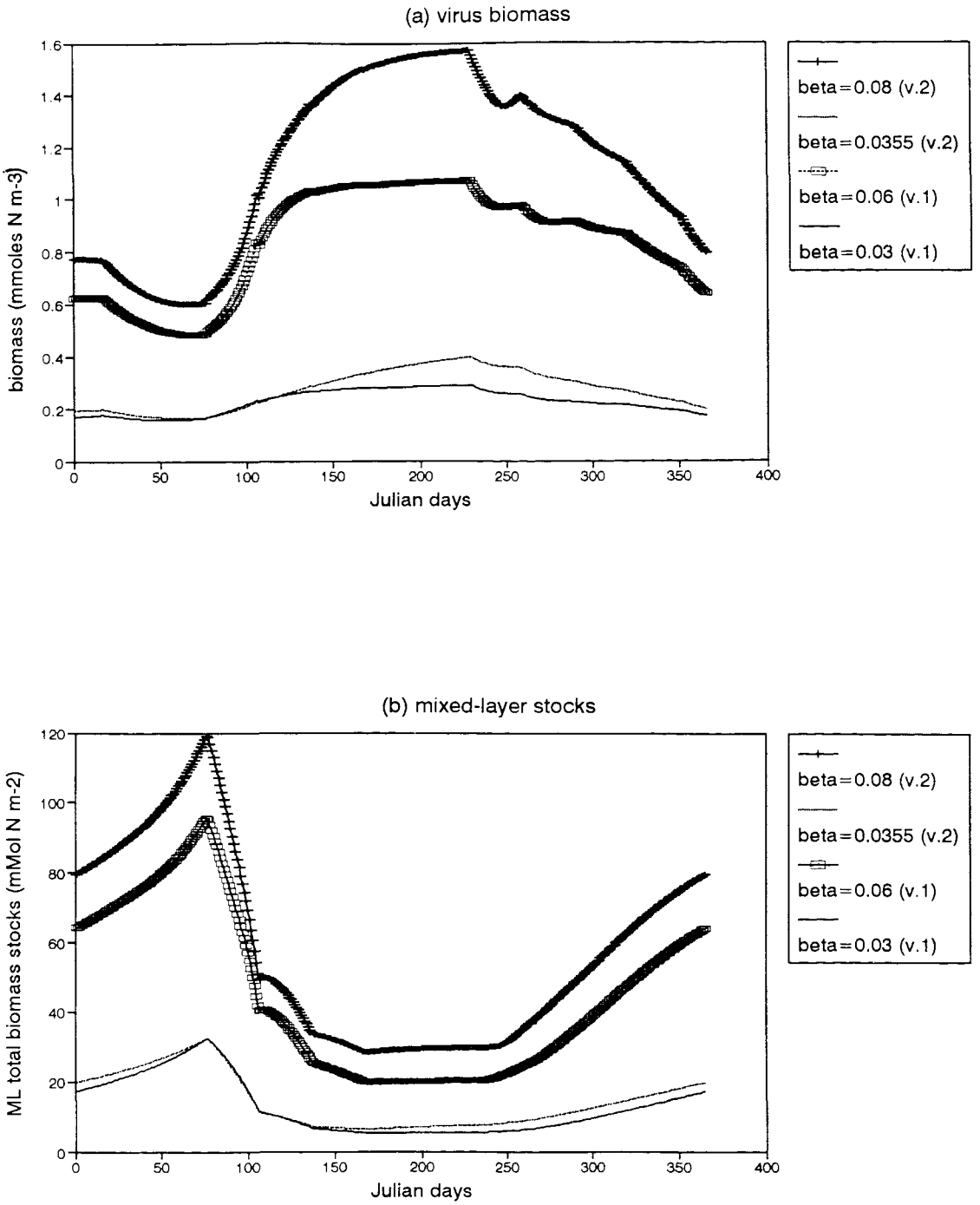

Figure 5.19 Comparison of the annual cycles of (a) virus biomass and (b) total mixed-layer stocks of viruses for minimum and maximum epidemics in versions 1 & 2 of the model. Version 1 - Max. (empty square), Min. (solid line) Version 2 - Max. (plus), Min. (dotted).

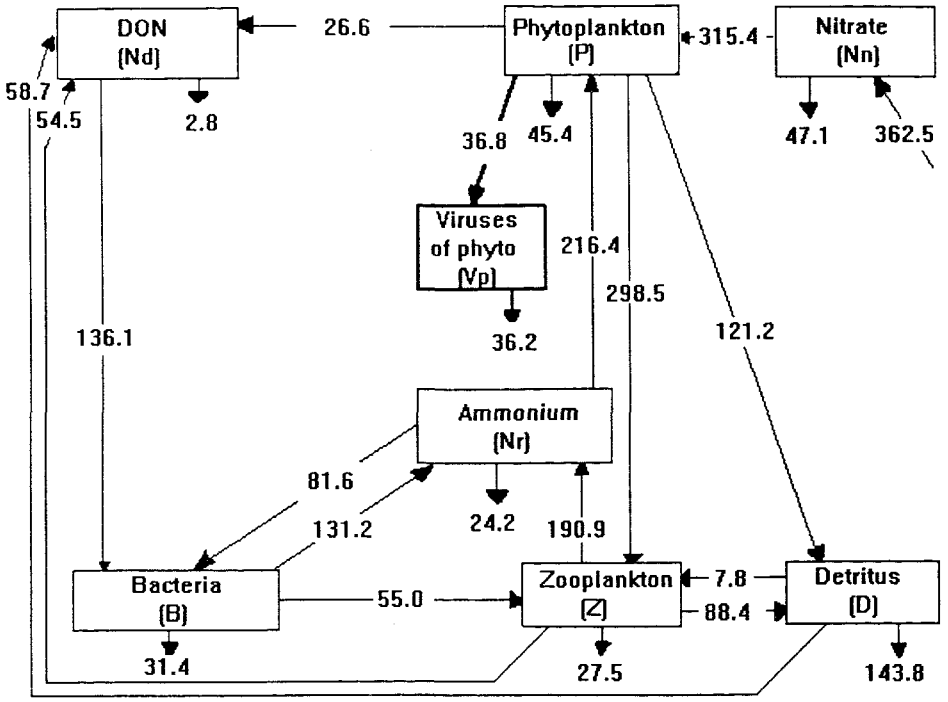

a Minimum epidemics Beta 8=0.0355 k8=1 sink=10 mixing= 0.01

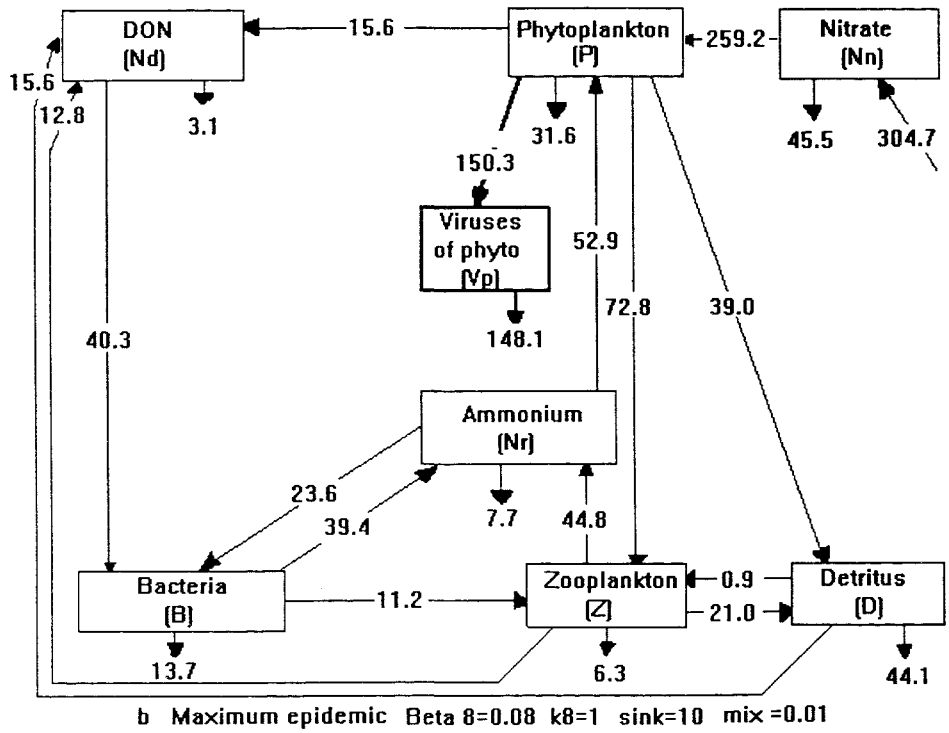

b Maximum epidemic Beta 8=0.08 k8=1 sink=10 mix =0.01

Figure 5.20 Annual inter-compartment flows of nitrogen for (a) minimum and (b) maximum epidemic simulations in version 2 with a mixing rate of 0.01m d^{-1}.

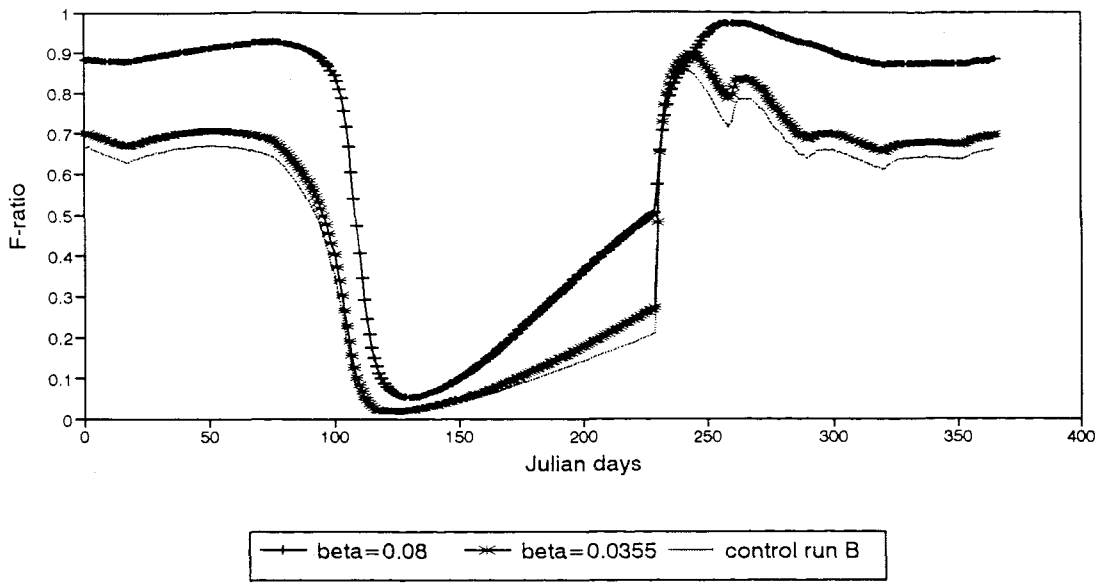

Figure 5.21 Comparison of f-ratios for minimum (star) and maximum (plus) epidemics and control run B (dotted).

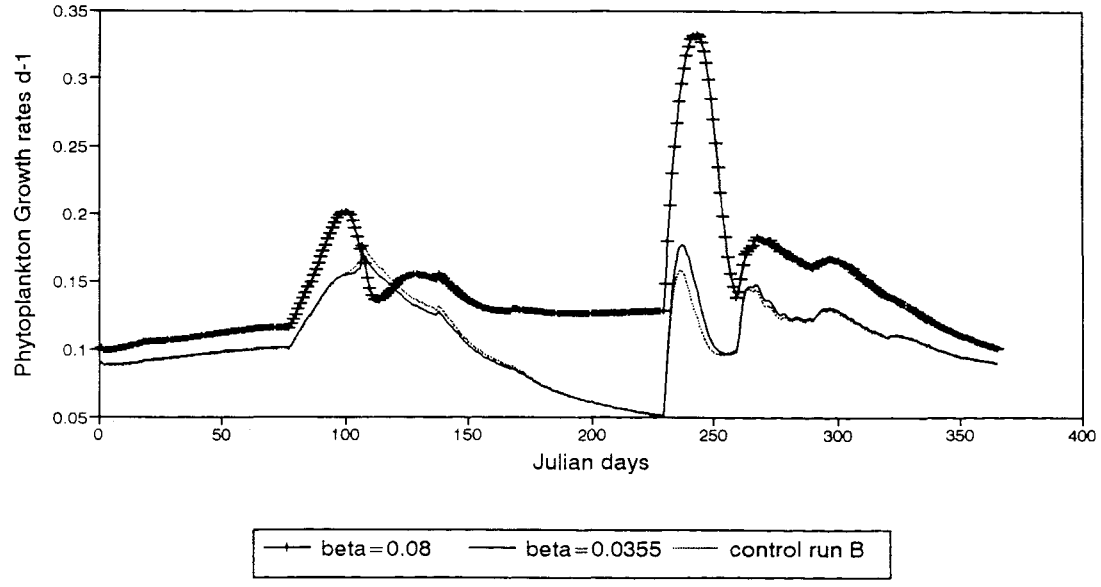

Figure 5.22 Seasonal variation of the specific phytoplankton growth rate μ_p for minimum (solid line) and maximum (plus) epidemic and control run B (dotted).

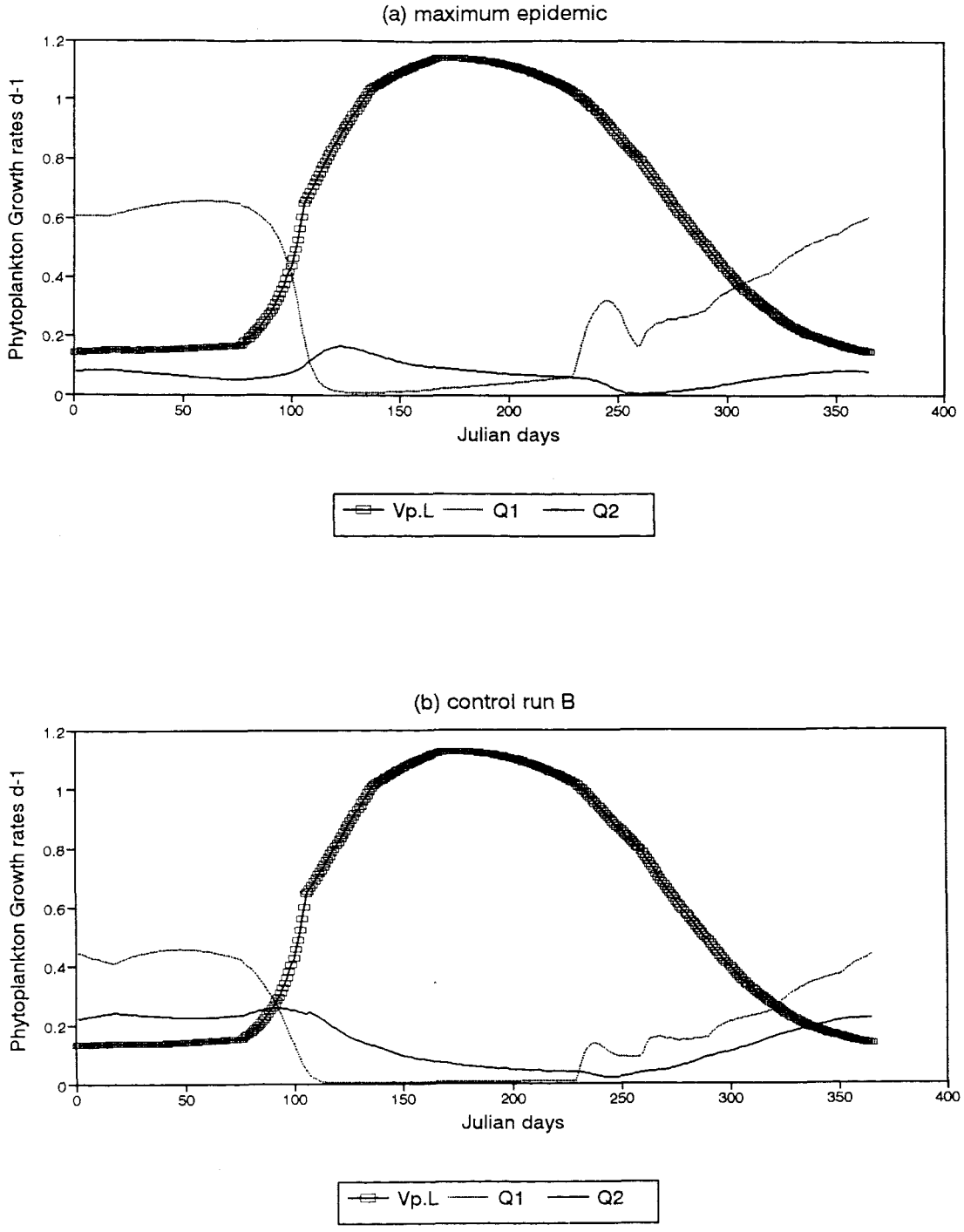

Figure 5.23 Control of phytoplankton growth rate by light (Vp.L) - empty square - and nutrients (nitrate - dotted; ammonium - solid line) limiting effects in (a) maximum epidemic and (b) control run B.

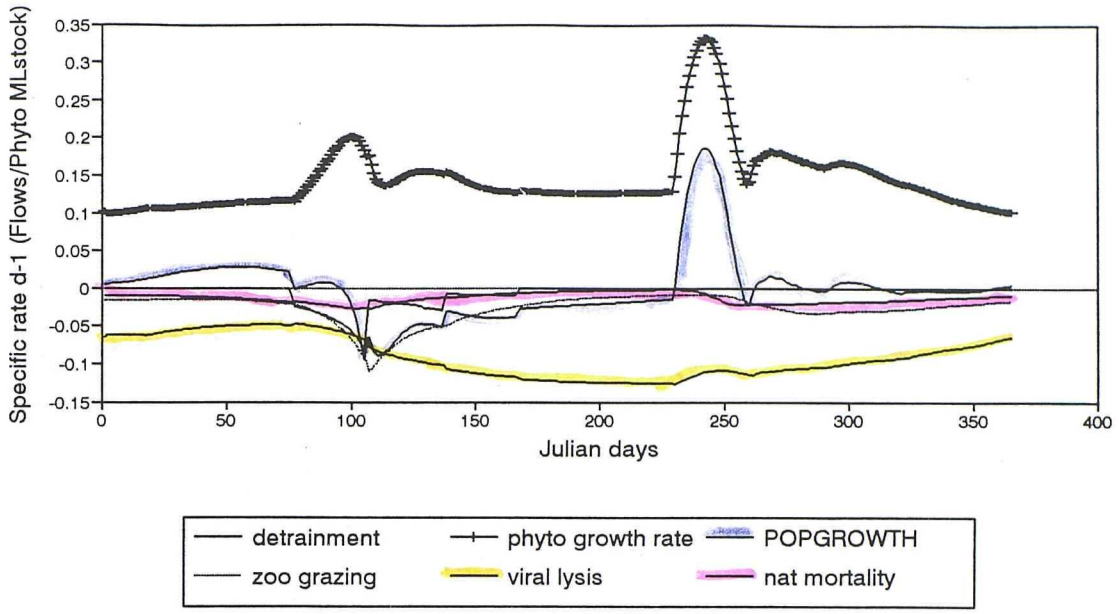

Figure 5.24 Specific rates of phytoplankton loss terms (detrainment - solid line; zooplankton grazing - dotted; viral lysis - yellow; natural mortality - red), phytoplankton growth rate (plus) and population growth (blue) for the maximum epidemic.

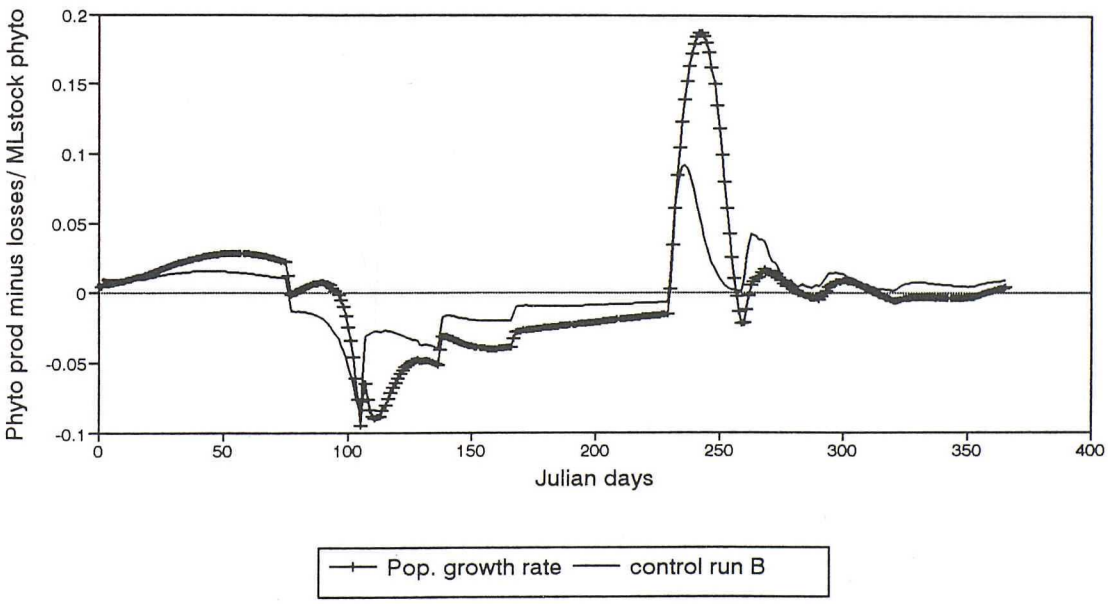

Figure 5.25 Growth rate of the phytoplankton population for the maximum epidemic (plus) and control run B (solid line).

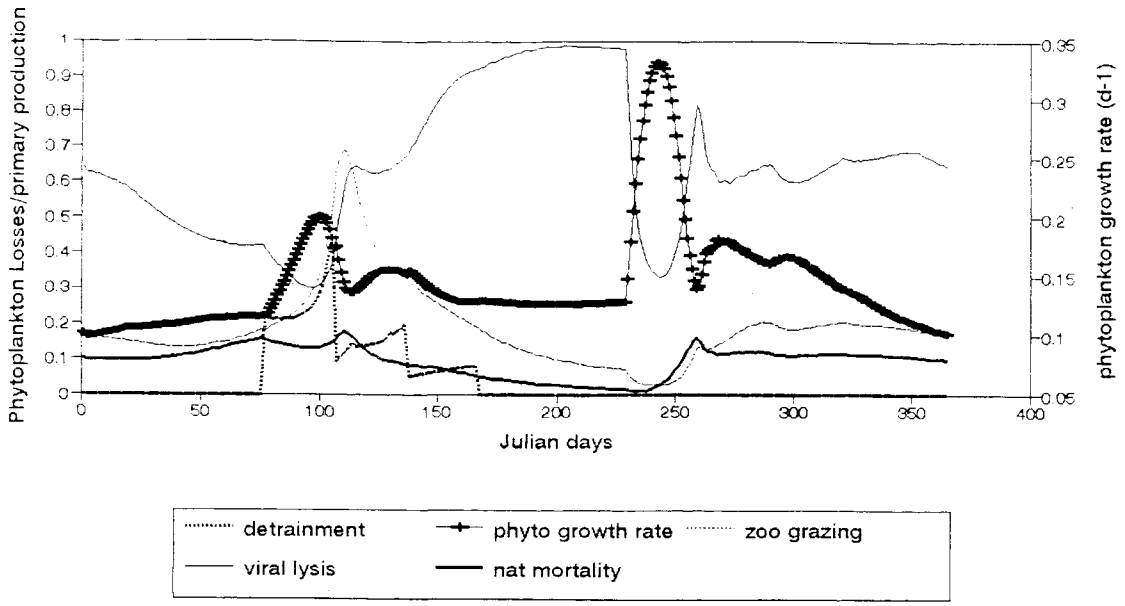

Figure 5.26 Seasonal changes in the specific loss rate of primary prodution for the maximum epidemic. Detrainment - heavy dotted; zooplankton grazing - dotted; virus lysis - solid line; natural mortality - heavy solid; growth rate of phytoplankton - plus.

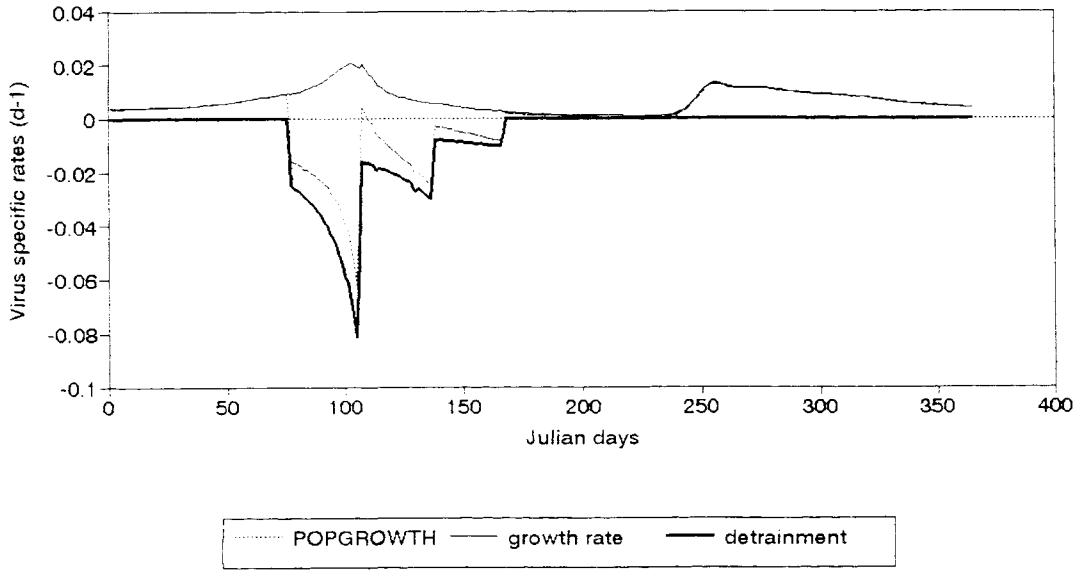

Figure 5.27 Seasonal cycle of net specific growth of virus biomass for the maximum epidemic. Population growth - dotted; growth rate - solid; detrainment - heavy solid.

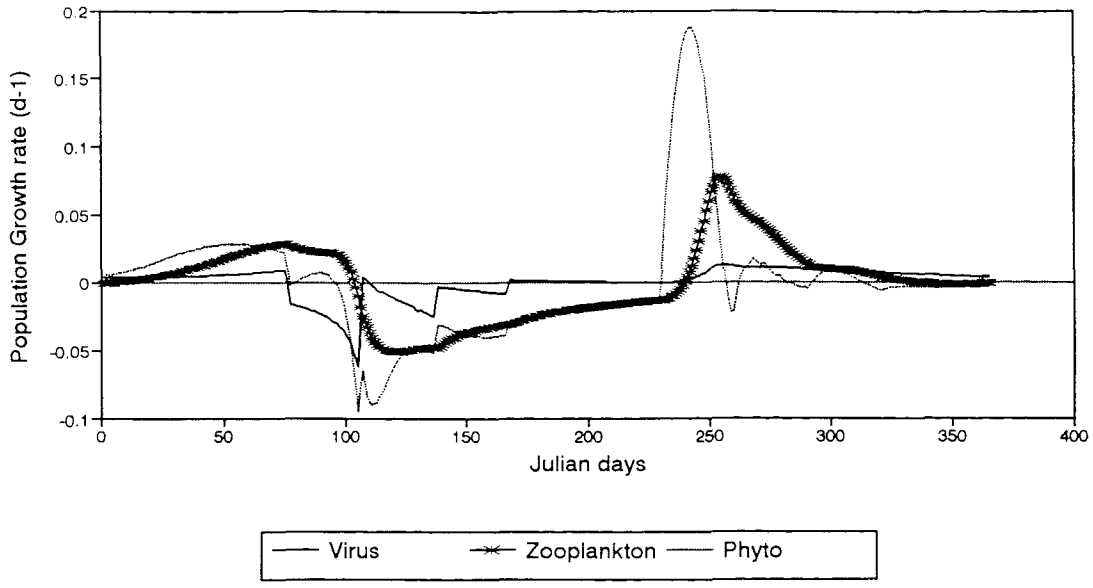

Figure 5.28 Population growth rate of virus (solid line), zooplankton (star) and phytoplankton (dotted) for the maximum epidemic.

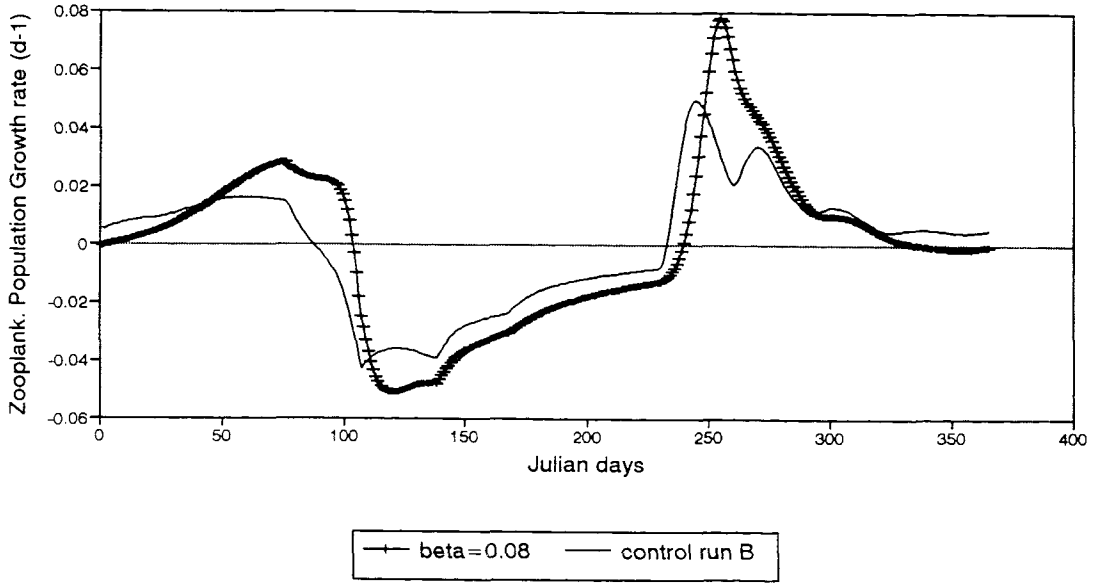

Figure 5.29 Growth rate of the zooplankton population for the maximum epidemic (plus) and control run B (solid).

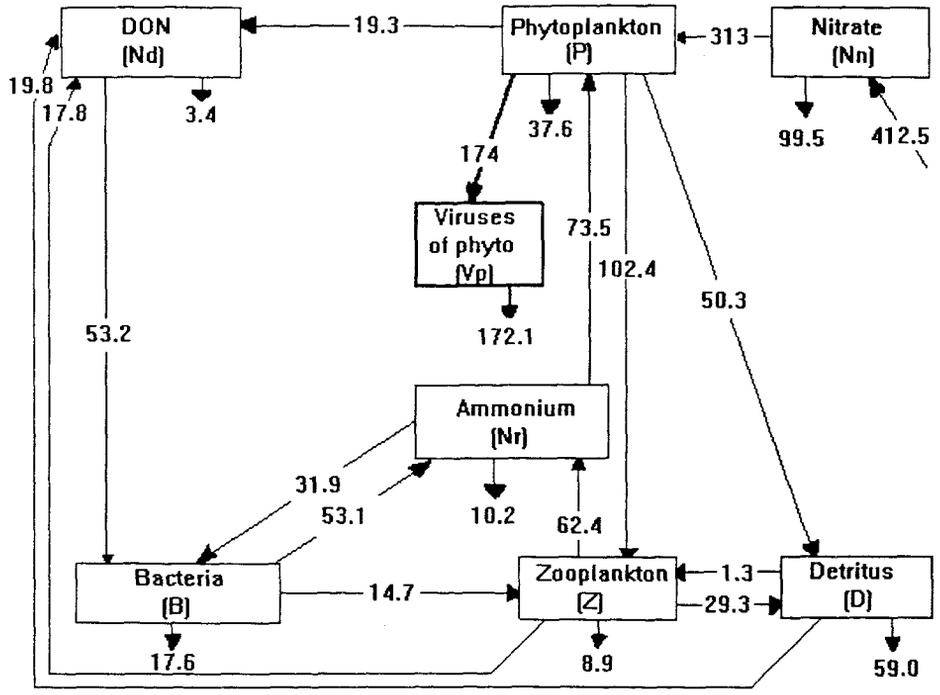

Figure 5.30 Annual intercompartment flows of nitrogen for maximum epidemic in version 2 with a mixing rate of 0.1m d^{-1}.

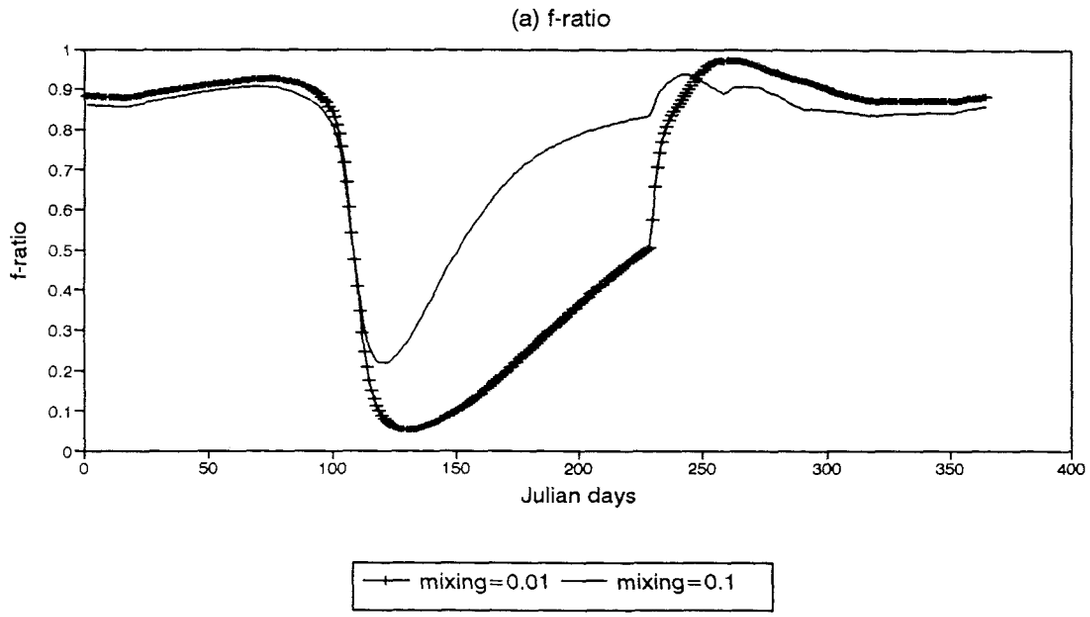

Figure 5. 31 Comparison of (a) f-ratios, (b) and (c) virus biomass for the maximum epidemic with a mixing rate of 0.01 m d^{-1} (plus) and 0.1 m d^{-1} (solid line).

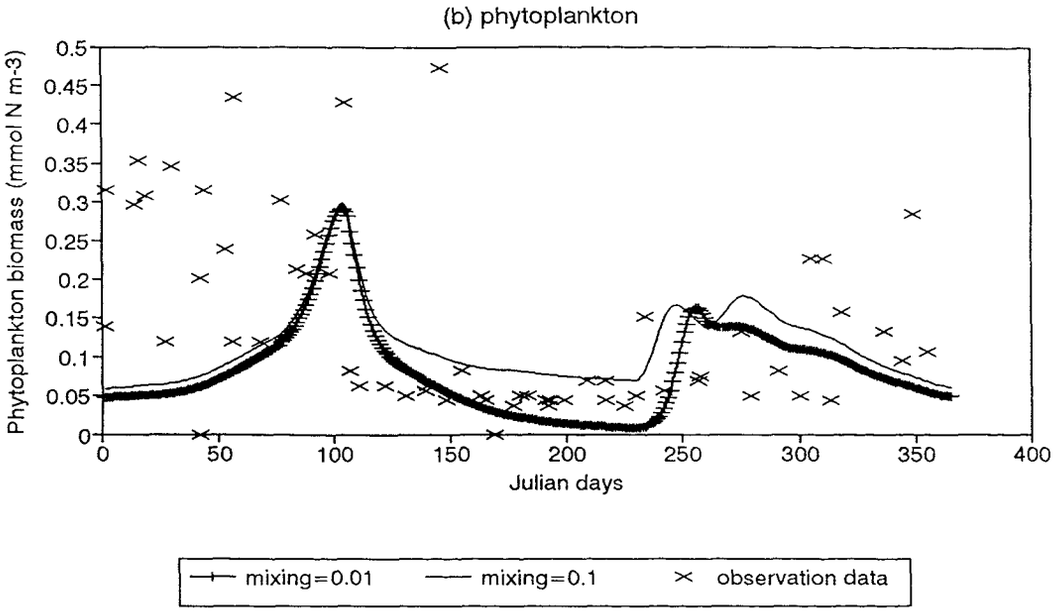

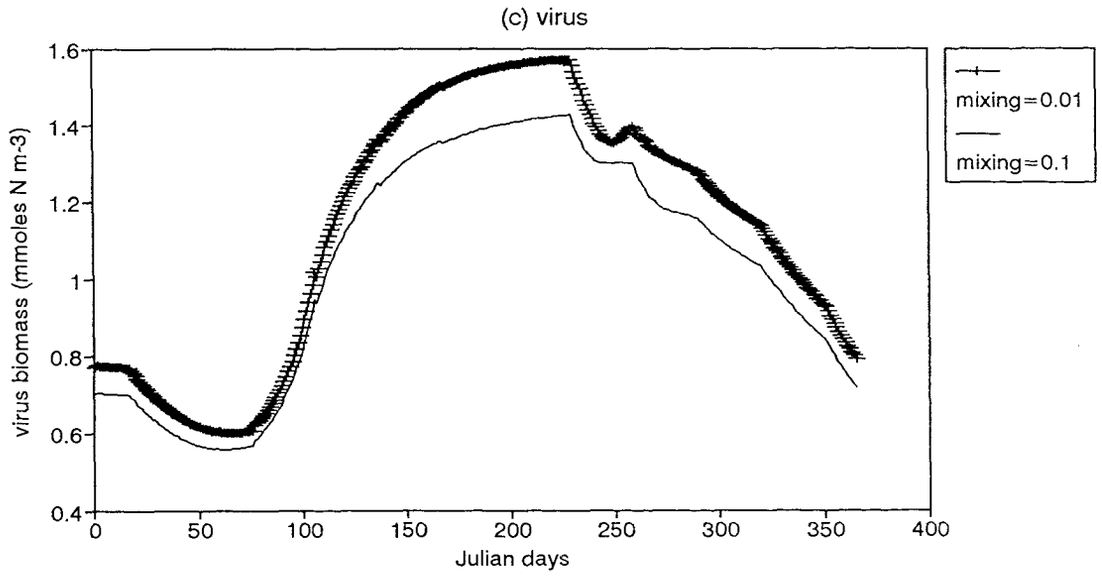

Figure 5.31 - continued

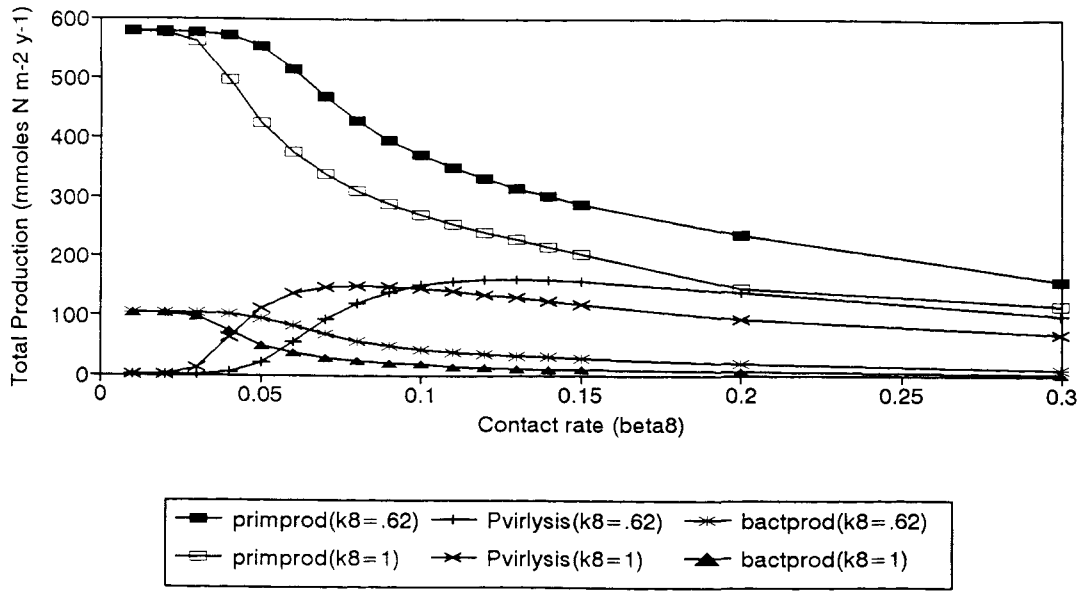

Figure 5.32 Variation in annual primary production (filled/empty square), bacterial production (star/triangle) and corresponding losses by phytoplankton viral lysis (plus/cross) in mMol N/m^2/year, plotted against increasing levels of the contact rate (beta8), using two levels of efficiency (k8=.62 and k8=1) for the biomass conversion from host cells into virus. Beta8 values between 0 - 0.3.

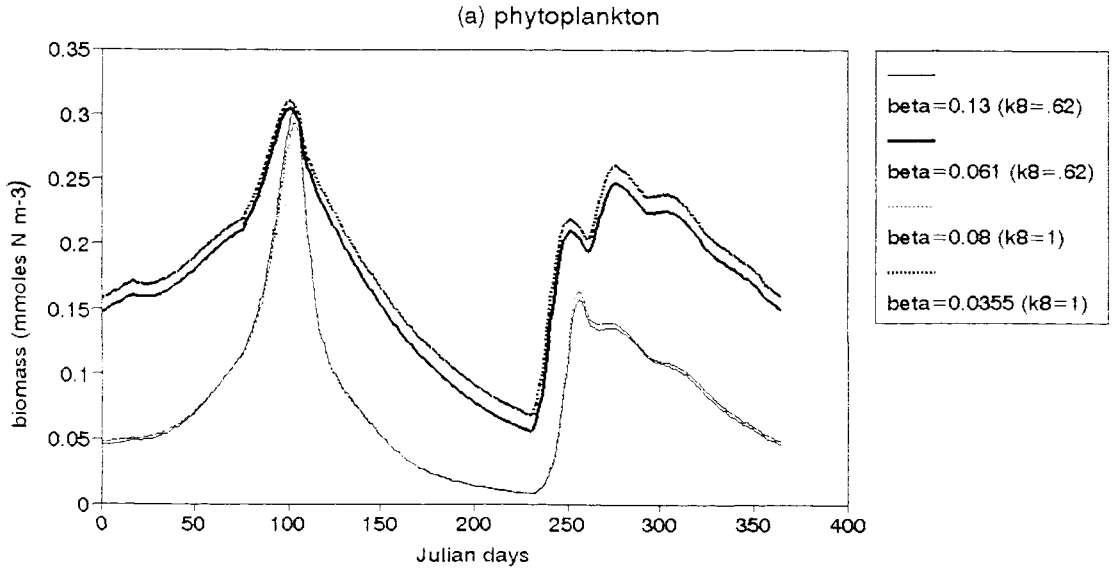

Figure 5.33 Annual cycle of (a) phytoplankton, (b) virus biomass and (c) total mixed layer stoks of viruses in minimum (heavy solid/solid/heavy dotted) and maximum (solid/plus/dotted) epidemics for two levels of eficiency (K8 =.62 and k8=1).

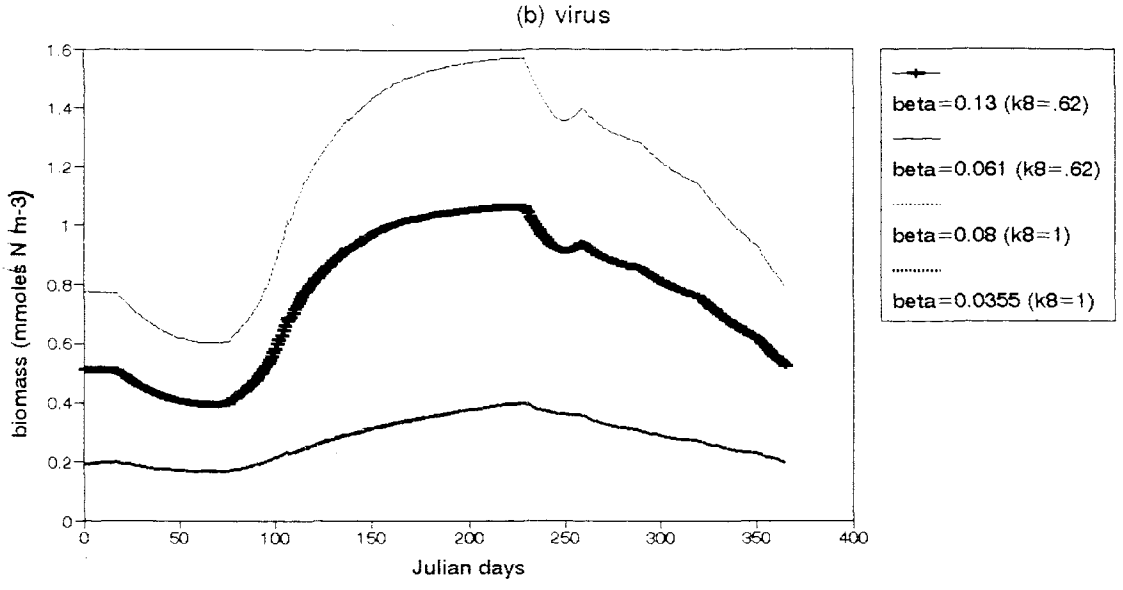

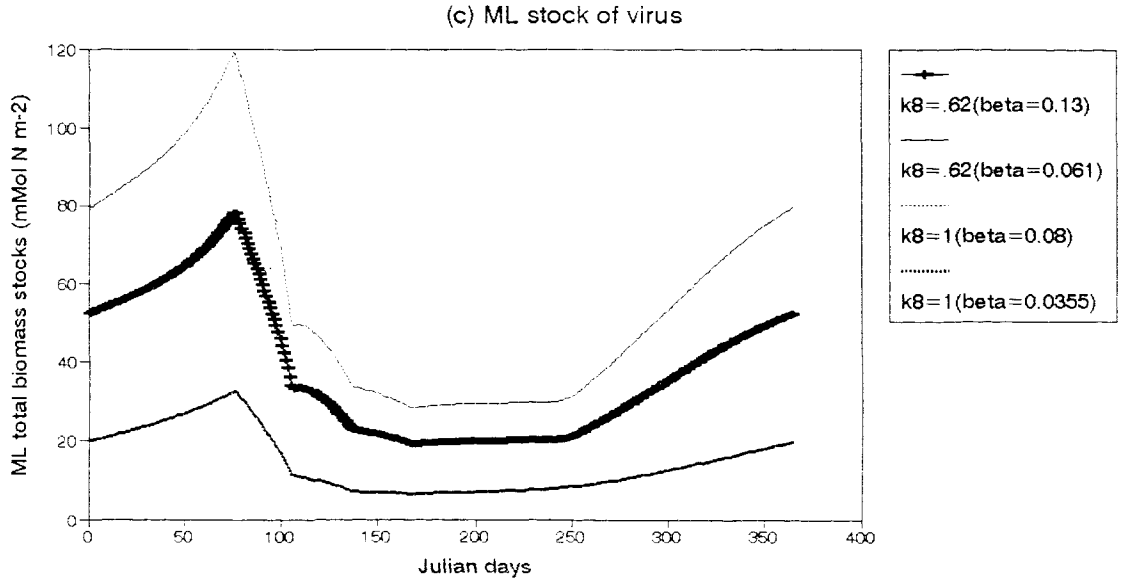

Figure 5.33 - continued

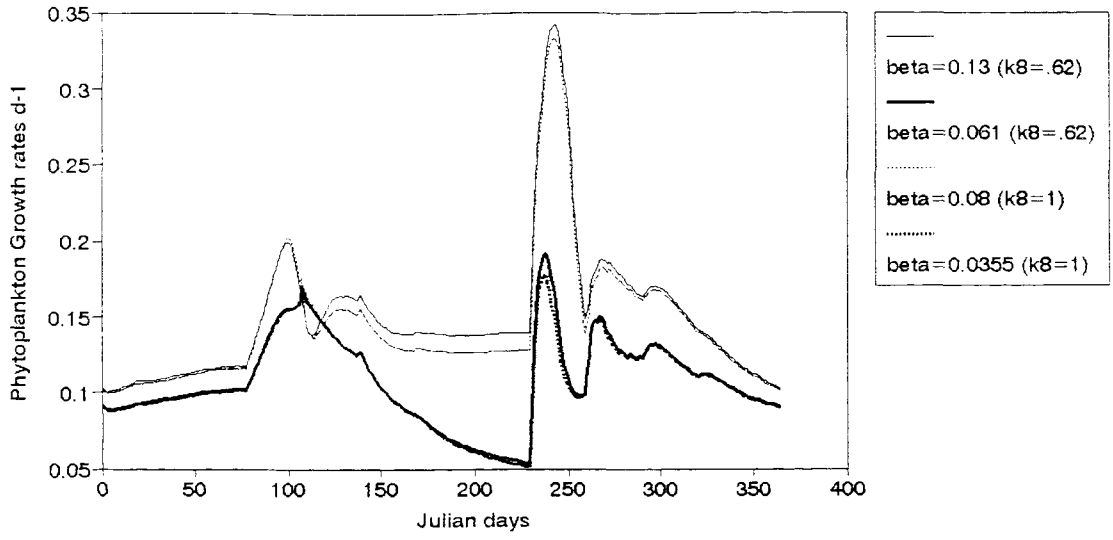

Figure 5.34 Annual cycle of phytoplankton growth rates in minimum (heavy solid/heavy dotted) and maximum (solid/dotted) epidemics for two levels of eficiency (K8 =.62 and k8=1).

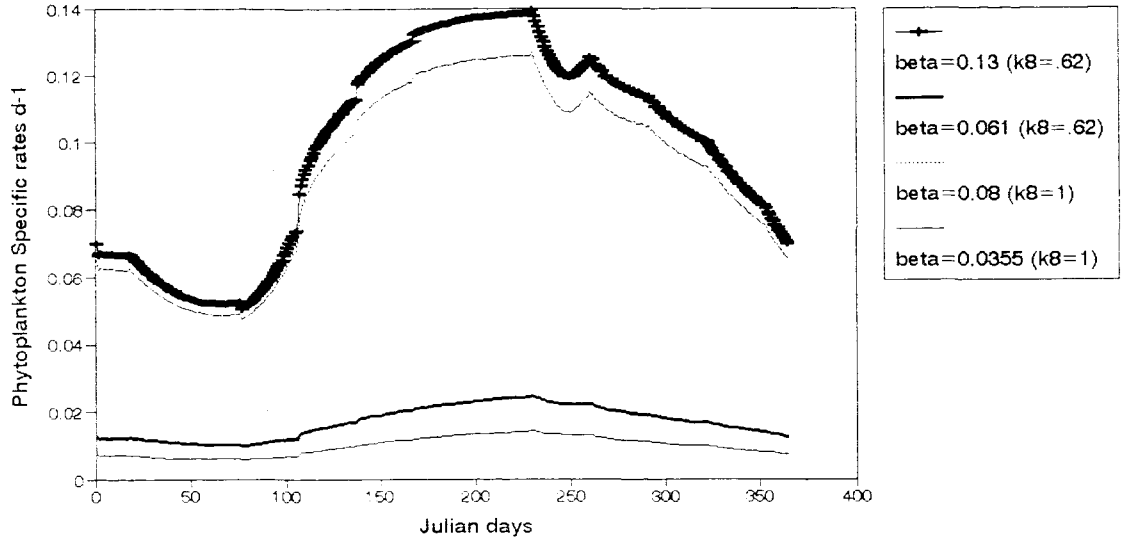

Figure 5.35 Annual cycle of phytoplankton specific rate of viral lysis in minimum (heavy solid/solid) and maximum (plus/dotted) epidemics for two levels of eficiency (K8 =.62 and k8=1).

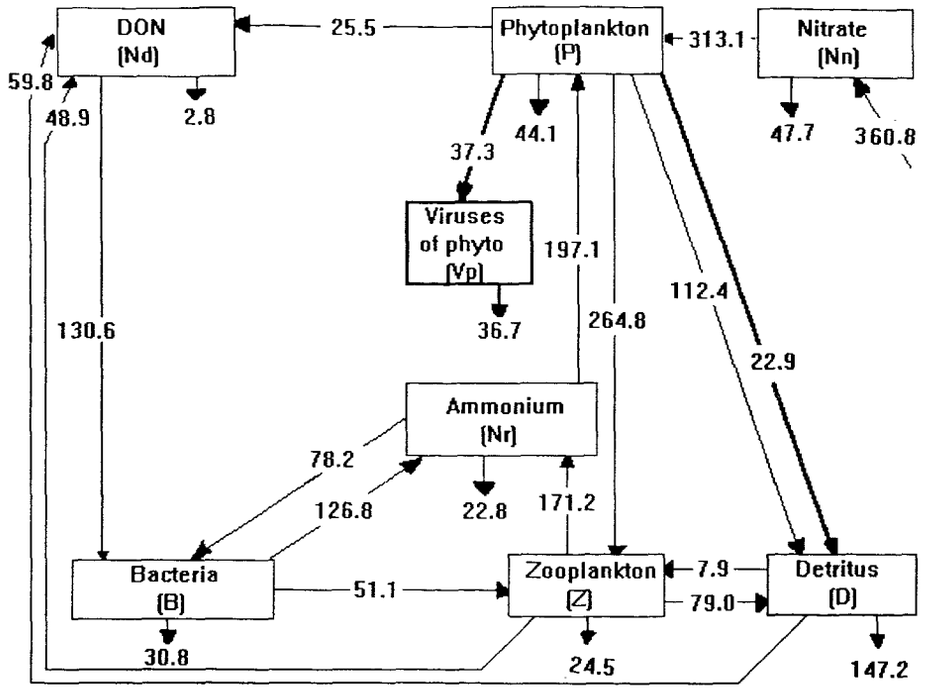

a Minimum epidemic Beta8=0.061 k8=.62 sink=10 mixing=0.01

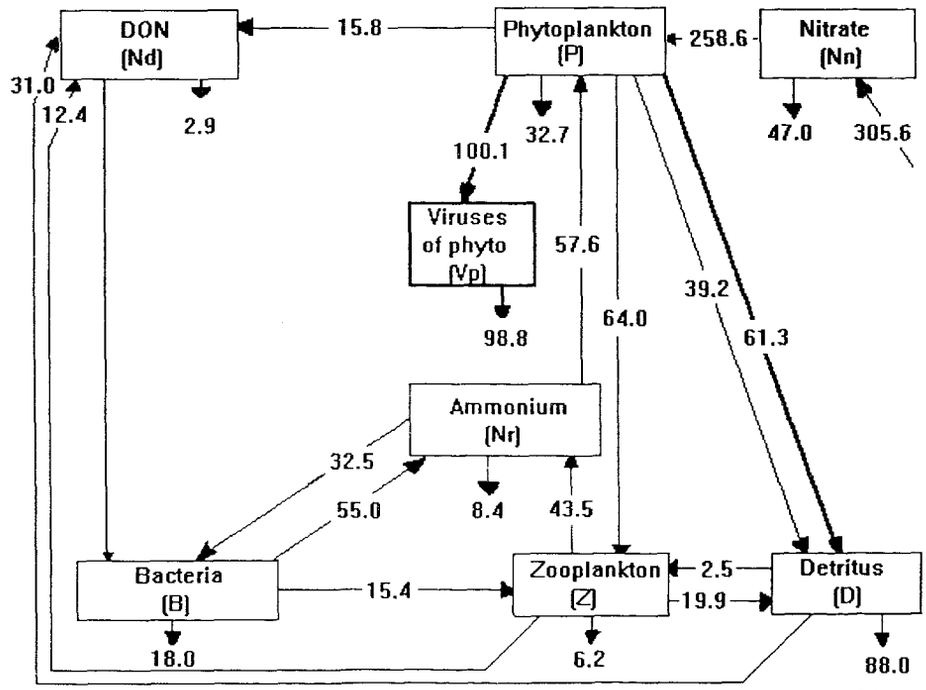

b Maximum epidemic Beta8=0.13 k8=.62 Mixing rate=0.001

Figure 5.36 Annual intercompartment flows of nitrogen for (a) minimum and (b) maximum epidemic for a level of eficiency of K8 =.62 in version 2 of the model with a mixing rate of 0.01m d^{-1}.

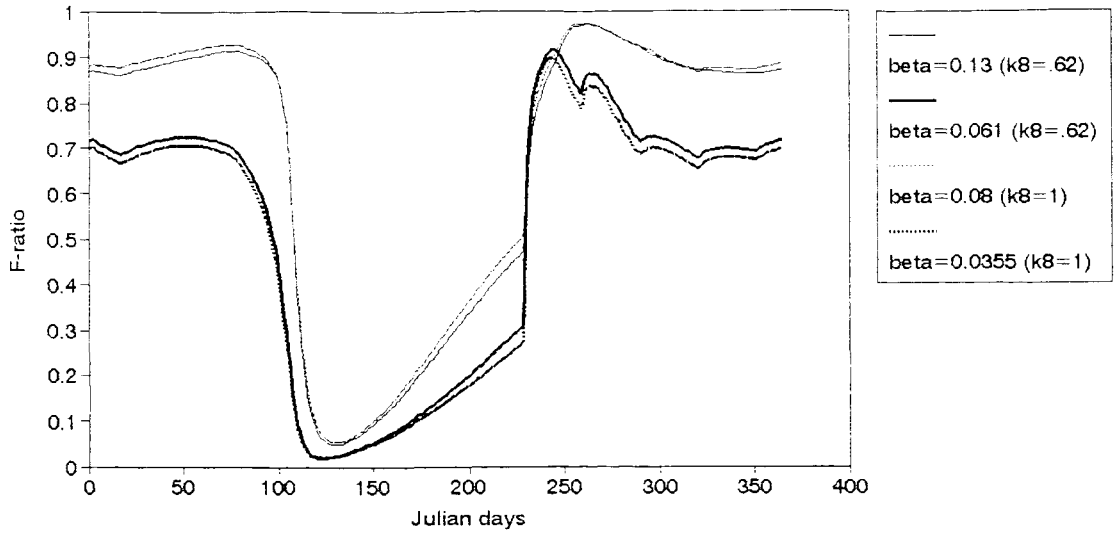

Figure 5.37 Comparison of f-ratios in minimum (heavy solid/heavy dotted) and maximum (solid/dotted) epidemics for two levels of eficiency (K8 =.62 and k8=1).

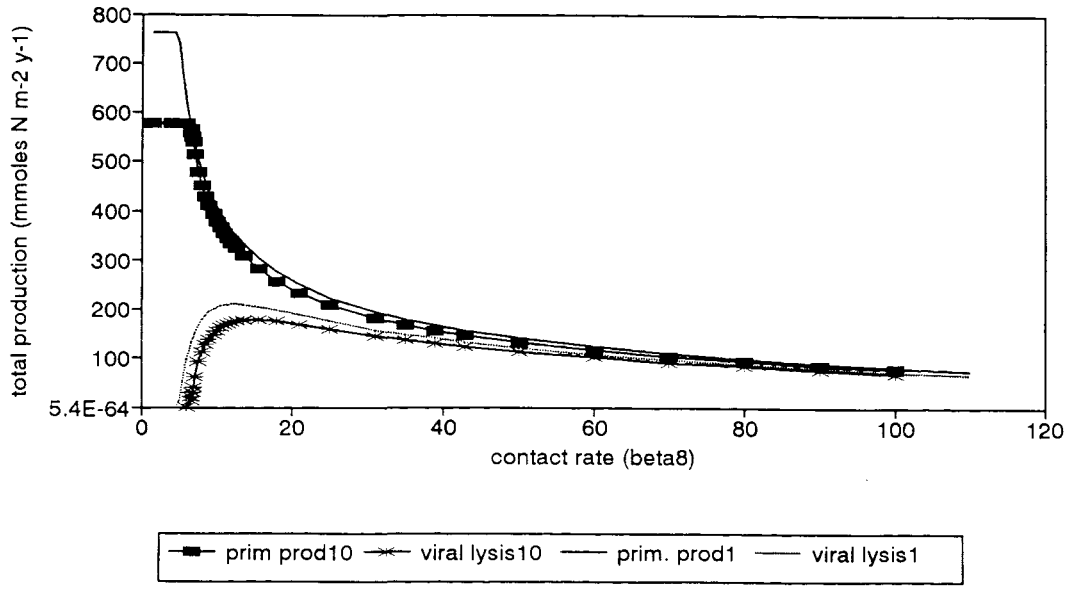

Figure 5.38 Variation in annual primary production (filled square/solid line) and corresponding losses by phytoplankton viral lysis (star/dotted) in mMol N/m^2/year, plotted against increasing levels of the contact rate (beta8), using two sinking rates of detritus (10 and 1 m d^{-1}). Beta8 values between 0 - 100.

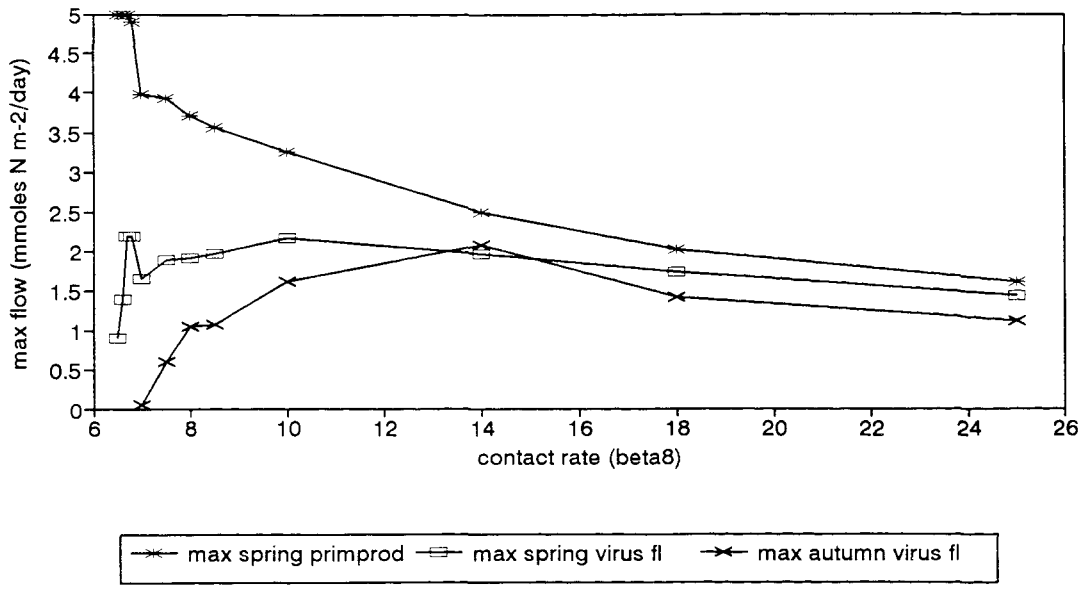

Figure 5.39 Variation in the maximum daily flows into viral lysis of phytoplankton during spring (empty square) and autumn (cross) blooms, compared with the maximum flow of primary production during the spring bloom (star) for increasing levels of the contact rate (beta8).

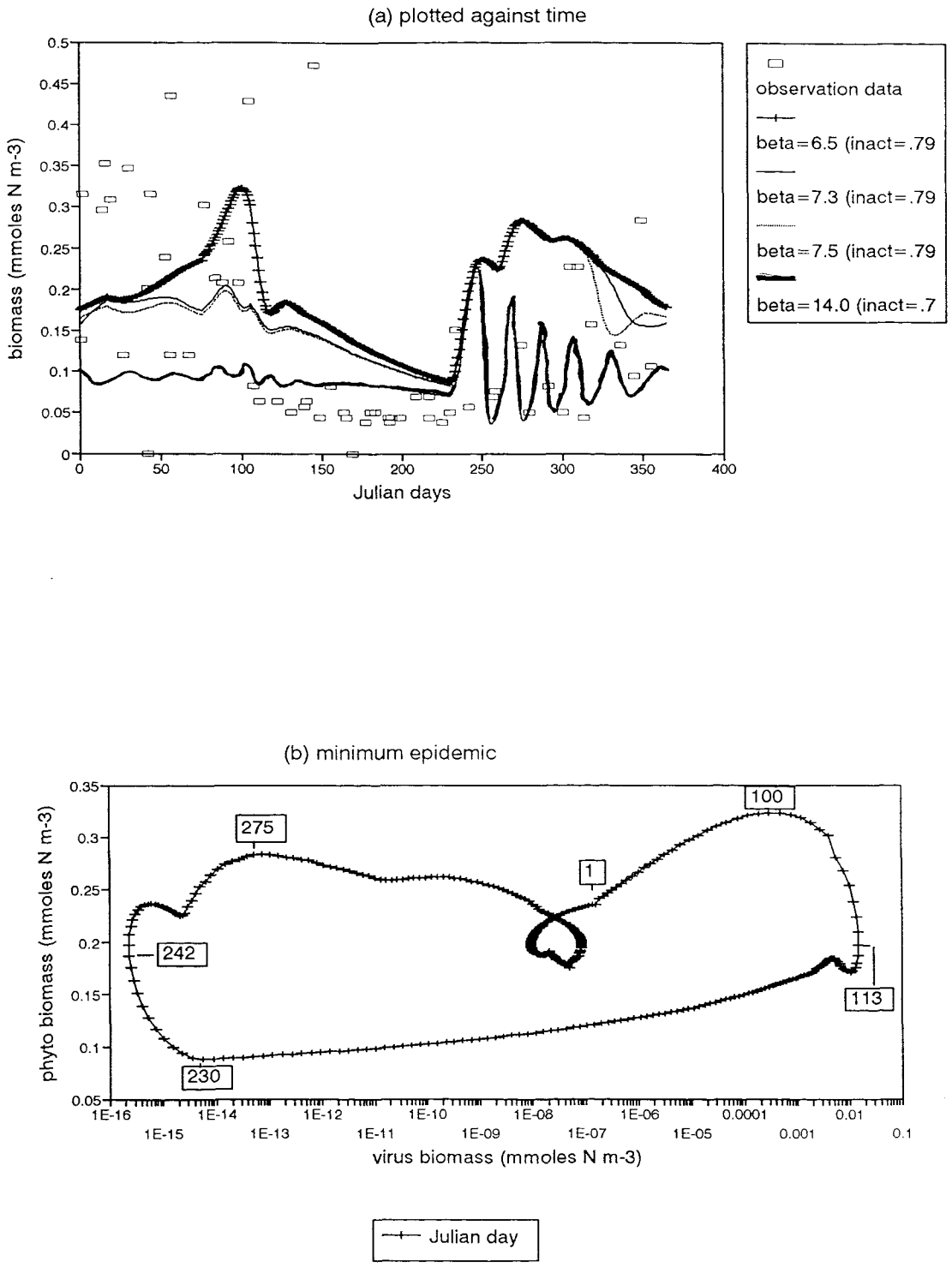

Figure 5.40 Annual cycles of phytoplankton biomass for minimum (plus), 2 intermediates (solid line and dotted) and maximum epidemics (red). (a) plotted against time; and plotted against virus biomass: (b) minimum epidemic, (c) maximum epidemic, (d) detail of maximum epidemic

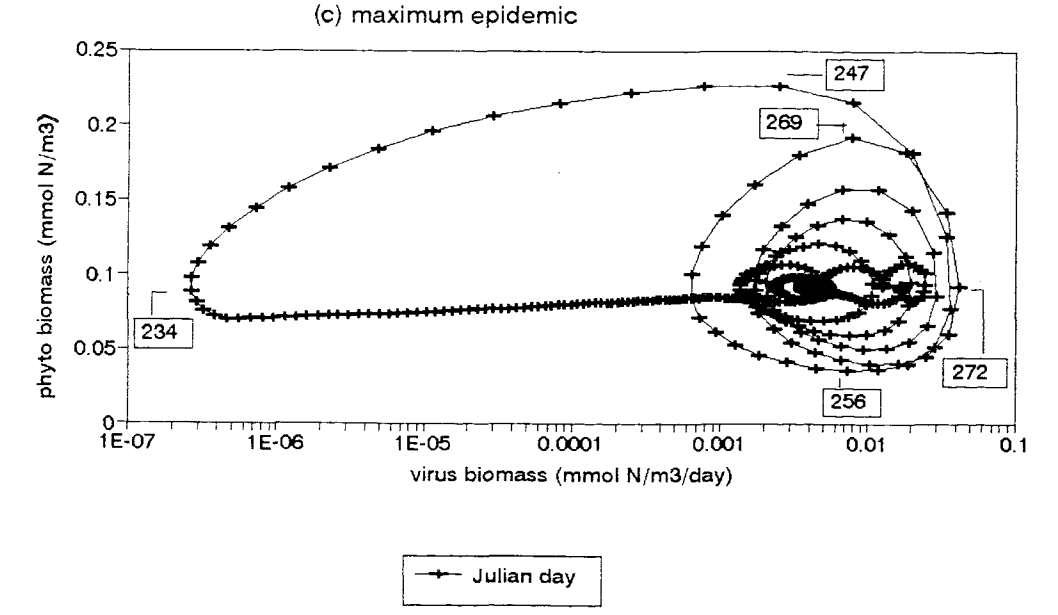

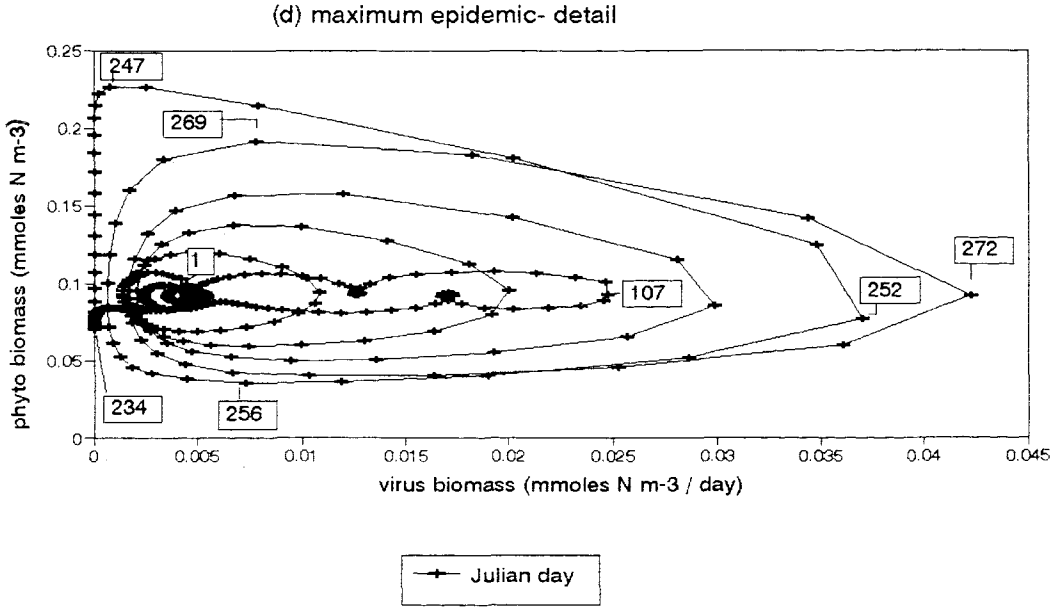

Figure 5.40 - continued

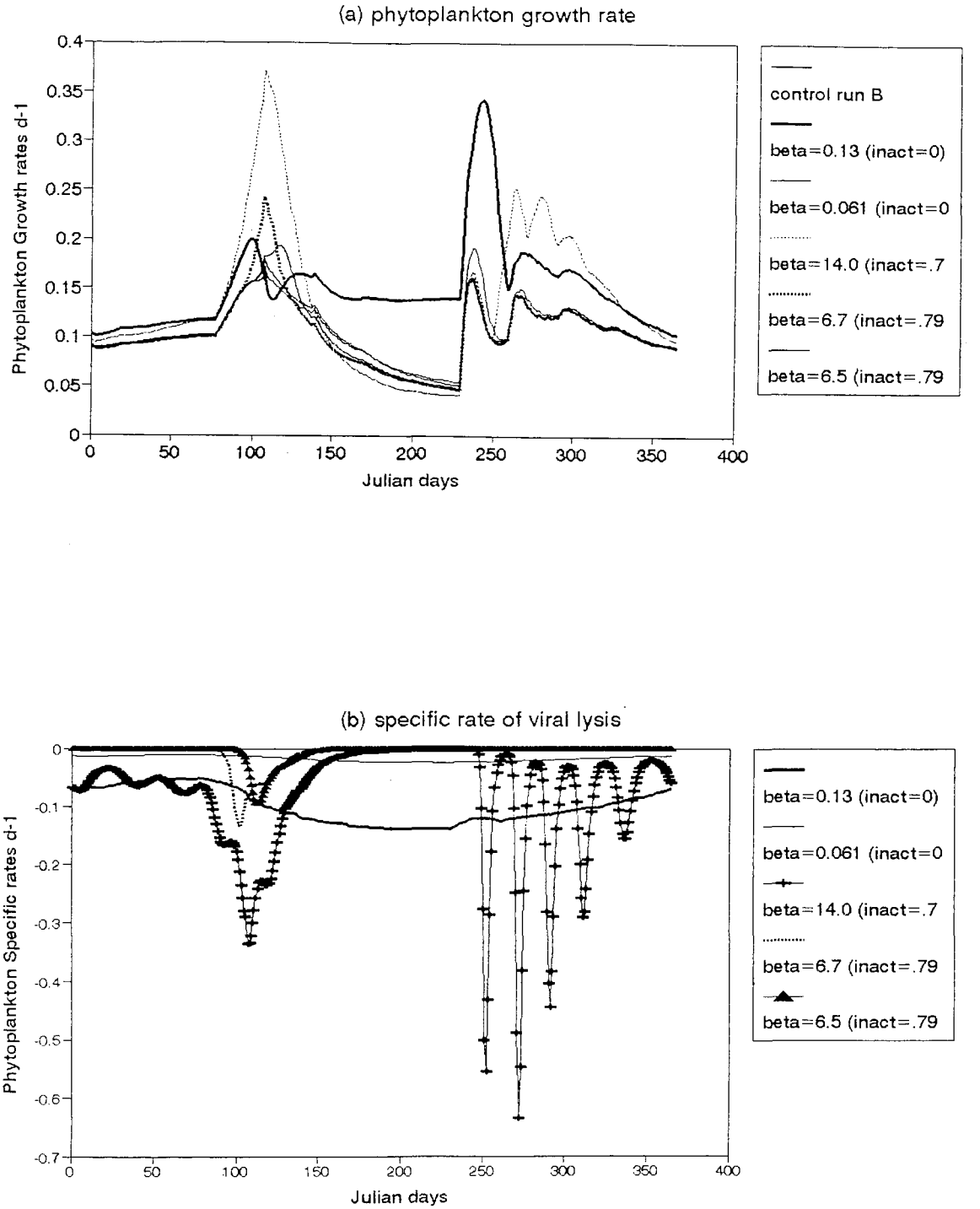

Figure 5.41 Annual cycles of phytoplankton (a) growth rate, (b) specific rate of viral lysis, for minimum (red/triangle/solid line), intermediate (heavy dotted), maximum epidemics (dotted/plus/heavy solid) for inactivation rates .792 and 0 d^{-1}, and control run B (yellow).

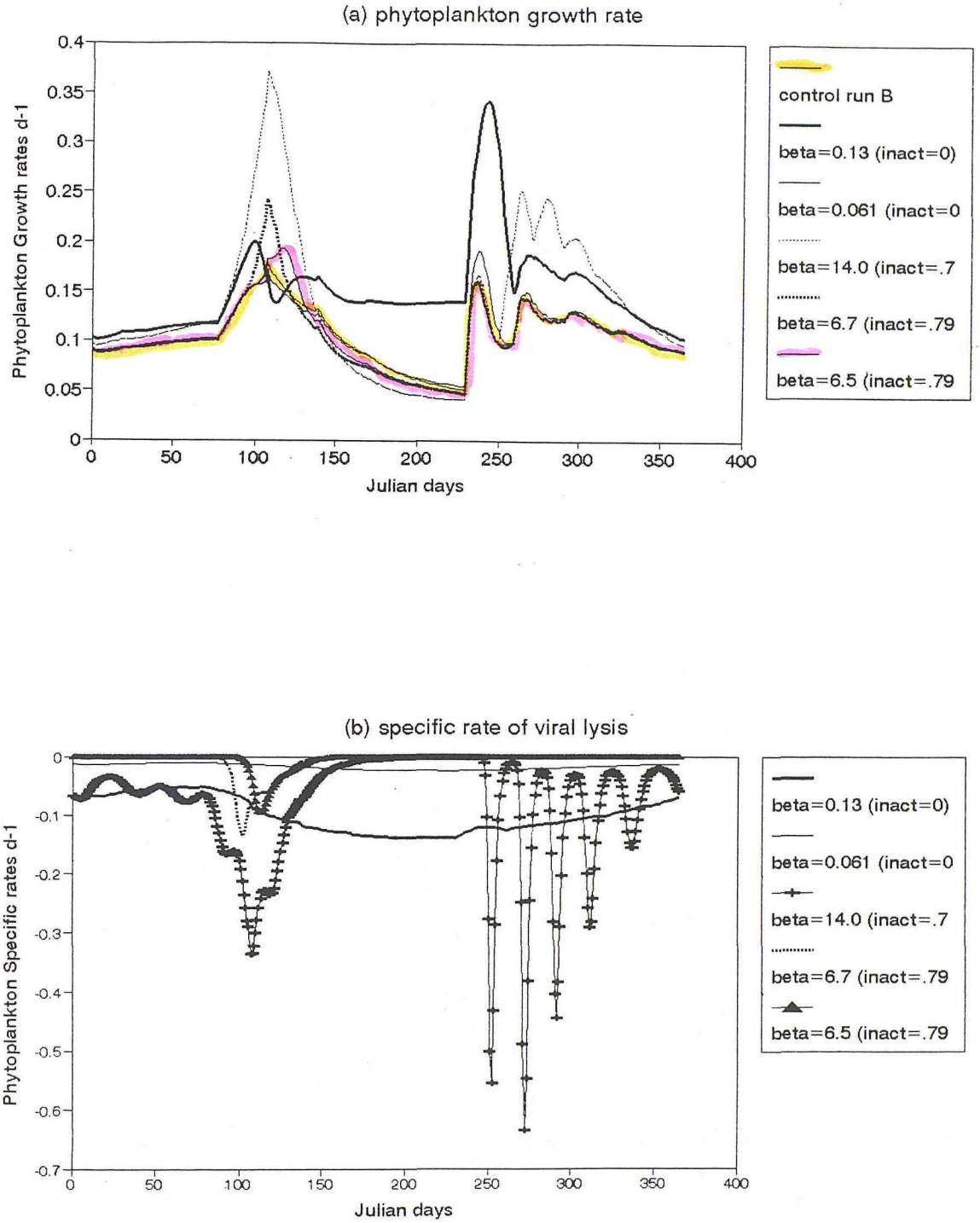

Figure 5.41 Annual cycles of phytoplankton (a) growth rate, (b) specific rate of viral lysis, for minimum (red/triangle/solid line), intermediate (heavy dotted), maximum epidemics (dotted/plus/heavy solid) for inactivation rates .792 and 0 d^{-1}, and control run B (yellow).

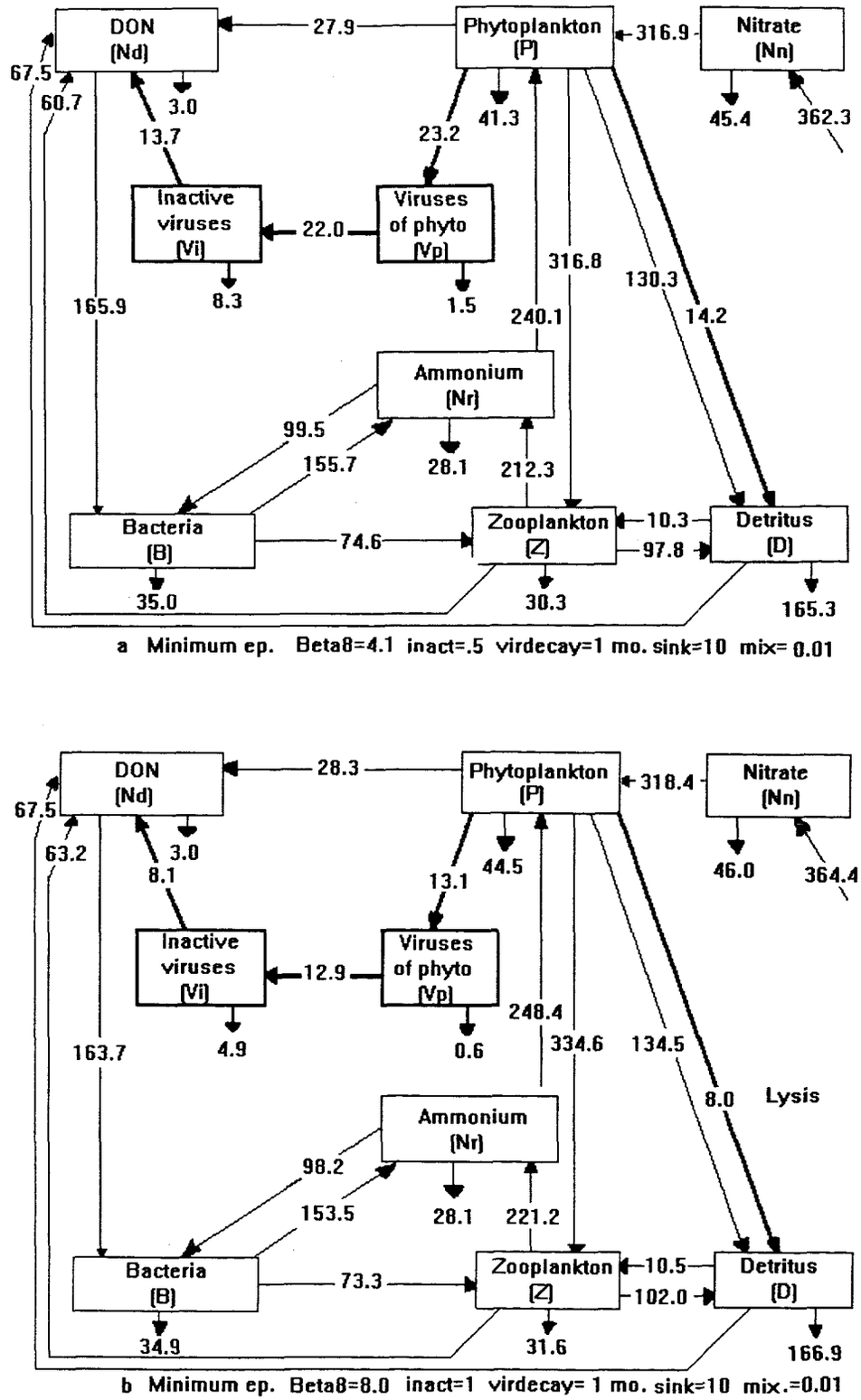

Figure 5.42 Annual intercompartment flows of nitrogen for (a),(b) minimum and (c),(d) maximum epidemic in version 4 for inactivation rates .5 and 1 d^{-1} and decay time of one month.

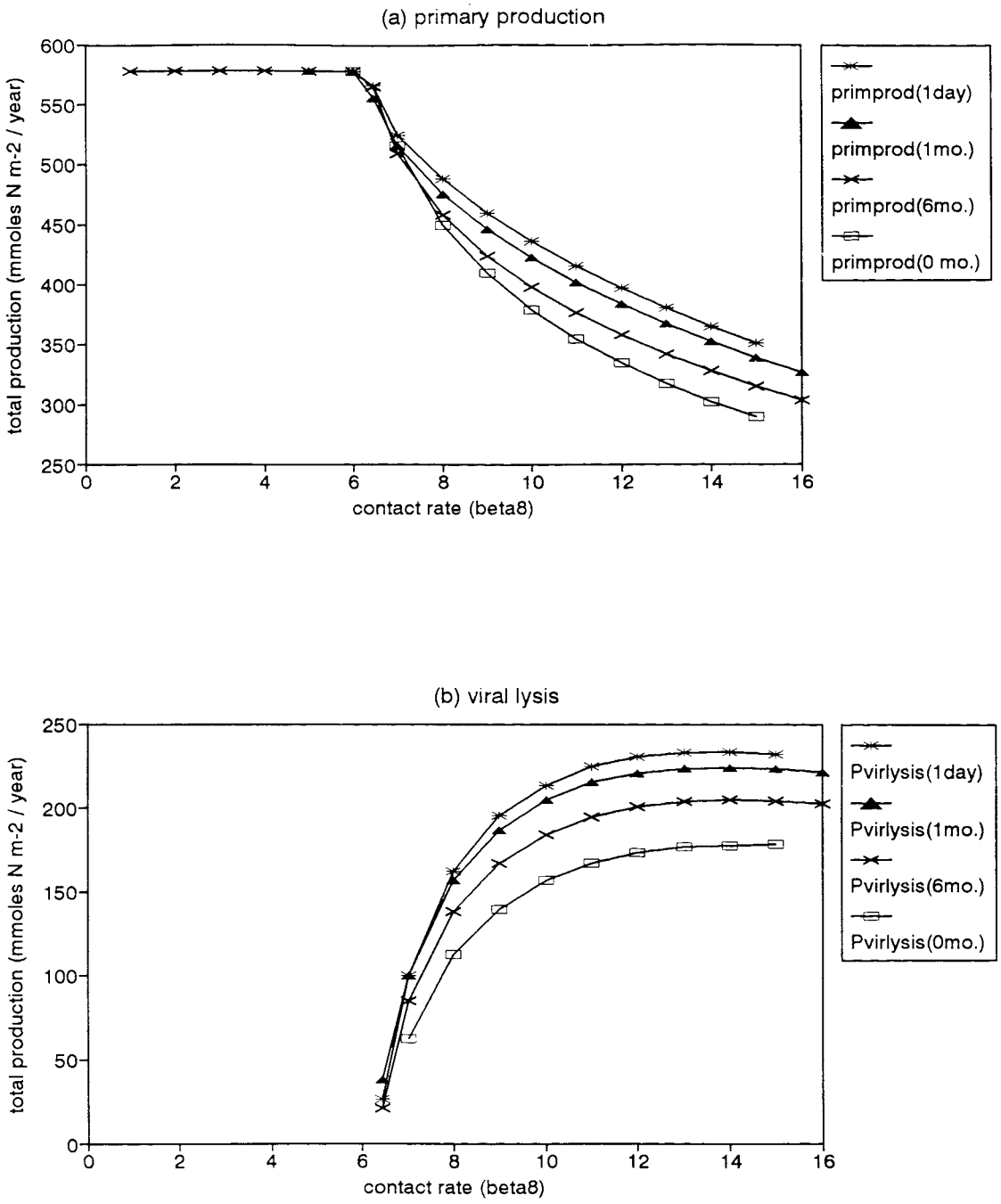

Figure 5.43 Variation in (a) annual primary production, (b) corresponding losses by phytoplankton viral lysis and (c) bacterial production in mMol N/m^2/year, plotted against increasing levels of the contact rate (beta8) for decay times of one day (star), 1 month (triangle), 6 months (cross) and no decay (empty square). Beta8 values between 0 - 16.

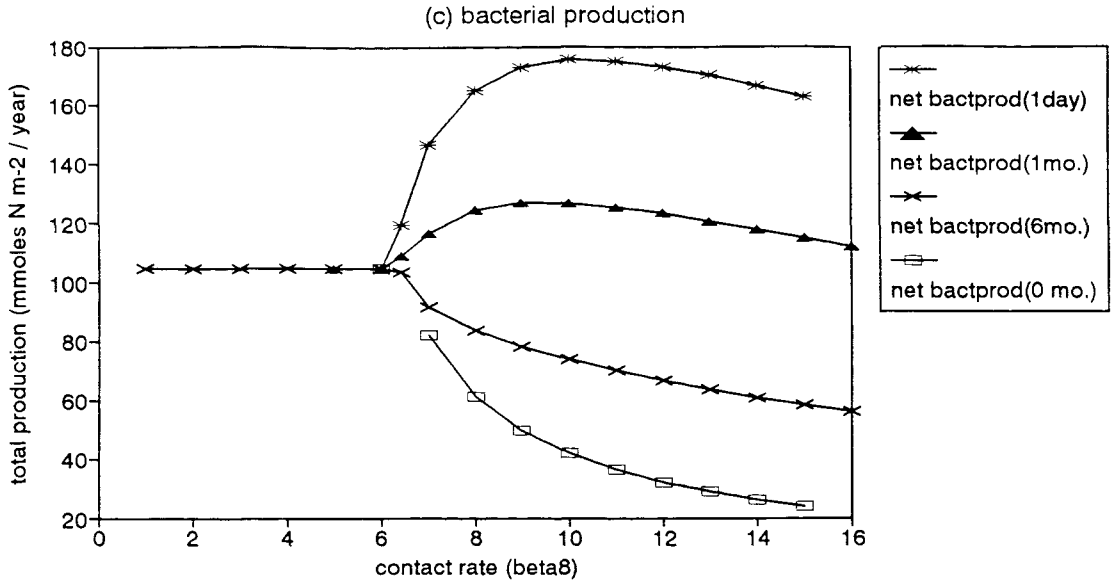

Figure 5.43 - continued

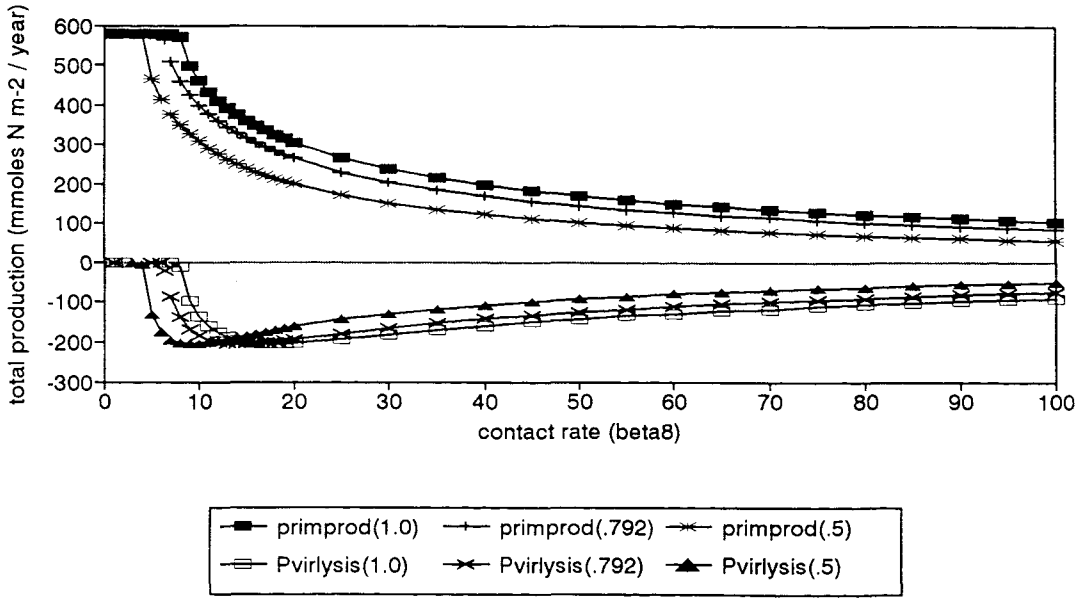

Figure 5.44 Variation in annual primary production (filled square/plus/star), and corresponding losses by phytoplankton viral lysis (empty square/cross/triangle) in mMol N/m^2/year plotted against increasing levels of the contact rate, for inactivation rates 1, .792 and .5 d^{-1}, respectively. Beta8 values between 0 - 100.

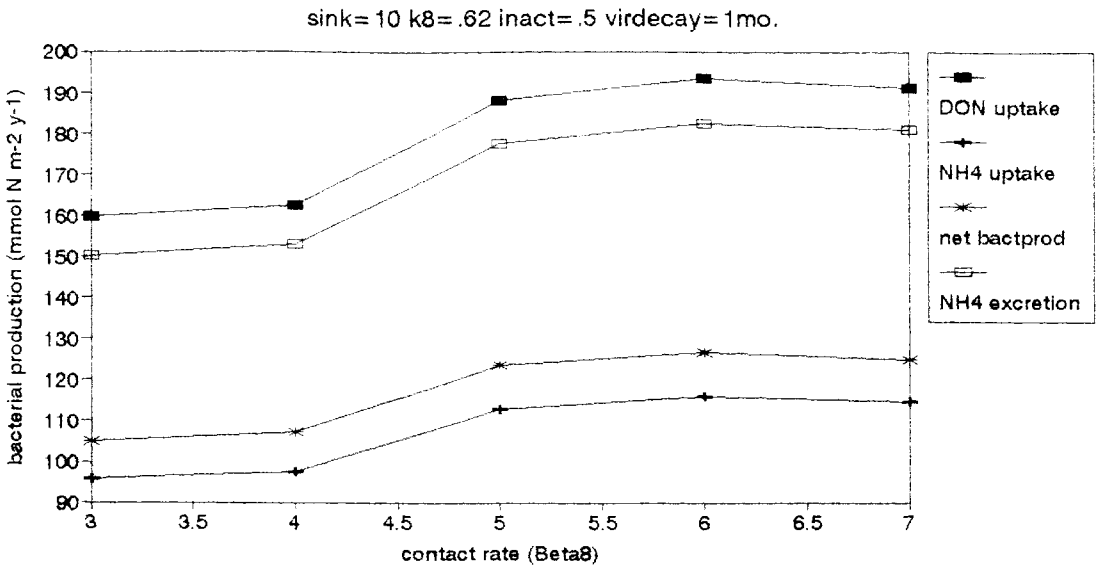

Figure 5.45 Variation in DON uptake (filled square), ammonium uptake (plus), net bacterial production (star) and ammonium excretion (empty square) of Bacteria, plotted against increasing levels of the contact rate for an inactivation rate of .5 d^{-1} and a decay time of one month.

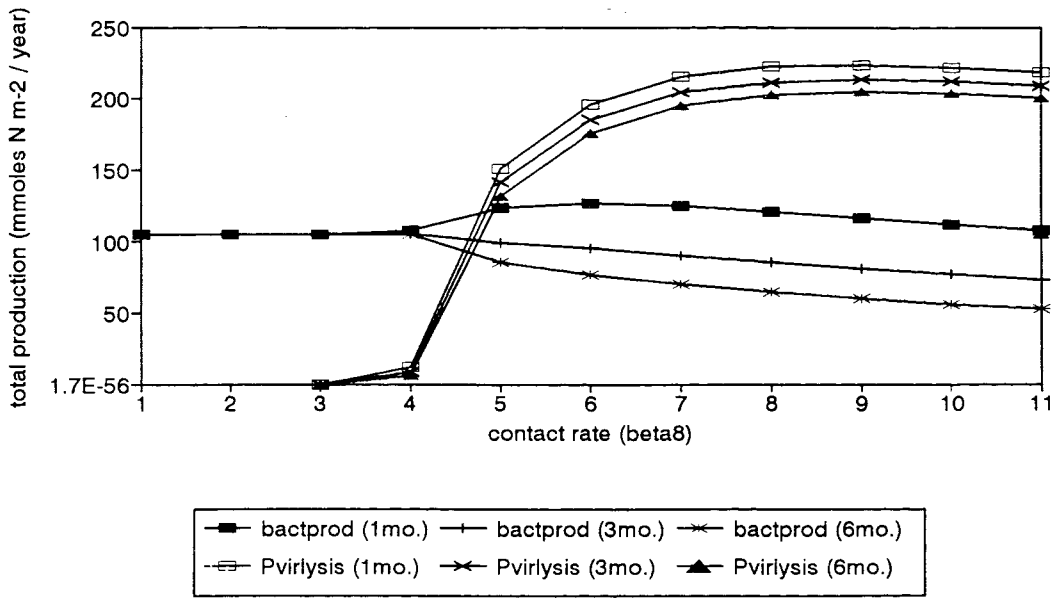

Figure 5.46 Variation in annual bacterial production (filled square/plus/star), and viral lysis of phytoplankton (empty square/cross/triangle) in mMol N/m^2/year, plotted against increasing levels of the contact rate, for decay times of one, three and six months, and an inactivation rate of .5 d^{-1}. Beta8 values between 0 - 11.

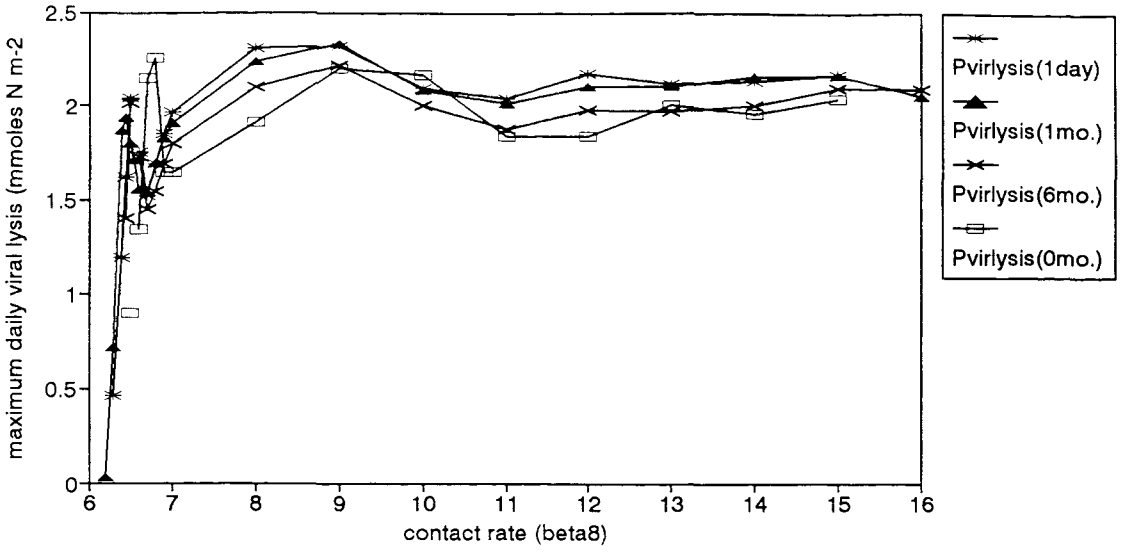

Figure 5.47 Variation in maximum daily flow into viral lysis in mMol N/m^2/day, plotted against increasing levels of the contact rate (beta8) for decay times of one day (star), 1 month (triangle), 6 months (cross) and no decay (empty square). Beta8 values between 0 - 16.

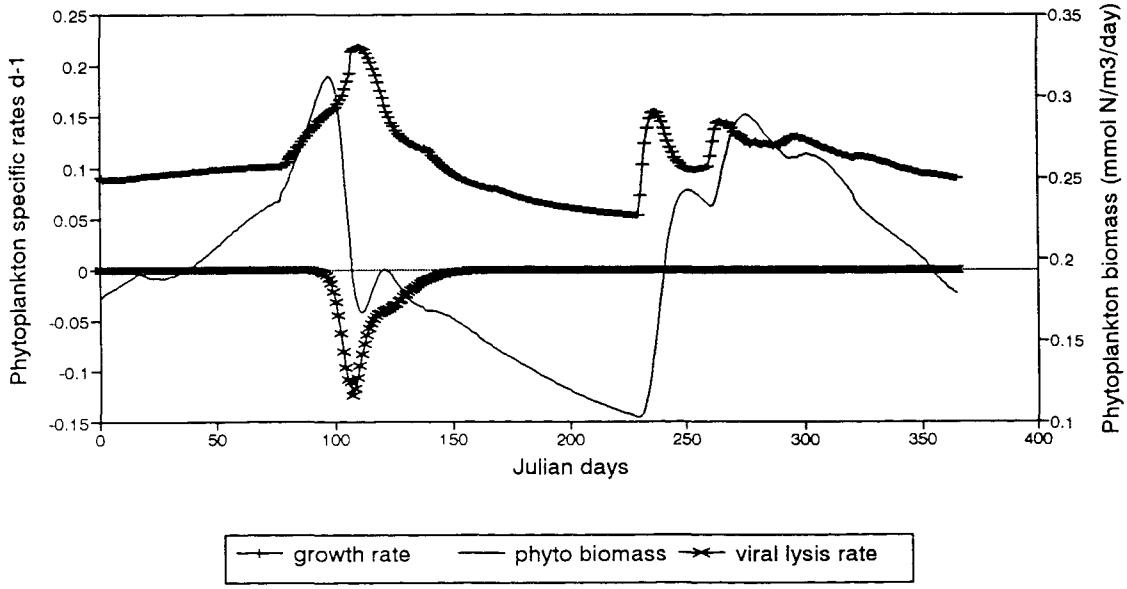

Figure 5.48 Seasonal cycle of phytoplankton growth rate (plus) and biomass (solid line) compared to the specific rate of viral lysis (cross) for a minimum epidemic with a decay time of six months.

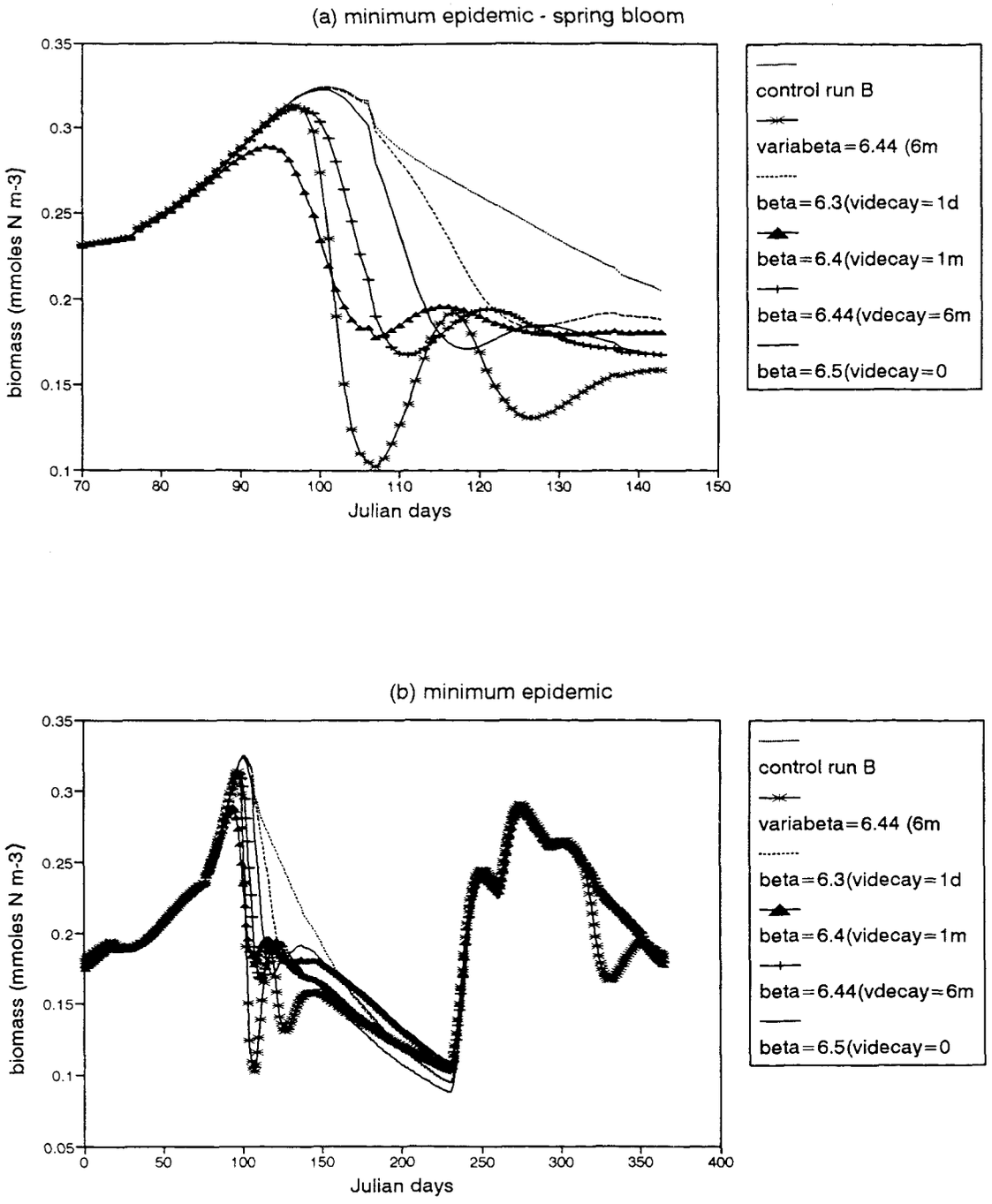

Figure 5.49 Collapse of the phytoplankton biomass in (a),(b) minimum and (c) maximum epidemics during the spring and autumn blooms for decay rates of one day (dashed), one month (triangle/heavy dotted), six months (plus/solid line), no decay (solid line/dotted) and variable contact rate of six months (star/green), compared to control run B (dotted/empty square).

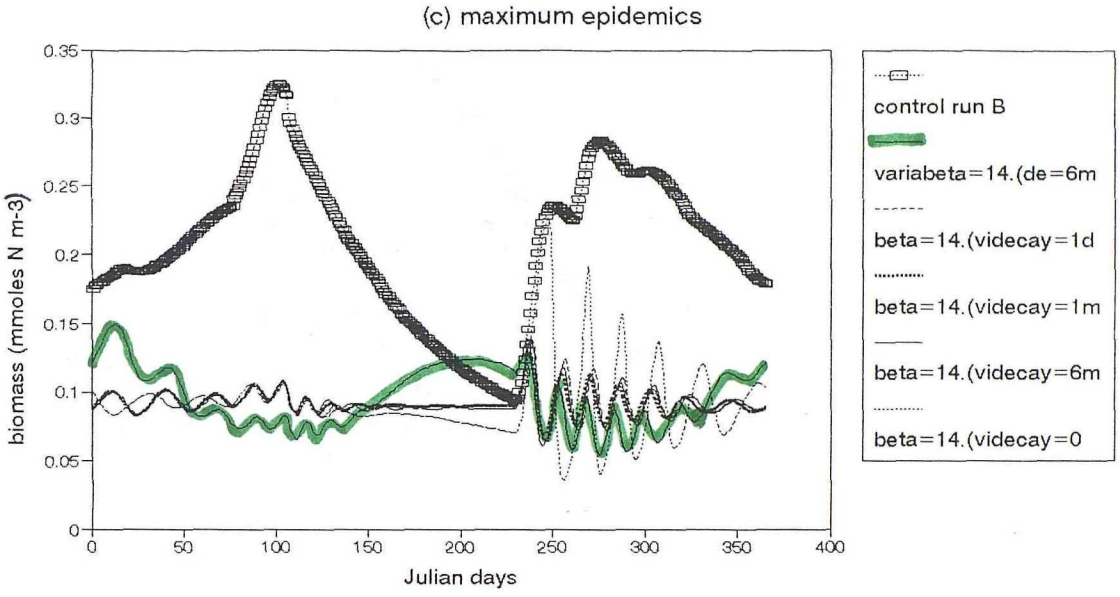

Figure 5.49 - continued

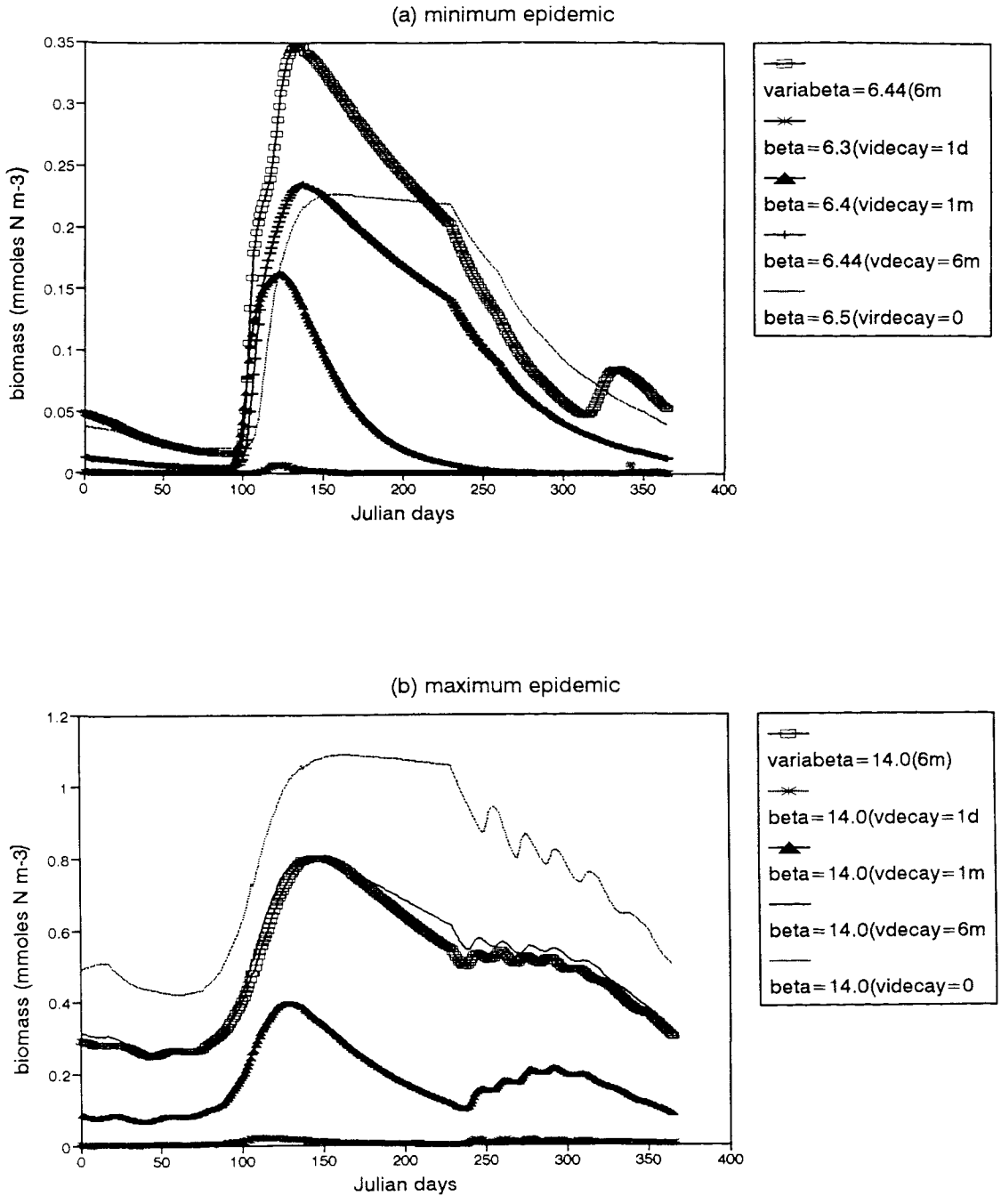

Figure 5.50 Annual cycle of inactivated viruses in (a) minimum and (b) maximum epidemics for decay times of one day (star), one month (triangle), six months (plus/solid line) and no decay (dotted) compared to a variable contact rate for six months decay (empty square).

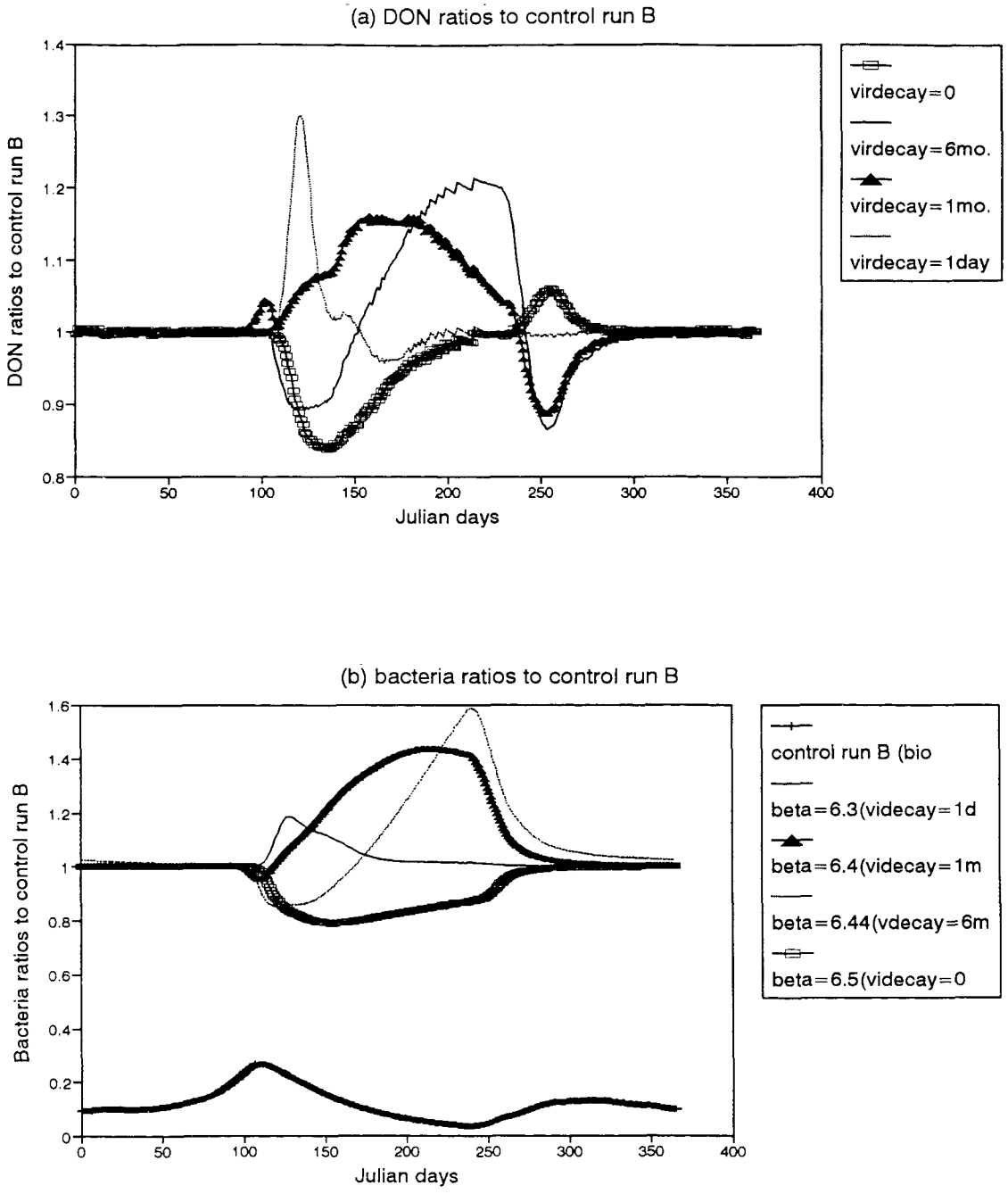

Figure 5.51 Ratios to control run B of (a) DON and (b) bacteria biomas for decay times of one day (dotted/solid line), one month (triangle), six months (solid line/dotted) and no decay (empty square), in minimum epidemic.

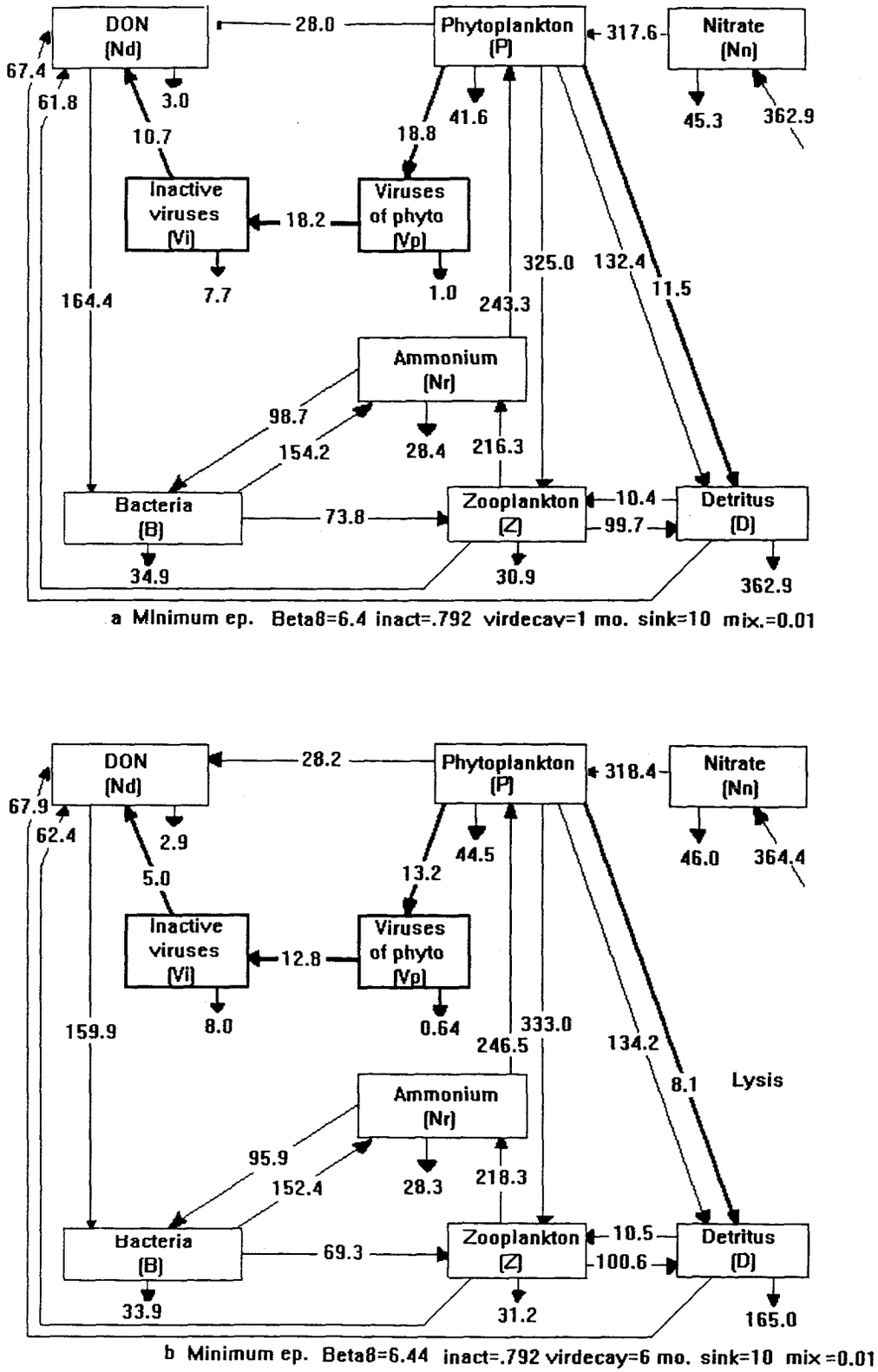

Figure 5.53 Annual intercompartment flows of nitrogen for (a),(b) minimum and (c),(d) maximum epidemic in version 4, for decay times of one and six months.

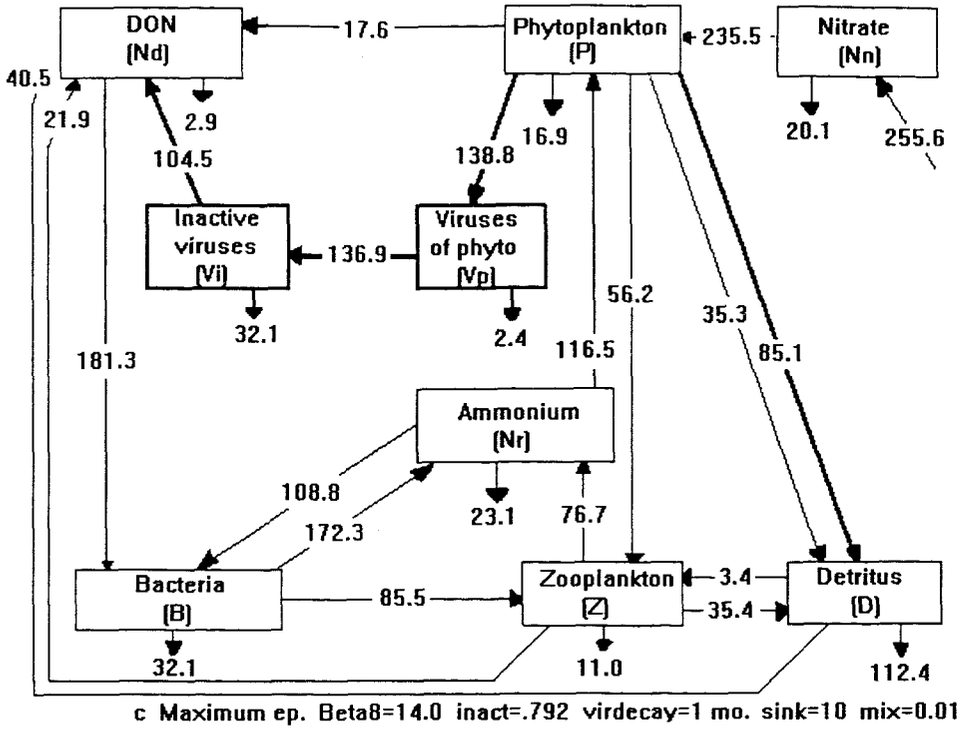

c Maximum ep. Beta8=14.0 inact=.792 virdecay=1 mo. sink=10 mix=0.01

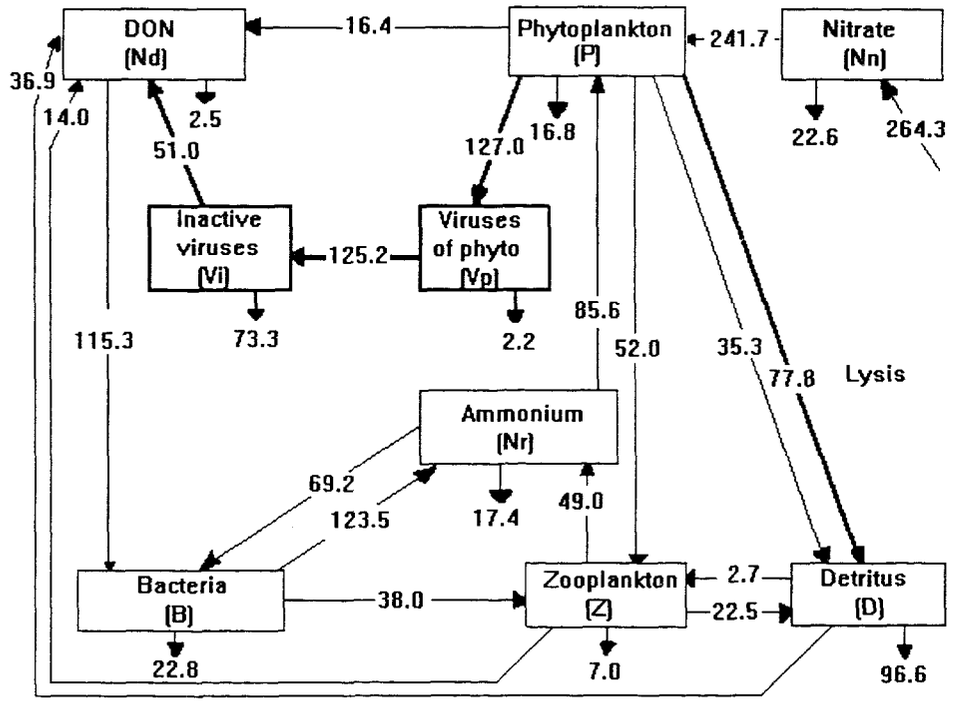

d Maximum ep. Beta8=14.0 inact=.792 virdecay=6mo. sink=10 mix=0.01

Figure 5.53 - continued

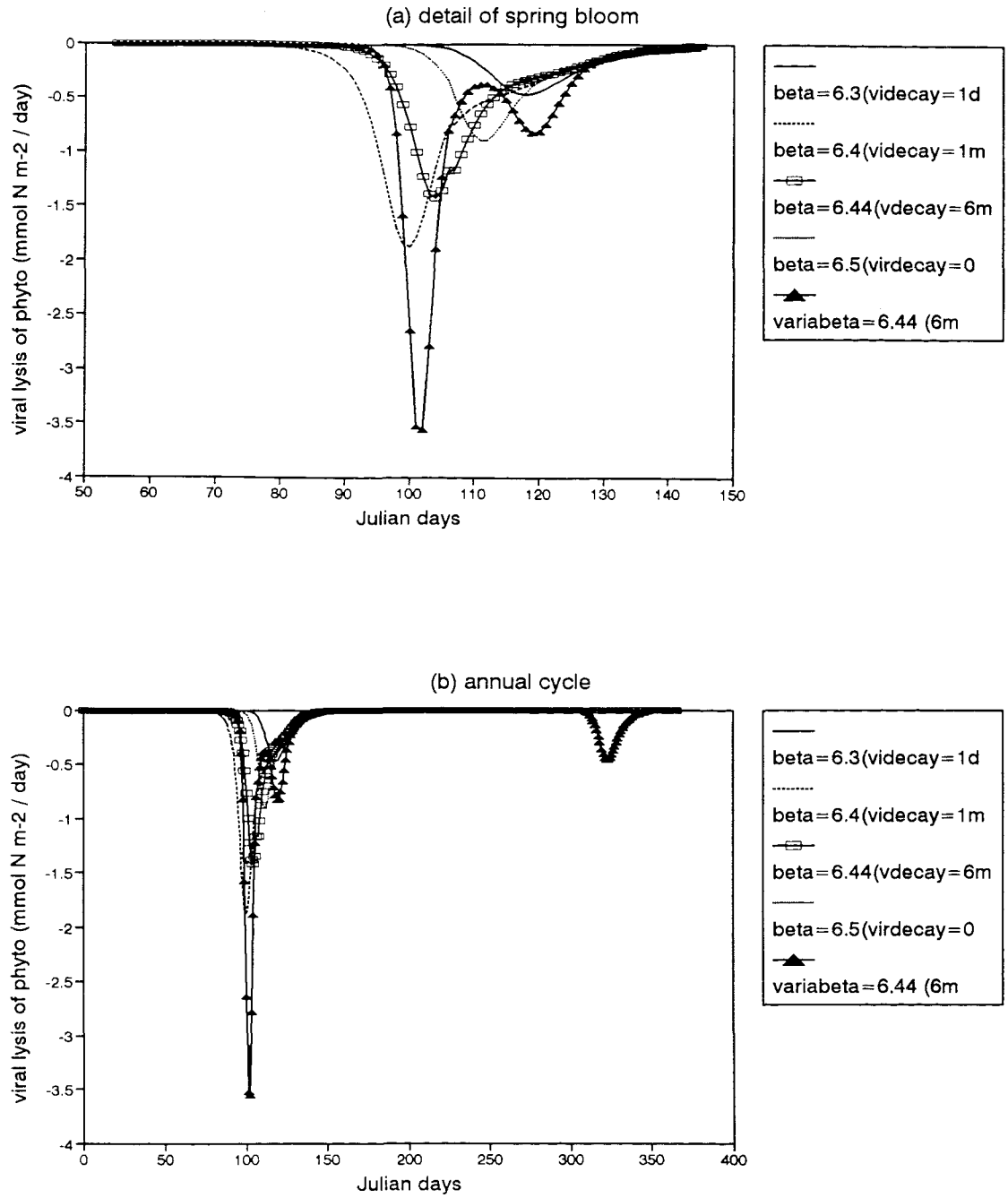

Figure 5.54 Temporal evolution of the phytoplankton loss fluxes (in mMol N/m^2/day) due to viral lysis in (a) and (b) minimum, (c) maximum epidemics. Decay times of one day (solid line), one month (dashed), six months (empty square), no decay (dotted) and variable contact rate of six months (triangle). (a) detail of spring bloom, (b) annual cycle.

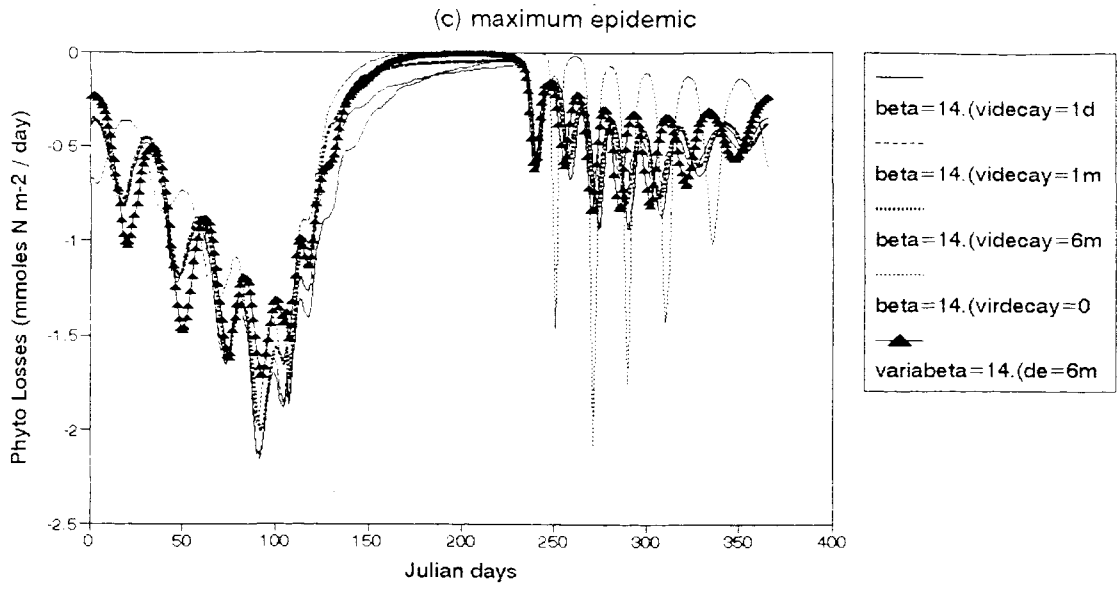

Figure 5.54 - continued

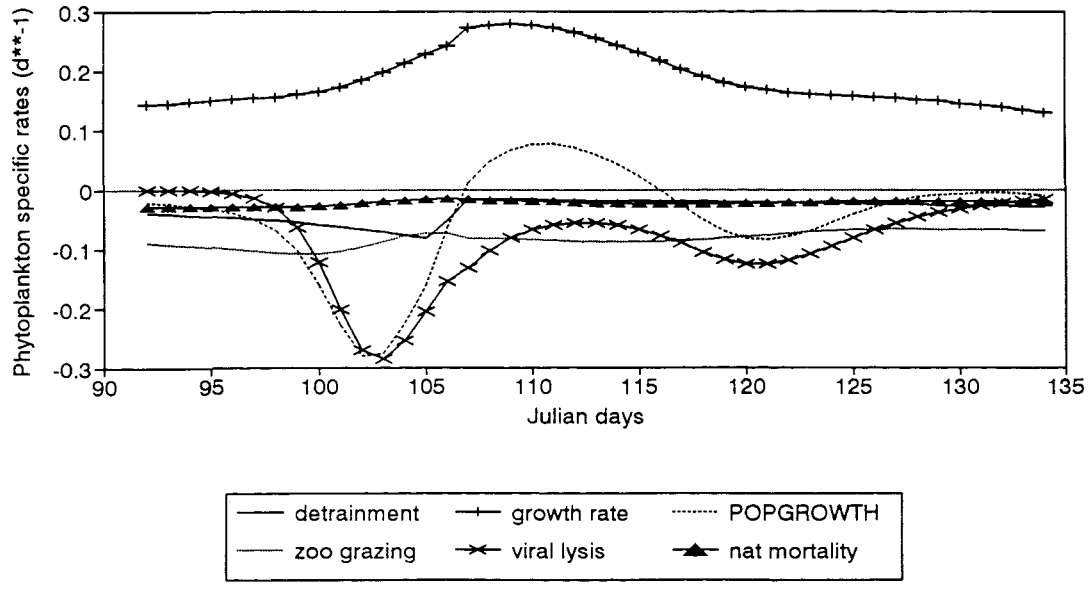

Figure 5.55 Temporal evolution of phytoplankton specific rates during the spring bloom for a minimum epidemic. Decay time of six months. Losses are: detrainmemt (solid line), zooplankton grazing (dotted), viral lysis (cross), natural mortality (triangle). Growth rate is represented by plus and population growth by dashed.

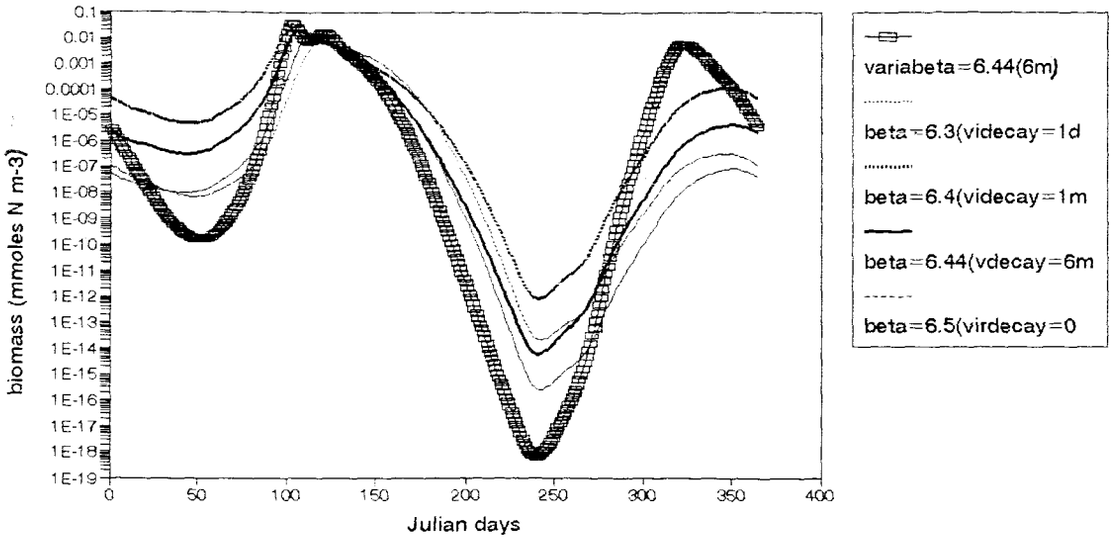

Figure 5.56 Annual cycle of active viruses in minimum epidemics for decay times of one day (dotted), one month (heavy dotted), six months (heavy solid) and no decay (dashed) compared to a variable contact rate for six months decay (empty square).

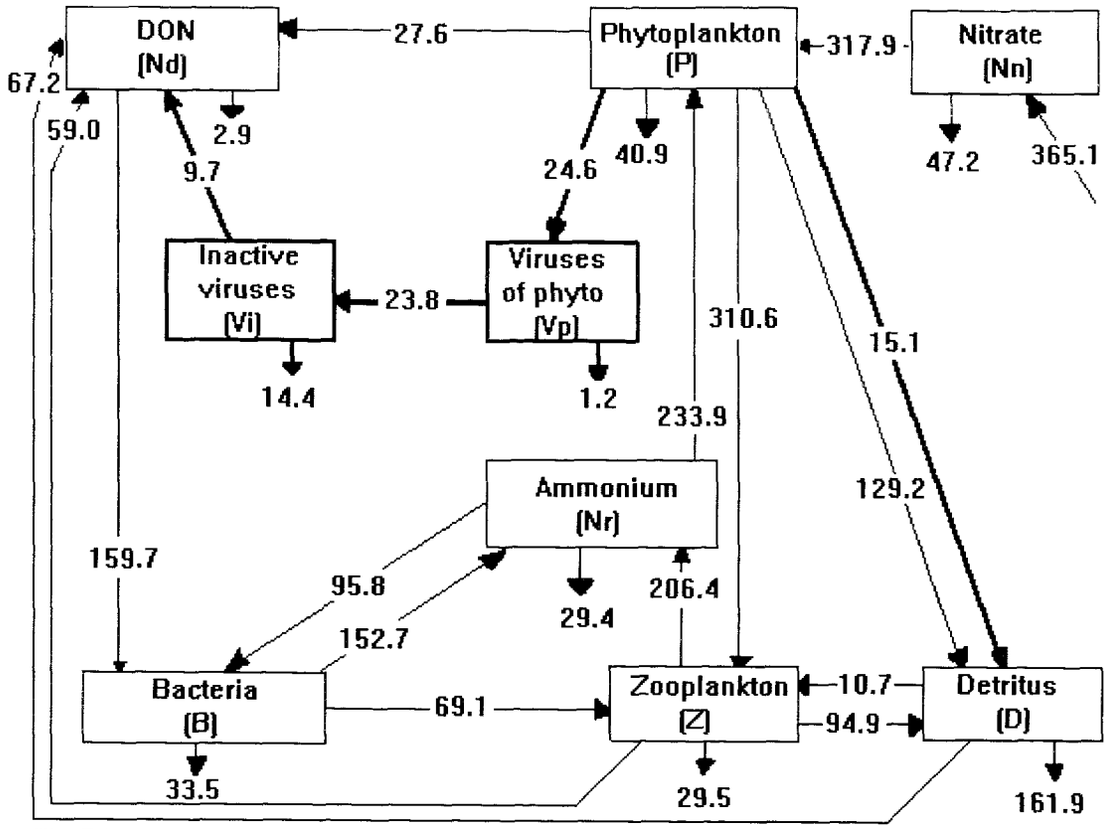

Fig 5.57 a Minimum ep. Beta=6.44 Inact=.792 Virdecay=6 mo. Sink=10 Mix=0.01

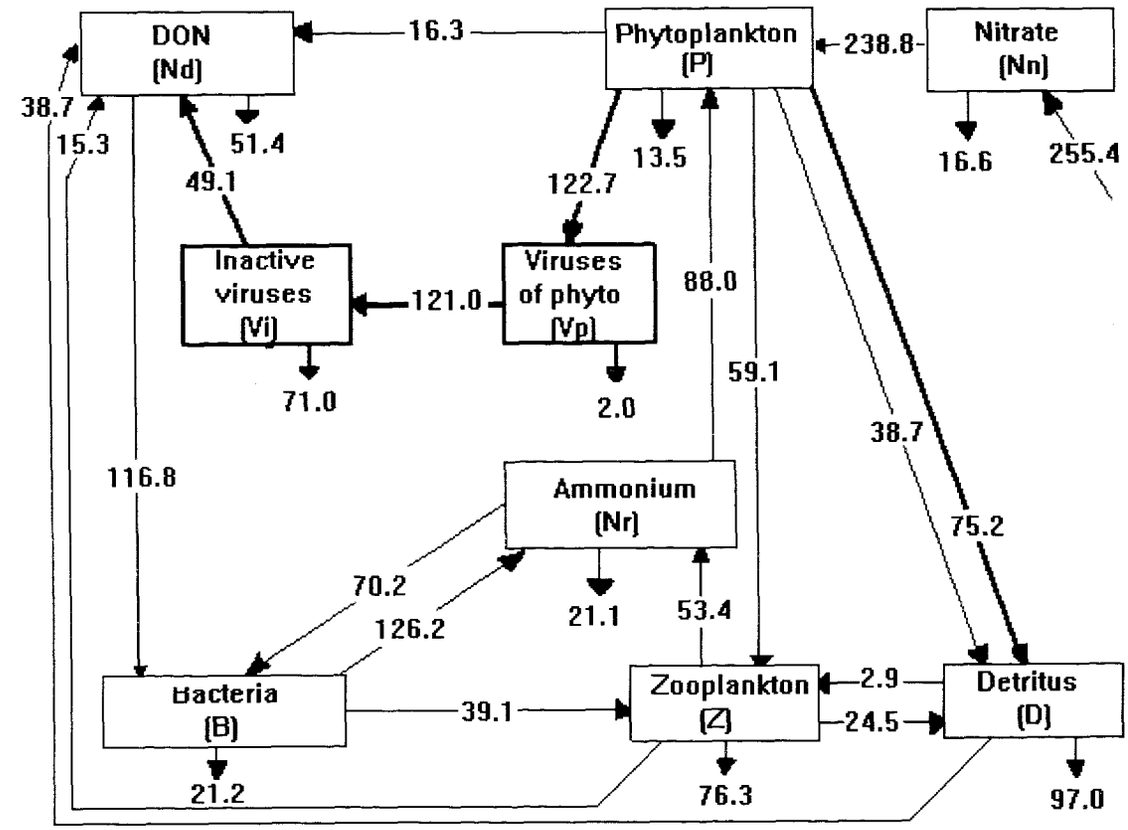

Fig. 5.57 b Maximum ep. Beta=14 Inact=.792 Virdecay=6mo. Sink=10 Mix=0.01

Figure 5.57 Annual intercompartment flows of nitrogen for (a) minimum and (b) maximum epidemic in version 5, for a variable contact rate with a decay time of six months.

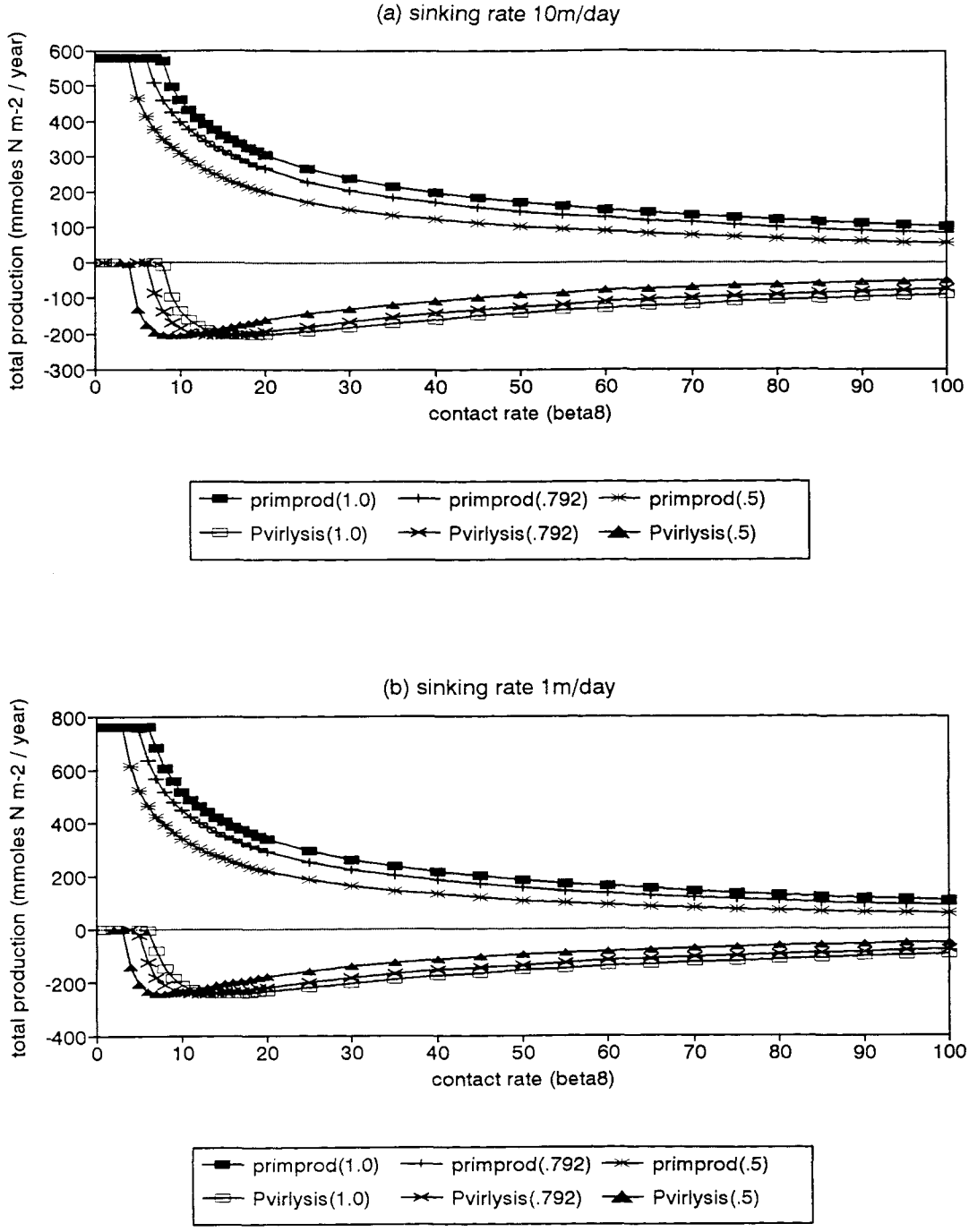

Figure 5.58 Variation in annual primary production (filled square/plus/star) and corresponding losses by phytoplankton viral lysis (empty square/cross/triangle) in mMol N/m^2/year, plotted against increasing levels of the contact rate (beta8). Inactivation rates of 1, .792 and .5 d^{-1} for a decay time of six months and a sinking rate of (a) 10m/day and (b) 1m/day. Beta8 values between 0 - 100.

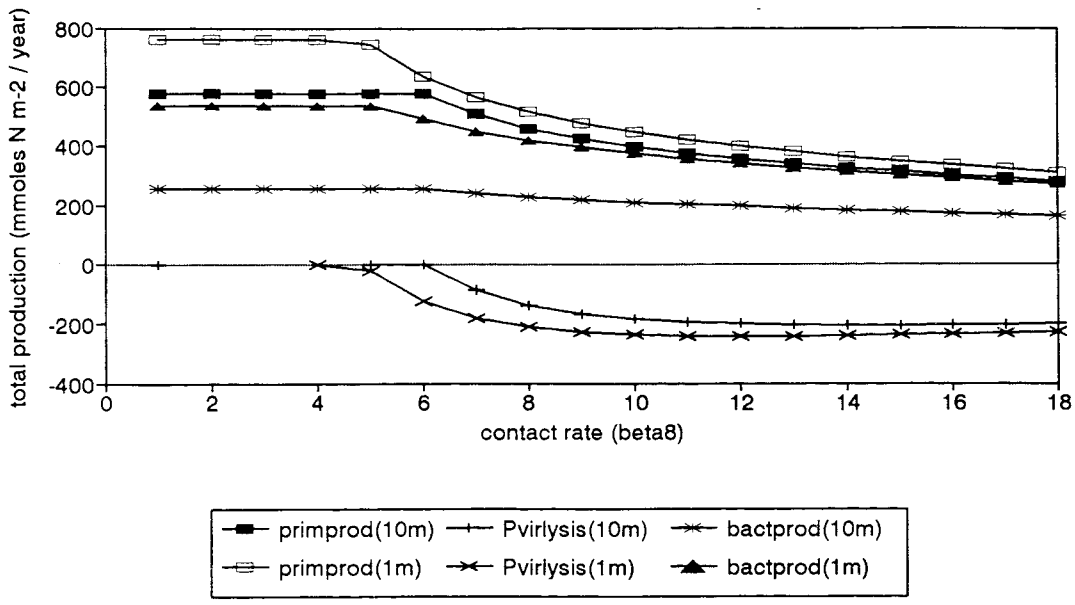

Figure 5.59 Variation in annual primary production (filled/empty square), corresponding losses by phytoplankton viral lysis (plus/cross) and bacterial production (star/triangle) in mMol N/m^2/year, plotted against increasing levels of the contact rate (beta8). Inactivation rate of .792 for a decay time of six months and sinking rates of 10m/day and 1m/day. Beta8 values between 0 - 18.

Chapter 6.

Results II - Epidemics of Bacterial Viruses.

6.1 Introduction

In chapter 5 the dynamics of phytoplankton viruses was investigated. The effect of contact rate increase from minimum to maximum epidemics on the temporal scale of phytoplankton and viral production was discussed and some general relationships between levels of inactivation and decay rates and the resulting scale of viral lysis were noted.

However, epidemics of bacterial viruses are probably the most important contributors for the biomass of inactivated viruses in the ocean (Cochlan et al. 1993). In this chapter the aim is to investigate the dynamics of bacterial viruses by varying the parameters found in the previous chapter to be most critical to describing the characteristics of an epidemic.

For reference purposes only, a characterisation of bacteria epidemics using the detritus pathway for lysed cell debris is presented in section 6.2 and is referred to as version 6.a. Results of simulations with a standard flow into DON of lysed bacterial debris are analyzed in § 6.3, thereby introducing the "official" version 6 of the model. A comparison to a simulation with a sinking rate of 1m/day is presented in § 6.4. Interannual variability on bacterial production due to natural oscillations in active viruses is discussed in § 6.5. The response of the epidemic to seasonally varying contact rates is analyzed in § 6.6, thereby introducing version 7 of the model. The effects of $\beta 9$, inactivation and decay time increases on production rate, growth rate and biomass are studied as well as the host-prey dynamics. The chapter ends with a summary and discussion of the conclusions reached from these numerical simulations.

Supporting tables and figures in this chapter:
version 6.a - Tables 6.1 to 6.4 and Figures 6.1 to 6.2,
version 6 - Tables 6.5 to 6.11 and Figures 6.3 to 6.13,
version 7 - Tables 6.12 to 6.19 and Figures 6.14 to 6.24.

Details of experimental characteristics for simulation runs can be found in the List of Tables and List of Figures.

6.2 Characterisation of bacteria epidemics using the detritus pathway for lysed cells

Phytoplankton primary production is very sensitive to the beginning of the bacterial epidemics (Fig. 6.1 & 6.4) declining 30.6% from 578.5 to **ca.** 400 mMol N m^{-2} yr^{-1} until the contact rate that yields the maximum annual output of viruses is reached. Thereafter primary production increases slightly. This pattern is identical in either six or one month decay simulations.

The total nitrogen uptake of bacteria represented by the gross bacterial production does not show any significant variation but increases very slightly (1.4%) during the mid-range of contact rates declining only 7.3% as the maximum output of viruses is reached.

However the net bacterial production (uptake of DON plus ammonium minus excretion of ammonium) is up to twice as high due mainly to a 74% decline in the excretion of ammonium with the increase in contact rate (Fig. 6.2). The effect is further emphasised because the uptake of DON and ammonium remained very high throughout the range of Beta9 values that were tested. Both increased 1.5% during the mid-range of contact rates and slowly declined by 4.5% and 12%, respectively as the Beta9 value for maximum output of viruses was reached. Therefore in bacterial epidemics the bacteria are net consumers of ammonium as opposed to net producers of ammonium which they are in phytoplankton epidemics.

Note that most nitrogen is diverted into viral lysis of bacteria whose output in the minimum epidemic (Table 6.1) is 24-32 mMol N m^{-2} yr^{-1} increasing to 187 mMol N m^{-2} yr^{-1} in the

simulation of maximum annual viral lysis for a decay rate of six months with an inactivation rate of .792 d^{-1} (Table 6.3).

The highest maximum daily flows into viral lysis occurred in the minimum epidemics (Table 6.1) during spring blooms and showed an increase with the inactivation rate from 2.1 to 3.2 and 3.7 mMol N m^{-2} d^{-1}.

Otherwise the three inactivation rates tested, .5, .792 and 1 d^{-1}, produced similar results. The contact rates for the minimum epidemics in the six months decay simulations were 7.5, 11.9 and 14.9, respectively. Likewise, similar results were obtained for one month decay simulations in epidemics of the maximum annual viral lysis (Table 6.2) for contact rates 16, 24 and 31.

The maximum viral lysis (Table 6.4) increases from 186.5 to 290.2 and 397.5 mMol N m^{-2} yr^{-1} when the decay time is shortened from six to one month and to one day, respectively. The maximum net bacterial production increases from 197.0 to 311.4 and to 422.4 mMol N m^{-2} yr^{-1} when the decay time is shortened from six to one month and to one day, respectively with an inactivation rate of .5 d^{-1}. That is two, three and four times the bacterial production of control run B.

Notice from Tables 6.3 & 6.4 that the maximum bacterial production and maximum viral lysis are reached at an ever lower contact rate for each increase in the decay rate. That is contrary to what was found in phytoplankton epidemics where some contact rate adjustment was needed in minimum epidemics but the contact rate for production maximums kept the same value in all decay simulations.

In comparison to the simulations of phytoplankton epidemic with identical decay time (Tables 5.5 & 6.3) the amount of nitrogen diverted at the maximum annual viral lysis in the bacteria epidemic is 8.7% lower in the six month decay simulation, 30% higher in the one month decay simulation and

70% higher in the one day decay simulation. Notice that there is a factor of three between contact rates for the minimum and maximum viral lysis in the six month decay simulation (Tables 6.1 & 6.3) as compared to a factor of two in the phytoplankton epidemics (Tables 5.4 & 5.5).

Furthermore, the contact rates in all bacteria epidemics are two times larger than their counterparts in phytoplankton epidemics.

Summary

In minimum epidemics the higher the inactivation rate of virus the more intense bacterial viral lysis becomes during spring blooms. Such differences are less marked in epidemics for the maximum annual viral lysis.

The one month and one day decay simulations produce higher maximum viral lysis than any phytoplankton epidemic and display an identical factor of two between contact rates for minimum and maximum epidemic.

6.3 Flow into DON of lysed bacterial debris

Bacteria are very small organisms therefore their lysed cell debris is thought to enter directly the pool of DON instead of first flowing through the detritus compartment. The impact of inactivation rate and decay time of inactivated virus on annual production rates and biomass levels will be investigated.

The overall reaction of the system to the new path for nitrogen cycling is similar to what was described in § 6.2 the difference being that bacteria and DON become more dynamic compartments in the model in terms of nitrogen flow (see flow networks, Fig. 6.3 a,b,c) whilst the other compartments suffer an up to 40% generalized reduction

compared to control run B.

For decay times of one month bacteria cycles three times more nitrogen than zooplankton and more than two and a half times that of total phytoplankton primary production (Fig. 6.3.c). For simulations with a six month decay time the nitrogen uptake of bacteria is 80% that of zooplankton and 60% that of phytoplankton in minimum epidemics (Fig. 6.3.a).

Decay times of fifty years yield bacterial uptakes of nitrogen similar to those of zooplankton and which are 64% that of primary production in maximum epidemic (Fig. 6.3.b).

In all these simulations regenerated primary production was up to five times lower than in control run B due to the diversion of ammonium in the system into viral synthesis. Any simulation of maximum epidemic or a minimum epidemic with a fast decay time will result in an uptake of ammonium up to twice that of its excretion by bacteria though the latter maybe up to 30% larger than control run B (Fig. 6.3.c).

The total phytoplankton primary production dropped by up to 35% compared to control run B due to the lower availability of ammonium for regenerated production. Consequently the phytoplankton loss to detritus by natural mortality decreased by up to 36%, the zooplankton grazing on phytoplankton dropped by 37% and so did its excretion of ammonia by up to 41%.

Overall, the annual rates of bacterial production and viral lysis are up to 2.6 times larger when the lysed bacterial debris flows directly into DON due to the faster cycling of matter (Fig. 6.4).

These simulations require contact rates only half as large as those using the fictitious detritus pathway.

The annual primary production declines gradually (Table

6.5.b) from 533 to 379 mMol N/m^2/year, a total drop of 28.9%, in the six month decay simulations when the contact rate is increased from the value for minimum epidemics to that for the maximum annual viral lysis.

A constant rate of annual primary production of *ca.* 379 mMol N/m^2/year (Table 6.5.c) is yielded in simulations with one month decay for all contact rates. By contrast, the equivalent simulation in § 6.2 (see Fig. 6.4) underwent a smooth decline until a similar bottom value was eventually reached.

A collapse of the bacteria spring bloom caused by viruses occurs in minimum epidemic for simulations with a decay time longer than one month (six months and fifty years, Fig. 6.5.a) in a way analogous to the events simulated in phytoplankton epidemics of § 5.11. The bacteria decline is initiated on days 94/107 respectively, four days before the phytoplankton decline in the six months simulation, and five days after the phytoplankton decline in the fifty year simulation. The bacterial concentration drops from 0.20 to 0.11 and from 0.27 to 0.06 mMol N/m^3 on days 102/123, respectively. Thus it takes nine days to reduce the bacterial biomass by a half in the six months simulation and thirteen days to reduce it by 3/4 in the fifty year simulation. By contrast, the bacteria biomass is kept at an almost steady concentration of *ca.* 0.16 mMol N/m^3 during the whole year in the one month decay simulation. The concentration of bacteria reaches its lowest levels of 0.09, 0.06 and 0.03 mMol N/m^3 in maximum bacterial epidemics (Fig. 6.5.b) for one month, six months and fifty year decay simulations. Notice that these steady levels are half those of the lowest values for minimum epidemics during the spring bloom. Although the concentration of bacteria is not constant the oscillations in spring are less than 10% around their average level. In autumn these oscillations are maintained for the one and six month simulations but for the fifty year simulation it becomes larger.

The concentration of inactivated viruses (Fig. 6.6) during summer, 0.9-1.2 mMol N/m^3 in maximum epidemics, is similar to the levels reached in phytoplankton epidemics but is twice to four times larger in minimum epidemics (0.5-0.8 mMol N/m^3). Notice that the maximum concentration of inactivated viruses decreases 38% for longer decay times in minimum epidemics. However this concentration increases 33% for longer decay times in maximum epidemics.

The phytoplankton biomass follows a pattern similar to control run A in all levels of bacterial epidemics (Fig. 6.7 a,b). The drop in phytoplankton biomass at the end of the spring bloom is well replicated here. Therefore viral epidemics of phytoplankton are not needed to adjust the simulated biomass to the observation data.

The phytoplankton losses (Fig. 6.8) to zooplankton grazing grow during spring and are over 100% of primary production between days 104-127 in six and one month decay simulations. These accumulate to the losses by detrainment (up to 60/90%, respectively) and natural mortality (20-30%) pushing the overall losses to twice the primary production levels thus causing the collapse of the spring phytoplankton bloom.

The analysis of the nutrient limiting factors showed that the phytoplankton bloom was not nutrient limited. Their relative abundances were twice those of control run B. Although the collapse is mainly attributed to zooplankton it is interesting that zooplankton concentration levels are lower than in control run B. The contributions to the ammonium flows show that the bacteria exudation declines 15 days before the peak of the phytoplankton bloom which is then sustained by zooplankton excretion and mortality. The same sequence of events take place in Control Run B.

The seasonal cycle of specific rate of bacterial production (Fig. 6.9 a,b) show that for the six months and

fifty years decay simulations the rate of uptake of DON and ammonium is constant throughout the year. The ammonium excretion rate declines slowly from winter to spring, drops at the end of the bacterial spring bloom, rises rapidly after the bloom, keeps a steady level during summer, drops again during the autumn bloom and rises slowly thereafter. The specific loss rate of bacterial production into viral lysis rises drastically during the spring bloom from days 115 to 120, and reaches a peak level of 3 mMol N m^{-2} d^{-1}, twice that of the bacterial production rate. Its rate drops to half that of bacterial production six days later, rising again on day 133 to twice its own previous value and declines slowly until day 160.

The processes outlined above are initiated twenty-five days earlier, with a magnitude 30% larger in the flows but 50% lower in the specific rates, when the decay time of inactivated viruses is shortened from fifty years to six months.

For one month simulations the uptake of DON increases gradually from the beginning of the year, reaches its maximum height after the spring bloom, maintains a constant level during summer and decreases gradually during the autumn bloom. In contrast the seasonal cycle of ammonium uptake shows the opposite trend; a slow decline from the beginning of the year dropping faster at the end of spring bloom, keeping a constant level during summer and increasing at the autumn bloom. The ammonium excretion is constant during the first 50 days of the year, declines slowly during the spring bloom and increases slowly immediately after. The specific loss rate of bacterial production into viral lysis ranges from 0.6 to 0.8 d^{-1} during the annual cycle.

Losses of ammonium to detrainment during the spring bloom are less important than gains to the ammonium pool by natural mortality of zooplankton as these represent up to 50% of the seasonal primary production.

The total nitrogen uptake of bacteria which at over 900 mMol N/m^2/year is 3 times larger than Control run B, is nearly constant at all levels of contact rate in epidemics with a decay time of one month (Table 6.6.c). However, it increases 37% from 312 to 429 mMol N/m^2/year with contact rate increase in simulations with a decay time of six months (Table 6.6.b). There is a modest 8% increase in the total nitrogen uptake of bacteria from 260 to 280 mMol N/m^2/year with contact rate increase in the fifty year decay simulations.

6.3.1 Summary

Viral lysis surpasses gross bacterial production (total nitrogen uptake by bacteria) for a short period during the spring bloom. The losses to zooplankton grazing and ammonium excretion during this period are low. Ammonium excretion dominates the annual cycle, except when surpassed by viral lysis during brief periods in spring and autumn, and is high in winter, low during spring, increases during summer (highest) declines during the autumn bloom, increasing again towards the end of this period. However, in one month decay simulations ammonium is second to viral lyses which is supreme in all seasons of the year.

Bacteria are net consumers of ammonium, regardless of decay time of inactivated viruses, in bacteriophage epidemics. The excretion of ammonium was always smaller than its uptake and declined with contact rate increase.

In conclusion, in bacteriophage epidemics viral lysis increases at the expense of ammonium excretion and due to rises in DON and ammonium uptake. Consequently it also diminishes the total ammonium pool, decreases regenerated primary production and increases the f-ratio.

Bacterial production will not exceed primary production

neither in minimum nor maximum epidemics if the decay time of inactivated viruses is long (6 months or more). Its maximum level will be 31 to 93% that of primary production at the most. However if the decay time is short (1 month or less) then viral lysis of bacteria can force the bacterial production to rise to levels twice that of primary production at any given level of viral epidemics. These findings are relevant for the discussion presented in Fuhrman (1992).

It was shown that longer decay times result in decreasing levels of the total nitrogen uptake by bacteria. This is consistent with the fact that less nitrogen is available to bacterial consumption because it is being retained for longer in the form of inactivated viruses.

Shortening the decay time results in a generalized increase in net bacterial production and viral lysis for all contact rates. There is also a generalized decrease in primary production although the range of values is much smaller in maximum epidemics.

It is possible to speculate that ocean samples where high bacterial productions have been measured may indicate that intense processes of viral lysis are taking place.

Epidemics of bacterial viruses display their control role by forcing the bacteria biomass to either collapse at bloom events or to keep at a nearly constant level throughout the year, depending on contact rate levels and decay rates.

The timing of bacterial collapse is initiated earlier for each increase in decay rate (shorter decay times). An increase in bacterial production driven by a faster cycling of nitrogen results in an earlier critical biomass of active viruses being reached which causes the bacterial collapse.

Although the contact rate is fixed the specific rate of viral lysis is variable and oscillates during the spring

bloom from values near zero to twice that of the rate of bacterial production. This results in an intense period of viral lysis of bacteria by mid-April lasting 5 to 10 days.

The concentration of inactivated viruses increases for longer decay times in maximum epidemics because nitrogen locked in viruses is not being broken down as fast into DON. By contrast the opposite happens in minimum epidemics because the dynamics of the bacterial compartment rises drastically for shorter decay times and more viruses are produced.

Notice that the contact rates needed for minimum and maximum epidemics are (1) lower than for simulations with a detritus pathway and (2) their value becomes also lower with increase in decay rates (shorter decay times).

6.4 Sinking rate of 1m/day

Following Fasham et al. (1990) a detritus sinking rate of 1m/day was experimented to evaluate its impact on the behaviour of bacterial epidemics.

The phytoplankton primary production is 30-42% larger, **ca.** 160 mMol N/m^2, in 1m/day simulations for the minimum epidemic. Nonetheless, its value is similar to those of 10m/day simulations in epidemics for the maximum rate of annual viral lysis.

The annual rate of viral lysis in 1m/day simulations for the minimum epidemic is similar to 10m/day simulations for long decay times and 13%, 83 mMol N/m^2, lower for short decay times (Tables 6.7.a & 6.5 a,b,c). Overall viral lysis is 48-57%, 156-428 mMol N/m^2, higher than 10m/day simulations in epidemics for the maximum rate of annual viral lysis.

Though overall net bacterial productions are 12-90%, 93-148 mMol N/m^2, larger in 1m/day simulations, the percental of

viral lysis are significantly lower due to the lower value of contact rates (and an increased excretion of ammonium in the six month decay simulation which rises the net bacterial production) (Table 6.7 a,b,c & 6.5 a,b,c).

Contact rates for 1m/day simulations are 25-48% lower than those for 10m/day simulations.

Contact rates required for minimum and maximum epidemics increase for longer decay times and decrease for shorter ones by as much as 17 to 50% (Table 6.7 a,b,c). It is therefore crucial to determine experimentally the decay time of inactivated viruses in seawater in order to validate the estimated contact rates of this model. A further constraint on the values of $\beta 8$ and $\beta 9$ can be given by the theoretical limit on contact rates (Murray & Jackson, 1992).

Faster decay times result in the percental increase of viral lysis relatively to net bacterial production in simulations of minimum and maximum epidemics. This value rises from 22% to 64% in simulations of fifty years to one month decay for minimum epidemics; and increases from 92% to 95% in the equivalent simulations for maximum epidemics (Tables 6.7 a,c).

The largest values in total bacterial uptake of nitrogen do not correspond to the highest values of net bacterial production due to asymmetries in the excretion of ammonium. Maximum net values are yielded at higher contact rates for any decay time (Tables 6.8 a,b,c,d).

The bacterial uptake of DON and ammonium plus excretion of ammonium increase under viral epidemics. Although the uptake of Ammonium increased three times, the most remarkable was the six fold increase in DON uptake.

The annual rates of primary production, net bacterial production and viral lysis are similar for a given decay time

under equivalent epidemics pressure (contact rates for minimum or maximum) for all inactivation rates (Tables 6.9 a,b).

However there is an increase in the maximum daily flow into lysis, from 3.29 to 4.72 mMol $N/m^2/day$, as the inactivation rate increases resulting in the peak value being reached systematically earlier in minimum epidemics (Table 6.9.a).

The primary production drops by a half, the net bacterial production increases by a factor of two, viral lysis rises by a factor of five, and the maximum daily flow into lysis hardly changes when the contact rate is increased from minimum to maximum epidemics in simulations of six months decay with a sinking speed of 1m/day (Table 6.8.a).

The primary production drops 23%, the net bacterial production increases by a factor of three (2.7), the viral lysis rises by a factor of seven (6.6), and the maximum daily flow into lysis hardly changes when the decay time of inactivated viruses is shortened from six to one month in simulations of minimum epidemics with a sinking speed of 1m/day (Table 6.7.a). The values of these parameters do not change significantly for decay times ranging from fifty years to one year. The maximum variation between one year and six months is a 27% decrease in the maximum daily flow into lysis.

The primary production hardly changes, the net bacterial production increases by a factor of two (2.2), viral lysis rises by a factor of three (2.5), and the maximum daily flow into lysis rises by a factor of two (2.2) when the decay time of inactivated viruses is shortened from six to one month in simulations of maximum epidemics (Table 6.7.c). However the values of these parameters increase only 39-59% when the decay time is shortened from fifty years to six months, with the exception of primary production which hardly changes.

The ratio of viral lysis to net bacterial production increases:

1- When the contact rate is risen from minimum to maximum epidemics, from 22% to 95%,

2- When the decay time is shortened from fifty years to one month

from 22% to 64% in minimum epidemics

from 92% to 95% in maximum epidemics

3- When the sinking speed of detritus is increased from 1 to 10m/day.

Summary

Contact rates are 25-48% lower in 1m/day simulations yet they yield higher rates of annual viral lysis and net bacterial production and also generally higher maximum daily flows into lysis in spite of the overall percentage of lysis being half to three quarters those of 10m/day simulations.

A 31-45% reduction of contact rates with faster decay times for bacteriophage epidemics is another qualitative difference from the pattern obtained in phytoplankton epidemics in which contact rates were identical independently of decay times for maximum epidemics.

The variation in production rates between fifty and one year decay is minimal. The transition between one year and six months yields an increase of 22% in net bacterial production and viral lysis. However the most significant changes in production rates were between six and one month decay simulations.

6.5 Interannual variability

The highest values for maximum daily viral lysis of bacteria are reached close to the values of minimum epidemic (Fig. 6.10).

Contact rates around the value of the minimum epidemic display considerable interannual variability on the size and timing of the collapse of the bacterial spring bloom (Fig. 6.11) as a result of small differences in the overwinter concentration of the active bacterial viruses.

Although viral lysis of bacteria does not affect the timing for the onset of bacterial blooms it nonetheless causes their early collapse thus not allowing the biomass of bacteria to climb to the peak levels of control run B.

Table 6.10 shows the overwinter concentration of active bacteriophages and corresponding bacteria concentration for each year of a ten year run of minimum epidemic, compared with the peak bacteria concentration and corresponding Julian day number together with peak concentrations of active bacteriophages during the spring bloom and the resulting peak concentration of inactivated viruses. Notice that the overwinter concentration of active viruses is decreasing every year very slightly whilst the overwinter concentration of bacteria is nearly constant. These values have an impact on the timing and concentration of the peak bacteria spring value which do show some variation in the first 6 years of the model run.
Lower overwinter concentrations of active viruses result in larger peak bacteria values the following spring.

The bacterial loss flows show that viral lysis is starting increasingly later for each new simulation year (Fig. 6.12) thus allowing the bacterial biomass to rise to higher levels (Fig. 6.11) and consequently excrete more ammonium that in turn fuels phytoplankton regenerated production (Table 6.11) during the final part of the spring bloom event. This results in the life of the phytoplankton bloom being extended for ca. 3 more days (Fig. 6.11) and also benefiting the zooplankton that follows on its wake.

The annual rate of viral lysis of bacteria is being

reduced for each consecutive year (Table 6.11) due to the accrued delay in the start of viral lysis in each year. Notice that viral lysis finishes always on the same day (Fig. 6.12) independently of the starting date.

The interannual variability does not occur at higher contact rates (Fig. 6.13).

Summary

It was shown that small changes in the overwinter concentration of viruses can introduce interannual variability in the ecosystem at low contact rates, which are manifested by changes in the size and timing of the collapse of bacterial blooms. These in turn are immediately reflected in the magnitude of daily bacterial viral lysis and in variations of the annual rates of viral lysis and regenerated production.

6.6 Inclusion of a variable contact rate

The infectivity of modelled viruses changes during the annual cycle due to the implementation of a variable contact rate. On par with changes in host density another physical justification for the seasonal variation in contact rate is lower viability of viruses during summer due to increased exposure to UV radiation as well as lower number of contacts between host and virus in winter due to dilution with the entrainment of deep waters into the mixed-layer.

6.6.1 Effects of $\beta 9$ increase on production rates

There is an increase in bacterial production with the increase in the level of contact rate with a peak located between minimum to maximum epidemic (Tables 6.12.a; 6.13.a; 6.14; 6.15; 6.16). There is an overall increase in the bacterial uptake of DON and ammonium which increases up to

80% and 29% for faster decay times (Tables 6.12.b; 6.13.b). The losses to viral lysis accompany the growth in bacterial production and divert an increasingly larger percental from 21% in minimum to 96% in maximum epidemic. Part of the lysed material flows into DON fuelling the nitrogen available for fast bacterial growth.

As a result of the nitrogen sequestered by viral synthesis the bacterial excretion of ammonium declines and consequently the regenerated primary production diminishes (Table 6.12.c) and thus total primary production decreases gradually. The lowest value it can reach is *ca*. 380 mMol N/m^2/year, which is 33% below control run B (Fig.6.14.a)

The lowest primary production is yielded by a contact rate in between minimum and maximum epidemics in one month decay simulations (Table 6.12.a) and after the maximum epidemic in six months decay simulation (Table 6.13.a). Thereafter there is a slow but steady increase in primary production as Beta9 increases in spite of a gradual decline in new production. This is due to a rise in regenerated production which results from the bacterial uptake of ammonium declining faster than the combined excretion of ammonium by zooplankton and bacteria which also decline as the contact rate increases (Tables 6.12.c; 6.13.b).

Overall net bacterial production ranges from 118 to 776 mMol N/m^2/year (Fig.6.14.b) according to decay time and contact rates and viral lysis (Fig. 6.14.c) ranges from 24 to 726 mMol N/m^2/year representing 21% to 96% of bacterial production. The maximum daily flow into lysis ranges from 1.6 to 9 mMol N/m^2/day in simulations with a variable contact rate.

The bacterial production and viral lysis in one month decay simulation with a variable contact rate are 4 to 55% lower than the fixed rate simulation with exception of maximum daily flow into viral lysis which are similar (tables

6.12.a and 6.5.c). This negative balance declines from minimum to maximum epidemic. The low rates in minimum epidemic are due to a decrease of bacterial uptake of ammonium and DON by more than 1/3 (tables 6.12.b and 6.6.c). However, the bacterial excretion of ammonium is unaffected and the regenerated production is higher (table 6.12.c) and consequently the primary production is 33% larger than in fixed contact rate simulations for the minimum epidemic. For longer decay times the overall differences in production rate is 4% lower for variable contact rate than fixed contact rate. Although the maximum daily flow into lysis can be up to 40 % larger in variable contact rate simulation.

A detailed analysis of tables 6.13.a, 6.14, 6.15, 6.16 and 6.17 reveals that the highest or lowest values for primary production, bacterial production, viral lysis of bacteria and maximum daily flow into lysis occupy a range of contact rates that include the intermediate levels between minimum and maximum epidemics. The typical sequence for simulations with a decay time longer than one month and a sinking rate of 10 m d^{-1} is first, at the lowest contact rate, the minimum annual viral lysis then the maximum daily flow into lysis followed by the maximum annual gross bacterial production which precedes the maximum annual net bacterial production then maximum annual viral lysis and finally the lowest annual primary production at the highest contact rate. The sequence of the later two steps is reversed for simulations with a decay time of one month (table 6.12.a).

Simulations for fixed contact rates show the same general pattern, but the gross bacterial production reverses with maximum daily flow for decay time of ten years or longer. For one month decay simulations the maximum daily flow reverses its place with the lowest primary production.

Summary

It was shown that the increase in contact rate determines an increase in bacterial production and viral lysis and a decline of ammonium excretion. This results in a decrease of primary production.

A sequence of production events became apparent when studying increasing levels of contact rate.

6.6.2 Effects of inactivation and decay time increase on production rates

The production rates of primary production, bacterial production and viral lysis yield almost constant values under increasing levels of inactivation rate in either minimum or maximum epidemics. However the maximum daily flow into viral lysis rises gradually from 1.91 to 7.33 mMol N/m^2/day with increasing inactivation rate in minimum epidemic simulations (Table 6.18.a. and fig. 6.15.a). A general trend of irregular increase is shown for maximum epidemic but within a shorter range of values, from 2.56 to 2.91 mMol N/m^2/day (Table 6.18.b and fig. 6.15.b).

Primary production shows a very slight increasing trend with decay time increase from one month to fifty years for minimum, intermediate and maximum epidemics (Tables 6.18.a, b, c). However there is a drastic drop in the rate of bacterial production from one to six months (394.4 to 152.2, 670.4 to 175.1, 769.7 to 331.6 mMol N m^{-2}/ year, for minimum, intermediate and maximum epidemics respectively) with a more gradual decline thereafter. Viral lysis follows the pattern of bacterial production decline though with some slight oscillations in minimum epidemics (Fig. 6.16.a). Maximum daily flow into lysis rises gradually with the increase in decay time in the epidemics which yield the largest daily flow into lysis (Fig.6.16.b) This pattern is also followed in minimum epidemics, with an unexplained drop for the ten year decay simulation. However the flow into lysis in

maximum epidemic reverses the pattern, declining with the increase in decay time (Fig.6.16.c) closely following the trend in bacterial production and annual viral lysis.

Summary

It was shown that increasing levels of the inactivation rate have negligible effect on the annual rates of primary production, bacterial production and viral lysis, though they change the size of maximum daily flow into lysis.

Bacterial production and viral lysis are extremely high in one month decay simulations and decline for longer decay time.

6.6.3 Effects of $\beta 9$ and decay time increase on biomass

The variable contact rate increases the amplitude of the oscillations on bacterial biomass in spring bloom in minimum epidemics (Fig.6.17.a). The height of bacterial biomass is higher than for fixed contact rate simulations but drops faster and to lower concentrations. Consequently two more secondary blooms are produced before the bacterial biomass of the six month and fifty year decay simulations converges on day 160 to the same biomass levels of fixed contact rate simulations and follow the same pattern for the rest of the year (Fig.6.17.a_1 and Fig. 6.6). Nonetheless the bacterial biomass continues to oscillate all the year long for the one month decay time simulation, reaching its highest value in summer and lowest in autumn, in contrast with the constant biomass level of the fixed rate simulation. This oscillation pattern is also present in maximum epidemics (Fig.6.17.b) for all decay time simulations which is in contrast with the constant level of fixed Beta simulations. However for the fifty year decay time simulation the autumn bloom displays several oscillations identical in amplitude and frequency to those in simulations for fixed contact rates which decrease gradually.

Consequently the biomass of active viruses displays oscillations also. The pattern is similar to the fixed rate simulations with differences in the bottom values of virus concentration before spring and autumn blooms (Fig. 6.18.a). These values are larger by six and three degrees of magnitude for six month and fifty years decay time in simulations for a variable contact rate.

The peak concentration of active viruses is reached on day 97 for one month decay and increasingly later for longer decay times (8 and 16 days later for six month and fifty year decay time simulations respectively). This is due to the latter having pre spring bloom concentrations which are six to 18 orders of magnitude lower and thus take slightly longer to reach a critical biomass in spite of an earlier start for their recover with the increase in decay time.

After the bloom the decline in the concentration of active virus is larger and takes slightly longer for longer decay times reaching a bottom value before the bacterial autumn bloom. A reversal on this pattern is shown for maximum epidemics (Fig. 6.18.b) where variable contact rates yield 10% lower peak concentrations of active viruses during the spring bloom than fixed contact rates. For the rest of the year the biomass differences are negligible even for the fifty year simulation where the displayed oscillation of biomass balance in the autumn bloom is solely due to timing differences.

The biomass cycle of inactivated virus in minimum epidemic for variable contact rate simulations has a similar pattern to that of fixed contact rate. However the difference between the peak concentrations for each decay time simulation is much smaller at less than 0.0465 mMol $N/m^2/day$. The peak biomass levels are up to 0.02 mMol $N/m^2/day$ higher in fifty year simulation and 0.3 mMol $N/m^2/day$ lower in one month in comparison to fixed $\beta 9$ simulations and are similar in six month simulations. The

differences shown in figure 6.19.a. for the six month simulation are mainly due to timing.

The concentration of inactivated viruses rises with the increase in decay time in maximum epidemics. The biomass levels are very similar to those of figure 6.6 and the differences are negligible.

Summary

The variable contact rate determines an oscillation of active viruses which changes and is reflected in the pattern of the bacterial biomass for all decay time simulations. By contrast the levels of bacterial biomass are nearly constant for fixed contact rate simulations.
The height of spring blooms is reached later for increased decay times.

6.6.4 Summary

Bacterial production rises for increasing levels of $\beta 9$, with peak values between minimum and maximum epidemic. The annual rate of viral lysis closely follows the variation in bacterial production, diverting an increasingly larger proportion of the latter with the increase of contact rate.

The production rates of bacterial production, viral lysis and primary production yield almost constant values under increasing levels of inactivation rate in either minimum or maximum epidemics.

The highest values of bacterial production (776.2 mMol N/m^2/year, seven times those of control run B) and viral lysis (726.5 mMol N/m^2/year) are reached in one month decay simulations.

Bacterial production and viral lysis decline with increasing decay times for minimum, intermediate and maximum

epidemics. However the values for bacterial production are never below those of control run B.

Maximum daily flow into lysis rises gradually with the increase in inactivation rate and decay time. It declines with the increase of decay time in maximum epidemic closely following the trend in bacterial production and annual viral lysis.

The overall synthesis of new viruses ranged from 15 to 450 mMol N/m^2 /year while the corresponding debris of lysed cells into DON ranged from 9 to 276 mMol N/m^2 /year.

The concentration of Bacteria oscillates around the biomass levels obtained for fixed contact rates throughout the annual cycle for decay time simulations of six and one month. The exception being the fifty year decay simulation which matches the pattern for the fixed contact rate simulation during the autumn bloom.

Increases in decay time force the amplitude of oscillations of active virus biomass to increase up to 27 orders of magnitude which results in their peak concentrations being reached increasingly later during the spring bloom.

The biomass of active viruses at the height of the bacteria spring bloom is 8-80% larger for minimum epidemics depending on decay time and 10% lower for maximum epidemics in comparison to fixed contact rate simulations.

The peak biomass of inactivated viruses is *ca.* 0.65 mMol N/m^2/day in minimum epidemics independently of decay time. By contrast it rises from 0.8 to 1.1 mMol N/m^2/day in maximum epidemics with the increase in decay time.

The average concentration of bacteria in minimum epidemics is twice that of maximum epidemics. By contrast the

lowest concentration of virus in minimum and maximum epidemics differs by four orders of magnitude.

6.6.5 Host-prey dynamics

It will be shown that seasonal changes in contact rate and in mixed-layer dynamics (Fig.6.20) affect the bacteria-virus dynamics.

One month decay simulation for minimum epidemic (Fig. 6.21.a and a_1) :

A fast decline in the concentration of bacteria and virus takes place between day 1 and 60 (day on which viruses reach their lowest value). This is due to a deepening of the mixed-layer depth which dilutes the concentration of both host and virus and is further reinforced by a lower value of the contact rate during this period.

The spring bloom takes place from day 60 to 90 and the viruses follow on the wake of the bacteria growth, increasing their concentration by three orders of magnitude partly due to the rise in value of the variable contact rate.

The increased concentration of viruses forces the collapse of the bacterial spring bloom. The bacteria reach their lowest value on day 99 with a concentration of 0.1079 mMol N/m^3.

A secondary bloom follows which rises the virus concentration to a peak 0.04796 mMol N/m^3 on day 108. From day 108 the contact rate lessens and bacteria bloom again, increasing rapidly in concentration. Their height is reached on day 197 whilst the virus concentration drops by two thirds.

This is followed by a drastic collapse of the bacterial bloom caused by the increase in contact rate from day 197 to 294. There is not a noticeable increase in virus because the simultaneous entrainment of waters into the mixed-layer dilutes the concentration and works against the build-up of viruses.

The concentration of bacteria increases from day 294 to the end of the year whilst the virus concentration declines because the mixed-layer continues to deepen and the variable contact rate decreases.

One month decay simulation for maximum epidemic (Fig. 6.21b):

The concentration of viruses on day one is the lowest of the year although it is four orders of magnitude larger than in minimum epidemic. By contrast the concentration of bacteria is large reaching a height on day 7 due to the low infectivity of viruses during this period.

The bacterial concentration collapses to half of its value on day 76 due to dilution caused by the deepening of the mix layer and the rising of the virus contact rate. The virus concentration increases twofold during the ensuing spring bloom whilst the bacterial concentration is kept constant until day 116 due to the pressure of a very high contact rate.

From day 116 to 196 the bacterial bloom grows and reaches a peak of 0.1214 mMol N/m^3 while the virus concentration declines slowly. This is due to the lessening of the contact rate and the increased availability of nitrogen for bacterial growth as a result of a short decay time of inactivated viruses.

Another collapse takes place until day 283 due initially to the nitrogen diverted by virus being larger than that produced by the undergoing bacterial bloom as a result of the rising of contact rate and then due to the dilution caused by the entrainment of waters into the mixed layer.

There is a fast increase in the concentration of bacteria from day 283 to the end of the year due to the lessening of the contact rate and consequently decline of virus concentration, which is further diluted by the

entrainment of waters into the mixed-layer.

The amplitude of the oscillations in bacterial concentration during the annual cycle does not surpass twice its lowest concentration.

Six month decay simulation for minimum epidemic (Fig.6.22a):

The concentration of viruses on day 1 is low at 1E-05 mMol N/m^3. It drops by seven orders of magnitude to 3.6 E-12 mMol N/m^3 on day 59 due to dilution caused by the deepening of the mixed-layer. The concentration of bacteria increases twofold and the height of the bacterial spring bloom is reached on day 101 and then collapses under the growing pressure of viruses. The peak concentration of viruses is reached five days later at 0.06 mMol N/m^3, an increase of ten orders of magnitude on pre-bloom concentrations partly driven by a twofold increase in contact rate. When the concentration of virus drops to one third due both to the lack of hosts and a lessening of the contact rate, a secondary bloom of bacteria takes place which rises the virus biomass to 0.045 mMol N/m^3. A third much smaller bloom of bacteria takes place on day 125 with a concentration of 0.023 mMol N/m^3. Afterwards the concentration of virus declines by twelve orders of magnitude due initially to the decline in contact rate and then from day 225 due to the deepening of the mixed-layer. A minimum annual concentration of 1.28 E-12 mMol N/m^3 is reached on day 252 in spite of a rise in contact rate which is not enough to compensate for the dilution effect, whilst the concentration of bacteria is kept constant. When the autumn bloom of bacteria is initiated the biomass of virus grows by ten orders of magnitude due to the increase of host biomass which coincides with the peak of the variable contact rate and is enough to overcome the dilution effect. Its concentration reaches 0.006 mMol N/m^3 on day 326 and then declines to a concentration of 1E-5 mMol N/m^3 on day 365 due to further deepening of the mixed layer and a downturn of the contact rate.

Six month decay simulation for maximum epidemic (Fig. 6.22b):

The range of concentrations of virus biomass varies by less than an order of magnitude in maximum epidemic. The bacteria concentration is three times lower than in minimum epidemic.

The concentration of viruses increases 2.5 times during the spring bloom while the bacteria biomass drops by 47% to reach its lowest value on day 110.

The virus contact rate is low and the biomass of bacteria is high in winter. The biomass of bacteria rises and reaches a peak concentration of 0.076 mMol N m^{-2} between days 17 and 29 then declines to *ca.* 0.04 mMol N m^{-2} on day 110, whilst the virus concentration reaches a peak 0.019 mMol N m^{-2}. Bacteria grow and reach another peak in mid-summer with a concentration of 0.076 mMol N m^{-2} on day 205 whilst the virus concentration drops due to a decline in contact rate. The downturn in mixed-layer depth entrains more water into the system which dilute both host and virus causing their collapse until day 240.

The concentration of bacteria continues to decline during the autumn bloom from days 240 to 321 due to the rise in virus concentration which is the result of an increase in contact rate. Then the lessening of the contact rate combined with the further deepening of the mixed-layer reduces the virus pressure and the bacteria concentration increases until the end of the year.

Fifty year decay simulation for minimum epidemic(Fig. 6.23a and $a_{1)}$:

The concentration of virus declines by four orders of magnitude to 4.07E-24 mMol N m^3 on day 51 due to the entrainment of water in the mixed layer which dilute the

virus concentration, whilst bacterial concentration is kept constant. Then the concentration of virus grows by 18 orders of magnitude accompanying the spring increase in bacteria biomass, which reaches 0.2687 mMol N m^3 on day 106. A critical biomass of virus is reached on this day, which forces the collapse of the bacteria bloom. Further increases in the concentration of viruses to a peak 0.074 mMol N/m^3 on day 113 (Fig. 6.22.a_1) depredates the bacteria concentration to a low 0.028 mMol N/m^3 on day 115.

An oscillation in bacteria and virus biomass ensues typical of predator prey systems which takes the virus biomass to a lower concentration of 0.01 mMol N m^3/day due not only to the inactivation rate but also to a lower concentration of bacteria. Once the virus pressure is reduced bacteria blooms again and reaches a concentration of 0.14 mMol N m^3 on day 121. This pattern is repeated once more and then the virus concentration declines from 0.015 mMol N m^3 on day 136 to its lowest value of E-29 mMol N m^3 on day 270. During the autumn bloom the virus concentration increases 11 orders of magnitude.

Fifty year decay simulation for maximum epidemic(Fig. 6.23b and $b_{1)}$:

The concentration of virus, driven by a twofold increase in contact rate, increases threefold from day 1 to 110 to a value of 0.014 mMol N m^{-3} which results in a 40% decrease in bacteria concentration. Thereafter the contact rate declines to its minimum value and the concentration of virus drops by twelve orders of magnitude to a low 3.02E-14 mMol N m^{-3} on day 254. The bacteria biomass declines slightly when the mixed-layer starts deepening at the end of this period. However the autumn bacterial bloom rises the concentration of bacteria threefold from 0.03 to 0.099 mMol N m^{-3} on day 277. A surge in virus growth driven by the upturn in bacterial growth and the increase in contact rate rises the virus concentration by eleven orders of magnitude in 26 days. The

peak concentration of viruses is reached at 0.02677 mMol N m^{-3} on day 280. A drop of 98% in virus biomass on day 289 due to the deepening of mixed-layer reduces the viral pressure and results in a sequence of six consecutive secondary blooms of bacteria in a typical host-prey pattern.

Summary

In a host-prey system the concentration of bacteria and viruses interact as follows : the concentration of virus declines when mixed layer deepens (dilution effect) and the contact rate declines (lower infectivity) and when the concentration of bacteria is low (less host); the concentration of bacteria increases when the pressure of virus is low or decreases, and when short decay times of inactivated viruses result in extra DON available; bacterial collapses are due to deepening of the mixed-layer, increase of contact rate (higher infectivity), pressure of virus concentration and low availability of nitrogen.

6.6.6 Effect of decay time on growth rate

The growth rate of bacteria displays large seasonal oscillations with peaks in spring and autumn (Fig. 6.24). A fast rise in growth rate is initiated increasingly earlier for either shorter decay times or higher levels of the contact rate. However the peak growth rates are reached 2-10 days later in spring bloom and 19-30 days later in autumn bloom than those of control run B. Notice that the rise to the peak is faster for the longest decay time simulations.

The bacteria growth rate for fast cycling of nitrogen is only 15% larger than for very slow cycling of nitrogen (50 year decay time) in maximum epidemic. Nonetheless the difference in decay time is not reflected in the level of growth rate for minimum epidemic.

The highest growth rates were reached by the end of the

spring bloom and ranged between 0.58 and 0.78 d^{-1}. These values represent a five to sixfold increase on the levels of control run B (0.13 d^{-1}).

6.7 Summary and discussion

In this chapter the dynamics of bacterial viruses and its effects on bacterial production, viral lysis and primary production has been investigated. This has been achieved through the analysis of results from 150 simulations in which the infectivity of viruses and the availability of DON has been varied, thus allowing the effect of differing levels of contact rate, inactivation rate, decay time and sinking speed of detritus on overall production rates and biomass to be examined.

Increasing the levels of fixed and variable contact rates yields higher bacterial production and viral lysis due mainly to an increase in the bacterial uptake of DON and also of ammonium.

The specific rate of viral lysis is variable on fixed contact rates and oscillates during the spring bloom from values near zero to twice that of the rate of bacterial production.

Seasonally varying contact rates do not change the annual rate of viral lysis above the values of fixed rates but have an impact on the intensity (size) of the flows during blooms and also influence the concentration of the bacterial biomass during these events.

Regenerated production declines with higher forcing of the contact rate because bacterial viruses divert an increasingly higher rate of bacterial nitrogen and thus the bacterial excretion of ammonium diminishes.

Altering the levels of inactivation does not

significantly affect the annual rates of bacterial production, viral lysis and primary production. However this results in an increase of the size of maximum daily flows into lysis which is due to a later collapse of the bacteria bloom.

Changes in decay time have an impact on the timing of bacteria collapse which is initiated earlier or later according to shorter or longer decay times. The exception is the one month decay simulation for a fixed contact rate in which the bacteria biomass is nearly constant throughout the year.

Elevated peak rates of bacterial growth occurred at the end of the spring bloom for all levels of decay time and contact rate. These high growth rates can be explained by faster cycling of nitrogen due to increased virus pressure on bacteria biomass during this period which intensify the direct flow into DON of lysed cell debris. This nitrogen can be immediately taken up by other bacteria.

The concentration of active viruses follows the pattern of bacteria variation though with larger oscillations of up to 27 orders of magnitude, which increase with decay time. As a result their peak concentration is reached increasingly later for longer decay times.

Increases in decay time result in a decline of bacterial production and viral lysis due to diminished availability of DON which is sequestered for longer periods in inactivated viruses.

A decrease of the detritus sinking rate increases drastically the bacterial production and viral lysis. This is due to a longer residence time in the mixed-layer of nitrogen that can be broken down into DON and thus become available for growth.

Host-prey dynamics of bacteria and viruses are affected by external factors some of which have been summarized above. Deepening of the mixed-layer, increase of contact rate, pressure of virus concentration and low availability of nitrogen result in bacteria decrease or collapse. Dilution effect, low infectivity and fewer hosts are responsible for the decline of virus concentration and increase of bacteria concentration.

This work has identified seven gradually increasing steps in a range of contact rates that describe different levels of epidemics.

- minimum annual viral lysis (referred to as minimum epidemic),
- maximum daily flow into lysis,
- maximum annual gross bacterial production (referred to as maximum annual uptake of nitrogen by bacteria),
- maximum annual net bacterial production,
- maximum annual viral lysis (referred to as maximum epidemic),
- minimum annual primary production.

The sequence of the second and third and of the last 2 steps reverses according to decay time or sinking speed of detritus.

6.8 Tables

Inactivation rate	Beta9	Primary production	Net Bacterial production	Viral lysis	Maximum daily flow into lysis
.5 d^{-1}	7.5	559.7	112.8	23.7	2.120(109)
.792 d^{-1}	11.9	554.8	114.0	32.3	3.156(101)
1 d^{-1}	14.9	556.9	113.4	28.5	3.717(103)

Table 6.1 Estimates of annual viral lysis, and the resulting net bacterial production and primary production, in mMol N/m^2/year, for minimum epidemics of bacterial viruses with inactivation rates of .5, .792 and 1 d^{-1}. Also shown, the maximum daily flow into viral lysis in mMol N/m^2 and day when achieved (in brackets). The lysed bacterial debris flows into the detritus compartment. The decay time of inactivated viruses was **six months**.

Inactivation rate	Beta9	Primary production	Net Bacterial production	Viral lysis	Maximum daily flow into lysis
.5 d^{-1}	16	387.9	309.8	290.2	2.684 (76)
.792 d^{-1}	24	387.9	313.3	292.4	2.739 (76)
1 d^{-1}	31	387.7	313.4	293.2	2.711 (76)

Table 6.2 Estimates of maximum annual viral lysis, and the resulting net bacterial production and primary production, in mMol N/m^2/year, for epidemics of bacterial viruses with inactivation rates of .5, .792 and 1 d^{-1}. Also shown, the maximum daily flow into viral lysis in mMol N/m^2 and day when achieved (in brackets). The lysed bacterial debris flows into the detritus compartment. The decay time of inactivated viruses was **one month**.

Decay time	Beta9	Primary production	Net Bacterial production	Viral lysis	Maximum daily flow into lysis
6 months	40	400.7	197.3	187.0	1.795 (76)
1 month	24	388.4	313.3	292.4	2.739 (76)
1 day	21	399.6	429.4	402.5	4.116 (76)

Table 6.3 Estimates of maximum annual viral lysis, and the resulting net bacterial production and primary production, in mMol N/m^2/year, for epidemics of bacterial viruses with decay times of inactivated viruses of six months, one month and one day. Also shown, the maximum daily flow into viral lysis in mMol N/m^2 and day when achieved (in brackets). The lysed bacterial debris flows into the detritus compartment. The inactivation rate was .792 d^{-1}.

Decay time	Beta9	Primary production	Net Bacterial production	Viral lysis	Maximum daily flow into lysis
6 months	25	401.4	197.0	186.5	1.755 (76)
1 month	15	387.9	311.4	290.2	2.702 (76)
1 day	14	397.2	422.4	397.5	3.996 (76)

Table 6.4 Estimates of maximum annual viral lysis, and the resulting net bacterial production and primary production, in mMol N/m^2/year, for epidemics of bacterial viruses with decay times of inactivated viruses of six months, one month and one day. Also shown, the maximum daily flow into viral lysis in mMol N/m^2 and day when achieved (in brackets). The lysed bacterial debris flows into the detritus compartment. The inactivation rate was .5 d^{-1}.

Beta9	Primary production	Net Bacterial production	Viral lysis of bacteria	Maximum daily flow into lysis
12.8	556.4	117.1	23.3 (20%)	3.036(120)
17	478.9	177.0	133.7 (76%)	2.226 (87)
36	395.2	207.6	195.0 (92%)	1.991 (76)

Table 6.5.a Estimates of annual totals of viral lysis of bacteria and corresponding percentage to net bacterial uptake of nitrogen (in brackets) compared with the resulting net bacterial production and phytoplankton primary production in mmol N/m2/yr. Also shown is the maximum daily flow into lysis in mmol N/m2/day and day when achieved (in brackets). Values are calculated for the minimum epidemic (Beta9=12.8), for the epidemic with the maximum net bacterial production (Beta9=17.0), and for the epidemic with the maximum annual output of viruses (Beta9=36.0). The lysed bacterial debris flows directly into the DON compartment and the decay time of inactivated viruses is **fifty years**. The sinking speed of detritus is 10m/day.

Beta9	Primary production	Net Bacterial production	Viral lysis of bacteria	Maximum daily flow into lysis
10.8	533.4	164.8	81.2 (49%)	3.734 (98)
18	379.8	354.0	321.0 (91%)	2.855 (76)
20	378.9	351.5	323.3 (92%)	2.808 (76)

Table 6.5.b Estimates of annual totals of viral lysis of bacteria and corresponding percentage to net bacterial uptake of nitrogen (in brackets) compared with the resulting net bacterial production and phytoplankton primary production in mmol N/m2/yr. Also shown is the maximum daily flow into lysis in mmol N/m2/day and day when achieved (in brackets). Values are calculated for the minimum epidemic (Beta9=10.8), for the epidemic with the maximum net bacterial production (Beta9=18.0), and for the epidemic with the maximum annual output of viruses (Beta9=20). The lysed bacterial debris flows directly into the DON compartment and the decay time of inactivated viruses is **6 months**. The sinking speed of detritus is 10m/day.

Beta9	Primary production	Net Bacterial production	Viral lysis of bacteria	Maximum daily flow into lysis
8	374.8	742.9	620.0 (83%)	5.008 (84)
12	378.9	803.5	741.4 (92%)	5.718 (76)
14	381.1	800.2	751.6 (94%)	5.767 (76)

Table 6.5.c Estimates of annual totals of viral lysis of bacteria and corresponding percentage to net bacterial uptake of nitrogen (in brackets) compared with the resulting net bacterial production and phytoplankton primary production in mmol N/m2/yr. Also shown is the maximum daily flow into lysis in mmol N/m2/day and day when achieved (in brackets). Values are calculated for the minimum epidemic (Beta9=8.0), for the epidemic with the maximum net bacterial production (Beta9=12.0), and for the epidemic with the maximum annual output of viruses (Beta9=14.0). The lysed bacterial debris flows directly into the DON compartment and the decay time of inactivated viruses is **1 month**. Fixed contact rates.

Beta9	Primary production	Net Bacterial production	Viral lysis of bacteria	Maximum daily flow into lysis
5.54	412.5	1418.0	1201.0(85%)	11.86 (90)
5.56	382.5	1711.0	1465.0(86%)	12.28 (90)
8.00	395.1	2428.0	2305.0(95%)	17.92 (76)

Table 6.5.d Estimates of annual totals of viral lysis of bacteria and corresponding percentage to net bacterial uptake of nitrogen (in brackets) compared with the resulting net bacterial production and phytoplankton primary production in mmol N/m2/yr. Also shown is the maximum daily flow into lysis in mmol N/m2/day and day when achieved (in brackets). Values are calculated for the minimum epidemic (Beta9=5.54), for the epidemic with the lowest primary prodution (Beta9=5.56), and for the epidemics with maximum net bacterial production and maximum annual output of viruses (Beta9=8.0). The lysed bacterial debris flows directly into the DON compartment and the decay time of inactivated viruses is **one day**. Fixed contact rates.

Beta9	DON uptake	Ammonium uptake	Ammonium excretion	Cell debris into DON
12.8	162.0	97.2	142.1	8.8
17.0	174.9	104.8	102.7	50.8
36.0	161.3	90.1	43.7	74.1

Table 6.6.a Estimates of annual totals of DON and Ammonium uptake compared to Ammonium excretion by the model bacteria in mmol N/m2/year. Values are calculated for the minimum epidemic (Beta9=12.8), for the epidemic with the maximum net bacterial production (Beta9=17.0), and for the epidemic with the maximum annual output of viruses (Beta9=36.0). The lysed bacterial debris flows directly into the DON compartment and the decay time of inactivated viruses is **fifty years**. Fixed contact rates.

Beta9	DON uptake	Ammonium uptake	Ammonium excretion	Cell debris into DON
10.8	195.5	117.3	148.0	30.9
15	279.5	159.1	103.8	110.5
18	288.4	151.9	86.3	122.0
20	287.7	141.5	77.7	122.9

Table 6.6.b Estimates of annual totals of DON and Ammonium uptake compared to Ammonium excretion by the model bacteria in mmol N/m2/year. Values are calculated for the minimum epidemic (Beta9=10.8), for the epidemic with the maximum ammonium uptake (Beta9=15.0), for the epidemic with the maximum net bacterial production (Beta9=18.0), and for the epidemic with the maximum annual output of viruses (Beta9=20.0). The lysed bacterial debris flows directly into the DON compartment and the decay time of inactivated viruses is **6 months.** Fixed contact rates.

Beta9	DON uptake	Ammonium uptake	Ammonium excretion	Cell debris into DON
8	634.5	302.7	194.3	235.6
12	725.3	207.5	129.3	281.8
14	729.4	181.6	110.8	285.6

Table 6.6.c Estimates of annual totals of DON and Ammonium uptake compared to Ammonium excretion by the model bacteria in mmol N/m2/year. Values are calculated for the minimum epidemic (Beta9=8.0), for the epidemic with the maximum net bacterial production (Beta9=12.0), and for the epidemic with the maximum annual output of viruses (Beta9=14.0). The lysed bacterial debris flows directly into the DON compartment and the decay time of inactivated viruses is **1 month**. Fixed contact rates.

Decay time	Beta9	Primary production	Net Bacterial production	Viral lysis	Maximum daily flow into lysis
50 years	7	674.2	260.3	58.3 (22%)	5.719 (118)
10 years	7	667.7	263.6	66.0 (25%)	6.018 (113)
1 year	6	688.6	287.5	69.5 (24%)	5.105 (112)
6 months	5.6	693.2	313.2	81.0 (26%)	4.025 (119)
3 months	5.4	658.8	392.5	149.0 (38%)	4.338 (116)
1 month	4.8	531.2	835.5	537.6 (64%)	4.01 (110)

Table 6.7.a Estimates of annual viral lysis, and the resulting net bacterial production and primary production, in mMol N/m^2/year, for minimum epidemics of bacterial viruses with decay times of inactivated viruses of fifty, ten and one year, plus six, three and one month. Also shown, the maximum daily flow into viral lysis in mMol N/m^2 and day when achieved (in brackets). The lysed bacterial debris flows directly into the DON compartment. The inactivation rate was .792 d^{-1}. Sinking speed of detritus 1m/day.

Decay time	Beta9	Primary production	Max. Gross Bacterial production	Viral lysis	Maximum daily flow into lysis
50 years	7	674.2	505.4 (260.3)	58.3 (22%)	5.719 (118)
10 years	7	667.7	508.6 (263.6)	66.0 (25%)	6.018 (113)
1 year	9	466.0	577.0 (403.6)	309.7 (77%)	3.501 (90)
6 months	9	411.9	695.9 (523.0)	429.4 (82%)	4.052 (87)
3 months	8	379.0	907.5 (713.4)	599.6 (84%)	4.769 (84)
1 month	6	381.1	1479.0 (1220.4)	1028. (84%)	7.461 (76)

Table 6.7.b Estimates of maximum gross bacterial production (net in brackets), corresponding annual viral lysis and the resulting primary production, in mMol N/m^2/year, for epidemics of bacterial viruses with decay times of inactivated viruses of fifty, ten and one year, plus six, three and one month. Also shown, the maximum daily flow into viral lysis in mMol N/m^2 and day when achieved (in brackets). The lysed bacterial debris flows directly into the DON compartment. The inactivation rate was .792 d^{-1}. Sinking speed of detritus 1m.

Decay time	Beta9	Primary production	Net Bacterial production	Viral lysis	Maximum daily flow into lysis
50 years	20	392.3	327.3 (405.6)	300.2 (92%)	2.8 (76)
10 years	20	389.6	335.2 (413.1)	308.4 (92%)	2.8 (76)
1 year	16	383.5	429.9 (527.0)	392.8 (91%)	3.3 (76)
6 months	15	383.9	520.6 (624.0)	479.6 (92%)	3.9 (76)
3 months	14	385.4	687.7 (798.6)	642.2 (93%)	5.0 (76)
1 month	11	389.5	1247.0 (1388.0)	1180. (95%)	8.7 (76)

Table 6.7.c Estimates of maximum annual viral lysis, and the resulting net bacterial production (with the total nitrogen uptake in brackets) and primary production, in mMol N/m^2/year, for epidemics of bacterial viruses with decay times of inactivated viruses of fifty, ten and one year, plus six, three and one month. Also shown, the maximum daily flow into viral lysis in mMol N/m^2 and day when achieved (in brackets). The lysed bacterial debris flows directly into the DON compartment. The inactivation rate was .792 d^{-1}. Sinking speed of detritus 1m/day.

Beta9	Primary production	Net Bacterial production	Viral lysis of bacteria	Maximum daily flow into lysis
5.6	693.2	313.2 (582.6)	81.0 (26%)	4.025 (119)
5.9	649.6	335.2 (596.2)	123.0 (37%)	4.912 (110)
9	411.9	523.1 (695.9)	429.4 (82%)	4.052 (87)
11	380.0	537.9 (679.0)	471.2 (88%)	3.899 (84)
15	383.9	520.6 (624.0)	479.6 (92%)	3.911 (76)

Table 6.8.a Estimates of annual totals of viral lysis of bacteria and corresponding percentage to net bacterial uptake of nitrogen (in brackets) compared with the resulting net and gross (in brackets) bacterial production and phytoplankton primary production in mmol N/m2/yr. Also shown is the maximum daily flow into lysis in mmol N/m2/day and day when achieved (in brackets). Values are calculated for the minimum epidemic (Beta9=5.6), for the epidemic with the maximum daily flow into lysis (Beta9=5.9), for the epidemic with the maximum gross bacterial production (Beta9=9), for the epidemic with the maximum net bacterial production which is also the epidemic with the minimum annual primary production (Beta9=11), and for the epidemic with the maximum annual output of viruses (Beta9=15). The lysed bacterial debris flows directly into the DON compartment and the decay time of inactivated viruses is **6 months**. Sinking speed of detritus 1m/day.

Beta9	Primary production	Net Bacterial production	Viral lysis of bacteria	Maximum daily flow into lysis
6	688.6	287.5 (550.7)	69.5 (24%)	5.105 (112)
9	466.0	403.6 (577.0)	309.7 (77%)	3.501 (90)
13	386.1	439.2 (558.7)	388.1 (88%)	3.581 (76)
14	381.9	437.3 (548.2)	391.8 (90%)	3.362 (76)
16	383.5	429.9 (527.0)	392.8 (91%)	3.323 (76)

Table 6.8.b Estimates of annual totals of viral lysis of bacteria and corresponding percentage to net bacterial uptake of nitrogen (in brackets) compared with the resulting net and gross (in brackets) bacterial production and phytoplankton primary production in mmol N/m2/yr. Also shown is the maximum daily flow into lysis in mmol N/m2/day and day when achieved (in brackets). Values are calculated for the minimum epidemic (Beta9=6) which is also the epidemic with the maximum daily flow into lysis, for the epidemic with the maximum gross bacterial production (Beta9=9), for the epidemic with the maximum net bacterial production (Beta9=13), for the epidemic with the minimum primary production (Beta9=14), and for the epidemic with the maximum annual output of viruses (Beta9=16). The lysed bacterial debris flows directly into the DON compartment and the decay time of inactivated viruses is **1 year**. Sinking speed of detritus 1m/day.

Beta9	Primary production	Net Bacterial production	Viral lysis of bacteria	Maximum daily flow into lysis
7	667.7	263.6 (508.6)	66.0 (25%)	6.018 (113)
7.1	660.9	263.8 (506.9)	71.3 (27%)	6.274 (111)
17	398.6	339.1 (431.1)	304.8 (90%)	2.997 (83)
20	389.6	335.2 (413.1)	308.4 (92%)	2.769 (76)
21	388.9	333.0 (407.1)	308.2 (93%)	2.719 (76)

Table 6.8.c Estimates of annual totals of viral lysis of bacteria and corresponding percentage to net bacterial uptake of nitrogen (in brackets) compared with the resulting net and gross (in brackets) bacterial production and phytoplankton primary production in mmol N/m2/yr. Also shown is the maximum daily flow into lysis in mmol N/m2/day and day when achieved (in brackets). Values are calculated for the minimum epidemic (Beta9=7) which is also the epidemic the maximum gross bacterial production, for the epidemic with the maximum daily flow into lysis (Beta9=7.1), for the epidemic with the maximum net bacterial production (Beta9=17), for the epidemic with the maximum annual output of viruses (Beta9=20), and for the epidemic with the minimum primary production (Beta9=21).
The lysed bacterial debris flows directly into the DON compartment and the decay time of inactivated viruses is **10 years**. Sinking speed of detritus 1m/day.

Beta9	Primary production	Net Bacterial production	Viral lysis of bacteria	Maximum daily flow into lysis
7	674.2	260.3 (505.4)	58.3 (22%)	5.719 (118)
7.3	656.2	260.7 (500.6)	72.2 (28%)	6.577 (110)
8.8	549.3	307.6 (495.4)	197.0 (64%)	3.193 (92)
17	403.3	330.3 (422.9)	295.4 (89%)	2.946 (84)
20	392.3	327.3 (405.6)	300.2 (92%)	2.77 (76)
22	390.1	323.4 (394.3)	299.9 (93%)	2.654 (76)

Table 6.8.d Estimates of annual totals of viral lysis of bacteria and corresponding percentage to net bacterial uptake of nitrogen (in brackets) compared with the resulting net and gross (in brackets) bacterial production and phytoplankton primary production in mmol N/m2/yr. Also shown is the maximum daily flow into lysis in mmol N/m2/day and day when achieved (in brackets). Values are calculated for the minimum epidemic (Beta9=7) which is also the epidemic with the maximum gross bacterial production, for the epidemic with the maximum daily flow into lysis (Beta9=7.3), for the epidemic with a viral lysis matching the Bacastow & Maier-Reimer (1991) requisites (Beta9=8.8), for the epidemic with the maximum net bacterial production (Beta9=17), for the epidemic with the maximum annual output of viruses (Beta9=20), and for the epidemic with the minimum primary production (Beta9=22).
The lysed bacterial debris flows directly into the DON compartment and the decay time of inactivated viruses is **50 years**. Sinking speed of detritus 1m/day.

Inactivation rate	Beta9	Primary production	Net Bacterial production	Viral lysis	Maximum daily flow into lysis
.5 d^{-1}	3.6	685.1	319.6	90.2 (28%)	3.29 (120)
.792 d^{-1}	5.6	693.2	313.2	81.0 (26%)	4.03 (119)
1 d^{-1}	7.1	686.3	316.0	87.1 (28%)	4.72 (117)

Table 6.9.a Estimates of annual viral lysis, and the resulting net bacterial production and primary production, in mMol N/m^2/year, for minimum epidemics with inactivation rates of .5, .792 and 1 d^{-1}. Also shown, the maximum daily flow into viral lysis in mMol N/m^2 and day when achieved (in brackets). The lysed bacterial debris flows directly into the DON compartment. The decay time of inactivated viruses was **six months**. Sinking speed of detritus 1m/day.

Inactivation rate	Beta9	Primary production	Net Bacterial production	Viral lysis	Maximum daily flow into lysis
.5 d^{-1}	10	384.6	516.2 (614.9)	478.0 (97%)	3.891 (76)
.792 d^{-1}	15	383.9	520.6 (624.0)	479.6 (92%)	3.911 (76)
1 d^{-1}	19	384.0	520.8 (623.6)	480.2 (92%)	3.913 (76)

Table 6.9.b Estimates of annual viral lysis, and the resulting net bacterial production (gross bacterial production in brackets) and primary production, in mMol N/m^2/year, for epidemics for the maximum annual output of bacterial viruses with inactivation rates of .5, .792 and 1 d^{-1}. Also shown, the maximum daily flow into viral lysis in mMol N/m^2 and day when achieved (in brackets). The lysed bacterial debris flows directly into the DON compartment. The decay time of inactivated viruses was **six months**. Sinking speed of detritus 1m/day.

	Year 1	Year 2	Year 3	Year 4	Year 5	Year 6	Year 7	Year 8	Year 9	Year 10
Overwinter Active Virus Concentration	0.185	6.18E-04	2.81E-04	2.09E-04	2.02E-04	2.03E-04	2.04E-04	2.05E-04	2.05E-04	2.05E-04
Peak Active Virus Concentration	0.02555 (109)	0.02906 (108)	0.0322 (109)	0.03339 (110)	0.03374 (110)	0.03264 (99)	0.03382 (110)	0.03382 (110)	0.03383 (110)	0.03383 (110)
Peak Inactive Virus Concentration	0.9237 (137)	0.7609 (137)	0.7107 (137)	0.6921 (137)	0.6848 (137)	0.6819 (137)	0.6808 (137)	0.6803 (137)	0.6802 (137)	0.6801 (137)
Overwinter Bacteria Concentration	0.1193	0.1042	0.1013	0.09944	0.09867	0.09841	0.09831	0.09827	0.09825	0.09825
Peak Bacteria Concentration	0.1316 (85)	0.1566 (82)	0.181 (89)	0.1905 (91)	0.194 (92)	0.195 (92)	0.1953 (92)	0.1955 (92)	0.1956 (93)	0.1957 (93)

Table 6.10 Overwinter concentration of active bacteriophages and corresponding winter bacteria concentration, compared with the resulting peak bacteria concentrations (in mmol N/m3) during the following spring bloom and corresponding day number (in brackets) together with peak concentrations of active bacteriophages during the same event and the resulting peak concentration of inactive virus during the annual cycle. Values are calculated for each consecutive year of a minimum epidemic of bacterial virus with a contact rate of 10.8 and a flow of lysed bacterial debris through the DON compartment. Decay time 6 months, inactivation rate .792 and sinking rate 10m/day

	Year 1	Year 2	Year 3	Year 4	Year 5	Year 6	Year 7	Year 8	Year 9	Year 10
Viral lysis of Bacteria	195.8 (47.4%)	114.4 (33.7%)	92.9 (28.8%)	85.5 (27.0%)	82.8 (26.4%)	81.8 (26.1%)	81.5 (26.0%)	81.3 (26.0%)	81.2 (26.0%)	81.2 (26.0%)
Regenerated Production	137.6	198.4	209.1	212.5	213.8	214.3	214.5	214.5	214.6	214.6
New Production	314.5	318.8	318.7	318.8	318.8	318.8	318.8	318.8	318.8	318.8
Total Production	452.1	517.2	527.8	531.4	532.6	533.1	533.3	533.4	533.4	533.4

Table 6.11 Estimates of annual totals of viral lysis of bacteria and corresponding percentage to total bacterial uptake of nitrogen (in brackets) compared with the resulting new and regenerated primary production in mmol N/m2/yr. Values are calculated for each consecutive year of a minimum epidemic of bacterial virus with a contact rate of 10.8 and a flow of lysed bacterial debris through the DON compartment. Inactivation rate .792, decay time six months, sinking rate 10 m/day.

Version 7 of the model: Introduction of variable contact rates in bacterial epidemics

Beta9	primary production	net bacterial production	viral lysis of bacteria	max. daily flow into lysis
8.6	498.1	394.4	278.7 (71%)	4.53 (95)
9.6	406.7	670.4	577.3 (86%)	6.29 (76)
11	379.5	769.5	696.5 (91%)	5.62 (76)
13	382.3	776.2	721.4 (93%)	5.65 (76)
15	384.8	769.7	726.5 (94%)	5.57 (76)

Table 6.12.a Estimates of annual totals of viral lysis of bacteria and corresponding percentage to net bacterial uptake of nitrogen (in brackets) compared with the resulting net bacterial production and phytoplankton primary production in mmol N/m2/yr. Also shown is the maximum daily flow into lysis in mmol N/m2/day and day when achieved (in brackets). Values are calculated for the minimum epidemic (Beta9=8.6), for the epidemic with the maximum daily flow into lysis (Beta9=9.6), for the epidemic with the lowest annual primary production (Beta9=11.0), for the epidemic with the maximum net bacterial production (Beta9=13.0), and for the epidemic with the maximum annual output of viruses (Beta9=15.0). Decay time of inactivated viruses is **one month.**

Beta9	DON uptake	Ammonium uptake	Ammonium excretion	Cell debris into DON
8.6	389.1	192.8	187.4	105.9
9.6	592.6	248.4	170.5	219.4
11	684.9	233.2	148.6	264.7
13	701.8	200.0	125.6	274.1
15	702.3	176.2	108.8	276.1

Table 6.12.b Estimates of annual totals of DON and Ammonium uptake compared to "DON" and Ammonium excretion by the model bacteria in mmol N/m2/year.
Values are calculated for the minimum epidemic (Beta9=8.6), for the epidemic with the maximum daily flow into lysis (Beta9=9.6), for the epidemic with the lowest annual primary production (Beta9=11.0), for the epidemic with the maximum net bacterial production (Beta9=13.0), and for the epidemic with the maximum annual output of viruses (Beta9=15.0). Decay time of inactivated viruses is **one month.**

Beta9	Regenerated Production	Ammonium excretion by Zooplankton	New Production
8.6	180.2	211.1	317.9
9.6	86.4	170.5	320.3
11	59.9	150.8	319.7
13	62.8	144.0	319.5
15	65.7	140.3	319.1

Table 6.12.c Estimates of annual totals of Regenerated Production, New Production and Ammonium excretion by zooplankton in mmol N/m2/year. Values are calculated for the minimum epidemic (Beta9=8.6), for the epidemic with the maximum daily flow into lysis (Beta9=9.6), for the epidemic with the lowest annual primary production (Beta9=11.0), for the epidemic with the maximum net bacterial production (Beta9=13.0), and for the epidemic with the maximum annual output of viruses (Beta9=15.0). Decay time of inactivated viruses is **one month**.

Beta9	primary production	net bacterial production	viral lysis of bacteria	max. daily flow into lysis
10.5	543.9	152.2	62.2 (41%)	5.26 (104)
11	524.8	175.1	94.4 (54%)	6.42 (98)
22	389.6	333.1	309.5 (93%)	2.84 (76)
24	387.2	331.6	311.0 (94%)	2.69 (76)
25	386.8	330.2	310.8 (94%)	2.63 (76)

Table 6.13.a . Estimates of annual totals of viral lysis of bacteria and corresponding percentage to net bacterial uptake of nitrogen (in brackets) compared with the resulting net bacterial production and phytoplankton primary production in mmol N/m2/yr. Also shown is the maximum daily flow into lysis in mmol N/m2/day and day when achieved (in brackets). Values are calculated for the minimum epidemic (Beta9=10.5), for the epidemic with the maximum daily flow into lysis (Beta9=11.0), for the epidemic with the maximum net bacterial production (Beta9=22.0), for the epidemic with the maximum annual output of viruses (Beta9=24.0), and for the epidemic with the lowest annual primary production (Beta9=25.0). Decay time of inactivated viruses is **six months**.

Beta9	DON uptake	Ammonium uptake	Ammonium excretion	Cell debris into DON
10.5	189.4	112.9	150.2	23.6
11	201.9	119.9	146.6	35.9
22	277.0	130.3	74.3	117.6
24	275.7	124.0	68.1	118.2
25	274.7	120.9	65.3	118.1

Table 6.13.b Estimates of annual totals of DON and Ammonium uptake compared to "DON" and Ammonium excretion by the model bacteria in mmol N/m2/year. Values are calculated for the minimum epidemic (Beta9=10.5), for the epidemic with the maximum net bacterial production (Beta9=22.0), for the epidemic with the maximum annual output of viruses (Beta9=24.0), and for the epidemic with the lowest annual primary production (Beta9=25.0). Decay time of inactivated viruses is **six months**.

Beta9	primary production	net bacterial production	viral lysis of bacteria	max. daily flow into lysis
11.8	531.3	151	77.0 (51%)	6.46 (95)
12	523.9	157.5	86.2 (55%)	6.61 (94)
25	398.6	268.1	248.7 (93%)	2.60 (76)
28	394.1	267.2	250.8 (94%)	2.33 (76)
34	391.5	260.5	248.2 (95%)	2.12 (76)

Table 6.14 . Estimates of annual totals of viral lysis of bacteria and corresponding percentage to net bacterial uptake of nitrogen (in brackets) compared with the resulting net bacterial production and phytoplankton primary production in mmol N/m2/yr. Also shown is the maximum daily flow into lysis in mMol N/m2/day and day when achieved (in brackets). Values are calculated for the minimum epidemic (Beta9=11.8), for the epidemic with the maximum daily flow into lysis (Beta9=12.0), for the epidemic with the maximum net bacterial production (Beta9=25.0), for the epidemic with the maximum annual output of viruses (Beta9=28.0), and for the epidemic with the lowest annual primary production (Beta9=34.0). Decay time of inactivated viruses is **one year**.

Beta9	primary production	net bacterial production	viral lysis of bacteria	max. daily flow into lysis
12	556.2	118.2	24.3 (21%)	4.15 (119)
14.1	529	131.9	62.0 (47%)	8.62 (98)
29	412.7	203.8	187.9 (92%)	2.17 (76)
36	403.7	202	190.6 (94%)	1.98 (76)
48	399.5	193.8	186.2 (96%)	1.59 (76)

Table 6.15 Estimates of annual totals of viral lysis of bacteria and corresponding percentage to net bacterial uptake of nitrogen (in brackets) compared with the resulting net bacterial production and phytoplankton primary production in mmol N/m2/yr. Also shown is the maximum daily flow into lysis in mMol N/m2/day and day when achieved (in brackets). Values are calculated for the minimum epidemic (Beta9=12), for the epidemic with the maximum daily flow into lysis (Beta9=14.1), for the epidemic with the maximum net bacterial production (Beta9=29), for the epidemic with the maximum annual output of viruses (Beta9=36), and for the epidemic with the lowest annual primary production (Beta9=48). The decay time of inactivated viruses is **ten years**.

Beta9	primary production	net bacterial production	viral lysis of bacteria	max. daily flow into lysis
12.9	546.7	121.8	34.2 (28%)	6.39 (112)
14.7	525	132.2	65.8 (50%)	8.95 (96)
30	413.3	198	182.7 (92%)	2.25 (288)
36	405.6	196.6	184.9 (94%)	1.94 (76)
49	400.4	188.4	180.9 (96%)	1.59 (76)

Table 6.16 Estimates of annual totals of viral lysis of bacteria and corresponding percentage to net bacterial uptake of nitrogen (in brackets) compared with the resulting net bacterial production and phytoplankton primary production in mmol N/m2/yr. Also shown is the maximum daily flow into lysis in mMol N/m2/day and day when achieved (in brackets). Values are calculated for the minimum epidemic (Beta9=12.9), for the epidemic with the maximum daily flow into lysis (Beta9=14.7), for the epidemic with the maximum net bacterial production (Beta9=30.0), for the epidemic with the maximum annual output of viruses (Beta9=36.0), and for the epidemic with the lowest annual primary production (Beta9=49.0). The decay time of inactivated viruses is **fifty years**.

Beta9	Primary production	Net Bacterial production	Viral lysis of bacteria	Maximum daily flow into lysis
6	679.0	290.8 (550.9)	67.0 (23%)	7.496 (110)
7	595.9	316.8 (547.1)	156.2 (49%)	8.557 (100)
10	471.5	401.4 (566.5)	321.0 (80%)	4.833 (76)
14	407.7	423.6 (540.6)	378.4 (89%)	4.027 (72)
18	391.1	416.8 (507.6)	386.6 (91%)	3.316 (76)
19	390.5	413.7 (499.7)	386.0 (93%)	3.218 (76)

Table 6.17. Estimates of annual totals of viral lysis of bacteria and corresponding percentage to net bacterial uptake of nitrogen (in brackets) compared with the resulting net and gross (in brackets) bacterial production and phytoplankton primary production in mmol N/m2/yr. Also shown is the maximum daily flow into lysis in mmol N/m2/day and day when achieved (in brackets). Values are calculated for the minimum epidemic (Beta9=6), for the epidemic with the maximum daily flow into lysis (Beta9=7), for the epidemic with the maximum gross bacterial production (Beta9=10), for the epidemic with the maximum net bacterial production (Beta9=14), for the epidemic with the maximum annual output of viruses (Beta9=19), and for the epidemic with the minimum primary production (Beta9=19). The lysed bacterial debris flows directly into the DON compartment and the decay time of inactivated viruses is **1 year**. Sinking speed of detritus 1m/day. Variable contact rates.

Inactivation rate	Beta9	Primary production	Net Bacterial production	Viral lysis	Maximum daily flow into lysis
.1 d^{-1}	1.5	518.9	182.2	99.6 (55%)	1.91 (110)
.3 d^{-1}	4.3	518.5	184.3	103.8 (56%)	3.57 (100)
.5 d^{-1}	6.8	534.1	164.4	77.4 (47%)	4.19 (103)
.792 d^{-1}	10.5	543.9	152.2	62.2 (41%)	5.26 (104)
1 d^{-1}	13.6	531.8	166.5	82.6 (50%)	7.33 (100)

Table 6.18a Estimates of annual viral lysis, and the resulting net bacterial production and primary production, in mMol N/m^2/year, for minimum epidemics with inactivation rates of .5, .792 and 1 d^{-1}. Also shown, the maximum daily flow into viral lysis in mMol N/m^2 and day when achieved (in brackets). The decay time of inactivated viruses was **six months**. Sinking speed of detritus 10m/day.

Inactivation rate	Beta9	Primary production	Net Bacterial production	Viral lysis	Maximum daily flow into lysis
.1 d^{-1}	3.3	386.9	322.5	302.0 (94%)	2.56 (76)
.3 d^{-1}	9	387.9	329.9	308.4 (93%)	2.76 (76)
.5 d^{-1}	15	387.6	331.2	301.1 (91%)	2.69 (76)
.792 d^{-1}	24	387.2	331.6	311.0 (94%)	2.69 (76)
1 d^{-1}	26	392.7	332.9	306.9 (92%)	2.91 (76)

Table 6.18b Estimates of annual viral lysis, and the resulting net bacterial production and primary production, in mMol N/m^2/year, for epidemics for the maximum annual output of bacterial viruses with inactivation rates of .5, .792 and 1 d^{-1}. Also shown, the maximum daily flow into viral lysis in mMol N/m^2 and day when achieved (in brackets). The decay time of inactivated viruses was **six months.** Sinking speed of detritus 10m/day.

Decay time	Beta9	Primary production	Net Bacterial production	Viral lysis	Maximum daily flow into lysis
50 years	12.9	546.7	121.8	34.2 (28%)	6.39 (112)
10 years	12	556.2	118.2	24.3 (21%)	4.15 (119)
1 year	11.8	531.3	151.0	77.0 (51%)	6.46 (95)
6 months	10.5	543.9	152.2	62.2 (41%)	5.26 (104)
1 month	8.6	498.1	394.4	278.7 (71%)	4.53 (95)

Table 19.a Estimates of annual viral lysis, and the resulting net bacterial production and primary production, in mMol N/m^2/year, for minimum epidemics of bacterial viruses with decay times of inactivated viruses of fifty, ten and one year, plus six and one month. Also shown, the maximum daily flow into viral lysis in mMol N/m^2 and day when achieved (in brackets). The inactivation rate was .792 d^{-1}. Sinking speed of detritus 10m/day.

Decay time	Beta9	Primary production	Net Bacterial production	Viral lysis	Maximum daily flow into lysis
50 years	14.7	525.0	132.2	65.8 (50%)	8.95 (96)
10 years	14.1	529.0	131.9	62.0 (47%)	8.62 (98)
1 year	12	523.9	157.5	86.2 (55%)	6.61 (94)
6 months	11	524.8	175.1	94.4 (54%)	6.42 (98)
1 month	9.6	406.7	670.4	577.3 (86%)	6.29 (76)

Table 6.19.b Estimates of annual viral lysis, and the resulting net bacterial production and primary production, in mMol N/m^2/year, for epidemics of bacterial viruses yielding the maximum daily flow into lysis with decay times of inactivated viruses of fifty, ten and one year, plus six and one month. Also shown, the maximum daily flow into viral lysis in mMol N/m^2 and day when achieved (in brackets). The inactivation rate was .792 d^{-1}. Sinking speed of detritus 10m/day.

Decay time	Beta9	Primary production	Net Bacterial production	Viral lysis	Maximum daily flow into lysis
50 years	36	405.6	196.6	184.9 (94%)	1.9 (76)
10 years	36	403.7	202.0	190.6 (94%)	2.0 (76)
1 year	28	394.1	267.2	250.8 (94%)	2.3 (76)
6 months	24	387.2	331.6	311.0 (94%)	2.7 (76)
1 month	15	384.8	769.7	726.5 (94%)	5.6 (76)

Table 6.19.c Estimates of maximum annual viral lysis, the resulting net bacterial production and primary production, in mMol N/m^2/year, for epidemics of bacterial viruses with decay times of inactivated viruses of fifty, ten and one year, plus six and one month. Also shown, the maximum daily flow into viral lysis in mMol N/m^2 and day when achieved (in brackets). The inactivation rate was .792 d^{-1}. Sinking speed of detritus 10m/day.

6.9 Figures

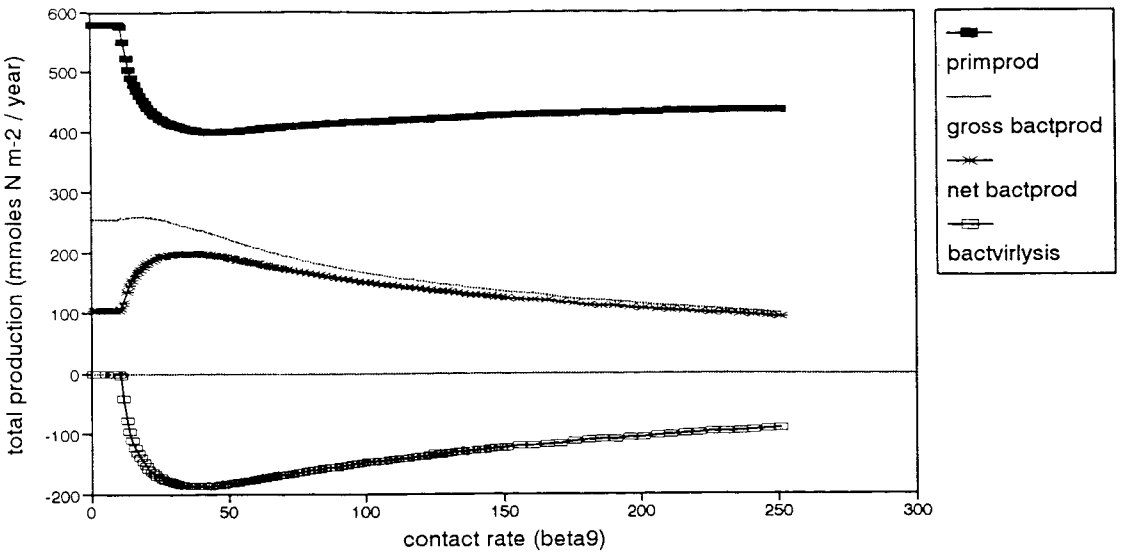

Figure 6.1 Variation in annual primary production (filled square), gross bacterial production (dotted), net bacterial production (star) and bacterial viral lysis (empty square) in mMol N/m^2 /year, plotted against increasing levels of the contact rate (Beta9) in single epidemic of bacterial viruses. Inactivation rate of .792 and sinking rates of 10m/day. Decay time six months.

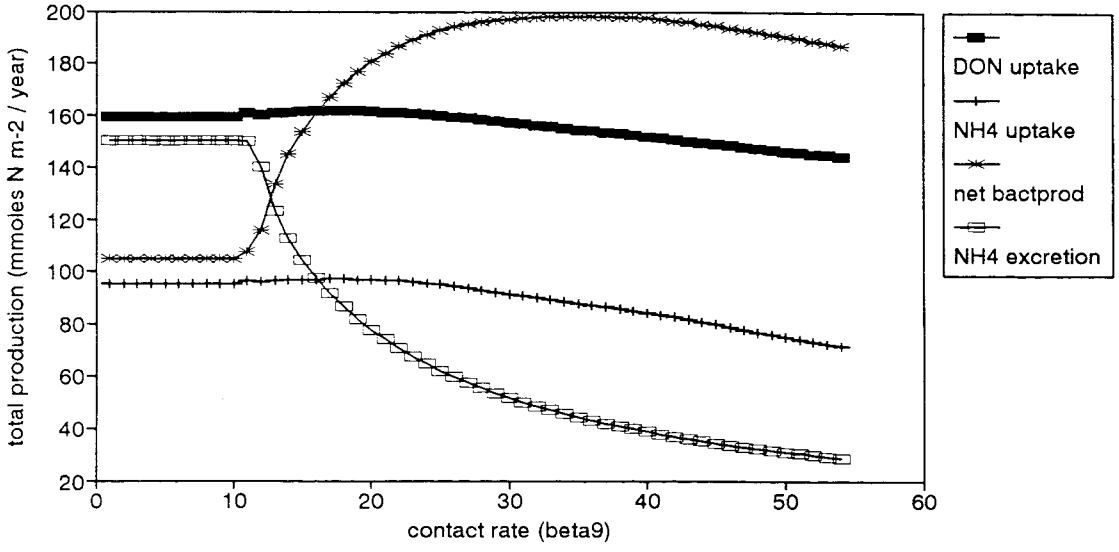

Figure 6.2 Variation in annual DON and ammonium uptake plus ammonium excretion by bacteria and net bacterial production plotted against increasing levels of the contact rate (Beta9) in single epidemic of bacterial viruses. Inactivation rate of .792 and sinking rates of 10m/day. Decay time six months.

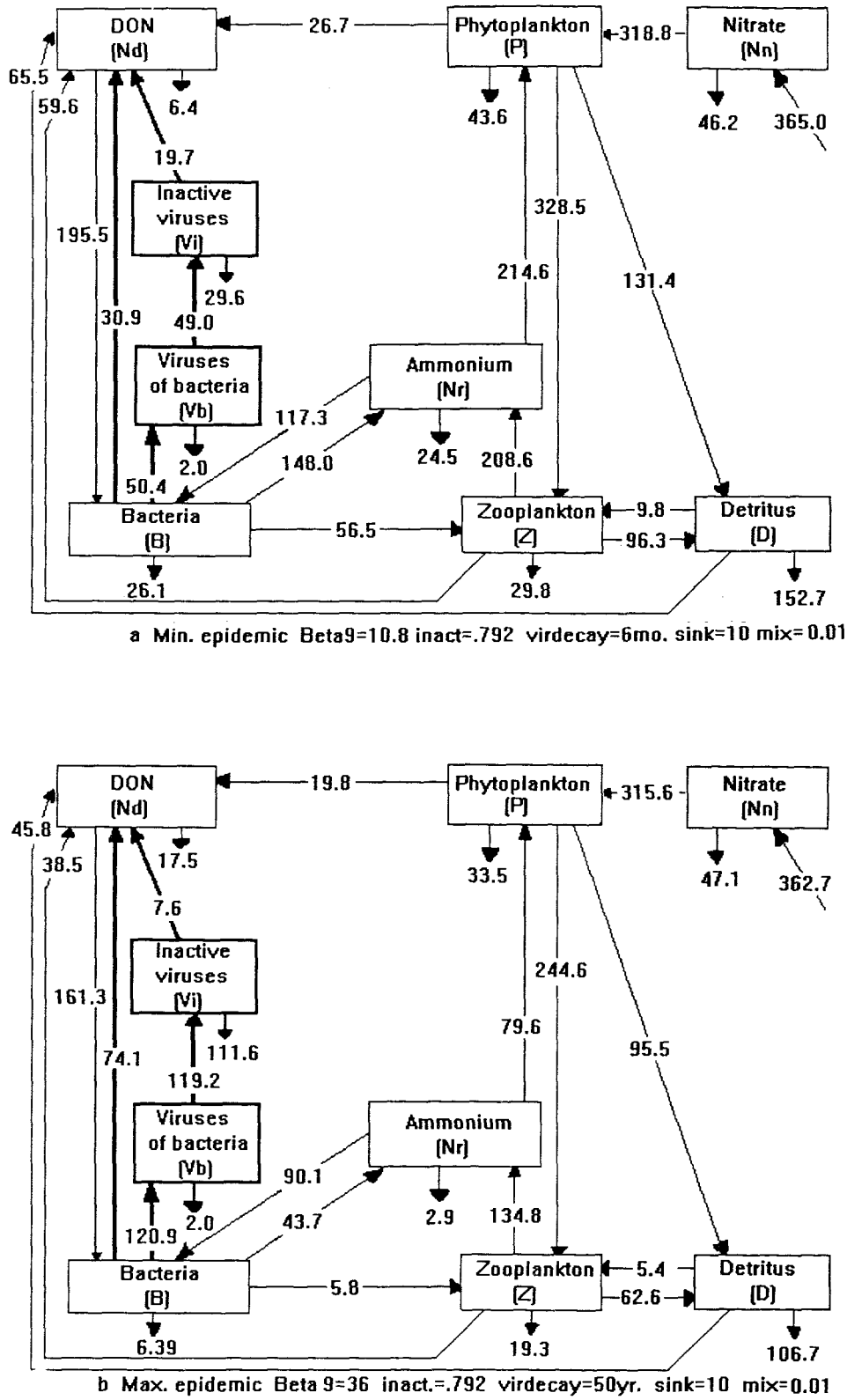

Figure 6.3 Annual intercompartment flows of nitrogen for (a), (c) minimum and (b) maximum epidemic, with a decay time of six months, one month and fifty years respectively.

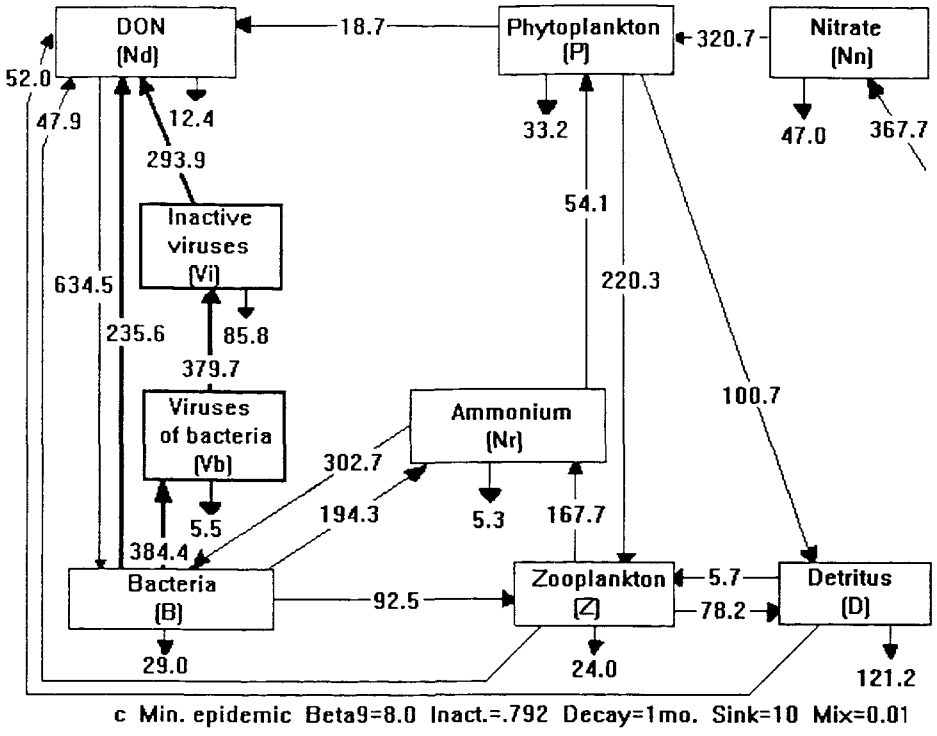

Figure 6.3 - continued

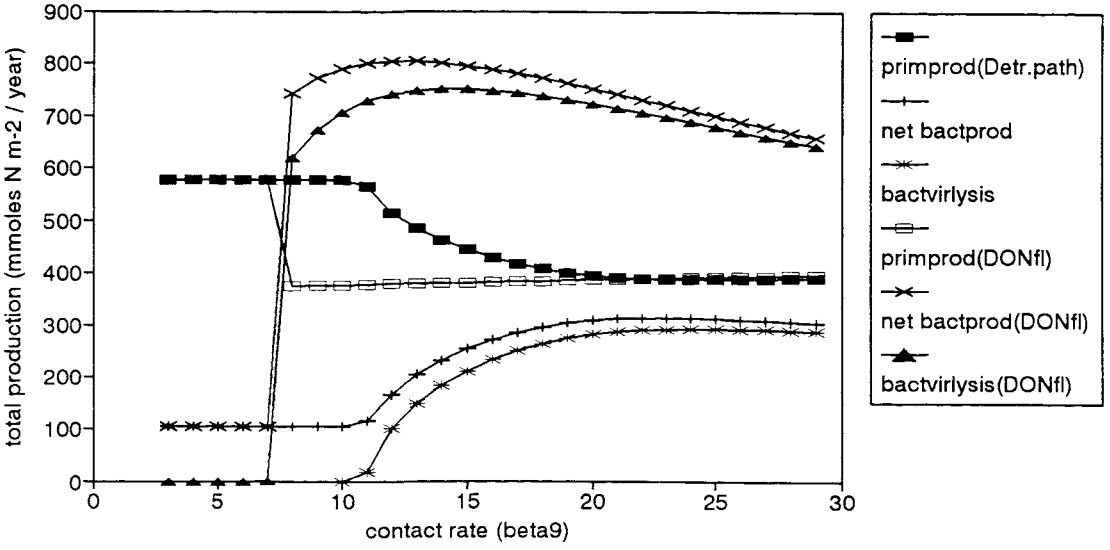

Figure 6.4 Variation in annual primary production (empty/filled square), bacterial production (cross/plus), bacterial viral lysis (triangle/star) in mMol N/m^2 /year, in simulations with a flow into DON of lysed bacterial debris, in comparison to simulations with a flow into detritus, plotted against increasing levels of the contact rate (Beta9). Inactivation rate of .792 and sinking rates of 10m/day. Decay time six months.

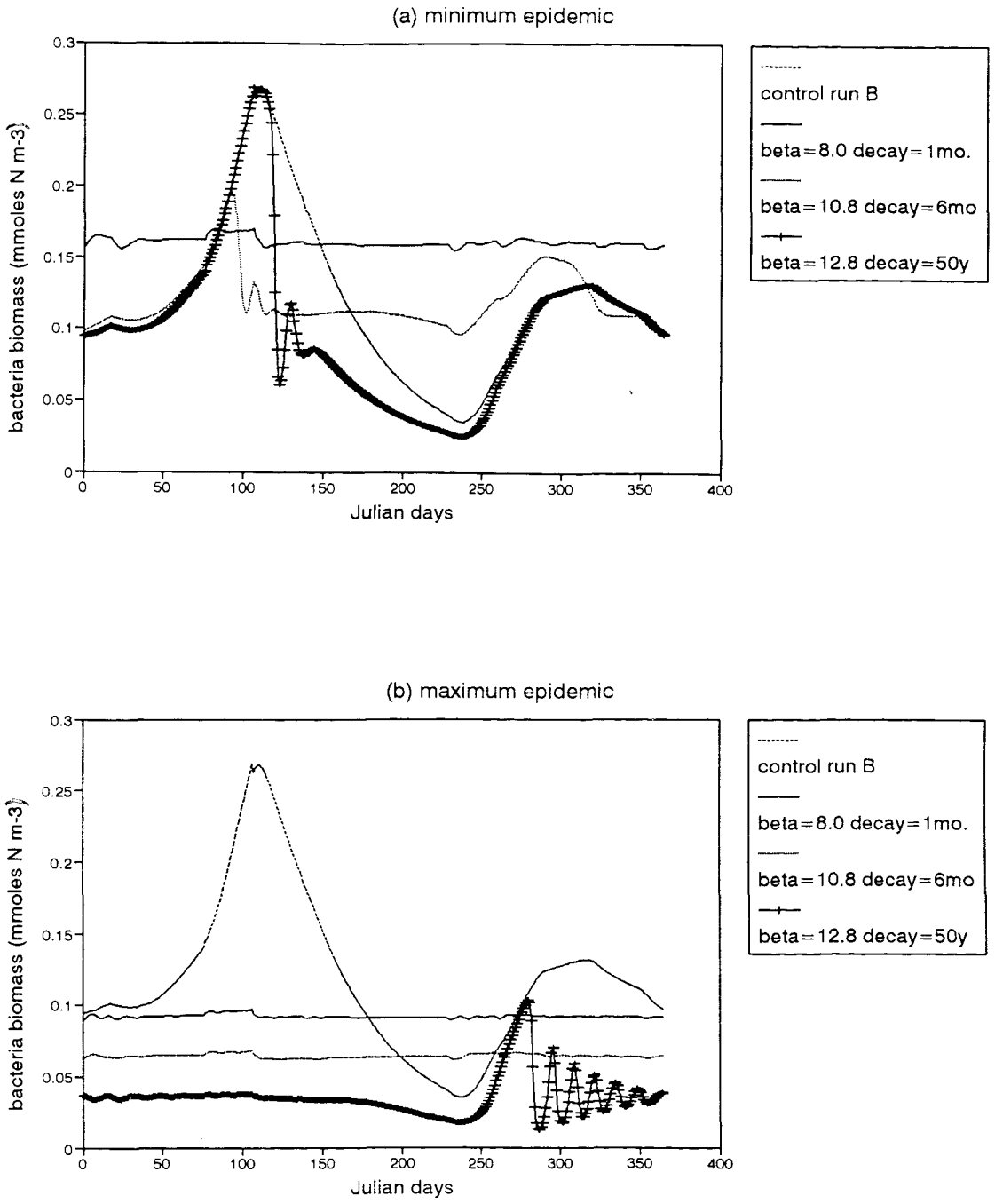

Figure 6.5 Annual cycle of bacterial biomass for decay rates of one month (solid line) six month (dotted) and fifty years (plus) compared to Control Run B (heavy dotted) for inactivation rate .792 and sinking rate 10m d^{-1} in Version 6 of the model. (a) minimum (b) maximum epidemics.

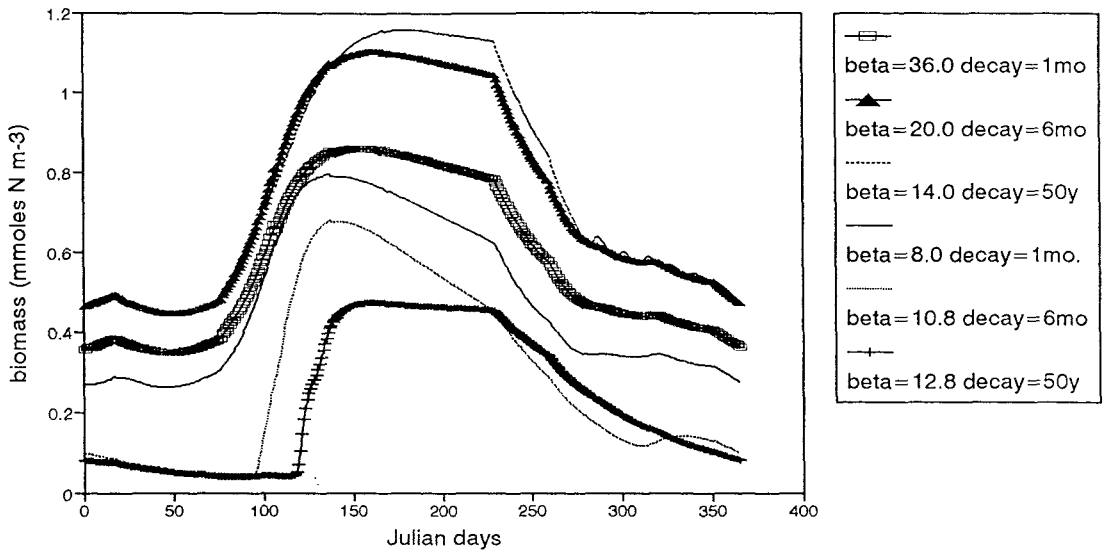

Figure 6.6 Annual cycle of inactivated viruses in minimum (solid/dotted/plus) and maximum epidemic (empty square/triangle/dashed) for decay times of one and six month and fifty years.

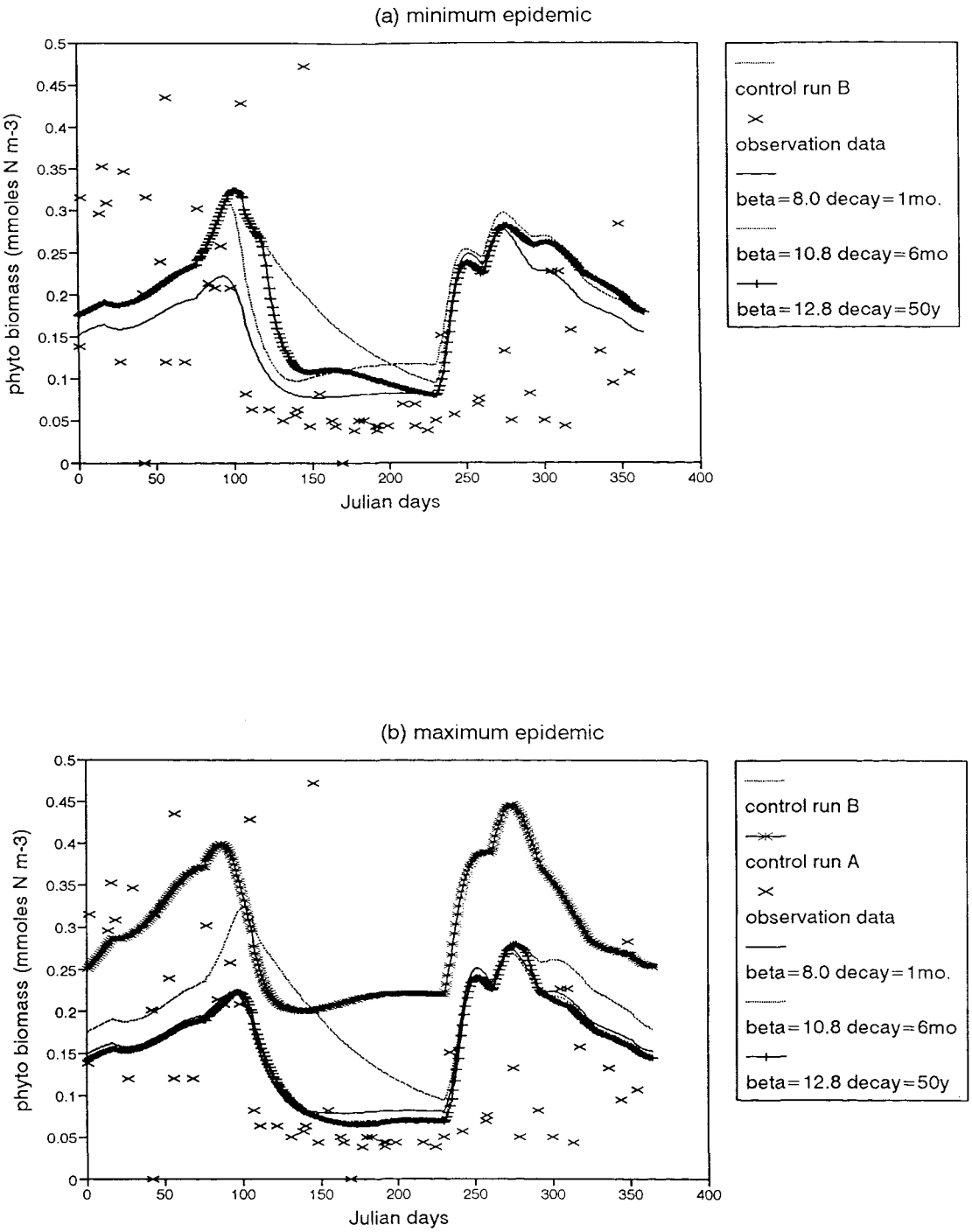

Figure 6.7 Annual cycle of phytoplankton biomass for decay rates of one month (solid line) six month (dotted) and fifty years (plus) compared to Control Run B (heavy dotted) and Control Run A (star), for inactivation rate .792 and sinking rate 10m d^{-1} in Version 6 of the model. (a) minimum (b) maximum epidemics.

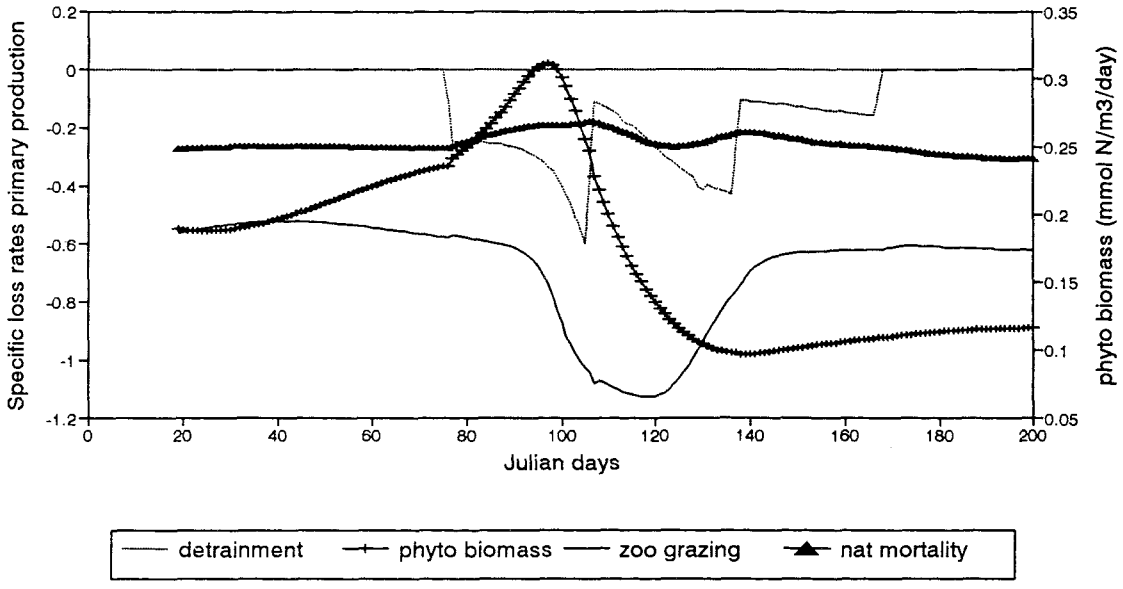

Figure 6.8 Seasonal changes in the specific loss rate of primary prodution for the minimum epidemic in the six month decay simulation. Detrainment - dotted; zooplankton grazing - solid line; natural mortality - triangle; phytoplankton biomass - plus.

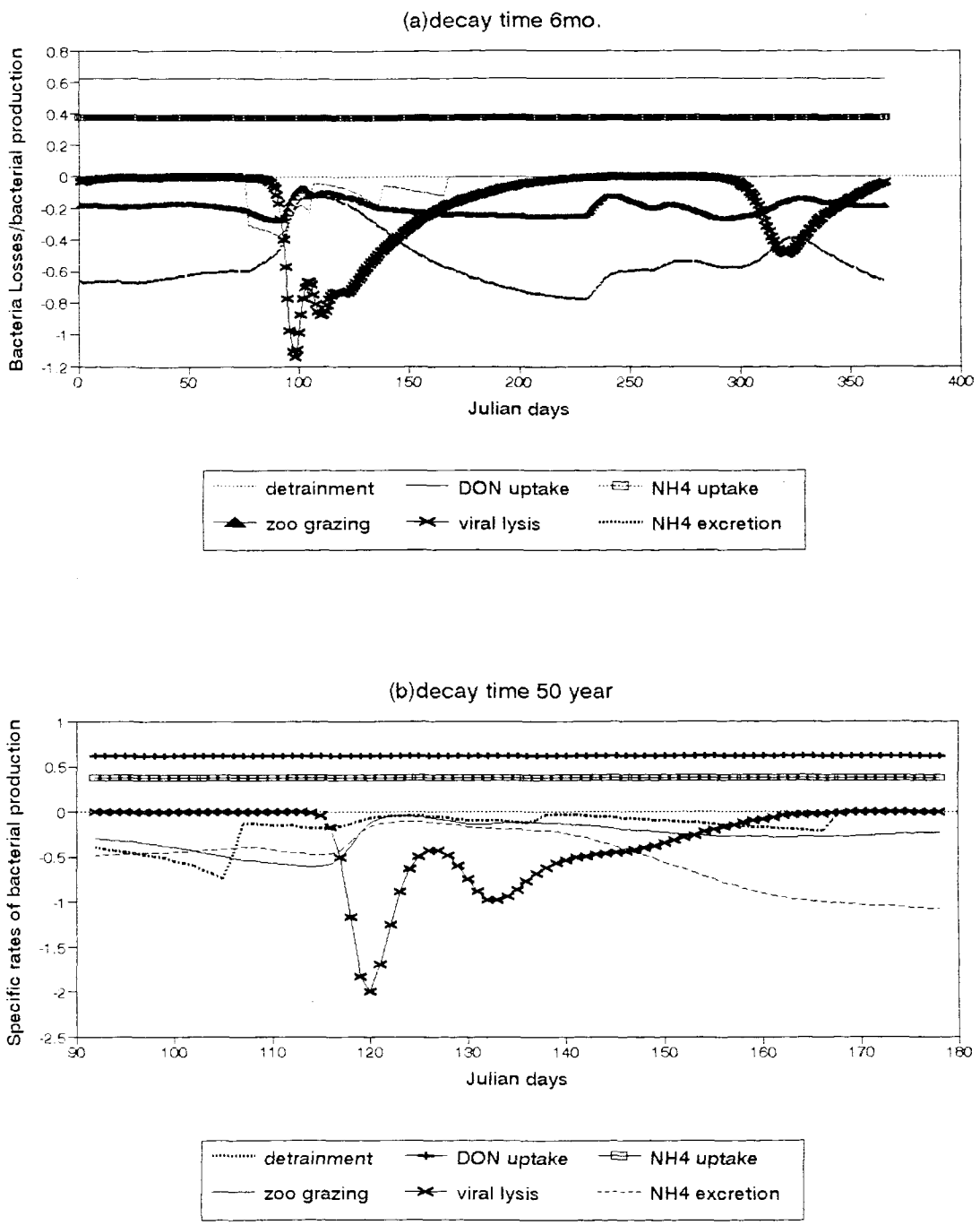

Figure 6.9 Seasonal cycle of specific rates of bacterial production in d^{-1} for the minimum epidemic in the (a) six month and (b) fifty year decay simulation. Detrainment - dotted; zooplankton grazing - solid line; DON uptake - plus; ammonium uptake - empty square; ammonium excretion - dashed; viral lysis - cross.

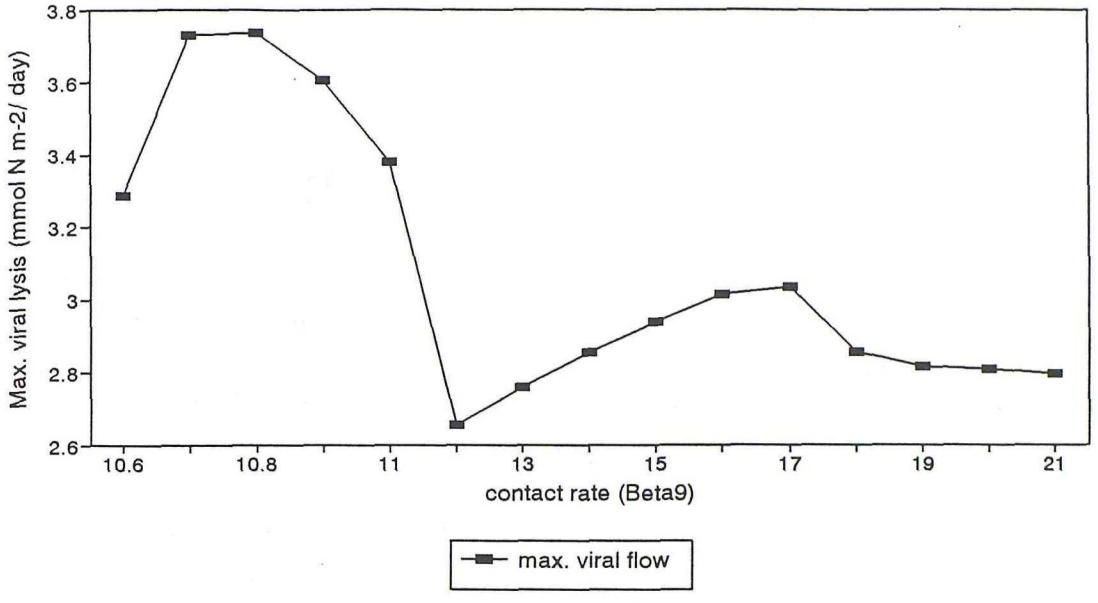

Figure 6.10 Variation in maximum daily flow into viral lysis in mMol N/m^2/day, plotted against increasing levels of the contact rate (beta9) for the 10th simulation year with a decay time of six months. Beta9 values between 10.6 - 21

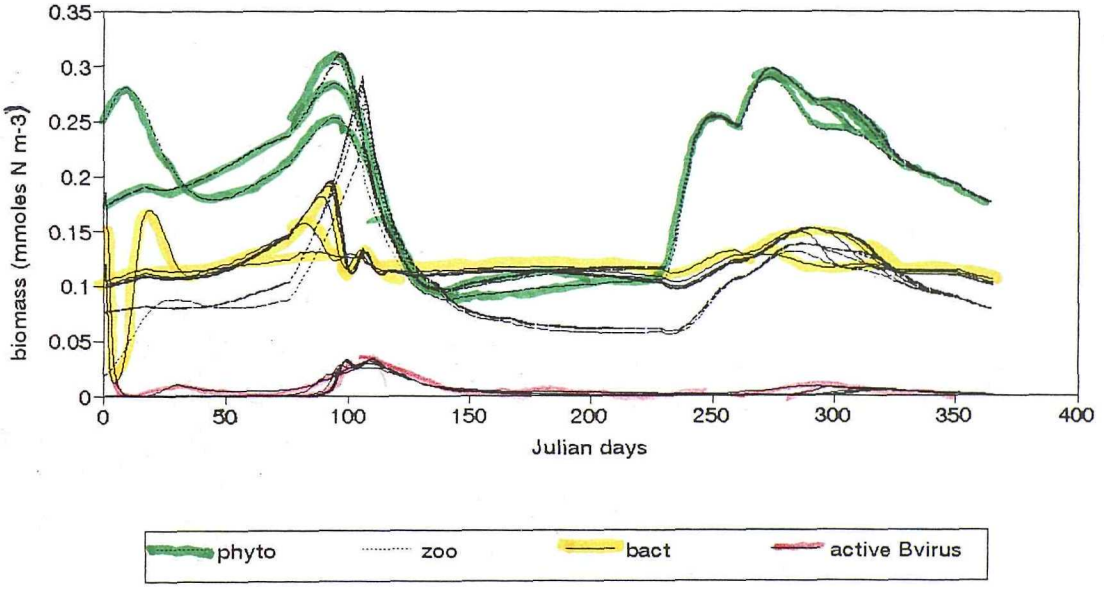

Figure 6.11 Annual cycle of bacteria (solid line), phytoplankton (green dotted), zooplankton (dotted) and active bacteriophage (red) biomass for a decay time of six months for ten consecutive years of a minimum epidemic. Inactivation rate .792 and sinking rate 10m d^{-1}.

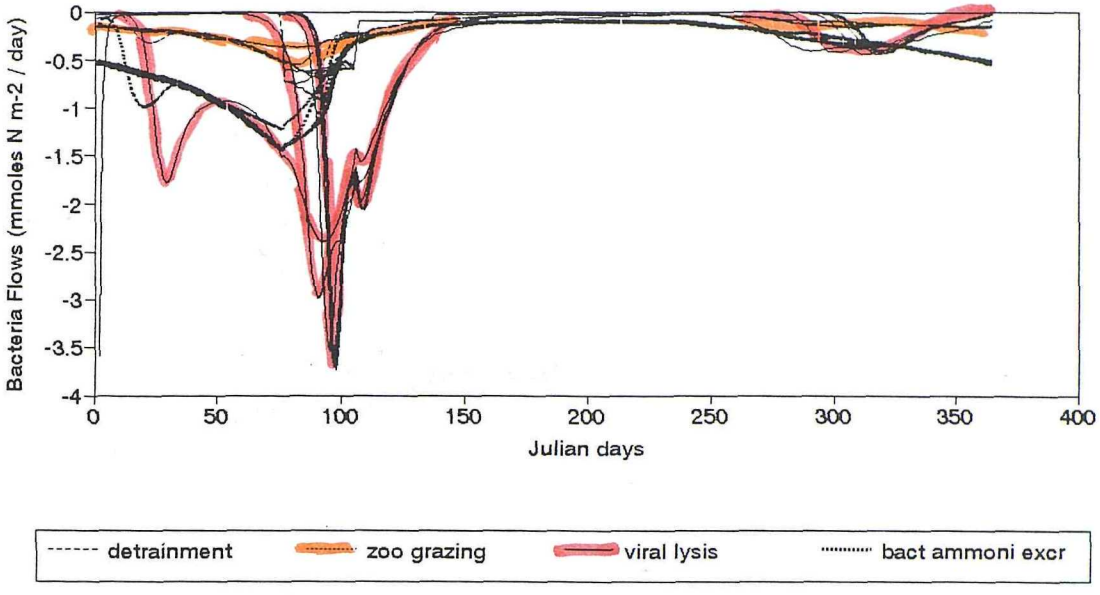

Figure 6.12 Temporal evolution of bacterial loss fluxes (in mMol N/m^2/day) due to viral lysis for ten consecutive years of a minimum epidemic with a decay time of six months. Inactivation rate .792 and sinking rate 10m d^{-1}.

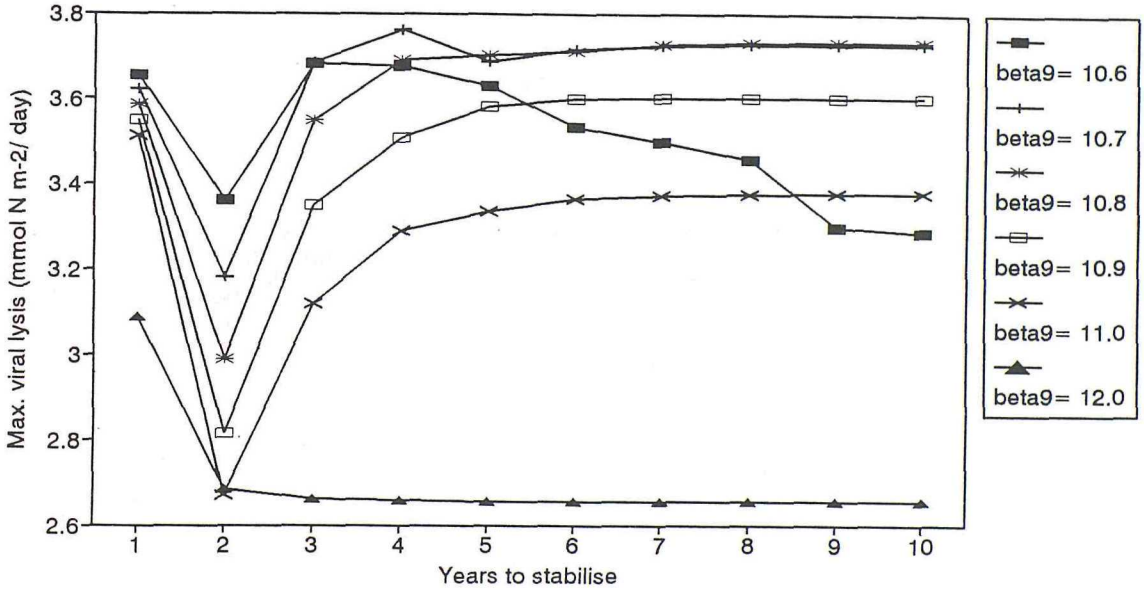

Figure 6.13 Variation in maximum daily flow into viral lysis in mMol N/m^2/day, plotted against time in years for a range of contact rates (beta9) from 10.6 to 12. Decay time of six months, inactivation rate .792 and sinking rate 10m d^{-1}.

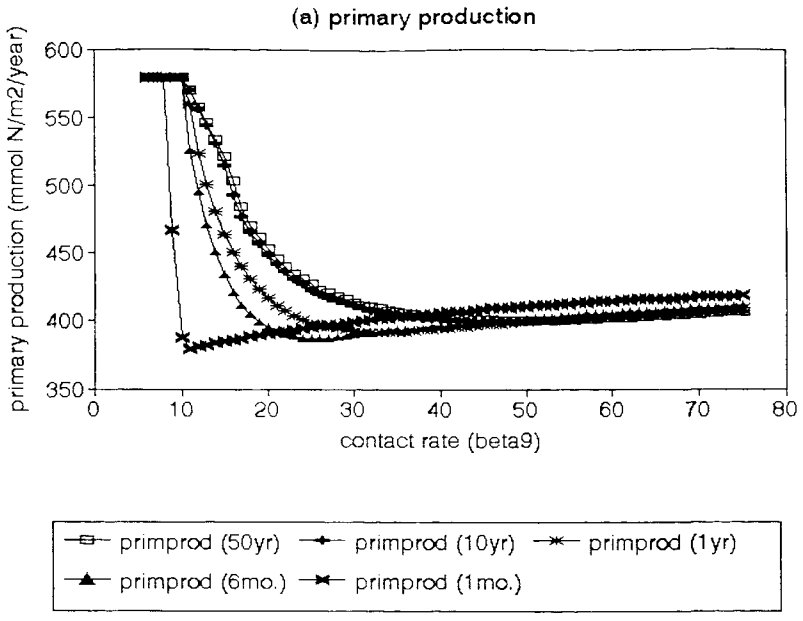

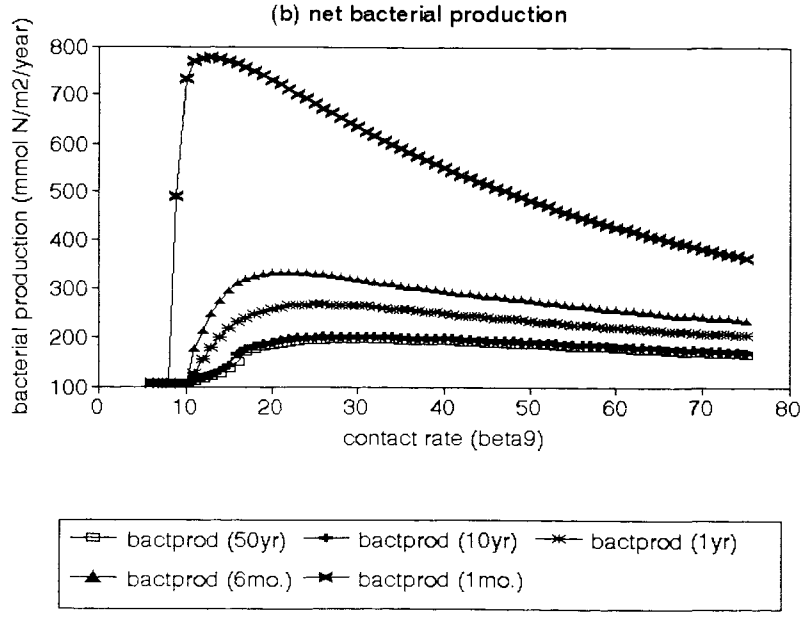

Figure 6.14 Variation in annual (a) primary production, (b) bacterial production and (c) bacterial viral lysis in mMol N/m^2 /year, plotted against increasing levels of the contact rate (Beta9), for decay times of fifty (empty square), ten (plus) and one year (star) plus six months (triangle) and one month (cross). Inactivation rate of .792 and sinking rates of 10m/day.

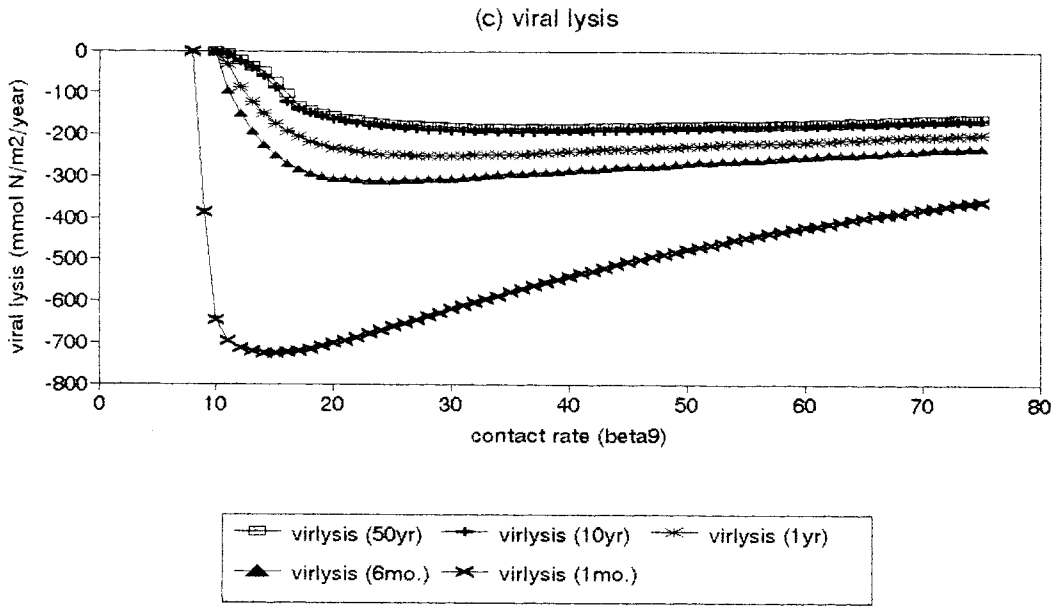

Fig 6.14 continued

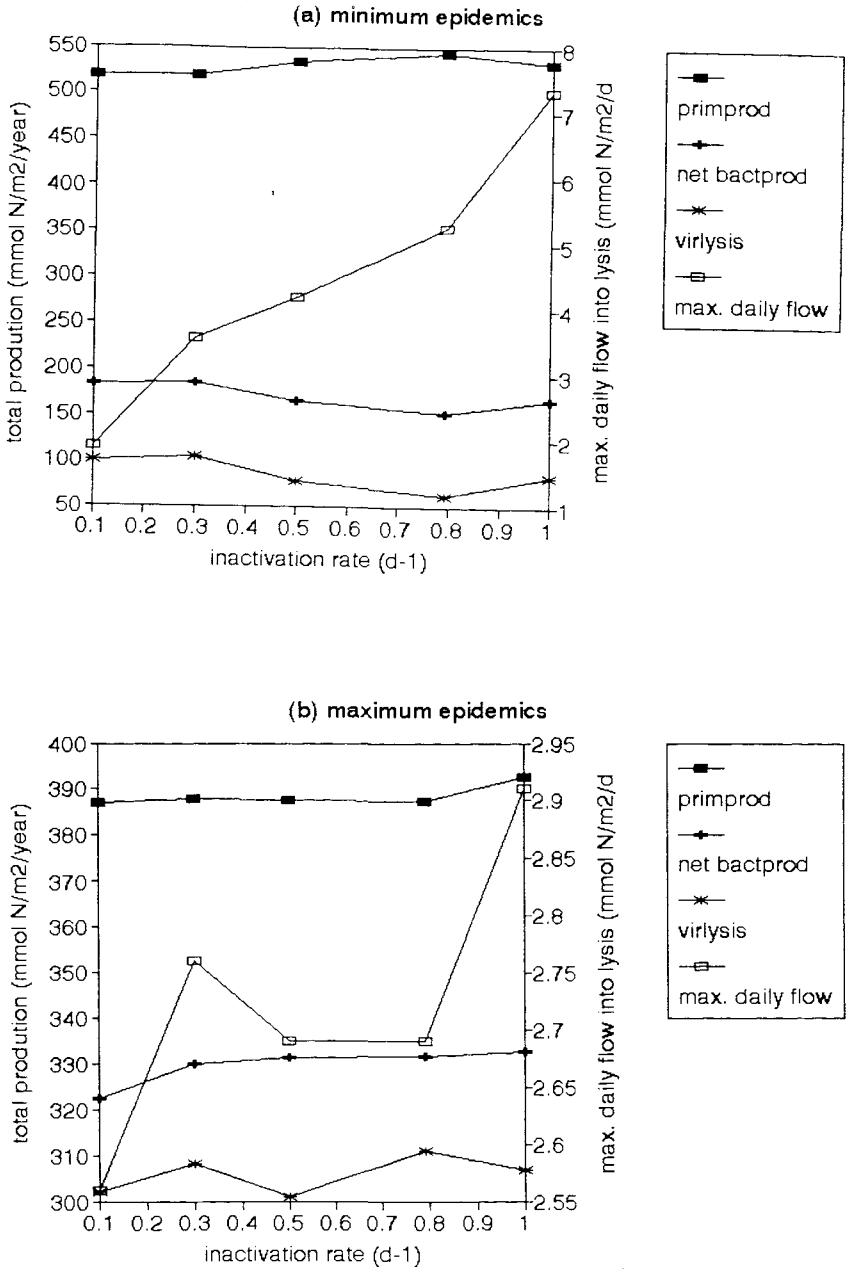

Figure 6.15 Changes in production rates of primary production (filled square), net bacterial production (plus), viral lysis (star) in mMol N/m^2/year, and the maximum daily flow into viral lysis (empty square) in mMol N/m^2 for epidemics of bacterial viruses, plotted against inactivation rates of .1, .3, .5, .792 and 1 d^{-1}. Decay time of six months. (a) minimum epidemics and (b) maximum epidemics.

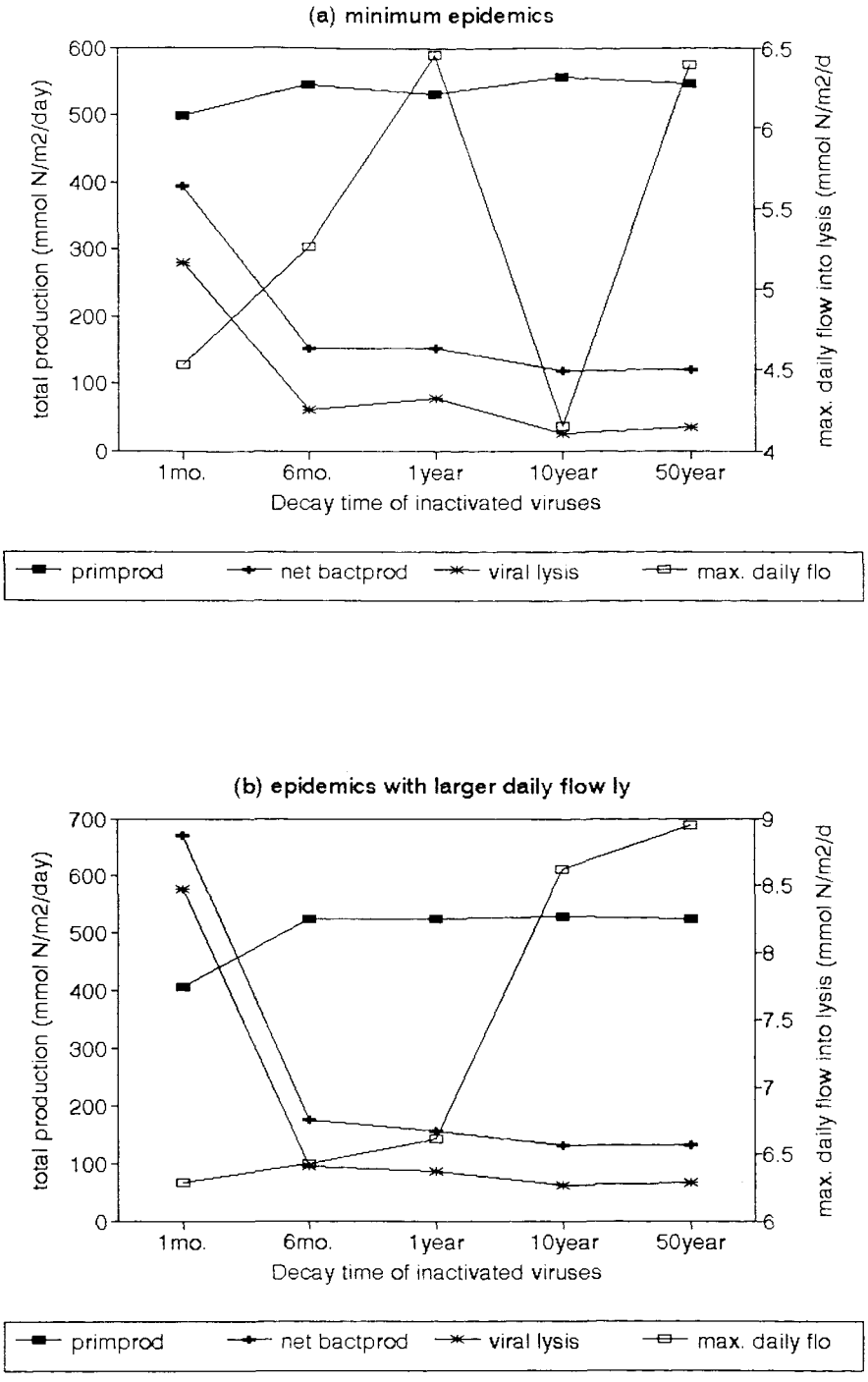

Figure 6.16 Estimates of annual viral lysis, the resulting net bacterial production, primary production, in mMol N/m^2/year, and the maximum daily flow into viral lysis in mMol N/m^2 for epidemics of bacterial viruses plotted against decay times of inactivated viruses of one and six months plus one, ten and fifty years. Inactivation rate .792 d^{-1}. Sinking rate 10m/day. (a) minimum epidemics, (b) epidemics with larger daily flows into lysis, (c) maximum epidemics.

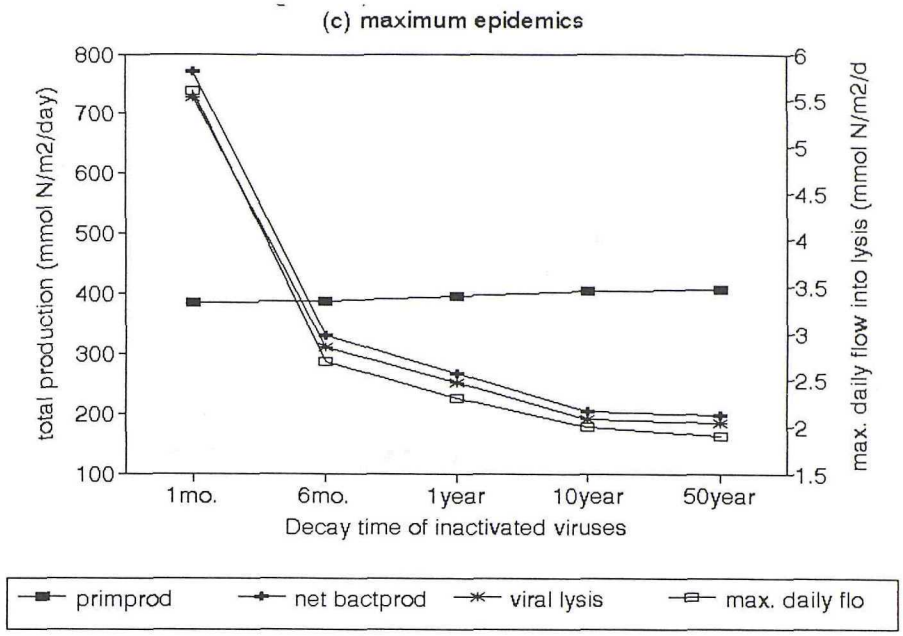

Figure 6.16 continued

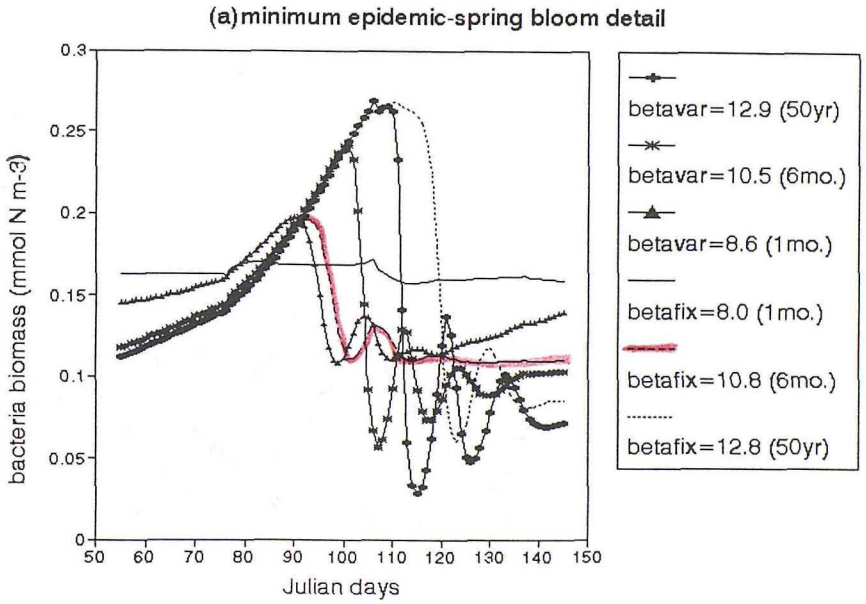

Figure 6.17 Collapse of the bacterial biomass in (a) minimum epidemic (a_1) variation in seasonal balance and (b) maximum epidemic during the spring and autumn blooms for decay rates of one month (triangle/solid line), six months (star/dashed or red) and fifty years (plus/dotted) for identical simulations with variable/fixed contact rates.

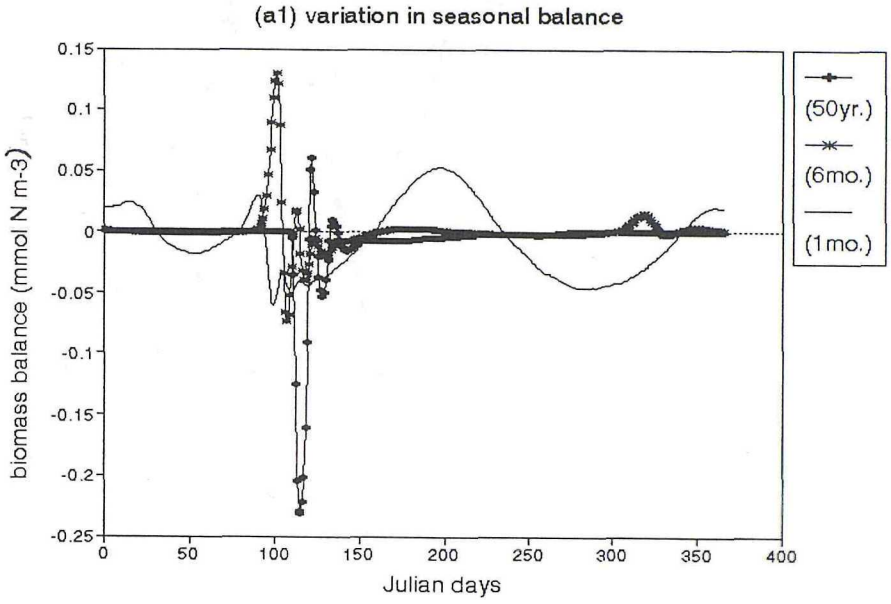

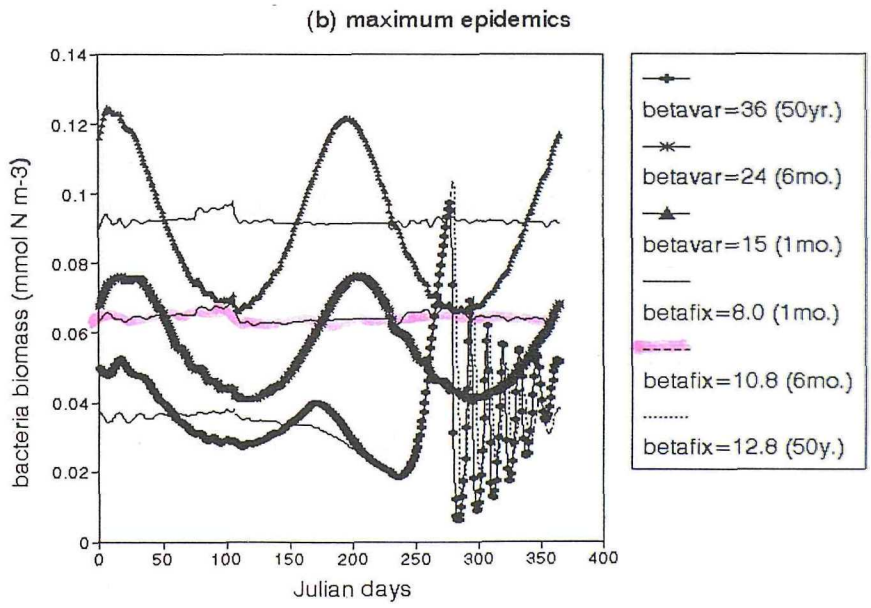

Figure 6.17 continued

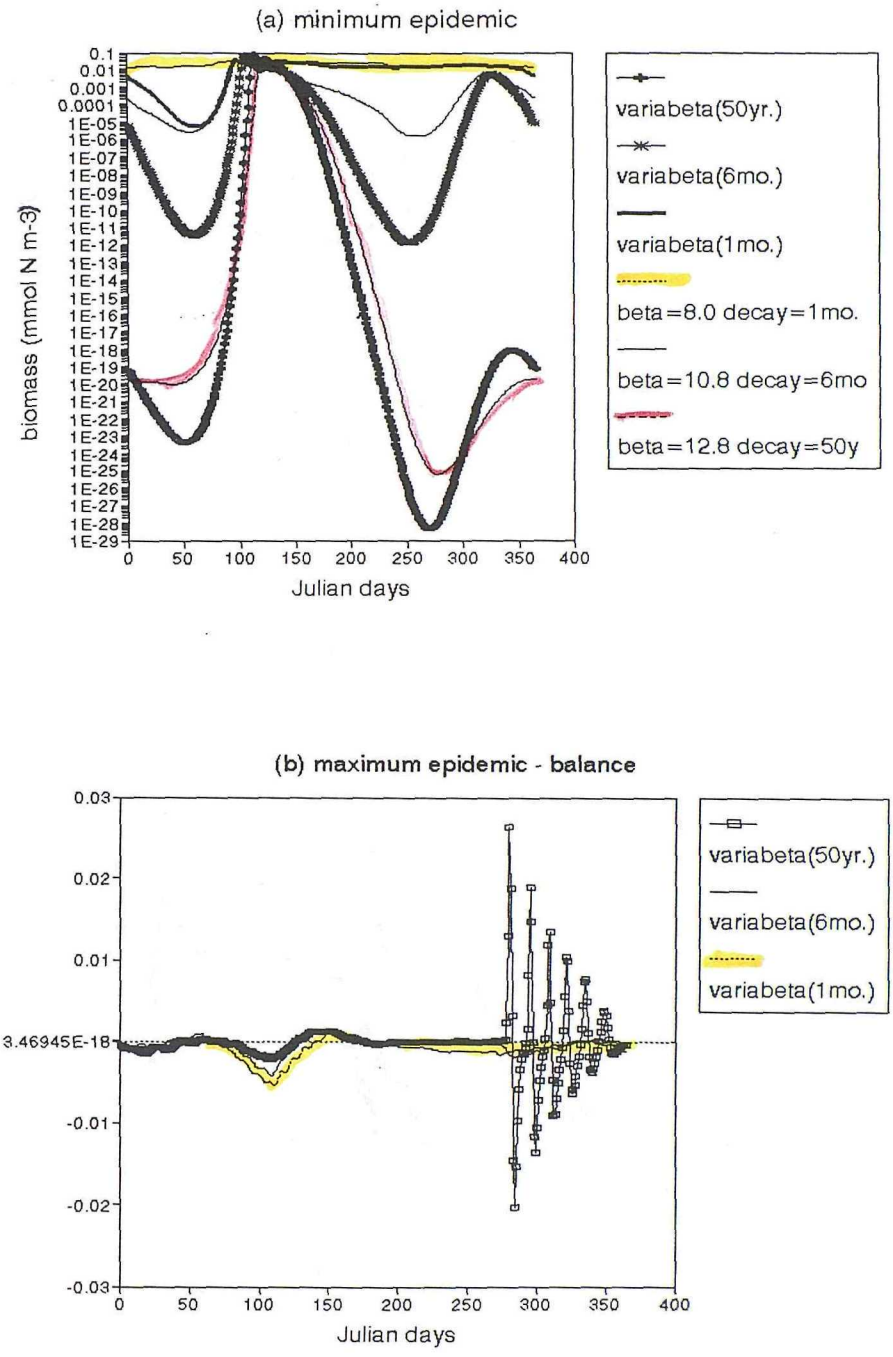

Figure 6.18 Annual cycle of active virus biomass in (a) minimum epidemic and (b) variation in balance for the maximum epidemic for decay rates of one month (heavy solid/yellow or dotted line), six months (star/blue or solid line) and fifty years (plus or empty square/red or dotted) for identical simulations with variable/fixed contact rates.

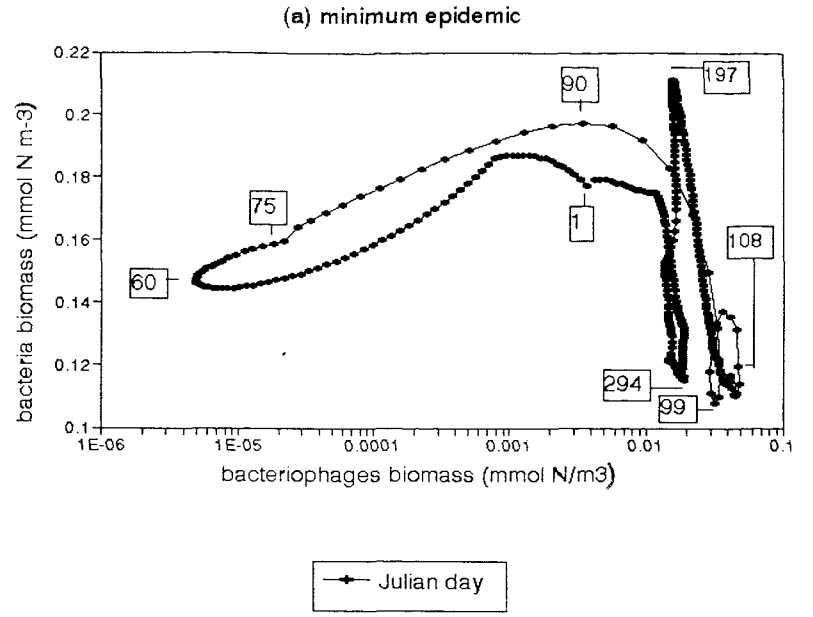

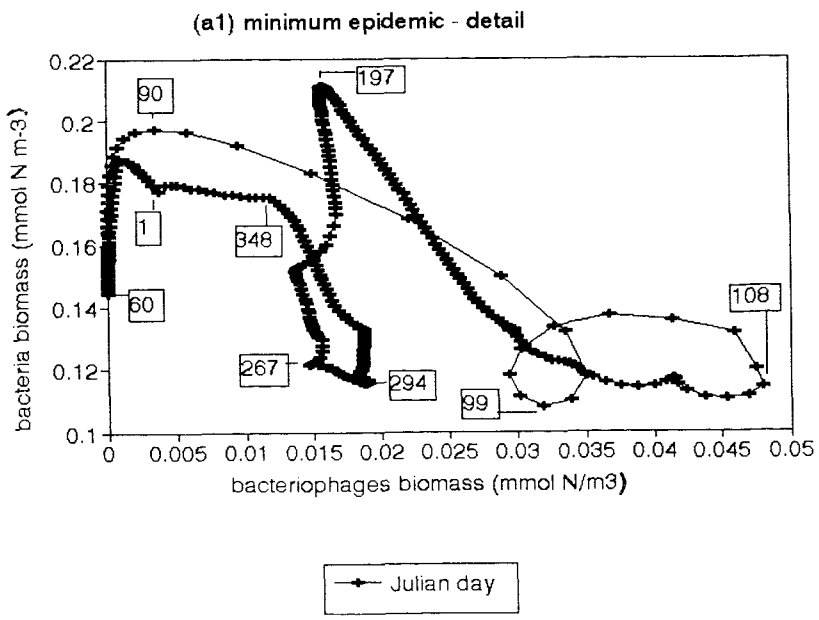

Figure 6.21 Seasonal variation of the host-prey dynamics of bacteria and virus biomass in simulations with a decay time of one month for (a) minimum epidemic, (a_1) detail and (b) maximum epidemic.

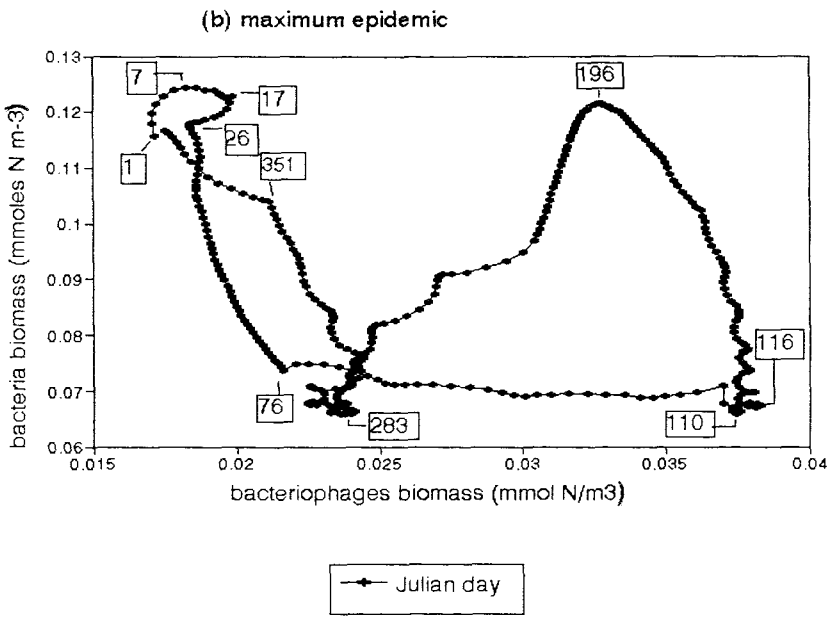

Figure 6.21 continued

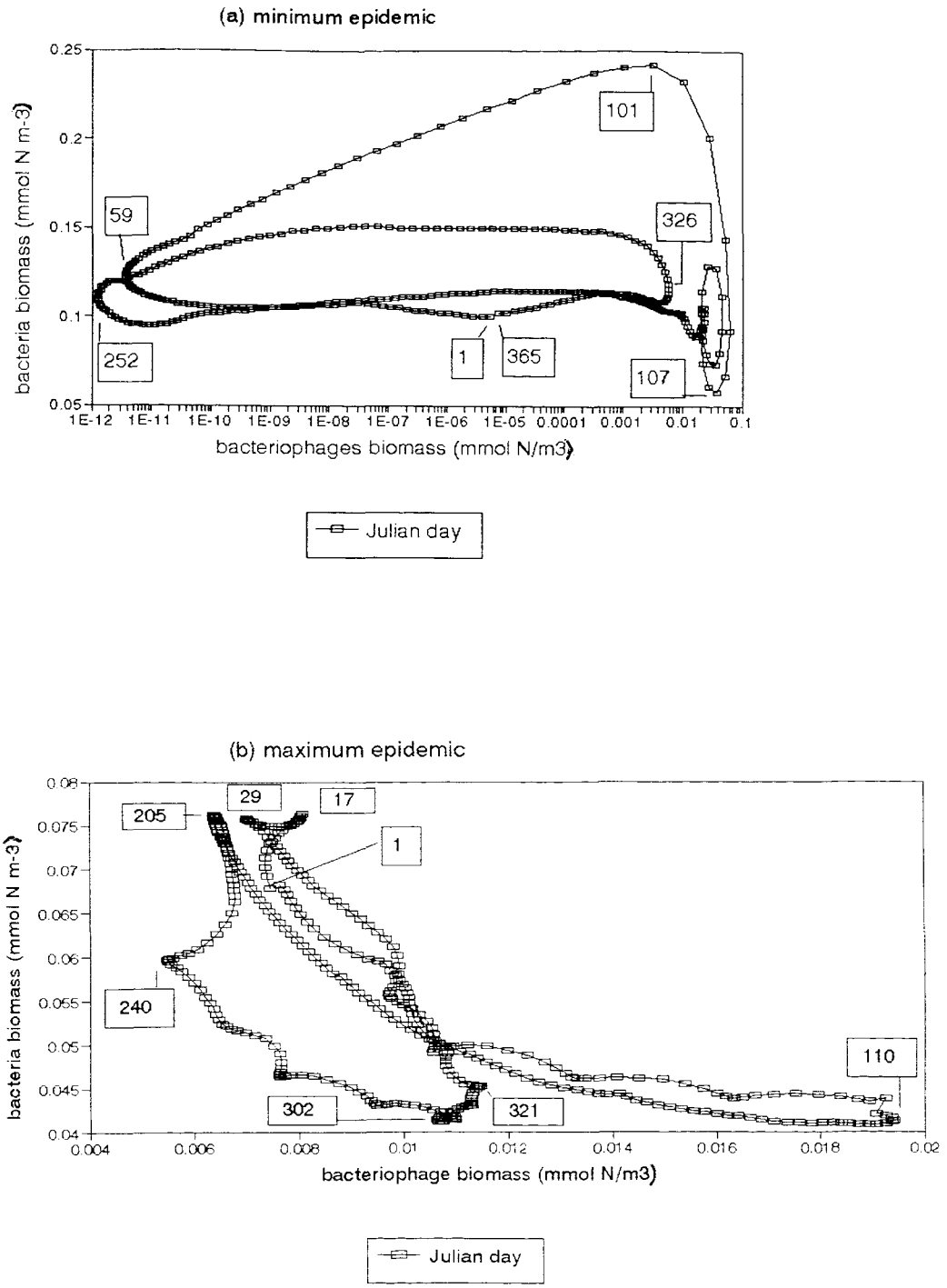

Figure 6.22 Seasonal variation of the host-prey dynamics of bacteria and virus biomass in simulations with a decay time of six months for (a) minimum and (b) maximum epidemic.

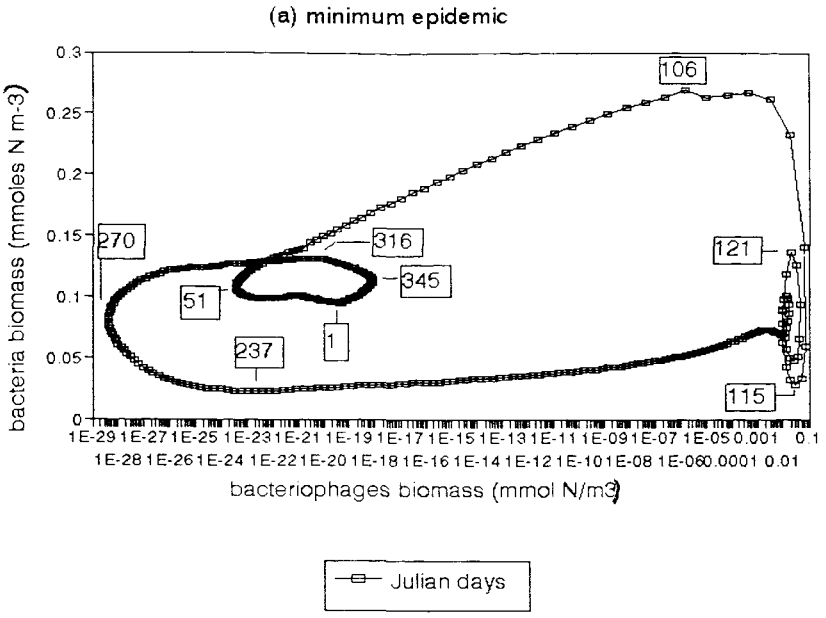

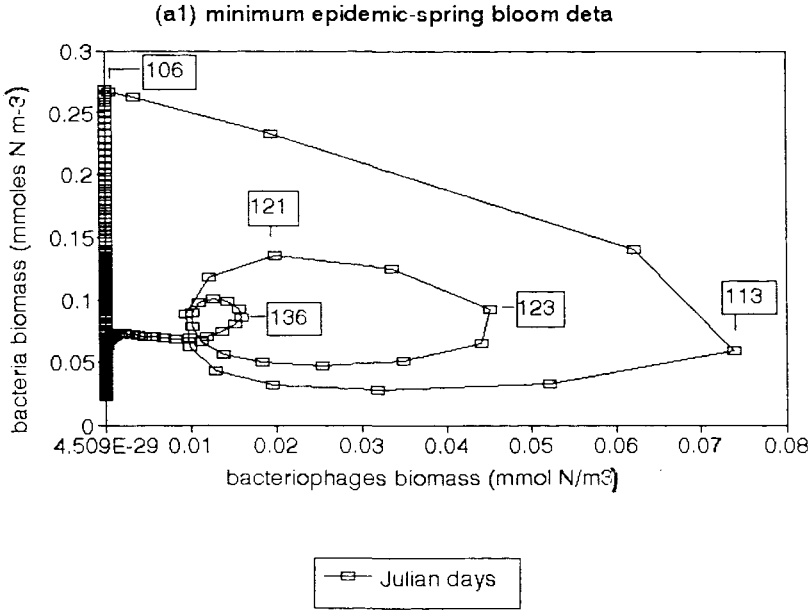

Figure 6.23 Seasonal variation of the host-prey dynamics of bacteria and virus biomass in simulations with a decay time of fifty years for (a) minimum epidemic (a_1) detail of spring bloom (b) maximum epidemic and (b_1) detail of autumn bloom.

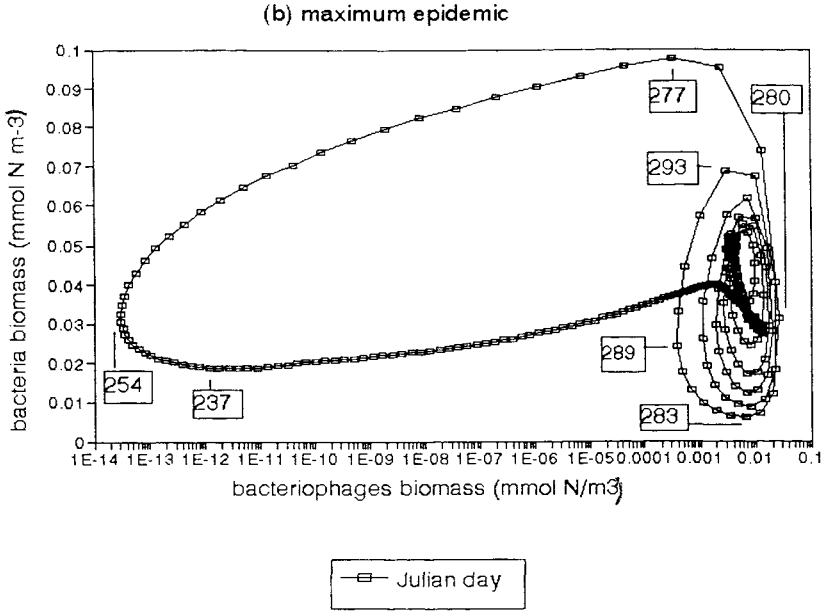

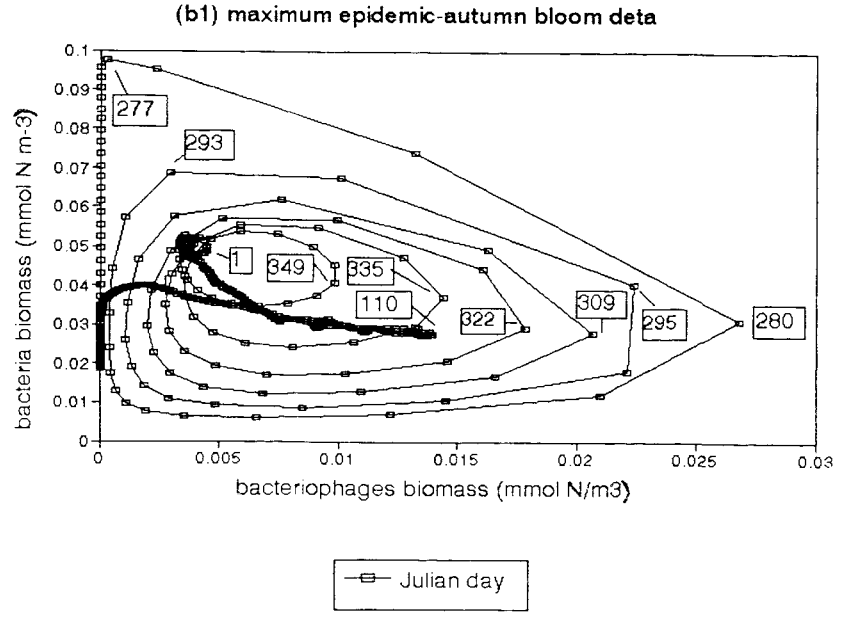

Figure 6.23 continued

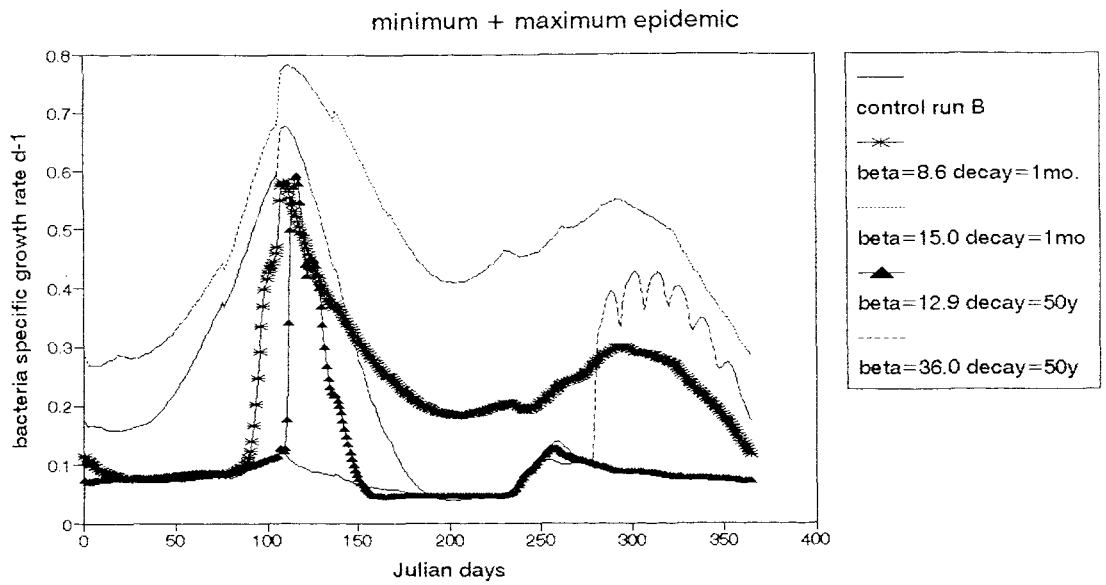

Figure 6.24 Variation in the seasonal cycle of specific growth rate of bacteria in minimum and maximum epidemics, for decay times of one month (star/dotted), fifty years (triangle/dashed) and control run B (solid line).

Chapter 7.

Results III - Simultaneous Epidemics of Bacterial and Phytoplankton Viruses.

7.1 Introduction

In chapter 5 and 6 the dynamics of phytoplankton and bacterial viruses were investigated separately. However, it is likely that both the bacteria and phytoplankton populations are at some stage of viral infection at any one time. Therefore in this chapter a simultaneous epidemic of bacterial and phytoplankton viruses is investigated thereby introducing version 8 of the model.

The experimental strategy is outlined in § 7.2. Results of simulations for increasing decay times of inactivated viruses and a sinking speed of detritus of 1 m/day and 10 m/day are presented in § 7.3 and § 7.4. In these sections the effect on overall production rates and biomass are studied. The response of the epidemic to seasonally varying contact rates is given special attention. In § 7.5 the conclusions reached from these numerical simulations are discussed.

7.2 Experimental Strategy.

A reference minimum value for the contact rate (Beta8) of phytoplankton viruses was determined to assure their coexistence at any level of bacteriophage epidemic for simulations with a sinking speed of detritus of 1 and 10m d^{-1}.

However the reference value should be taken as an upper limit on the infectivity of phytoplankton viruses as it forced the phytoplankton biomass to concentration levels of moderate to maximum epidemic.

Nonetheless lower levels of Beta8 may survive equally well the impact of lesser epidemics of Beta9. Any change on

the levels previously found for single epidemic indicated an alteration in the infectivity of viruses and was due to competition for nitrogen.

In order to investigate the effect of changes in the reference $\beta 8$ on the fate of the epidemic of phytoplankton viruses against increased levels of the competing epidemic of bacterial viruses over 100 simulations were carried out.

Likewise the effect of changes in the reference $\beta 9$ on the fate of the epidemic of bacterial viruses against increased levels of $\beta 8$ was studied.

The effect of changes in decay time on production rates and biomass were studied for joint epidemics with $\beta 8$ and $\beta 9$ set alternately to minimum and maximum epidemic. The decay times under scrutiny were one, three and six months plus fifty years and were carried out in simulations for a sinking speed of detritus of 1 and 10m d^{-1}.

The impact of variable contact rates on production rates and biomass were determined for 1m and 10m simulations and compared to the results for fixed contact rates under similar conditions.

7.3 Sinking speed of detritus 1m/day

7.3.1 Impact of changes in the reference Beta8/Beta9 value on the production rates for increased levels of bacterial/phytoplankton epidemic

Simultaneous epidemics using the contact rate values obtained for single minimum epidemics in both the bacteria and phytoplankton viral populations have a very delicate balance and yield low rates of viral lysis which increase for shorter decay times.

The contact rate of phytoplankton viruses had to be

increased on average 54% on the minimum value for a single epidemic in order to sustain any level of the coexisting epidemic of bacteriophages. Figure 7.1a shows that for Beta8=8.3 the annual rate of phytoplankton viral lysis declines 82% between values of Beta9 8 - 30 and keeps a low but constant value of **ca.** 33 mMol N m^{-2} yr^{-1} for higher levels of Beta9.

Values for Beta8 below that for the new minimum will result in the epidemic of phytoplankton viruses being driven to extinction under increased levels of the bacteriophage epidemic. Figure 7.1b shows that for Beta8=8.0 the annual rate of phytoplankton viral lysis declines 98% from Beta9=8.0 and becomes negligible from Beta9=25.0.

Values for Beta8 above the minimum for simultaneous epidemics show smaller decreases and become constant at higher levels of annual viral lysis. Figure 7.1c shows that for Beta8=12.0, maximum epidemic of phytoplankton viruses, the annual rate of phytoplankton viral lysis declines 31% between values of Beta9 11 to 30 and then becomes constant at 144 mMol N/m^2/year matching the value of bacterial viral lysis.

By contrast, the maximum value reached by bacterial viral lysis is lower for each of these increases in the reference Beta8.

Increases in the infectivity of phytoplankton viruses have a large impact on the epidemic of bacteriophages which decreases gradually and can be driven to extinction no matter the minimum value chosen for Beta9 (fig. 7.2).

Increases in contact rate result in a initial decline in primary production which is then kept nearly constant for higher levels of Beta9 (fig. 7.3a). Gross and net bacterial production plus bacterial viral lysis increase initially and then decline slowly as the contact rate rises (fig. 7.3b).

This pattern is identical for all decay time simulations.

7.3.2 Impact of changes in decay time on production rates

Increases in decay time result in a decline of production rates in simulations for simultaneous epidemics thus following the same pattern of single epidemics for phytoplankton or bacteria.

Tables 7.1 a,b show the results for simulations of simultaneous epidemics in which the phytoplankton viruses are set to maximum epidemic and the bacterial viruses are set for minimum or maximum epidemic.

The total viral lysis yielded in the simultaneous epidemic with a minimum Beta9 is 631.9 mMol N/m^2/year for one month decay time and decreases 43%, 56% and 64% for three months, six months and fifty years, respectively.

The total viral lysis yielded in the simultaneous epidemic with a maximum Beta9 is 1180.0 mMol N/m^2/year for one month decay time and decreases 47%, 70% and 73% for three months, six months and fifty years, respectively.

The lowest values of total viral lysis for simultaneous epidemics are 230 mMol N/m^2/year for minimum and 308 mMol N/m^2/year for maximum epidemic of bacteria with phytoplankton set to maximum epidemic.

7.3.3 Impact of a variable contact rate on biomass and production rates

The collapse of phytoplankton biomass at the end of the spring bloom was found in previous chapters to be the result of either bacteriophage or phytoplankton viral epidemics. A low contact rate on bacteriophage epidemics resulted in the drop of phytoplankton biomass occurring 50 days later (day

150) in comparison to simulations for a higher contact rate. Collapses which result solely from epidemics of phytoplankton viruses occurred even earlier (chapter 5 and 6).

A simultaneous epidemic for minimum lysis in both the bacteria and phytoplankton populations results in a variation of the concentration of phytoplankton biomass similar to that of a single bacteria epidemic (figures 7.4.a and 7.4.b) and produces an identical peak concentration of inactive viruses. The viral lysis by phytoplankton viruses is minimal at 4.2 mMol N m^{-2} $year^{-1}$ while the viral lysis by bacteria is four times higher at 18 mMol N m^{-2} $year^{-1}$.

However the concentration levels of bacteria are above those of the observed data for Bermuda station "S" and thus higher fixed and variable contact rates of bacteriophages have been tested that crop down the bacteria biomass.

A comparison of the effect of fixed and variable contact rates on biomass was investigated in simultaneous epidemic with a fifty year decay time for Beta8=8.3, minimum and Beta9=19, maximum.

For fixed contact rates (Figure 7.5.a) the bacterial biomass was nearly constant for 3/4 of the year with a concentration of 0.07 mMol N m^3 d^{-1} and then increased at the autumn bloom to 0.17 mMol N m^3 d^{-1} and displayed typical oscillations of predator-prey interaction. This is due to the high contact rate of bacterial viruses (see chapter 6, § 6.6.5).

The phytoplankton biomass which is under the attack of viruses with low infectivity, is kept at a nearly constant biomass of 0.17 mMol N m^3 d^{-1} from the beginning of the year then declines 44% at the end of the spring bloom. It is kept at a nearly constant level during summer at 0.09 mMol N m^3 d^{-1} increasing to 0.3 mMol N m^3 d^{-1} during the autumn bloom.

When a variable contact rate was introduced for the same average contact rate (Figure 7.5.b) the bacterial biomass displayed a similar behaviour to the fixed contact rate simulation though with some oscillations in the initial 3/4 of the year (0.1 to 0.05 mMol N m^3 d^{-1}).

The initial phytoplankton biomass was slightly larger at 0.2 mMol N m^3 d^{-1} and collapsed twenty five days earlier to 0.1 mMol N m^3 d^{-1} then had a secondary bloom which reached a peak concentration on day 100 at 0.15 mMol N m^3 d^{-1}. Thereafter followed the pattern of the fixed contact rate simulation with the difference of a collapse in the autumn bloom which dropped the biomass concentration to 0.09 mMol N m^3 d^{-1} followed by a secondary bloom.

The variable contact rate introduces in the phytoplankton biomass a secondary bloom in spring and autumn and increases all production rates by 1.5% to 38% with the exception of maximum daily flow into lysis which increases by 2.3 times (table 7.2).

7.4 Sinking speed of detritus 10m/day

7.4.1 Impact of changes in the reference Beta8/Beta9 value on the production rates for increased levels of bacterial/phytoplankton epidemic

The difficulty in balancing the epidemics of phytoplankton and bacterial viruses which was found for 1 m sinking rate is maintained in simultaneous epidemics for a detritus sinking speed of 10 m.

The minimum contact rate for phytoplankton epidemic had to be increased to Beta8=9.0, which is 8.4% above the value for simultaneous epidemics in 1m/day simulations, in order to sustain any level of the coexisting epidemic of

bacteriophages (Fig. 7.8.a).

The annual rate of phytoplankton viral lysis declines 75% from 140.2 to 35.14 mMol N m^{-2} yr^{-1} between the values of Beta9 16 - 50 and keeps a nearly constant value thereafter in simulations for a decay time of 50 years. The bacterial viral lysis rises from 0 to 175.9 mMol N m^{-2} yr^{-1} within the same frame of reference.

Values of Beta8 below the new minimum will result in the epidemic of phytoplankton viruses being driven to extinction for increased levels of Beta9 (fig. 7.8.b).

Increases in the infectivity of phytoplankton viruses have a large impact on the epidemic of bacteriophages which can be driven to extinction no matter the minimum value chosen for Beta9 (fig. 7.9.a) as in previous simulations.

However when the contact rate of phytoplankton viruses is excessively high it causes the phytoplankton lysis to go over its maximum and start declining thus allowing the bacteriophages to initiate a rise in bacterial viral lysis (fig. 7.9.b).

This rising lysis of bacteria happens in spite of a declining uptake of nitrogen by bacteria and a falling primary production.

Simulations for a sinking speed of 10m/day (fig. 7.9 a,b) follow a similar pattern to 1m/day simulations though with 33% lower bacterial lysis and bacterial production rates and 14% to 20% lower primary production and phytoplankton viral lysis. Furthermore peak values are reached at higher contact rates (beta9).

7.4.2 Impact of changes in decay time on production rates

The decline of bacterial production rates and phytoplankton and bacterial viral lysis with the increase in decay time follows the pattern of 1m/day simulations (Fig. 7.9 a,b). However the primary production increases slightly for longer decay times and lower values of the contact rate.

The results for simulations of simultaneous epidemics in which phytoplankton and bacterial viruses are set to minimum epidemic are presented in Table 7.5.

The total viral lysis yielded in the simultaneous epidemic with a minimum Beta9 is 650.1 mMol N/m^2/year for one month decay time and decreases 63% and 75% for six months and fifty years, respectively.

The lowest value of total viral lysis for simultaneous epidemics is 159.8 mMol N/m^2/year for minimum epidemic and a decay time of fifty years.

7.4.3 Impact of a variable contact rate on biomass and production rates

The concentration of bacteria is kept at a nearly constant level of 0.1 mMol N m^{-3} d^{-1} throughout the year for a joint epidemic with fixed contact rates of β8=8.0 and β9=12.0, both corresponding to minimum epidemic, and a decay time of six months (fig. 7.10a).

A similar result in single epidemic of bacteriophages could be obtained only for simulations with a decay time of one month.

Furthermore the phytoplankton biomass exhibits a temporal evolution and concentration levels similar to the observed data for Bermuda. This simulation for six months decay time fits very well the observations.

The variable contact rate induces an earlier collapse of the phytoplankton spring bloom which takes place on days 60 and 63 for the fifty year (fig. 7.11b) and the six month (fig. 7.10b) decay time simulations and is 30 and 25 days earlier than for fixed contact rates (fig. 7.10a and fig. 7.11a).

Consequently it also gives rise to two secondary phytoplankton blooms in spring and one in autumn which are due to enhanced predator-prey interaction driven by the elevated contact rate of viruses during these events.

It also introduces oscillations in the biomass of bacteria during spring, summer and autumn which range from 0.07 to 0.17 mMol N m^{-3} d^{-1} and from 0.04 to 0.13 mMol N m^{-3} d^{-1} in six months and fifty year decay time simulations, respectively.

Most production rates decrease by 10% to 31% in six month decay time simulations but remain nearly constant for fifty year decay time simulations. The exceptions are the maximum daily flow into lysis which increase by up to 2.5 times and 3.5 times, respectively (table 7.6).

The viral lysis by phytoplankton viruses in simultaneous minimum epidemics ranged from 66 to 72 mMol N m^{-2} $year^{-1}$ while the viral lysis by bacteria ranged from 90 to 578.7 mMol N m^{-2} $year^{-1}$. These values increased for shorter decay times.

7.5 Discussion

It is not easy to find the contact rates for a balanced epidemic of bacterial and phytoplankton viruses because the nitrogen resources they share are limited.

They depend on phytoplankton primary production either directly (phytoplankton viruses) or indirectly (bacterial viruses assimilate the nitrogen that bacteria obtained from

the DON exuded by phytoplankton).

Most crucial, however is that bacterial viruses control the amount of nitrogen excreted as bacterial ammonium and therefore available for regenerated primary production.

A similar effect is obtained by lessening the natural mortality of phytoplankton which makes more nitrogen available to lysis of phytoplankton and less to detritus, zooplankton (hence a decline in ammonium) and DON. The cumulative effect forces a decline in bacterial production and hence the production of bacteriophages.

Attempts to use the low contact rate values determined for single epidemics of phytoplankton and bacterial viruses made the balance of the joint epidemic to become very sensitive and prone to collapse under increased levels of any of the contact rates into a single epidemic of favour driving the other to extinction.

For identical values of the contact rate bacteria yielded larger productions and cycled more nitrogen than phytoplankton due to their higher specific growth rate under viral attack (see figures 5.55 and 6.24) which is twice that of phytoplankton.

However increases in the infectivity of bacteriophages have a limited impact on the epidemic of phytoplankton viruses and are unable to drive them to extinction if a minimum value of Beta8 is respected. There is a maximum drop of 25-42% (*ca.* 108 mMol N m^{-2} $year^{-1}$) on phytoplankton viral lysis when the minimum epidemic of bacterial viruses is established but no decline thereafter with the increase in bacteriophage infectivity.

Nonetheless increases in the infectivity of phytoplankton viruses have a large impact on the epidemic of bacteriophages which decreases gradually and can be driven to

extinction. This happens because the viral epidemic of phytoplankton by diverting nitrogen into the making of new viruses strangles the supply of nitrogen to bacteria directly and indirectly. Hence the decline in bacterial production which forces a decrease in bacteriophage production.

A limit on the availability of nitrogen in the system sets the maximum value of joint viral lysis at *ca.* 309 mMol N m^{-2} $year^{-1}$ for 50 year decay time simulations, at *ca.* 480 mMol N m^{-2} $year^{-1}$ for 6 months decay time simulations and at *ca.* 1200 mMol N m^{-2} $year^{-1}$ for 1 month decay time simulations with sinking speed of detritus of 1m/day.

The simulated biomass of phytoplankton was lower than the observational data for Bermuda in simulations for a sinking speed of 1m/day in which the value of Beta8 was large and corresponded to a maximum epidemic of phytoplankton viruses in the joint epidemic with bacteriophages.

Nonetheless the simulated biomass of phytoplankton was similar to the observational data for Bermuda in simulations for a low value of Beta8 corresponding to a minimum epidemic.

The simulated biomass of bacteria could be fitted to the observational data for Bermuda (Fasham, 1990) by forcing a moderate to high contact rate on bacteriophages for simulations with a decay time longer than three months. This suggests that free living bacteria in the open ocean are permanently under the control of viruses that crop down the bacteria biomass. An alternative explanation is that the bacteria are heavily grazed by zooplankton (Fasham 1995, personal communication).

However bacteria exhibited a nearly constant concentration during the annual cycle when the decay time of inactivated viruses was short, 1 to 3 months, for any level of contact rate.

The peak concentration of inactivated viruses in 1m/day simulations was 1.65 mMol N m^{-3} d^{-1} which was up to 2 times higher than in 10m/day simulations. Their pattern of temporal variation is not very sensitive to changes in the level and seasonality of contact rates.

Variable contact rates increased the overall production rates in 1m/day simulations by contrast to 10m/day simulations where the rate of bacteria related processes decreased and phytoplankton related processes increased. This pattern was also found for single epidemics.

Bacteria are the main beneficiaries of slow detritus sinking speed because their longer residence time in the mixed-layer allows for a more complete breakdown of organic matter into DON which can then be used by bacteria.

Therefore bacterial production and hence viral lysis are very sensitive to the sinking speed of detritus in contrast to phytoplankton viral lysis.

Analysis of fluxograms (Fig. 7.7 a,b,c) has shown that on average 98% and 98.8% of the losses in the population of active viruses of phytoplankton and bacteria, respectively, are due to inactivation by natural ultra-violet radiation. The percentage of losses is unrelated to decay time (table 7.3).

The amount of nitrogen exported to the deep ocean (Fig. 7.7 a,b,c) by detrainment in the form of active and inactivated viruses in simulations for a decay time of one and six months and fifty years is similar, at 155.7-193.1 mMol N m^{-2} $year^{-1}$. By contrast the contribution of the sinking flux of detritus is three to five times lower at 41.8-47.9 mMol N m^{-2} $year^{-1}$ (Table 7.4).

However these simulations differ on the amount of nitrogen that is available to the ecosystem from viral

breakdown.

This virus derived nitrogen continues flowing within the mixed-layer, enhancing mostly bacterial production, and increases with the shortening of decay time (table 7.4) from 1.2 to 115.6 to 560.8 mMol N m^{-2} $year^{-1}$ for fifty years, six months and one month, respectively.

Minimum simultaneous epidemic in both the bacteria and phytoplankton population are dominated by bacterial viral lysis.

7.6 Tables

Decay time	Beta8	Beta9	Gross bacterial production	Bacterial viral lysis	Total viral lysis
1 month	12.0	5.2	997.2	443.5	631.9
3 months	12.0	6.5	547.1	155.8	359.0
6 months	12.0	7.3	384.6	59.8	276.8
50 years	10.0	12.0	253.2	50.2	230.0

Table 7.1a Variation in gross bacterial production, bacterial viral lysis and total viral lysis in mMol N m^{-2} $year^{-1}$ for decay times of one, three and six months plus fifty years, in simultaneous epidemics of phytoplankton and bacterial viruses in which the contact rate **Beta9 is set to minimum epidemic**. Inactivation rate is .792 d^{-1} and sinking speed of detritus is 1m/day.

Decay time	Beta8	Beta9	Gross bacterial production	Bacterial viral lysis	Total viral lysis
1 month	12.0	12.0	1208	1026	1180
3 months	12.0	17.0	610.4	488.2	638.6
6 months	12.0	21.0	424.7	236.6	384.0
50 years	10.0	29.0	267.0	198.3	308.3

Table 7.1b Variation in gross bacterial production, bacterial viral lysis and total viral lysis in mMol N m^{-2} $year^{-1}$ for decay times of one, three and six months plus fifty years, in simultaneous epidemics of phytoplankton and bacterial viruses in which the contact rate **Beta9 is set to maximum epidemic**. Inactivation rate is .792 d^{-1} and sinking speed of detritus is 1m/day.

Decay time	Beta8	Beta9	Primary productio	Phyto viral lysis	Net Bacterial productio	Gross Bacterial productio	Bacteria viral lysis	Bac. max. daily flow	Total viral lysis
1 month	min 7	min 4.8	525.7	5.3	845.8	1167	546.3	4	551.6
	8	8	366.4	45.7	1226	1419	1113	8.1	1158.7
	8	10	368.1	47.5	1223	1378	1146	8.4	1193.5
	8.3	10	361.2	65.9	1206	1361	1130	8.2	1195.9
	9	10	347.4	96.7	1178	1333	1102	7.8	1198.7
	9	12	348.7	97.4	1161	1290	1105	7.8	1202.4
6 months	5.2	6	viruses of phytoplankton die						
	8	12	369.3	26.1	518.2	647.4	460.4	3.86	486.1
	8	MVL 21	385.2	9.9	494.4	568.3	469.6	3.8	479.5
	10	max 12	327	117	415.1	544.4	359.8	2.78	476.8
50 years	8	8	viruses of bacteria die						
	min 8.3	19	368.7	58	280.6	363.1	251.9	2.34	309.9
	8	23	367.3	44.58	289.9	357.6	268.2	2.3	312.8
	10	min 12	385.8	181.2	113.5	253.2	50.2		231.4
	10	MBP 19	336.2	124.5	206.7	289.3	178.7	2.14	303.2
	10	MVL 23	331	114.7	215.6	283.5	194.6	1.7	309.3

Table 7.1c Variation in primary production, viral lysis of phytoplankton, net and gross bacterial production, viral lysis of bacteria, bacterial maximum daily flow into lysis and total viral lysis for decay times of one month, six months and fifty years, in simultaneous epidemics of phytoplankton and bacterial viruses. The inactivation rate is .792 d-1 and the sinking speed of detritus is 1m/day.
Note: MVL - maximum viral lysis. MBP - maximum bacterial production

Contact rate	Gross bact. production	Bact. viral lysis	Primary production	Phytop. viral lysis	Max. daily flow into lysis	Total viral lysis
Fixed $\beta 8=8.3$ $\beta 9=19.0$	363.1	251.9	368.7	58.0	Phyto 1.0 (Day 96) Bac 2.34 (Day 76)	309.9
Variable	369.5	255.8	379.2	62.2	Phyto 2.34 (day 78) Bac 3.23 (Day 74)	318.0
Increase	1.7%	1.5%	8.8%	7.1%	P- 2.3 x B- 38%	2.5%

Table 7.2 Variation in gross bacterial production, bacterial viral lysis, primary production, phytoplankton viral lysis, total viral lysis in mMol N m^{-2} $year^{-1}$ and maximum daily flow into lysis in mMol N m^{-2} d^{-1} for **fixed and variable contact rates** in simultaneous epidemics of phytoplankton and bacterial viruses. The decay time is **fifty years**, the inactivation rate is .792 d^{-1} and sinking speed of detritus is 1m/day.

Decay time	Beta8	Beta9	Inactivation (%)	
			viruses of phytoplankton	viruses of bacteria
1 months	8.0	8.0	97.8%	98.8%
6 months	8.0	12.0	96.9%	98.8%
50 years	8.3	19.0	97.9%	98.5%

Table 7.3 Variation in overall percentage of active viruses of phytoplankton and bacteria inactivated by natural UV radiation for **one** and **six months** and **fifty years** decay time simulations, in simultaneous epidemics of phytoplankton and bacterial viruses. Inactivation rate is .792 d^{-1} and sinking speed of detritus is 1m/day.

	fixed contact rates		variable contact rates
	1 month	6 months	50 years
Beta8	8.0	8.0	8.3
Beta9	8.0	12.0	19.0
Primary production	366.4	369.3	379.1
Lysed bacterial debris into DON	422.9	175.0	97.2
Breakdown of inactivated viruses into DON	560.8	115.8	1.2
Detrainment of inactivated viruses	147.0	179.1	189.9
Sinking flux of detritus	47.9	44.8	41.8

Table 7.4 Variation in the losses by detrainment of inactivated viruses, primary production, flow of lysed bacterial debris into DON, breakdown of inactivated viruses into DON and sinking flux of detritus in mMol N m^{-2} $year^{-1}$ for decay times of one and six months plus fifty years, in simultaneous epidemics of phytoplankton and bacterial viruses. Inactivation rate is .792 d^{-1} and sinking speed of detritus is 1m/day.

Decay time	Beta8	Beta9	Gross bact. prod.	Bact. viral lysis	Total viral lysis	Maximum daily flow
1 month	9.0	8.0	894.4	578.7	650.1	B-4.355 (76) P-1.258 (95)
6 months	8.0	12.0	344.1	151.4	217.7	B-1.74 (95) P-1.657 (93)
50 years	8.0	18.0	223.0	90.0	159.8	B-1.43 (90) P-1.36 (94)

Table 7.5 Variation in gross bacterial production, bacterial viral lysis, total viral lysis in mMol N m^{-2} $year^{-1}$ and maximum daily flow into lysis in mMol N m^{-2} d^{-1} for decay times of one and six months plus fifty years, in simultaneous epidemics of phytoplankton and bacterial viruses in which contact rates **Beta8 and Beta9 are set to minimum epidemic**. Inactivation rate is .792 d^{-1} and sinking speed of detritus is 10m/day.

Decay time	Gross bact. production	Bact. viral lysis	Primary production	Phytop. viral lysis	Max. daily flow into lysis	Total viral lysis
6 months $\beta 8=8.0$ $\beta 9=12.0$	309.5	103.9	437.2	88.1	Phyto 4.147 (day 72) Bac 3.512 (Day 86)	191.9
50 years $\beta 8=8$ $\beta 9=18$	226.7	89.1	436.3	72.8	Phyto 3.907 (day 74) Bac 5.051 (Day 72)	161.9

Table 7.6 Variation in gross bacterial production, bacterial viral lysis, primary production, phytoplankton viral lysis, total viral lysis in mMol N m^{-2} $year^{-1}$ and maximum daily flow into lysis in mMol N m^{-2} d^{-1} for **variable contact rates** in simultaneous epidemics of phytoplankton and bacterial viruses. The decay time of inactivated viruses is **six months** and **fifty years**. The inactivation rate is .792 d^{-1} and sinking speed of detritus is 10m/day.

7.8 Figures

Simulations with a sinking speed of detritus of 1m/day and an inactivation rate of viruses .792 d^{-1}

(a) Beta8=8.3

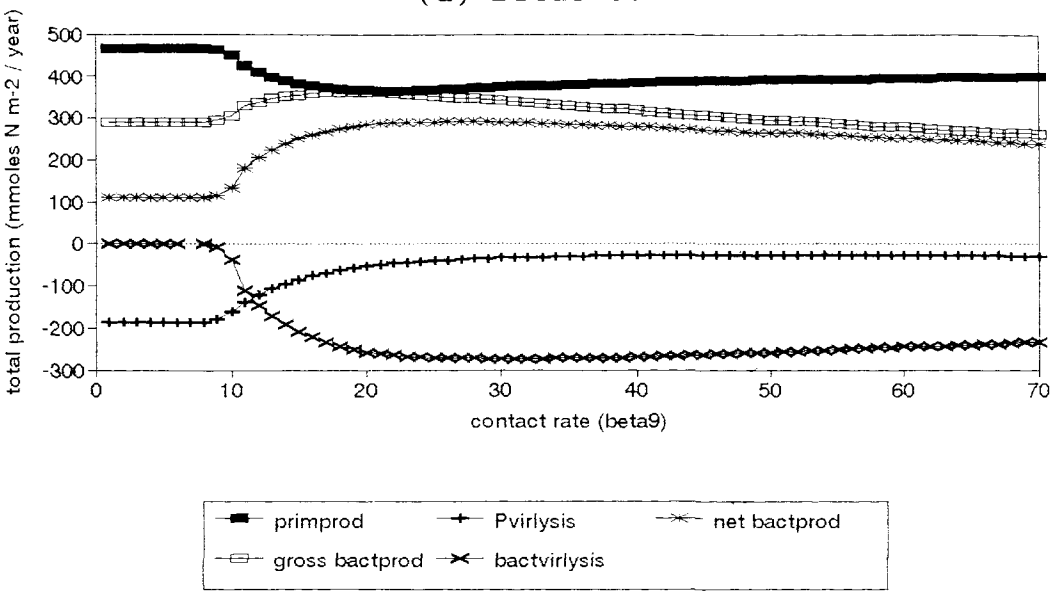

(b) Beta8=8.0

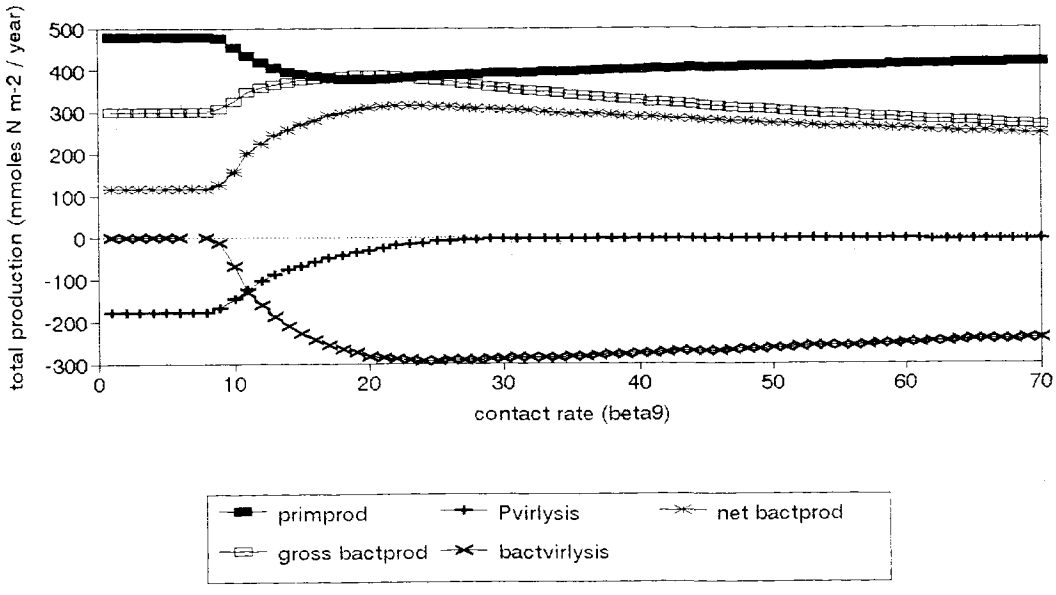

Figure 7.1 Variation in annual primary production (filled square), bacterial production (star) and corresponding losses by phytoplankton lysis (plus) and bacterial viral lysis (square) in mMol N/m^2/year, plotted against increasing levels of the contact rate (beta9) in simultaneous epidemics of phytoplankton and bacterial viruses for a **50 year** decay in inactivated viruses. The contact rate of phytoplankton viruses is fixed at (a) beta8=8.3 (b) beta8=8.0 and (c) beta8=12.0.

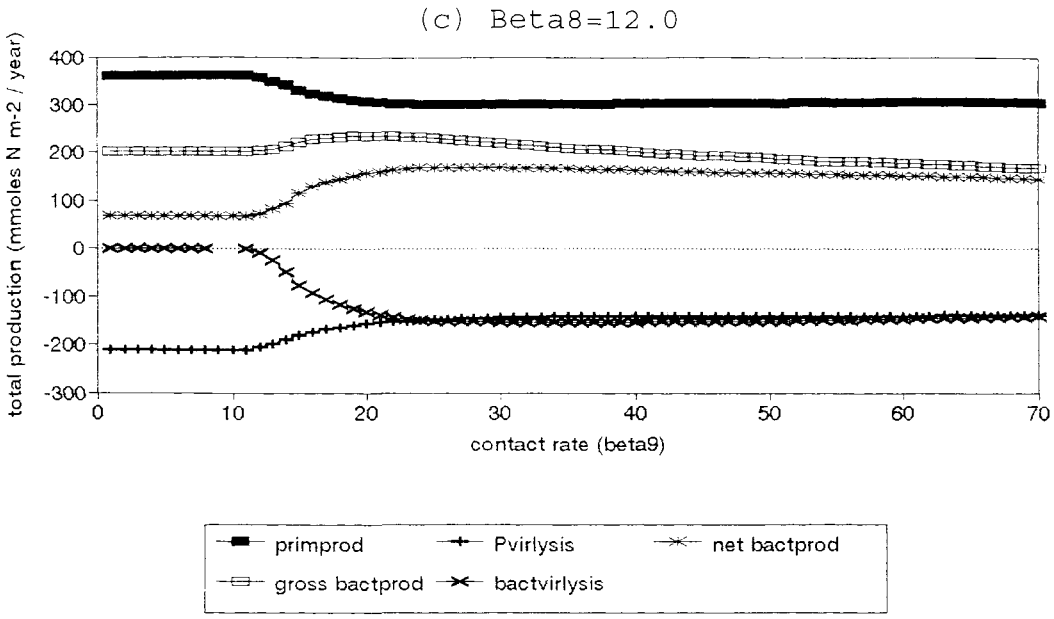

Figure 7.1 continued

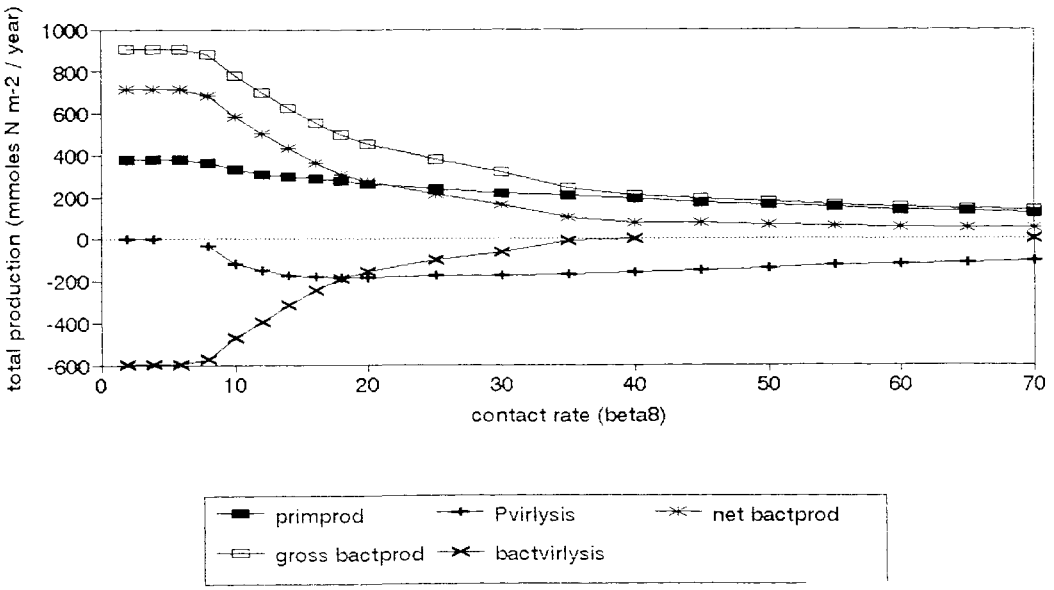

Figure 7.2 Variation in annual primary production (filled square), gross bacterial production (empty square), net bacterial production (star) and corresponding losses by phytoplankton lysis (plus) and bacterial viral lysis (cross) in mMol N/m^2/year, plotted against increasing levels of the contact rate (beta8) in simultaneous epidemics of phytoplankton and bacterial viruses for a **3 month** decay in inactivated viruses. The contact rate of bacterial viruses (beta9) is fixed at 8.0,

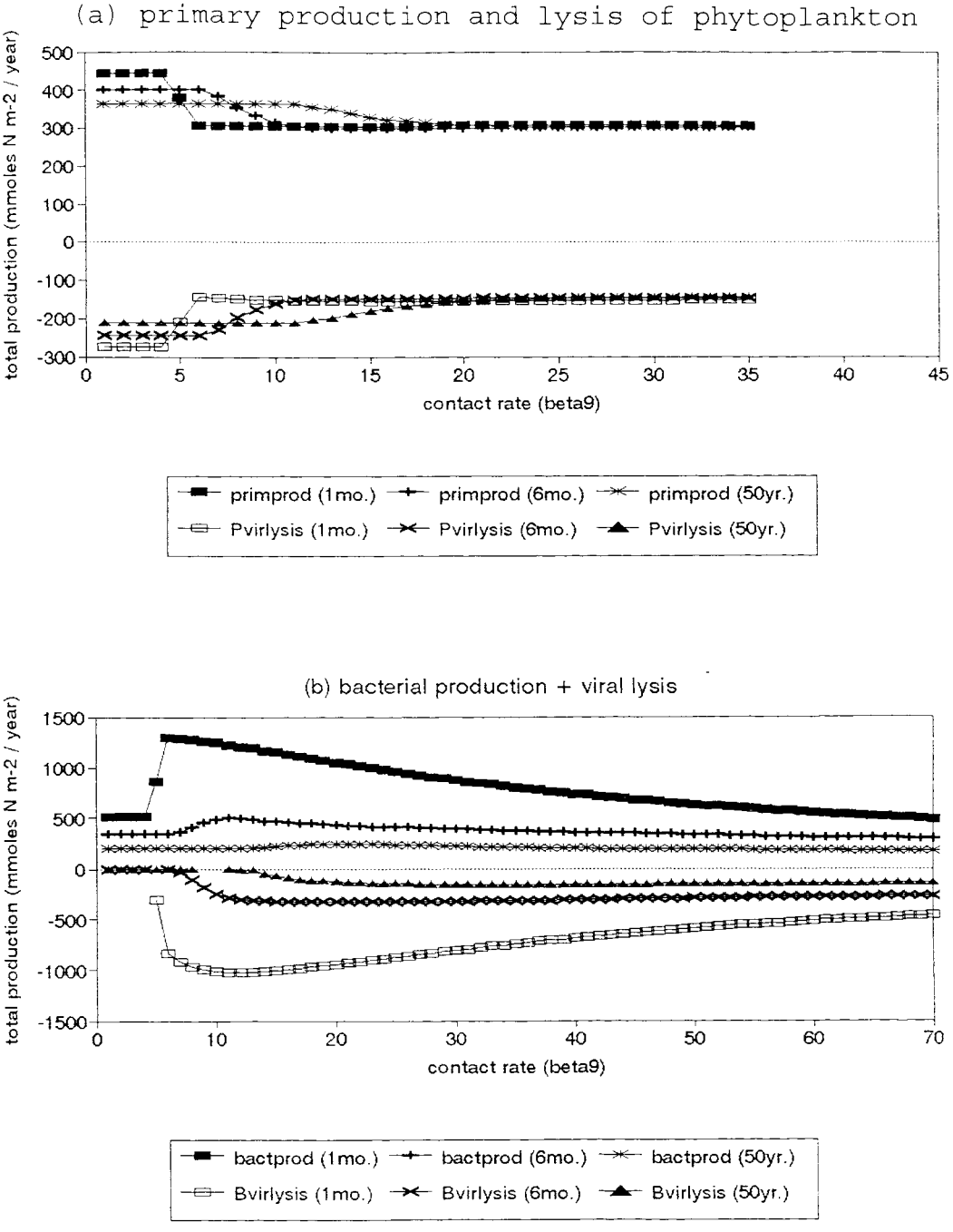

Figure 7.3 Annual production rates (in mMol N/m^2/year) and corresponding losses by viral lysis plotted against increasing levels of the contact rate (beta9) in simultaneous epidemics of phytoplankton and bacterial viruses for different levels of decay in inactivated viruses. Beta8 is fixed at 12.0 and Beta9 ranges from 0 to 35 or 70. Positive values represent productions for viral decays of 1 month (filled square), 6 months (plus) and 50 years (star). Negative values represent viral lysis for decays of **1 month** (square), **6 months** (cross) and **50 years** (triangle). (a) primary production and lysis of phytoplankton (b) gross bacterial production and lysis of bacteria.

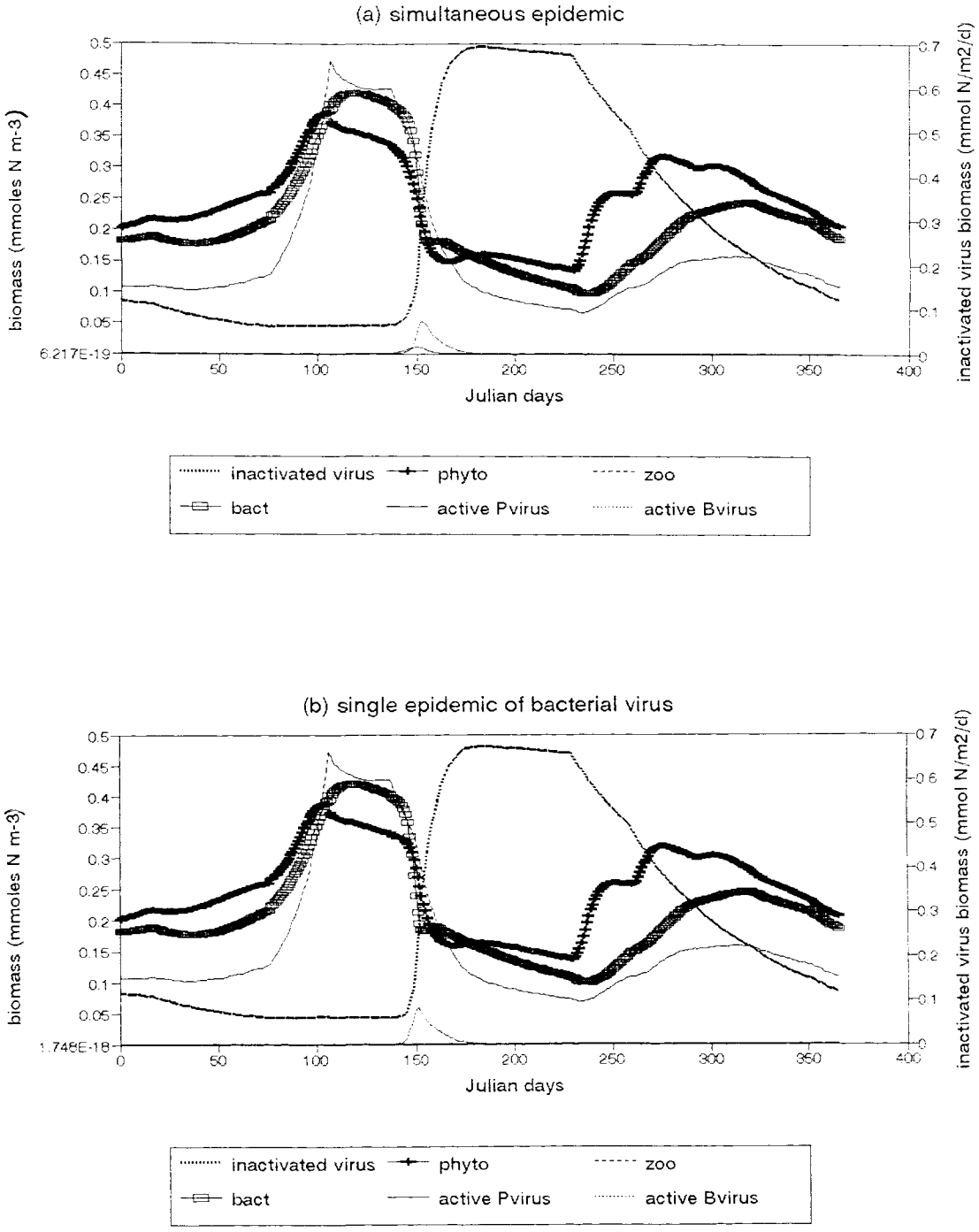

Figure 7.4 Annual cycles of phytoplankton (plus), bacteria (empty square), zooplankton (dashed), active viruses of phytoplankton (solid line) and bacteria (dotted) plus inactivated viruses (heavy dotted) concentration in (a) simultaneous epidemic for Beta8=5.2 and Beta9=6.0; (b) for single epidemic of bacterial viruses for Beta9=6.0. The decay time of inactivated viruses is **fifty years**.

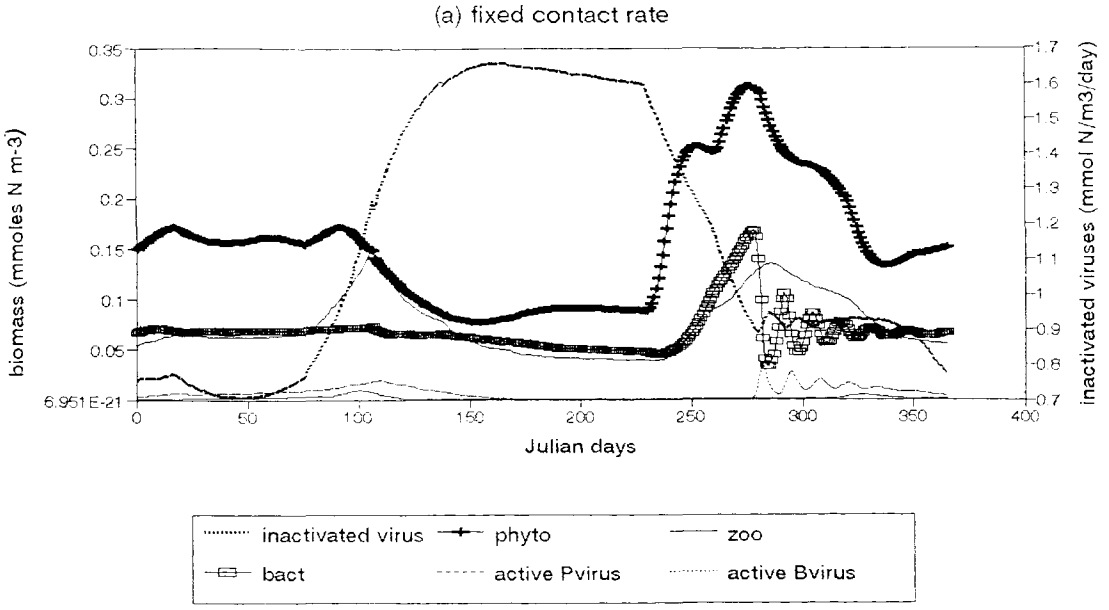

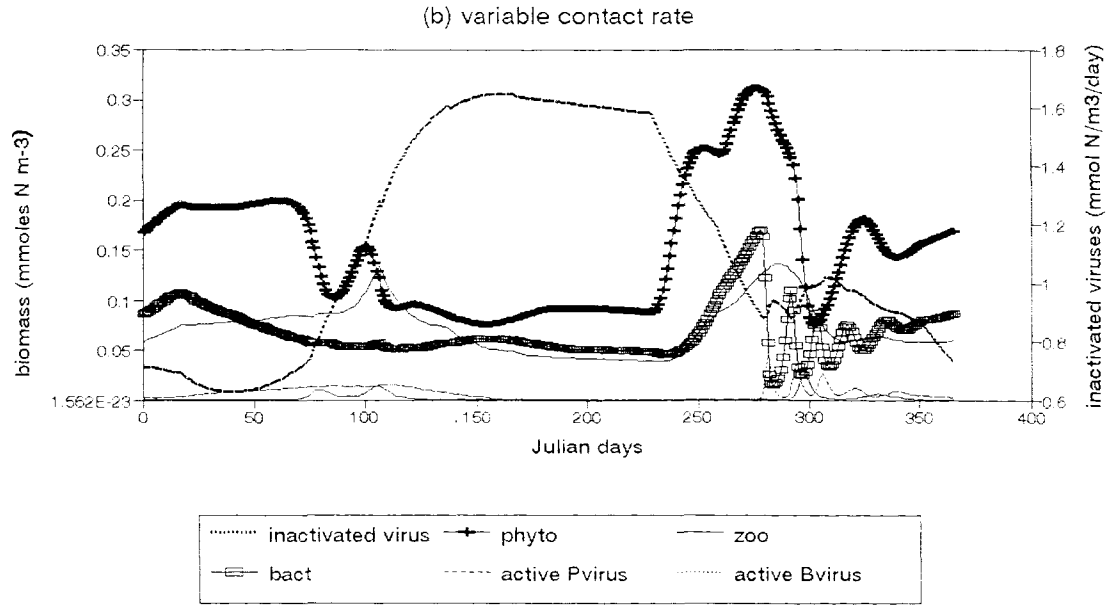

Figure 7.5 Annual cycles of phytoplankton (plus), bacteria (empty square), zooplankton (dashed), active viruses of phytoplankton (solid line) and bacteria (dotted) plus inactivated viruses (heavy dotted) concentration in a simultaneous epidemic for Beta8=8.3 and Beta9=19.0. The decay time of inactivated viruses is **fifty years**. (a) fixed contact rates (b) variable contact rates.

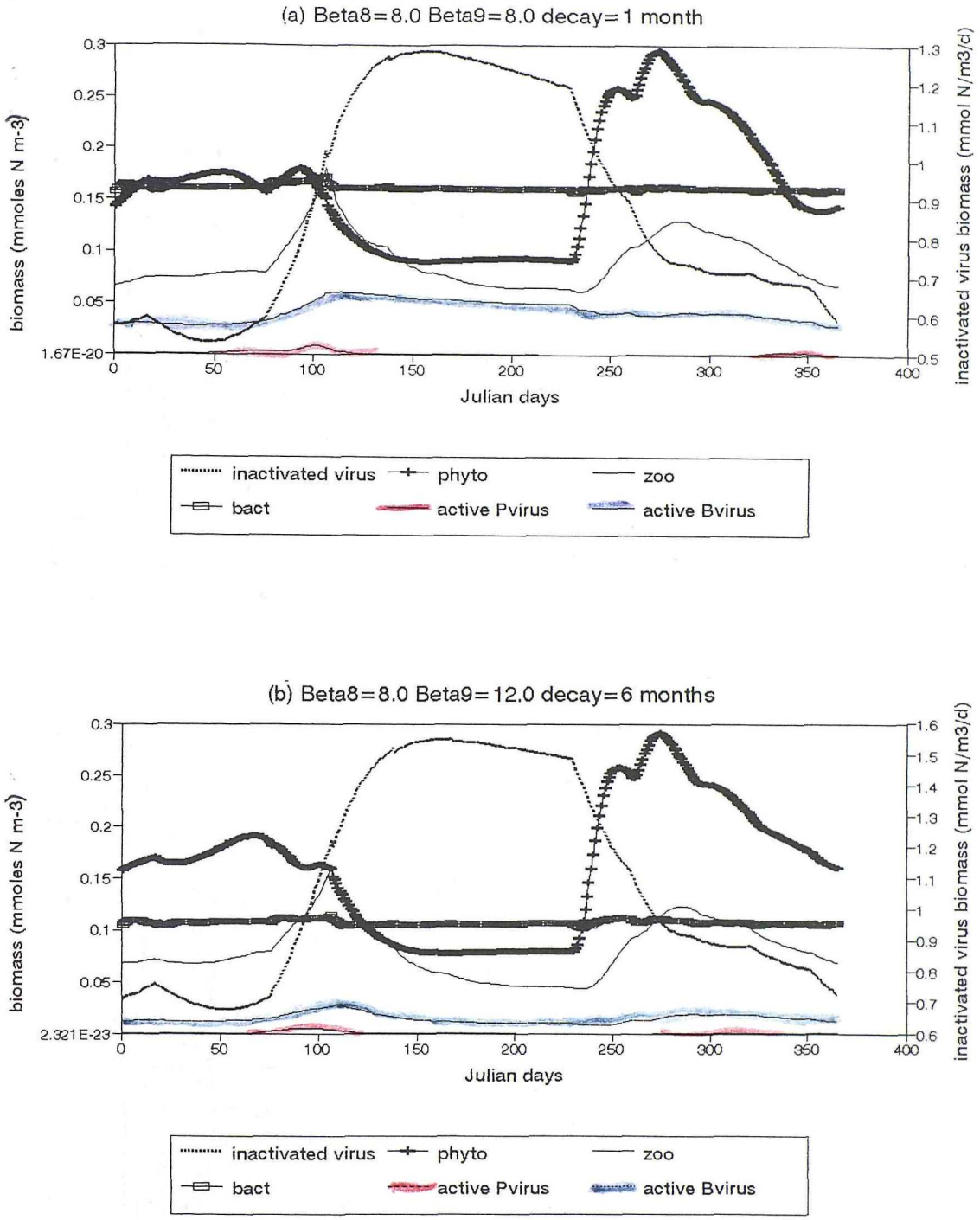

Figure 7.6 Annual cycles of phytoplankton (plus), bacteria (empty square), zooplankton (solid line), active viruses of phytoplankton (red) and bacteria (blue) plus inactivated viruses (heavy dotted) concentration in a simultaneous epidemic with fixed contact rates for (a) Beta8=8.0, Beta9=8.0 and decay time of inactivated viruses is **one month** (b) Beta8=8.0, Beta9=12.0 and decay time is **six months**.

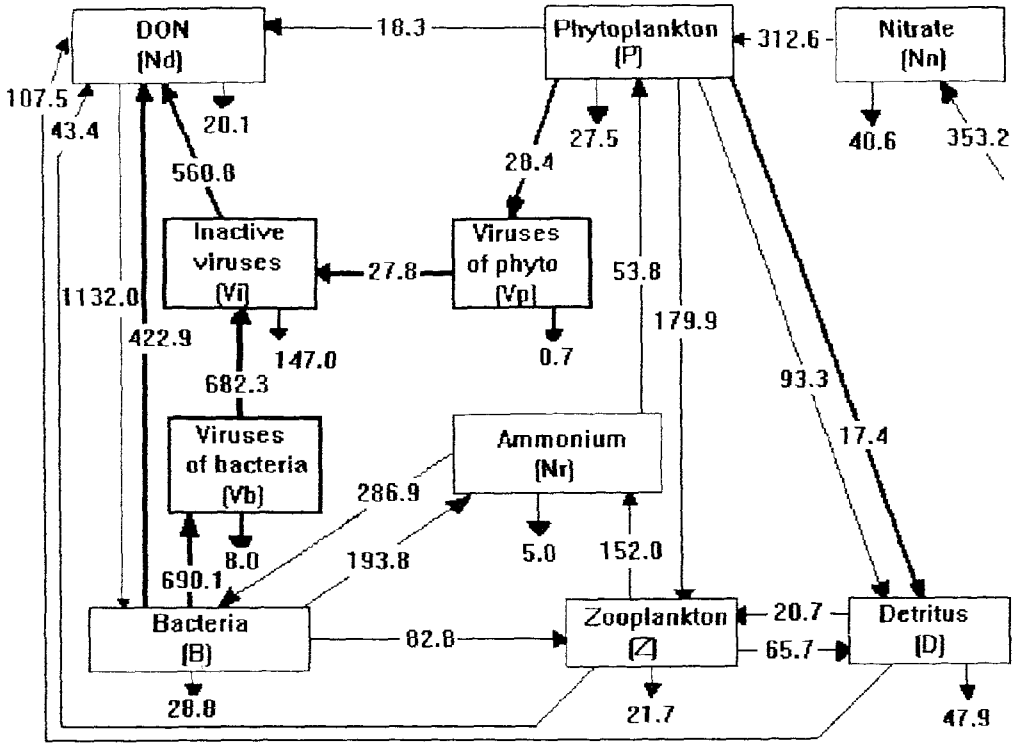

Fig.7.7 a Beta8=8 Beta9=8 Sink=1m/day Decay=1mo Inact=.792 Mix=0.01

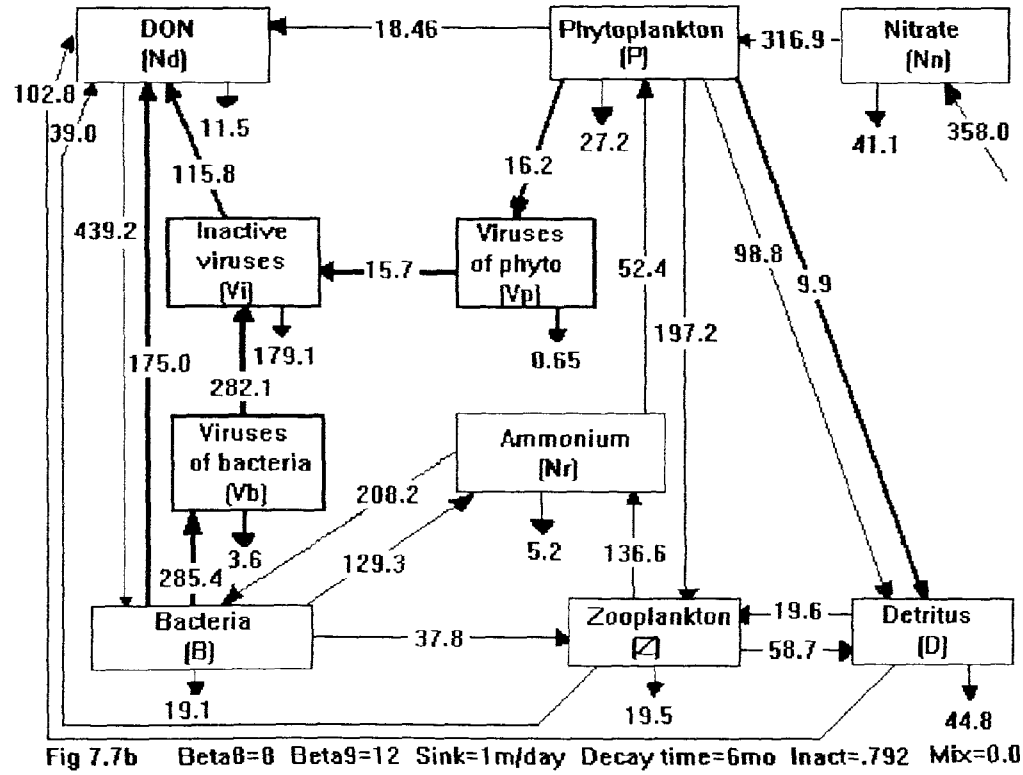

Fig 7.7b Beta8=8 Beta9=12 Sink=1m/day Decay time=6mo Inact=.792 Mix=0.01

Figure 7.7 Annual intercompartment flows of nitrogen for (a) Beta8=8.0, Beta9=8.0 (b) Beta8=8.0, Beta9=12.0 (c) Beta8V=8.3, Beta9V=19.0, with a decay time of **one** and **six months** and **fifty years** respectively.

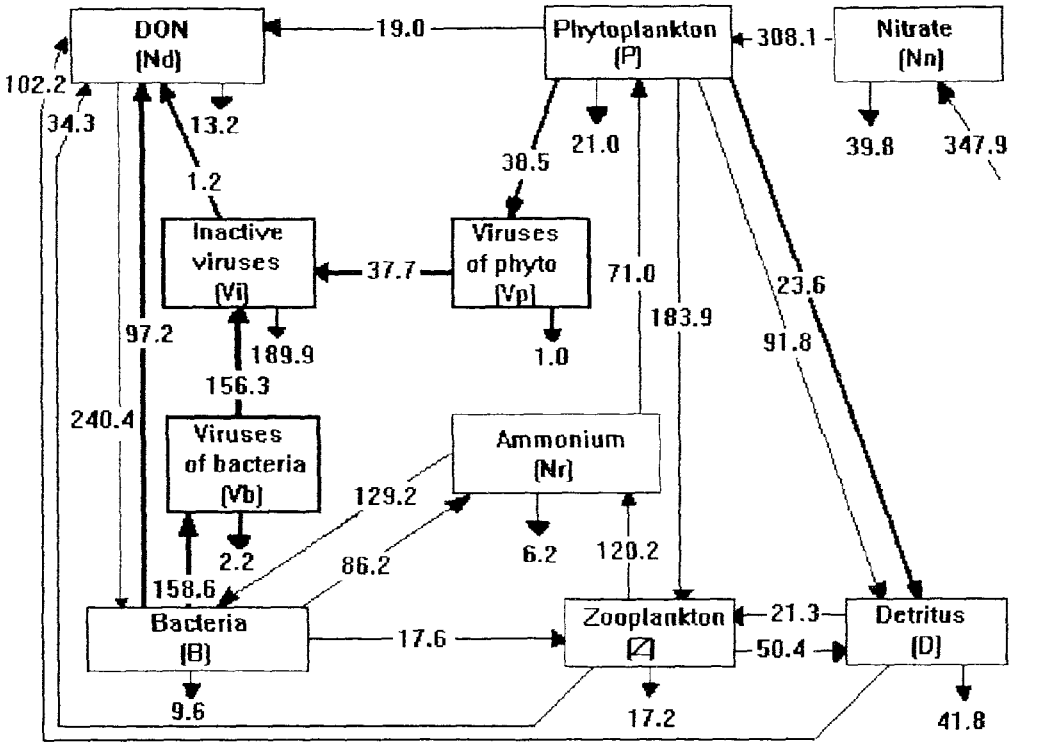

Fig. 7.7 c Beta8V=8.3 Beta9V=19 Sink=1m/d Decay=50 years Inact=.792 Mix= 0.01

Figure 7.7.c - continued

Simulations with a sinking speed of detritus of 10m/day and an inactivation rate of viruses .792 d^{-1}

(a) beta8=9.0

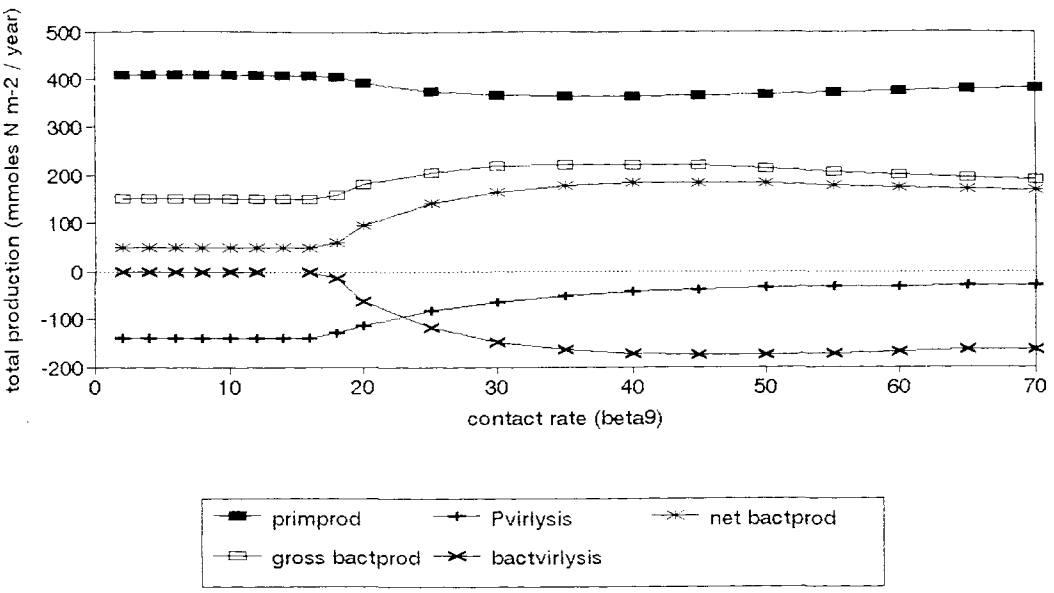

(b) beta8=8.3

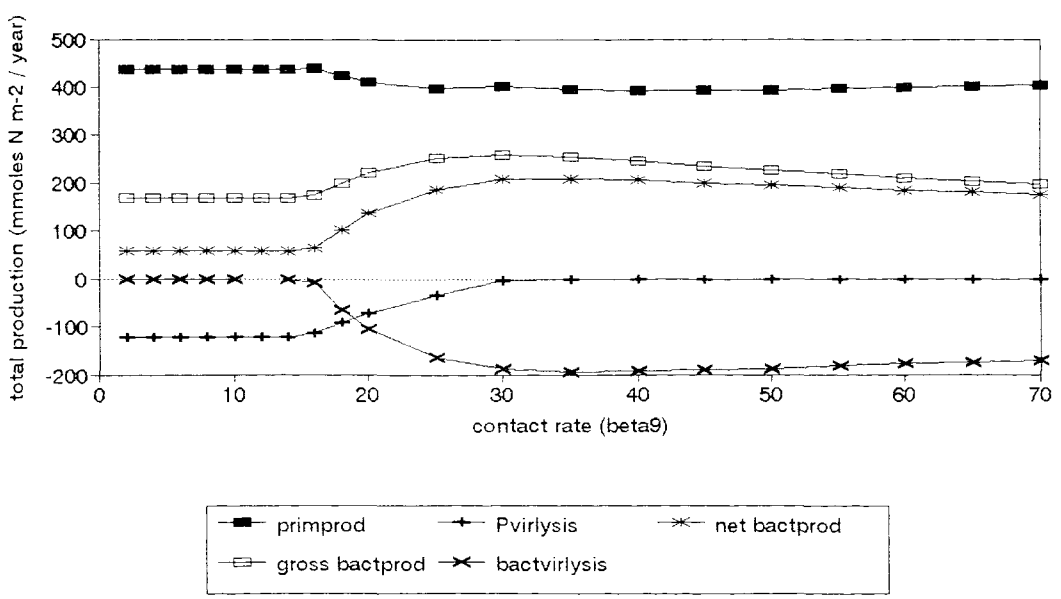

Figure 7.8 Variation in annual primary production (filled square), bacterial production (star) and corresponding losses by phytoplankton lysis (plus) and bacterial viral lysis (square) in mMol N/m^2/year, plotted against increasing levels of the contact rate (beta9) in simultaneous epidemics of phytoplankton and bacterial viruses for a **50 year** decay in inactivated viruses. The contact rate of phytoplankton viruses is fixed at (a) beta8=9.0 (b) beta8=8.3.

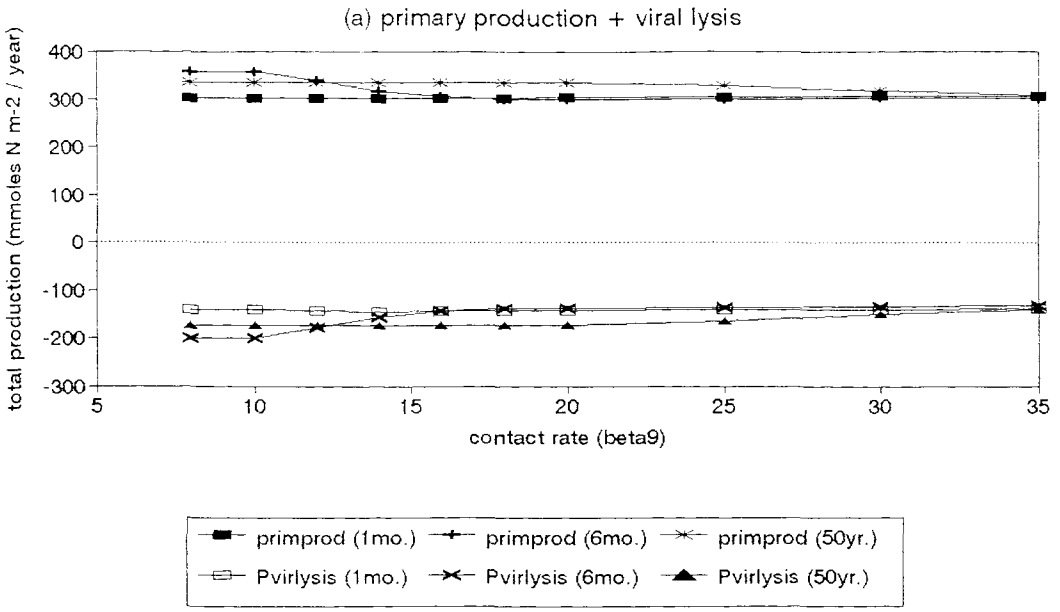

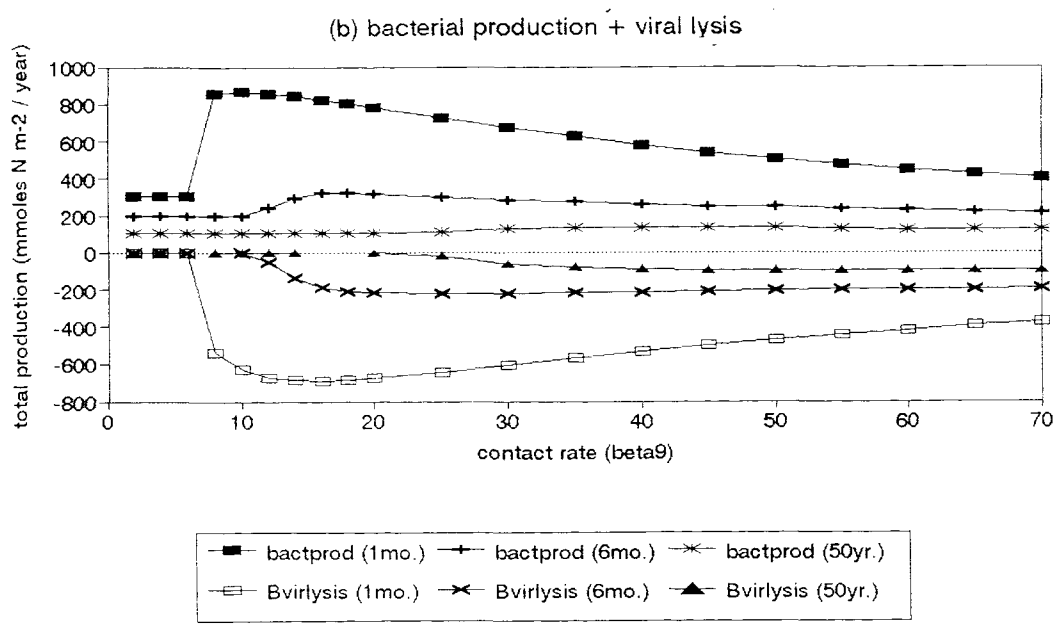

Figure 7.9 Annual production rates (in mMol N/m^2/year) and corresponding losses by viral lysis plotted against increasing levels of the contact rate (beta9) in simultaneous epidemics of phytoplankton and bacterial viruses for different levels of decay in inactivated viruses. Beta8 is fixed at 12.0 and Beta9 ranges from 0 to 35 or 70. Positive values represent productions for viral decays of 1 month (filled square), 6 months (plus) and 50 years (star). Negative values represent viral lysis for decays of **1 month** (square), **6 months** (cross) and **50 years** (triangle). (a) primary production and lysis of phytoplankton (b) gross bacterial production and lysis of bacteria.

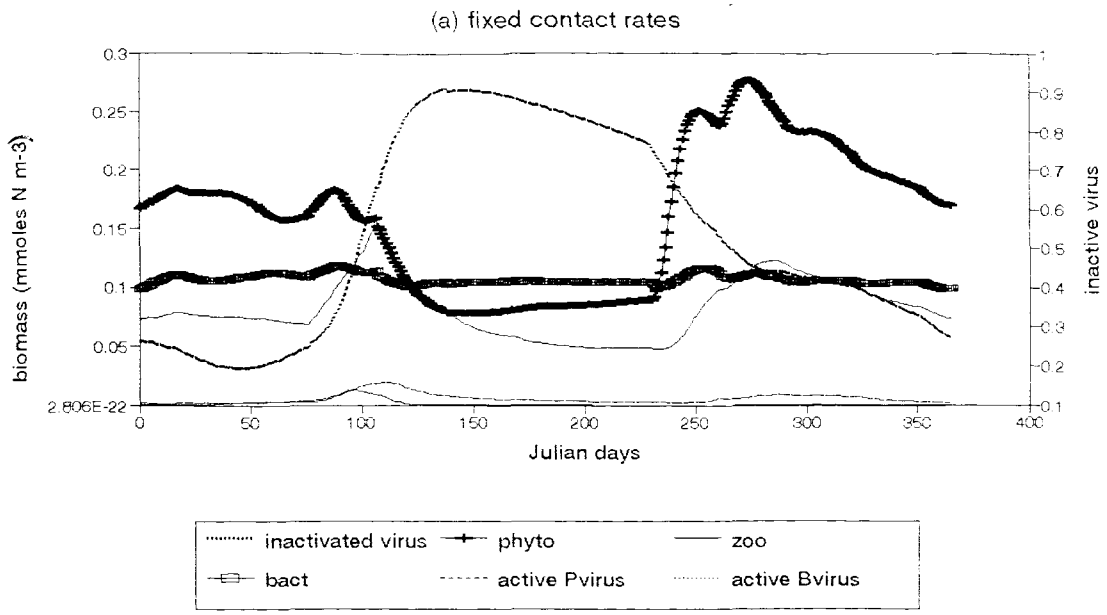

(b) variable contact rates

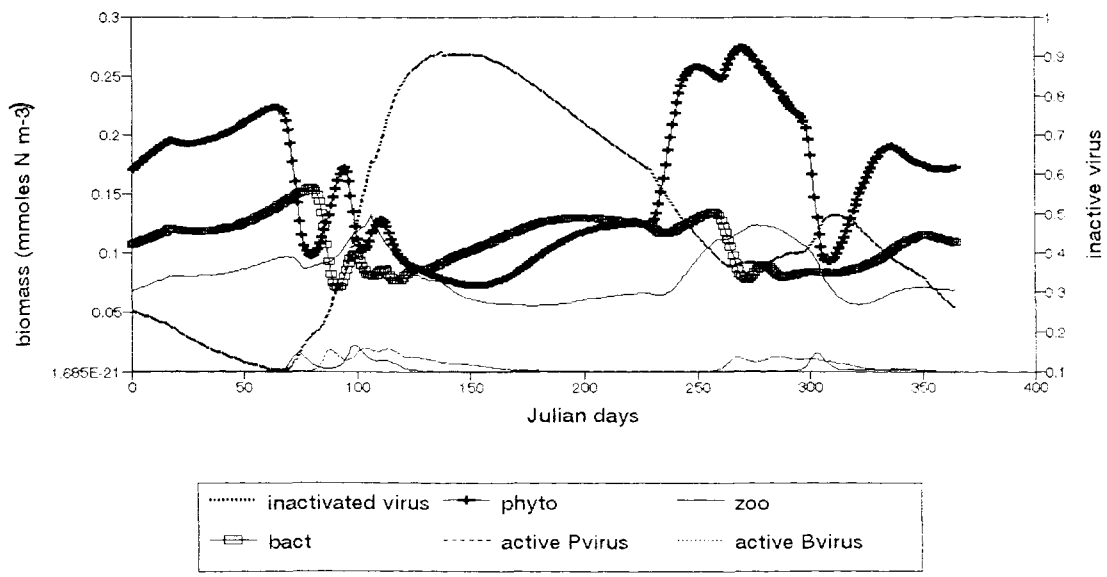

Figure 7.10 Annual cycles of phytoplankton (plus), bacteria (empty square), zooplankton (dashed), active viruses of phytoplankton (solid line) and bacteria (dotted) plus inactivated viruses (heavy dotted) concentration in a simultaneous epidemic for Beta8=8.0 and Beta9=12.0. The decay time of inactivated viruses is **six months**. (a) fixed contact rates (b) variable contact rates.

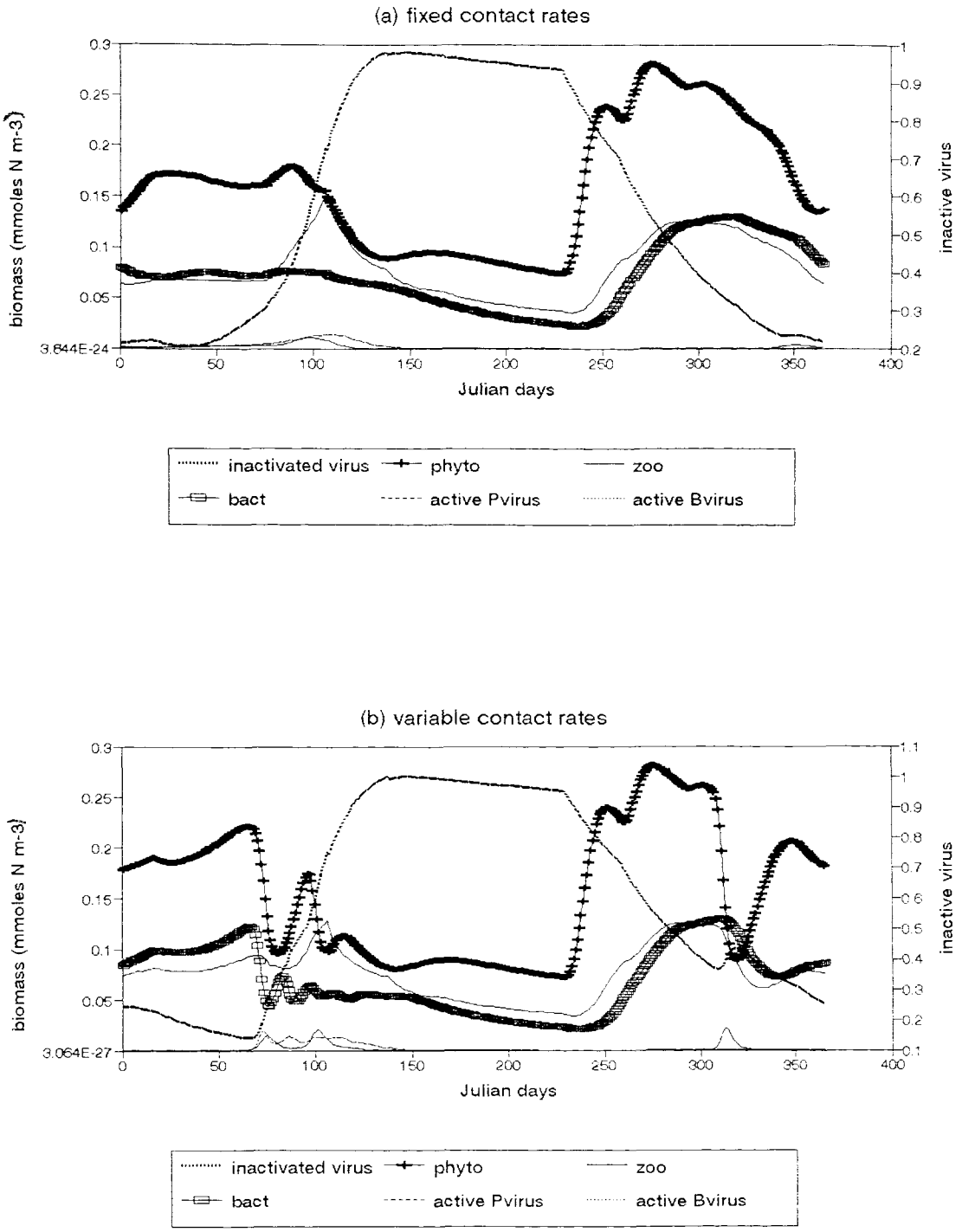

Figure 7.11 Annual cycles of phytoplankton (plus), bacteria (empty square), zooplankton (dashed), active viruses of phytoplankton (solid line) and bacteria (dotted) plus inactivated viruses (heavy dotted) concentration in a simultaneous epidemic for Beta8=8.0 and Beta9=18.0. The decay time of inactivated viruses is **fifty years**. (a) fixed contact rates (b) variable contact rates.

Chapter 8.

Discussion and Conclusions.

8.1 Introduction

This chapter summarises the results and the conclusions reached from this modelling investigation. The objectives of the project are reviewed in § 8.2. Section 8.3 presents a discussion of the results and the main conclusions. An evaluation of its limitations is presented in § 8.4. Possible directions for future work in this field are suggested in § 8.5.

8.2 Objectives of the investigation

The main aims for this modelling work were:

1. To determine theoretically and numerically whether there is a viral solution to the DOC enigma,
and
2. To investigate the dynamics of viral epidemics in a marine ecosystem and its repercussion in the biological production, as a way to understand the bloom collapses observed in the ocean.

The more specific goals of the project were to determine:

1.(a) the conditions under which the concentration of inactivated viruses may approach the 1.1 - 2.1 μMol N l^{-1} of the author's estimated DOC-class 6 concentration (Suzuki, 1988) for Bermuda surface waters based on the total DOC measurement in Michaels et al., 1994.

1.(b) the conditions under which the rate of viral lysis may yield the 2.2 Mol C m^{-2} $period^{-1}$ required to explain the imbalance between net export and measured loss of carbon in the upper 150m of Bermuda (Michaels et al., 1994).

1.(c) the conditions under which the annual rates of viral lysis may approach the 325 mMol N m^{-2} $year^{-1}$ (for a C/N ratio of 4) required by the subsurface consumption rate of Bacastow & Maier-Reimer (1991).

2.(a) the impact of viral epidemics on biological production.

2.(b) to investigate the host-prey dynamics in phytoplankton-virus and bacteria-virus systems.

These objectives have been met, within the limitations of the modelling approach.

In order to obtain numerical evidence to support the hypothesis that viruses are the answer to the DOC enigma an epidemics model based on Fasham et al. (1990) and Fasham (1993) ecosystem model of the upper ocean has been developed. Two new compartments have been added due to the host specific nature of the virus infection: viruses of phytoplankton and viruses of bacteria. A third new compartment of inactivated viruses was also added due to the natural processes of inactivation by ultra-violet radiation in the euphotic zone.

The epidemics model has been integrated over a ten year period and has been shown to produce annual cycles of phytoplankton and bacteria biomass that fit the observational data for Bermuda Station "S" in 1958-1960.

The equations governing the interaction of viruses with phytoplankton, bacteria, DON, each other and the mixed-layer have been presented in chapter 3.

Over two thousand simulations have been executed. The effect of differing levels of contact rate, inactivation rate, decay time of inactivated viruses and sinking speed of detritus on overall production rates and biomass were investigated. Chapter 5 dealt specifically with phytoplankton epidemics, while chapter 6 investigated bacterial epidemics

and chapter 7 studied joint simultaneous epidemics.

8.3 Discussion of results and conclusions

Marine ecosystems in the open ocean act as a "biological pump" transferring organic matter from the euphotic zone to the deep ocean at an estimated rate of 10 gigatons of carbon per year (Sarmiento, 1992). The organic matter created by the photosynthetic uptake of inorganic carbon and nutrients (new production) subsequently flows through the food web and finally leaves the upper layers moving into the oceanic interior. The relative rates of transfer of carbon and nutrients from sinking to nonsinking forms are of particular importance to the efficiency of this pump.

The scientific evidence presented in chapter two is that large horizontal and vertical gradients in DOC concentrations are present in the upper ocean and as pointed out by Toggweiler (1990, 1992) these can not survive the tendency of the circulation to reduce them unless large amounts of DOC production and remineralization are taking place. Though recent developments have scaled down the global size of the new pool (Suzuki, 1993) time-series measurements have detected large changes in DOC concentrations during the spring bloom in the North Atlantic which indicated that 20-40% of DOC can turn over in days (Kirchman et al., 1991 and Ducklow et al., 1993).

The natural processes that control the source and rate of production of DOC at this magnitude in the upper ocean, as well as its subsurface remineralization rate and lifetime, are not known but are required to explain the ocean's global distribution of nutrients.

A large imbalance between dissolved inorganic carbon (DIC) consumption, DOC production and the fallout of

particulate material measured by sediment traps in the upper 150m of Bermuda has been reported (Michaels et al., 1994).

The extremely high molecular weight of viruses (chapter 2, § 2.1) and their composition of DNA/RNA and protein make them very resistant to chemical oxidation and microbial degradation conferring them all the characteristics for a potentially long decay time.

By virtue of all these attributes and their minute dimensions that allow them to be considered as dissolved, a link between viruses and the semi-labile DOC was established by the author:

Viruses increase the residence time of C, N and P in the euphotic zone. While these biogenic elements are sequestered into the viral DNA and protein coat they remain in the upper ocean in the form of semi-refractory free-floating virus particles. This could explain why the bulk of the new pool of DOC is concentrated near the surface.

It would also explain why the carbon sequestered from primary producers is not detected in sediment traps.

The breakdown rate of marine viruses is not known. While conclusive data from laboratory experiments is not forthcoming one interim solution would be to take the estimate of 50 years for the breakdown of semi-labile DOC advanced by Bacastow & Maier-Reimer (1991) and Togweiller (1989). This was the lifetime required by global circulation models to explain the ocean's global distribution of nutrients.

Viral epidemics by specific lytic viruses in the phytoplankton and bacteria populations burst the infected cells releasing into the water new viruses the size of which (10-400nm) and burst size (20-200 phages) vary significantly across species.

The phages released in a single burst may be calculated to contain 1.5 to 3 times as much DNA (and therefore biomass) as a single bacterium, assuming the burst size to be 50 to 100 and the DNA content of individual bacteria and phages to be 2.6 and 0.08 fg respectively (Furhman & Azam, 1982, Borsheim et al.1990). Therefore the biomass of an infected bacterium is more than three times higher than that of a healthy bacterium.

The "soup" of cellular components in addition to viruses that is released into the water when the infected phytoplankton or bacteria cell bursts due to viral lysis (chapter 2, § 2.1) can be taken up immediately by other bacteria fuelling a DOC-bacteria loop (Bratbak et al., 1990; Fuhrman, 1992) which can potentially increase the bacterial production above the value for primary production (Table 6.7.b and Fig. 6.4). This hypothesis was tested in order to reconcile the high turnover rates of DOC measured by Kirchman et al. (1991) in the North Atlantic spring bloom which were due to an apparent fast consumption of DOC.

This project has studied the response of primary production and bacterial production in the upper ocean to lysis caused by epidemics of phytoplankton and bacterial viruses. The dynamics of the epidemic is driven by the contact rate between virus and host-cell $\beta 8$ (or $\beta 9$), attenuated by an efficiency rate of biomass conversion k8, and is controlled by a inactivation rate provided by natural Ultra-violet radiation $\mu 8$ (or $\mu 9$).

The project has concentrated on a range of contact rates between minimum and maximum epidemic. These were defined to be the minimum annual viral lysis required to sustain the virus at an endemic level in the population and the maximum annual viral lysis, respectively.

The attribution of contact rates for simultaneous epidemics on phytoplankton and bacteria is difficult because

they interact with each other and their interaction is driven by the availability of nitrogen.

However, the resources in nitrogen are limited and depend ultimately on the ability of the autotrophic component (phytoplankton) to synthesise organic nitrogen.

Seasonally varying contact rates do not change the annual rates of viral lysis but have an impact on the intensity (size) of the flows during blooms (Fig. 5.54) and also influence the concentration of the biomass during these events (Fig. 5.49 and Figs. 6.17 a,b & 6.18a).

Inactivation rates of 0, .1, .3, .5, .792 and 1 d^{-1} were explored in the model experiments (Tables 5.2, 5.3, 6.9 & 6.18). However, the reference value used throughout this study was .792 d^{-1} as the average inactivation rate of marine viruses by natural UV radiation was determined to be *ca.* .8 d^{-1} by Suttle & Chen (1992). Nonetheless, the rate of inactivation being dependent on solar radiation is bound to vary throughout the day and also from area to area according to latitude and cloud cover.

Increases in inactivation rate, discussed in detail in chapters 5, 6 and 7, resulted in lower or similar annual production rates but much higher maximum daily flow into lysis of bacteria during bloom events (Fig. 6.15). The slowdown in the build-up of viruses forced by the inactivation delays the collapse of the bloom and allows the concentration of the host population to continue to rise before a critical biomass of active viruses can be reached.

This model has explored a range of decay rates of inactivated virus from 0 to 1 d^{-1}, namely; no decay, slow decay, moderate, fast and instantaneous decay, corresponding to 0, 50 years, 10 years, 1 year, 6 months, 3 months, 1 month and 1 day, respectively (Tables 6.7 & 6.19).

However, it is not realistic to expect these decay times to be shorter than 1 month (see chapter 2). Recent works by Cowie & Hedges (1994), Keil & Kirchman (1993, 1994) and Heissenberger & Herndl (1994) reported the decay of high molecular weight proteins in water to take longer than six months. Evidence of intact viruses in large concentrations in very old sediments collected in the sea bottom by marine geologists and proteins identified in fossilized marine organisms (Collins et al., 1991, 1992) points to an even longer decay time. That is not surprising considering that DOM in ocean water is known to be over four thousand years old (Bauer et al., 1992; Williams & Druffel, 1988).

The peak concentration of inactivated viruses in joint epidemics (Fig. 7.4 & 7.5) ranged from 0.7 to 1.7 mMol N m^{-3} in May-June according to the level of contact rate, decay time and sinking speed of detritus. The 0.7 mMol N m^{-3} concentration is equivalent to the $1.13*10^{8}$ virus per ml average data on intact bacteriophages reported from ocean samples (Bergh et al.1989; Bratbak et al. 1990). The 1.7 mMol N m^{-3} peak concentration is equivalent to $2.75*10^{8}$ virus per ml. Both estimates of viral numbers are within the range of values obtained by the new method of epifluorescence microscopy (Hennes & Suttle, 1995) and also by estimates based on the seawater content of coated high molecular weight dissolved DNA (Maruyama et al. 1993). They are also within the range of estimates based on direct counting of viruses under the electron microscope (Proctor & Fuhrman, 1990). The number of viruses was estimated using a C/N ratio of 3.5 and 0.26 fg C per virus (Fuhrman, 1992).

The concentration of 1.7 mMol N m^{-3} in inactivated viruses nearly matches 1.8 mMol N m^{-3}, the class-6 fraction of semi-labile DOC estimated by the author for Bermuda station "S" (see chapter 2, § 2.3) based on HTCO measurements by Michaels et al. (1994). This value was obtained for simulations with a sinking rate of 1m/day and decay times of six months and fifty years for different levels of Beta8 and

Beta9 either in fixed or variable contact rates (see chapter 7, Figs. 7.5 a,b & 7.6.b).

The annual cycle of modelled inactivated viruses replicates well the timing and pattern of seasonal variation in total DOC concentration measured at the U.S. JGOFS Bermuda time-series station (Carlson et al. 1994) (Fig. 4.14) albeit with concentration values that are a fraction of those observed.

The timing and pattern of seasonal variation in the concentration of modelled inactivated virus agree with that of observations for other areas of the ocean which found a strong seasonal pattern on the annual cycle of virus with the highest concentrations in the summer and lowest in the winter (Jiang & Paul, 1994; Smith et al. 1992).

The peak concentration of inactivated viruses in the model should be considered only as the potential biomass in the absence of removal by marine snow (Kepkay, 1994). In coastal areas flocculation processes would remove most of the inactivated viruses to the bottom of the water column but in the open ocean that is less likely to occur due to the much lower concentration of organic matter. Furthermore most of those aggregates dissolve again in the upper 100m of the ocean which would release the viruses.

To estimate the total concentration of "dissolved" organic nitrogen at any one time one must add the concentration of active and inactivated virus to that of the base DON.

However the concentration of labile DON is ten times lower than that of inactivated viruses.

The peak value of labile DON concentration in minimum epidemics, 0.07 to 0.1 mMol N m^{-3} d^{-1} showed a threefold increase on the 0.023 mMol N m^{-3} d^{-1} value for Standard Run B.

The concentration of labile DON follows the pattern of the blooms of active virus for decay times longer than one month and follows the pattern of inactivated virus biomass in simulations for a decay time of one month.

The availability of nitrogen in the system sets a limit on the maximum value of joint viral lysis according to the decay time of inactivated viruses (see chapter 7, § 7.5).

Maximum joint viral lysis ranges from ca 1200 to 480 to 309 mMol N m^{-2} $year^{-1}$ for one month, six months and fifty years decay times simulations with a sinking speed of detritus 1m/day (Table 7.1b).

The joint viral lysis of bacteria and phytoplankton in minimum epidemics may contribute 159.8 - 650.1 mMol of nitrogen m^{-2} per year (table 7.3), corresponding to 559.3 - 2275.4 mMol carbon m^{-2} per year, to the DOC pool in Bermuda for decay times of fifty years and one month, respectively. A very conservative C/N ratio of 3.5, which is the value between DNA and proteins was used, as on average viruses are composed by 50% DNA and 50% protein. A value of 4 would still be an acceptable option and would yield even higher production rates. The above estimates for viral lysis would increase twofold in maximum epidemic and by up to 63% if a sinking speed of detritus of 1m/day was used instead.

The annual viral production in the one month decay simulation for minimum epidemic is enough to explain the 2.2 Mol C m^{-2} vanishing every year from Bermuda (Michaels et al., 1994). These are required to explain the imbalance between organic carbon exported out of the euphotic zone, measured by sediment traps, and the higher amounts expected from in situ production inferred from dissolved inorganic carbon consumption.

A short decay time of inactivated viruses of only one month may be supported by data on the turnover time of dissolved organic phosphorous (DOP), an element exclusive to

nucleic acids, that is reported to have a cycle of 22-49 days (Cho, 1990).

The author suggests that the reason why DOC measurements in Bermuda using HTCO machines (66 μMol l^{-1}) do not show an increase in the fraction of dissolved organic carbon and hence do not reflect the impact of viral production is due to the now common practice of using 0.2 μm filters to remove particulate material from DOC samples after the divulging of Suzuki's original work.

Although most viruses (20-200 nm) are still smaller than the pore size of the new generation of DOC filters 90% of them are retained in these filters (Paul et al, 1991). Notice that this material is not analyzed by chemists nor by biologists and is always discarded. Therefore the biomass of virus in these samples is not accounted for and is routinely ignored.

Annual rates of viral lysis of 308-318 mMol N m^{-2} $year^{-1}$ (Table 7.2) were obtained for simulations with a decay time of inactivated viruses of fifty years and a sinking speed of detritus of 1m/day. These productions were reached for fixed and variable contact rate simulations where Beta8 was set to minimum and Beta9 to intermediate and maximum epidemic. Therefore the model results on viral lysis match the magnitude and lifetime of the inputs of the yet unknown semi-labile DOC required by the subsurface consumption rate of Bacastow & Maier-Reimer's (1991) global circulation model.

The contribution of viral lysis to the carbon cycle is in two ways: the cell debris of lysed hosts (38% of the total) enter in the short term biogeochemical cycles while the viruses themselves (62% of the total) enter in the long term biogeochemical cycles. The relative scale of lysed debris turnover in the model (38%) is similar to that observed by Kirchman et al. (1991) and Chen & Wangersky (1993) for DOC turnover in the upper ocean (20-40% and 1/3 to 50%, respectively) and its relative decay time of 1 d^{-1} is

commensurate with the decay time of .1 to .5 d^{-1} measured for this labile pool (see chapter 1, § 1.1 and chapter 2, § 2.1).

The export of nitrogen into the oceanic interior by detrainment in the form of active and inactivated viruses, 193 mMol N m^{-2} $year^{-1}$, is four times larger than that transferred by sinking detritus particles, 42 mMol N m^{-2} $year^{-1}$ (see chapter 7 in § 7.5, Fig. 7.7 a,b,c and Table 7.4). This confirms the postulate of Toggweiler (1990) on the relative contribution of dissolved and particulate organic carbon to the biological pump.

The model results on viral production do not lend support to the viral source of the total "extra" DOC originally claimed by Suzuki.

Viral lysis of phytoplankton represents between 5-7% of annual net primary production in minimum epidemics but a much higher 150% for a short period during bloom events. In addition, viral lysis of bacteria represents 28-71% of the annual gross bacterial production and diverts twice the rate of the daily bacterial production at the height of the spring bloom.

These large short-term fluxes into lysis last for less than a week and would thus be easily missed by sampling cruises. The size of the largest flows (5-7 mMol N m^{-2} d^{-1} or 0.1 mMol C m^{-3} d^{-1} see table 7.4) is less than a tenth of what is needed to explain the 1.3 to 6.6 mMol C m^{-3} of daily oscillations of DOC for the North Atlantic (Ducklow et al., 1993). Furthermore they are also only a sixth of the size of oscillations in marine viruses measured in Norwegian waters (0.65 mMol C m^{-3} d^{-1} corresponding to $5*10^7$ virus per ml).

However, these results on viral production are valid only for the Bermuda station "S" area. They do not represent a top ceiling on viral production due to its dependency on primary production which itself is dependent on the nitrate

concentration at the start of the spring bloom, whose quantity is very latitude dependent. Therefore, the scale of virus production can be higher or lower than what was obtained for Bermuda and is bound to vary from one ocean province to another.

In this work the epidemics of phytoplankton viruses were given special attention because up to now the frequent observation of collapse of phytoplankton blooms have not been properly understood and explained. These very often occur in the absence of known limiting factors.

The model results suggest that the collapse of the spring bloom may be due to either direct predation by specific phytoplankton viruses or to a drop in regenerated production caused by a reduction of bacterial excretion of ammonium when bacteria are subjected to viral lysis.

Simulations for joint epidemics have shown that the contribution of bacteria to viral synthesis is several times larger than that of phytoplankton.

Epidemics of bacterial viruses exert their control role by forcing the bacteria biomass to either collapse at bloom events or to keep at a nearly constant level throughout the year, depending on contact rate levels and decay times.

It was shown that the increase in contact rate stimulates a growth in gross and net bacterial production and viral lysis and a decline of ammonium excretion which in turn induces a decrease of primary production.

Furthermore bacterial production rates and hence viral lysis increase drastically for slower sinking speeds of detritus and for shorter decay times of inactivated viruses.

The larger availability of nitrogen for bacteria consumption in one month decay simulations stabilizes the bacteria biomass at a constant level throughout the year. However for decay times longer than one month a surge of bacteria biomass followed by a collapse occurs at the spring bloom for low levels of the contact rate.

Nonetheless peak rates of bacterial growth of *ca.* .6 to .8 d^{-1} (Fig. 6.24) occurred at the end of the spring bloom for all levels of decay time and contact rate as a result of faster cycling of nitrogen due to increased virus pressure which intensified the direct flow into DON of lysed cell debris. The immediate availability of nitrogen drives the ensuing DON-bacteria-phage loop which enhances all bacteria related processes during the event.

The peak bacterial growth rates obtained with the model are four to six times higher than that of Control Run B for the same event (Fig. 6.24). Nonetheless they are within the range obtained with the radiolabeling techniques of thymidine and leucine incorporation. Heissenberger & Herndl (1994) reported bacterial growth rates of 1.18 d^{-1} for grazed cultures and 0.67 d^{-1} for ungrazed cultures. Therefore one suggests that viral pressure is the analoge of grazing by flagellates which was shown by Heissenberger & Herndl to keep the bacterial community in a more juvenile, active stage with higher growth rates.

Reiterating, epidemics of bacteria are characterised by a large increase in bacterial production and viral lysis for increasing contact rates which suggest that ocean samples where high bacterial productions are measured are undergoing intense viral lysis.

Bacteria become net consumers of ammonium under viral epidemics as the increase in DON and ammonium uptake is accompanied by a significant decline in ammonium excretion, due to the diversion of nitrogen into the synthesis of new

viruses (Fig. 6.2 and Tables 6.6 a,b,c, Tables 6.12b & 6.13b see also chapter 6, § 6.2 and § 6.3.1).

Furthermore the model results have shown that the C/N ratio of 4 in bacteria cannot be maintained at all levels of epidemics due to an asymmetry in the uptake of DON and ammonium as the contact rate increases (see chapter 6, § 6.4).

The two results above are relevant to the discussion of the most appropriate measurement of bacterial productivity being the net or gross bacterial uptake of nitrogen (Bronk et al., 1994).

As yet it is difficult to actually measure changes in the uptake pattern of bacteria. However more accurate information on the rates of ammonium and DON production and uptake by both bacteria and phytoplankton will be available with the advent of new techniques for their measurement (Bronk et al., 1994).

The primary production does not benefit from the increase in bacterial activity because most of the nitrogen diverted from the DON-bacteria loop is lost to the synthesis of new viruses. Furthermore regenerated production declines due to a decreasing excretion of ammonium by zooplankton which reinforces the viral induced decline in bacterial ammonium.

Although primary production declines under joint viral epidemics to values below those estimated by Fasham et al. (1990) for Bermuda Station "S" and yielded by control run B (578 mMol N m^{-2} $year^{-1}$) they are still reasonable considering that the range of values measured by the BATS programme of the JGOFS Time Series at this site can vary nearly twofold between years (109 - 172 g C/m^2/year). Significant interannual variability in the depth of the winter mixed layers, spring surface nitrate concentrations and the

magnitude of the spring bloom and consequently primary production were found at this station (Michaels, 1994 and Michaels et al., 1994).

The major controlling factor on the simulated biomass of active viruses was inactivation by natural ultra-violet radiation which caused an estimated 98% of total annual losses (Table 7.3) while detrainment came second with only 2%. Nonetheless the losses to inactivation are probably overestimated by the model during the winter deepening of the mixed-layer. The reason being that the penetration of ultra-violet radiation decreases exponentially with depth whereas the inactivation parameter in the model is a constant calculated originally for the upper 30 metres of the open ocean.

It was shown in chapter 5, § 5.14 that the reason why in minimum epidemic zooplankton controls the first part of the phytoplankton blooms and the viruses the second part is due to the delay in the build-up of active viral biomass which has to increase by several orders of magnitude to $2.8*10^6$ virus particles per ml from their very depressed pre-bloom levels of just one virus per every $20m^3$.

The peak concentration of active viruses is reached during the decay phase of blooms and their bottom concentration is reached before the onset of the autumn bloom. Active viruses are below the detection limit of electron microscopy which is 10^4 virus/ml, for most of the annual cycle.

The amplitude of the oscillation in active phytoplankton and bacterial viruses concentration increases for variable contact rates, longer decay times and low values of the contact rate and is negligible for larger contact rates.

A high infectivity on viruses allows for their critical biomass to be sustained all year long at high levels enabling

viruses to respond more quickly to changes in the dynamics of their hosts. The more closely coupled relationship with the host population lessens the impact of mixed-layer dynamics and UV inactivation on the simulated oscillation of virus concentration.

Interannual variability in the size and timing of spring bloom collapses in both the bacteria and phytoplankton populations was found to be dependent on small oscillations in the overwinter concentration of active viruses of bacteria (Tables 6.10 and 6.11, see chapter 6, § 6.5).

A delay in the build-up of active virus biomass due to their lower initial concentration allows bacterial biomass to reach higher levels (Fig. 6.11) and excrete more ammonium which fuels regenerated production thus extending the life of the phytoplankton bloom for up to 3 days.

It is suggested that the above processes can be triggered by changes in mixed layer depth driven by occasional storms which dilute the concentration of viruses.

Another ecological implication of viral lysis is that the large number of viral particles produced during the spring bloom which the model estimates put at twice to four times the size of phytoplankton biomass will curtail the penetration of light in the mixed layer.

A large number of viral particles will affect the diffraction of light which is most important at the sub-micrometer scale and is repercuted in changes in the photosynthetic available radiation (PAR) for phytoplankton.

This is of special relevance to remote sensing estimates of primary production where the impact of sub-micrometer particles of the size of bacteria (0.30 to 0.55 μm in diameter; Fuhrman, 1981; Sieracki et. al., 1985) have been estimated to account for 80% of the diffraction of light (Trevor Platt, personal communication in 1993).

Host-prey dynamics of phytoplankton (Fig. 5.4b and 5.40 b,c,d), bacteria (Fig. 6.23 a,a1,b,b1) and viruses are

driven by oscillations in the concentration of active viruses and their hosts in a typical predator-prey pattern, emphasized by changes in mixed-layer depth and by seasonal variation of the contact rate (Fig. 6.20).

Low concentration of viruses enable phytoplankton and bacteria biomass growth which result in the build-up of virus biomass with consequent collapse of the bacteria and phytoplankton blooms. A decline in virus concentration due to the lack of hosts lowers the pressure on bacteria and phytoplankton which bloom again.

The concentration of viruses declines also due to dilution when the mixed layer deepens and their infectivity lessens due to a downturn in the contact rate.

Bacteria and phytoplankton increase when the pressure of viruses is low or decreases, and when nitrogen is available due to short decay time of inactivated viruses. Phytoplankton and bacteria collapses result from enhanced infectivity of viruses due to the increase of contact rate, pressure of virus concentration and low availability of nitrogen.

Thus, this project has successfully studied the impact of viral epidemics on ecosystem dynamics and their contribution to the production of dissolved organic matter in the upper ocean. A much improved fit to the observations of phytoplankton and bacteria biomass for Bermuda Station "S" was obtained with this model for the joint epidemics of bacteriophage and phytoplankton viruses.

Nonetheless the fit should not be overemphasized as the phytoplankton biomass of observations is estimated from chlorophyll concentrations and thus is not an accurate representation of the actual phytoplankton biomass. Furthermore there are other model changes (zooplankton grazing, variable carbon/chlorophyll ratios) that can also give better fit (Fasham 1995, personal communication). Fasham has also produced a better fit using the FDM model and

optimising it to the data. However see comments in Sarmiento (1992).

The original aims, given in § 8.2 above, have been addressed within the limitations of a numerical modelling approach. The main conclusions of this work can be summarized as follows:

1 - This project has shown that marine viruses with their dynamics and peculiar biogeochemistry can explain two apparently conflicting aspects of the ocean's pool of DOC: the fraction that turns over rapidly in hours to days, which was detected by HTCO machines, and the other fraction that is remineralized very slowly in timescales of months to years that contributes to the bulk of DOC in the upper ocean. The author suggested the former to be lysed bacterial and phytoplankton cell debris and the latter to be inactivated viruses.

2 - The model results on DON/DOC production suggest that viruses are possibly also the main contributor to the pool of dissolved organic phosphorous (DOP) in the open ocean as the latter is mainly composed of dissolved nucleic acids (DNA/RNA) and 5'-nucleotides (ATP) (Cho, 1990).

3 - The role of marine viruses in the regulation of the size and timing of phytoplankton and bacteria blooms and their collapses has been determined. Their impact on overall production rates has been assessed and the importance of their partnership in bacterial trophodynamics demonstrated:

(a) - Viral epidemics are controlled by contact rates, inactivation rate, decay time of inactivated viruses and sinking speed of detritus.

(b) - In general the timing for the onset of blooms is unchanged by viral epidemics but their termination is hastened by viruses in the form of collapses. Therefore the

time span of the bloom and its magnitude are lower than that for control run B. However under certain conditions the bacterial biomass is kept constant throughout the year.

(c) - Variable contact rates increase the amplitude of biomass oscillation on active viruses, increase the size of flows into viral lysis, forces a more abrupt collapse of phytoplankton and bacteria blooms which give rise to secondary blooms.

(d) - Primary production and regenerated production decline for any level of viral epidemic.

(e) - Viral lysis enhance bacterial production through a partnership of viruses and bacteria in microbial trophodynamics.

(f) - Bacteria becomes the most important compartment in the ecosystem model in terms of nitrogen cycling, even surpassing phytoplankton, when the decay time of inactivated viruses is short. However bacterial production does not exceed primary production neither in minimum nor maximum epidemics when the decay time of inactivated viruses is longer than three months.

Finally, one has to conclude that the now unveiling relationships between viruses and their ecosystem with their far-reaching possible implications for biogeochemical cycles is a theme that is becoming ever more interesting!

8.4 Limitations of the study

8.4.1 Limitations of the biological model

Fasham et al. (1990) and Fasham (1993) discuss the difficulties faced in the adequate parameterisation of the ecosystem model, which are mainly due to the lack of

understanding of fundamental biological processes and limit the ability of the model to accurately predict planktonic interactions in the upper ocean.

The DON released by phytoplankton in this model is assumed to be a constant 5%. However, recent studies in the ocean found that 75% of nitrate uptake by phytoplankton is excreted in the early part of blooms as DON and then reabsorbed when the nitrate is exhausted (Bronk et al., 1994; Collos, 1992). This can be thought of as extracellular storage of organic nitrogen (see chapter 3, § 3.4.3). Bacteria will compete with phytoplankton for the utilisation of this DON.

The new methods that have been developed to isolate DON (Bronk & Glibert, 1991, 1993) enable its release and uptake rates to be quantified (see chapter 3, § 3.4.9). Therefore it is the author's opinion that a new formulation for nitrogen uptake incorporating DON feedback into the phytoplankton compartment ought to be included in future ecosystem models.

8.4.2 Limitations of the epidemic model

There are no datasets available in the U.S. JGOFS Bermuda Atlantic Time-series Study (BATS) to check if the variations in the seasonal cycle of modelled viruses are accurate.

The viral epidemic was modelled on the assumption that marine viruses are lytic. This assumption was based on the results of 20 years of research at Cold Spring Harbour, Massachusetts, USA, by the biomedical community who found that the nature of the majority of marine viruses is lytic (Cairns et al., 1992). However the present marine biology community seems to be unaware of this past body work of research by the biomedical community and until recently suggested by extrapolation that marine viruses are lysogenic or temperate at the image of freshwater viruses 90% of which

are temperate. Nonetheless Wilcox & Fuhrman (1994) have shown that the mechanism of virus production in seawater is lytic rather than lysogenic.

Temperate viruses present as prophages in bacteria can only be inducted by chance contact with UV radiation or collision with another particle and should therefore be modelled differently.

It is well known that viruses are host specific ie. that one type of virus will attack solely one host species but not infect a different species. Therefore, it may be argued that because Fasham's model lumps together diverse species into a single phytoplankton compartment the results on viral production would be flawed. The reasoning is that in the real world no species would bloom twice, once in Spring and again in the Autumn, as there is a succession of plankton blooms each of them by a different species and with a much shorter duration than allowed for in Fasham's model. Consequently, the build-up of phytoplankton or bacteria specific viral biomass would be much smaller than in the present model and the newly produced viruses would not be able to infect the next incoming bloom. Furthermore, the majority would probably have been removed by the time the right host bloomed again. However, the quantitative bacterial species composition and diversity are presently unknown which precludes a more detailed model description of the specificity of virus/host interactions driving the epidemics.

Nevertheless, one must state that the basic dynamics of the epidemic are correct since lytic infection is dependent on encounter frequency and determined by the product of virus and host (bacteria or phytoplankton) concentration. Moreover, flow results show that the inactivation rate imposed on viruses drastically limits the number of active viruses in the system for most contact rates not allowing them to reach a threshold which would make the autumn bloom collapse. The latter event coincides with the deepening of the mixed-layer

which dilutes the virus concentration further. Thus, the autumn bloom does not contribute to a large build-up of viral biomass. In terms of viral contribution to the DOC that remarkable aspect may balance any potential overestimate from the spring bloom.

The validation of the contact rates suggested by the model is a sensitive task to accomplish as these were obtained by iteration. The contact rate was assumed to be the fraction of the population that became infected by viruses. This value, which was small in the early versions of the model, had to be increased by a factor of 100 after the introduction of the .8 d^{-1} inactivation rate in order to sustain minimum epidemics.

The theoretical contact rate for bacteria estimated by Murray & Jackson (1992) is 9.1 x 10^{-5} s^{-1} or nearly 8 d^{-1} which is within the range of values used throughout this work for minimum to medium epidemics. That limit on contact rate value can also encompass maximum epidemics if lower values for the inactivation rate are used.

8.4.3 Possible critics to the epidemic model

For those who have still doubts on the applicability of a viral epidemics which is intrinsically host specific to a model where phytoplankton and bacteria are represented by an amalgamation of species into one single compartment the author would like to make a remark. Viral lysis is a density dependant process therefore it would be easy to include in Fasham's original model a density dependant mortality to phytoplankton and bacteria that would account for viral mortality. Fasham's model B already has such a formulation for phytoplankton mortality though not for bacteria.

Then it would be a question of including a compartment for semi-labile DON with inputs from the bacteria and phytoplankton compartments reflecting the flow of high-molecular weight particles (viruses) that are not readily

taken up by bacteria. This compartment of semi-labile DON would have an output to the compartment of labile DON with a given decay time of one, three, six months or longer according to what laboratory experiments may in the future determine.

An additional link would be needed between the bacteria and labile DON compartments reflecting the direct flow of small-molecular weight particles released from the host cell during lysis and which are readily taken up by other bacteria. The material released by cell lysis of phytoplankton is slightly more difficult to assign. If the phytoplankton is composed of small size species like picoplankton then the flow of lysed material apart from the viruses themselves should go into labile DON. Otherwise, if the phytoplankton is composed of diatoms then the flow of lysed materials should go into detritus.

A flow network of this nature is for all purposes almost identical to the one used in the present model and would probably display the same behaviour as well as conduce to similar results.

8.5 Future directions

This project has provided a significant and up-to-date contribution to the undergoing investigation on the role of marine ecosystems in the less known aspects of carbon cycling.

Future work should include a white noise random variation in the average contact rate (see chapter 3, § 3.2) as demonstrated by Rand & Wilson (1991). The variable contact rate used in the model implements solely a seasonal component and is thus incomplete in face of recent developments in the field of epidemiology.

To incorporate viruses into models of global biogeochemical cycles it is vital that research be conducted on viral decay times into labile DON and processes controlling it. The model proved extremely sensitive to the values of this parameter which had a large impact on bacterial production and viral lysis.

An explicit model for the detritus compartment, involving the formation of algal flocs by physical coagulation processes and their subsequent sinking, should be developed in view of the high sensitivity of the epidemic model to changes in the sinking speed of detritus.

Future studies should determine the role of viruses on the succession of "monospecific" plankton blooms. Thus, there is a need to divide the phytoplankton population in 2 or 3 sub-compartments based on differences of size, growth rate and contribution to the sinking flux. The author would suggest picoplankton, nanoflagellates and diatoms.

A DON feedback loop into the phytoplankton compartment should be included in future versions of the model.

In this era of concern over the global change there is a pressing need for models able to predict with consistency simulations of annual carbon cycles. Therefore, it would be worth including a carbon cycle into this model.

8.5.1 Proposed experiment to test the resistance of viral capsids to breakdown by the UV method of DOC measurement

The following experiment could not be completed due to mechanical failure of two 20 year old UV machines.

A seawater sample is concentrated by differential ultra-centrifugation at 250,000 g to isolate and increase the

number of viruses for the experiment.

By means of negative-staining electron microscopy a viral counting is performed on the concentrate before and after the DOC experiment.

For the DOC measurement, two aliquots of the concentrate are used to run two independent DOC machines simultaneously: one using the UV method (conventional DOC measurement) and another using Suzuki's technique.

Then, the residual liquid of the DOC machines (UV and Suzuki's) are examined in the electron microscope and compared.

If the residual liquid of Suzuki's machine contains no virus but the UV machine's residual liquid still has them, then my hypothesis is correct, meaning that viruses are indeed contributing to the "new" DOC signal. Whether they can account for the total DOC in class 6 or even for a substantial part of the excess DOC measured by Suzuki in the other molecular weight classes depends on whether there is enough viral component in this particular sample as well as in the ocean itself (see 2.1.4 and 2.2.5).

However, it is extremely important that these analysis be performed on fresh samples because viruses are extremely efficient at sticking onto other particles and therefore will attach to the walls of the sample bottle very quickly. I faced this problem after the processing of my virus samples by ultracentrifugation. When it took me more than 24 hours to analyse by electron microscopy the fresh concentrate of viruses I would not find any virus as they would diffuse through the water into the periphery and adsorb irreversibly to the walls of the centrifuge tube. Sorptive losses of DOM to container walls is recognised as a thorny problem especially in acidified and freshwater samples (Hedges & Farrington, 1993).

APPENDIX A.
Model Parameters and Initial Conditions.

Table 1. Model Parameters

This table gives the values assigned to the parameters used in the model equations for the standard run. The choice of these values is discussed in Fasham et al. (1990).

Parameter	Symbol	Value
PAR/Total irradiance	-	0.41
Cloudiness	-	4 Oktas
Light attenuation due to water	k_w	0.04 m^{-1}
Cross-thermocline mixing rate	m	0.01 m d^{-1}
Sub-mixed layer concentration of nitrate	N_0	2 mMol N m^{-3}
Phytoplankton maximum growth rate (Bermuda)	V_p	2.9 d^{-1}
Initial slope of P-I curve	α	0.025 (W m^{-2})$^{-1}d^{-1}$
Light attenuation by phytoplankton	k_c	0.03 m^2 (mMol N)$^{-1}$
Half-saturation constant for nitrate uptake	k_1	0.5 mMol m^{-3}
Half-saturation constant for ammonium uptake	k_2	0.5 mMol m^{-3}
Phytoplankton maximum specific mortality rate	$\mu 1$	0.05 d^{-1}
Phytoplankton half-saturation constant for mortality	k_5	0.2 mMol m^{-3}

Phytoplankton DON exudation fraction	γ	5%
Ammonium inhibition parameter to nitrate uptake	ψ	1.5 (mMol N m^{-3})$^{-1}$
Zooplankton maximum growth rate	g	1.0 d^{-1}
Zooplankton half-saturation constant for ingestion	k_3	1.0 mMol m^{-3}
Zooplankton assimilation efficiency	$\beta1, \beta2, \beta3$	75%
Zooplankton maximum loss rate	$\mu2$	0.3 d^{-1}
Zooplankton half-saturation constant for the loss rate	k_6	0.2 mMol m^{-3}
Fraction of zooplankton losses going to DON	δ	20%
Fraction of zooplankton losses going to ammonium	ϵ	70%
Zooplankton feeding preferences	p1,p2,p3	0.5,0.25,0.25
Bacterial maximum uptake rate	V^b	2.0 d^{-1}
Bacterial excretion rate	$\mu3$	0.05 d^{-1}
Bacterial half-saturation constant for uptake	k_4	0.5 mMol m^{-3}
Ammonium/DON uptake ratio for bacteria	η	0.6
Detrital sinking rate	V	10 m d^{-1}
Detrital breakdown rate	$\mu4$	0.05 d^{-1}

Virus contact rate (phytoplankton)	β_8	as a function of b_0 and b_1
Virus contact rate (bacteria)	β_9	as a function of b_0 and b_1
Average contact rate	b_0	0-16 d^{-1}
Seasonal component of contact rate	b_1	0 or 30%
Phase synchronization of the variable contact rate	t_0	16 (phyto) 35 (bacteria)
Virus assimilation efficiency	k_8	62%
Virus inactivation rate	$\mu 8, \mu 9$	50%-100% d^{-1}
Decay rate of inactive viruses into DON	$\mu 10$	0.0328767 d^{-1} 0.0109589 d^{-1} 0.0054794 d^{-1} 0.0027397 d^{-1} 0.0002739 d^{-1} 0.0000547 d^{-1}
Detrital fraction of phytoplankton viral lysis	k_7	38%
DON fraction of bacterial viral lysis	k_9	38%

Table 2. Initial values.

This table gives a summary of the initial values used in the ecosystem model for Bermuda Station "S". These values were taken from version 1 of control run A after it had been run to equilibrium.

Parameter	Symbol	Value
Mixed Layer Depth	h	103 m
Phytoplankton	P	0.2520 mMol N/m^3
Zooplankton	Z	0.0197 mMol N/m^3
Bacteria	B	0.1193 mMol N/m^3
Virus of phytoplankton	Vi_p	0.1850 mMol N/m^3
Virus of bacteria	Vi_b	0.1850 mMol N/m^3
Inactive viruses	I_{vir}	0.1850 mMol N/m^3
Labile Dissolved Organic Nitrogen	N_d	0.0105 mMol N/m^3
Ammonium	N_r	0.0759 mMol N/m^3
Nitrate	N_n	0.5186 mMol N/m^3
Detritus	D	0.0725 mMol N/m^3

APPENDIX B.

Julian Days and Corresponding Dates.

Table D1.

This table gives the Julian day and corresponding date for the 1st of each month for a five year period. The start day of the simulations presented in this work is Julian day 1.

Date	Julian day				
1st Jan.	1	366	731	1096	1461
1st Feb.	32	397	762	1127	1492
1st Mar.	60	425	790	1155	1520
1st Apr.	91	456	821	1186	1551
1st May	121	486	851	1216	1581
1st Jun.	152	517	882	1247	1612
1st Jul.	182	547	912	1277	1642
1st Aug.	213	578	943	1308	1673
1st Sep.	244	609	974	1339	1704
1st Oct.	274	639	1004	1369	1734
1st Nov.	305	670	1035	1400	1765
1st Dec.	335	700	1065	1430	1795

APPENDIX C.

Conversion of Viral Numbers into Viral Biomass.

The average DNA content of bacteriophages is about 0.08 fg of DNA per virus (standard deviation of 0.06; n=96 [data from Laskin & Lechevalier, 1978]).

The average reported number of virus particles at the height of the Spring bloom is 10^7 per ml (Bratbak, 1990; Paul et al., 1991).

The viral DNA is composed of 16.2% nitrogen and is about 50% of the particle's weight which is mostly composed of proteins (Laskin & Lechevalier, 1978).

To estimate the biomass of the viral population in the model currency (mMol N m3) the following formula was used:

$$x \text{ fento} * 10^{-15} \text{ g / amu} = \text{Mols}$$

Nitrogen has an atomic mass unit (amu) of 14. Thus 10^7 virus per ml will correspond to 1.85×10^{-2} mMols N m3.

This value is an underestimation of the total viral population because the samples are prefiltered through 0.2-μm filters to remove bacteria and other microorganisms for viral enumeration. Recently, it has been found that most of the viruses (an average of 60%, and often 90%) are retained on the 0.2-μm filters in the process of filtering water (Paul et al, 1991).

It seems that the interception of the viruses is dependant upon the amount of particulate matter available for viral adsorption. Thus, one would expect that the viral countings performed during a bloom event are underestimated by at least 90%, if not more.

Therefore, correcting for that factor will give an estimated concentration of $18.5 \pm 32.4 * 10^{-2}$ mMol N m^{-3} for the total viral population at the height of a spring bloom.

This value is comparable to that of the observational data for the total phytoplankton population in spring blooms at Bermuda Station "S", which is $10 \pm 45 * 10^{-2}$ mMol N m^{-3} (Fasham et al.,1990).

Even though, one must be aware that this value corresponds only to the easily identifiable virus phagues whose tails have not been damaged. When performing viral countings under the electron microscope most virus will be taken to be detrital particles and will consequently be dismissed.

REFERENCES.

Altabet, M. A. (1989). Particulate new nitrogen fluxes in the Sargasso Sea. Journal of Geophysical Research, 94: 12771-12779.

Alperin, M.J. & Martens, C.S. (1993). Dissolved organic carbon in marine pore waters: a comparison of three oxidation methods. Marine Chemistry, 41: 135-145.

Amon, R.M.W. & Benner, R. (1994). Rapid cycling of high-molecular-weight dissolved organic matter in the ocean. Nature, 369: 549-552.

Anderson, R. M. & May, R. M. (1979). Population biology of infectious diseases: part I. Nature 280: 361-367.

Anderson, R. M., May, R. M. & McLean, A. R. (1988). Possible demographic consequences of AIDS in developing countries. Nature 332: 228-234.

Anderson, R. M. (1991). The Kermack-Mckendrick Epidemic Threshold Theorem - Discussion. Bull. Math. Biol. 53: 3-32.

Anderson, T. R. (1992). Modelling the influence of food C:N ratio, and respiration on growth and nitrogen excretion in marine zooplankton and bacteria. J. Plankt. Res., 14: 1645-1671.

Atkinson, C.A. (1989). Progress in the development of the optimization of plankton ecosystem dynamics. Model for prediction of ocean light transmission. (manuscript).

Azam, F., Fenchel, T., Field, J.G., Gray, J.S., Meyer-Reil, L.A. & Thingstad, F. (1983). The ecological role of water-column microbes in the sea. Mar. Ecol. Prog. Ser., 10: 257-263.

Bacastow, R. & Maier-Reimer, E. (1991). Dissolved organic carbon in modeling oceanic new production. Global Geochemical

Cycles, 5: 71-85.

Bauer, J.E, Williams, P.M. & Druffel, E.R.M. (1992). ^{14}C activity of dissolved organic carbon fractions in the north-central Pacific and Sargasso Sea. Nature, 357: 667-670.

Benner, R. & Strom, M. (1993). A critical evaluation of the analytical blank associated with DOC measurements by high-temperature catalytic oxidation. Marine Chemistry 41: 153-160.

Bergh, O, Borsheim, K. Y., Bratbak, G. & Heldal, M. (1989). High abundance of viruses found in aquatic environments. Nature 340: 467-468.

Bird, D.F., Maranger, R. & Karl, D.M. (1993). Palmer LTER: Aquatic virus abundances near the Antarctic Peninsula. Antarctic Journal of the U.S., 28(5): 234-235.

Borsheim, K. Y, Bratbak, G. & Heldal, M. (1990). Enumeration and biomass estimation of planktonic bacteria and viruses by transmission electron microscopy. Appl. Environ. Microbiol. 56: 352-356.

Boehme, J., Frischer, M.E., Jiang, S.C., Kellogg, C.A., Pichard, S., Rose, J.B., Steinway, C. & Paul, J.H. (1993). Viruses, bacterioplankton, and phytoplankton in the southeastern Gulf of Mexico: distribution and contribution to oceanic DNA pools. Marine Ecology Progress Series, 97: 1-10.

Bratbak, G., Heldal, M., Nordland, S. & Thingstad, T. F.(1990). Viruses as partners in spring bloom microbial trophodynamics. Appl. Environ. Microbiol. 56: 1400-1405.

Bratbak, G., Egge, J.K. & Heldal, M. (1993). Viral mortality of the marine alga *Emiliania huxleyi* (Haptophyceae) and termination of algal blooms. Mar. Ecol. Prog. Ser. Vol. 93: 39-48.

Brian, P. & Morel, F.M.M. (1991). Amine oxidases of marine phytoplankton. Appl. Environ. Microbiol., Vol.57, 8: 2440-2443.

Bronk, D.A., Glibert, P.M. & Ward, B.B. (1994). Nitrogen uptake, dissolved organic nitrogen release, and new production. Science, 265: 1843-1846.

Butler, E.I., Knox, S. & Liddicoat, M.I. (1979). The relationship between inorganic and organic nutrients in sea water. J. mar. biol. Ass. U.K., 59: 239-250.

Cairns, J., Stent, G.S. & Watson, J.D. Editors (1992). Phage and the Origins of molecular biology. Expanded edition. Cold Spring Harbour Press. 366 pp. ISBN 0-87969-407-6

Cano, R.J. & Borucki, M.K. (1995). Revival and identification of bacterial spores 25-to-40-Million-Year-Old in Dominican Amber. Science, 268: 1060-1064.

Carlson, C.A., Ducklow, H.W. & Michaels, A.F. (1994). Annual flux of dissolved organic carbon from the euphotic zone in the northwestern Sargasso Sea. Nature, 371: 405-408.

Chen, W. & Wangersky, P.J. (1993). High-temperature combustion analysis of dissolved organic carbon produced in phytoplankton cultures. Mar. Chem., 41: 167-172.

Cho, B.C. (1990). Significance of dissolved nucleic acids in dissolved organic phosphorous (DOP) pool and their dynamics in oceanic phosphorous cycle. The Jounal of the Oceanological Society of Korea, 25, 3:145-150.

Cochlan, W.P., Wikner, J., Steward, G.F., Smith, D.C. & Azam, F. (1993). Spatial distribution of viruses, bacteria and chlorophyll *a* in neritic, oceanic and estuarine environments. Marine Ecology Progress Series, 92: 77-87.

Collins, M.J., Muyzer, G., Westbroek, P., Curry, G.B., Sandberg, P.A, Xu, S.J., Quinn, R. and MacKinnon, D. (1991). Preservation of fossil biopolymeric structures: conclusive immunological evidence. Geochim. Cosmochim. Acta, 55: 2253-2257.

Collins, M.J., Westbroek, Muyzer, G. & de Leeuw, J.W. (1992). Experimental evidence for condensation reactions between sugars and proteins in carbonate skeletons. Geochim. Cosmochim. Acta, 56: 1539-1544.

Collos, Y. (1992). Nitrogen budgets and dissolved organic matter cycling. Mar. Ecol. Prog. Ser., 90: 201-206.

Confer, D.R. & Logan, B.E. (1991). Increased bacterial uptake of macromolecular substrates with fluid schear. Appl. Environ. Microbiol., Vol.57, 11: 3093-3100.

Cottrell, M.T. & Suttle, C.A. (1995). Dynamics of a lytic virus infecting the photosynthetic marine picoflagellate Micromonas pusilla. Limnology and Oceanography, 40(4): 730-739.

Cowie, G.L. & Hedges, J.I. (1994). Biochemical indicators of diagenetic alteration in natural organic matter mixtures. Nature, 369: 304-307.

De Baar, H.J.W., Brussaard, C., Hegeman, J., Schijf, J. & Stoll, M.H.C. (1993). Sea-trials of three different methods for measuring non-volatile dissolved organic carbon in seawater during the JGOFS North Atlantic pilot study. Marine Chemistry, 41: 145-152.

Ducklow, H.W. & Fasham, M.J.R. (1992). Bacteria in the Greenhouse: Modelling the role of oceanic plankton in the global carbon cycle. *In* Environmental Microbiology (ed. Ralph Mitchell), Wiley-Liss, Inc, New York.

Ducklow, H.W., Kirchman, D.L., Quinby, H.L., Carlson, C.A. & Dam, H.G. (1993). Stocks and dynamics of bacterioplankton carbon during the spring bloom in the eastern North Atlantic Ocean. Deep-Sea Research II, Vol.40, 1/2: 245-263.

Dugdale, R. C. & Goering, J. J. (1967). Uptake of new and regenerated forms of nitrogen in primary productivity. Limnol. Oceanogr., 12: 196-206.

Ebenhoeh, W. (1988). Coexistence of an unlimited number of algal species in a model system. Theoretical Population Biology 34: 130-144.

Eppley, R.W. (1990). Nitrate use by plankton in the eastern subtropical North Atlantic, March-April 1989. Limnol. Oceanogr. 35(8): 1781-1787.

Evans, G.T. (1988). A framework for discussing seasonal succession and coexistence of phytoplankton species. Limnol. Oceanogr., 33: 1036-1037.

Evans, G.T. & Parslow, J.S. (1985). A model of annual plankton cycles. Biological Oceanography, Vol.3, 3: 327-345

Fasham, M.J.R. (1993). Modelling the oceanic biota. in The Global Carbon Cycle (ed. M. Heimann), Springer-Verlag.

Fasham, M.J.R. (1985). Flow analysis of materials in the marine euphotic zone, in Ecosystem Theory for Biological Oceanography, R.E. Ulanowicz and T. Platt, eds., Can. Bull. Fish. Aquat.Sci., 213, 139-162.

Fasham, M.J.R., Ducklow, H.W.& McKelvie, S.M. (1990). A nitrogen-based model of plankton dynamics in the oceanic mixed layer. Journal of Marine Research 48:591-639.

Fasham, M.J.R., Sarmiento, J.L., Slater, R.D., Ducklow, H.W., and Williams, R. (1993). Ecosystem behaviour at Bermuda

station "S" and Ocean Weather Station "India": A general circulation model and observational analysis. Global Biogeochemical Cycles, Vol.7, 2, 379-415.

Fenchel, T. (1988). Marine plankton food chains. Ann. Rev. Ecol. Syst., 19: 19-38.

Fischman, J. (1995). Evolutionary Biology. Have 25-Million-Year-Old bacteria returned to life?. Science, 268: 977.

Fitzwater, S.E. & Martin, J.H. (1993). Notes on the JGOFS North Atlantic Bloom Experiment - Dissolved organic carbon intercomparison. Marine Chemistry, 41: 179-185.

Frischer, M. (1993). Bacteria hold the key to genetic pollution. Journal of General Microbiology, Vol.139, p 753.

Frost, B. W. (1987). Grazing control of phytoplankton stock in the open subarctic Pacific Ocean: a model assessing the role of mesozooplankton, particularly the large calanoid copepods Neocalanus spp. Mar. Ecol. Prog. Ser., 39: 49-68.

Fuhrman, J. (1992). Bacterioplankton roles in cycling of organic matter: The microbial food web. in Primary Productivity and Biogeochemical Cycles in the Sea. (ed. P.G. Falkowski & A.D. Woodhead), Plenum Press, New York.

Fuhrman, J. (1981). Influence on method on the apparent size distribution of bacterioplankton cells: Epifluorescence microscopy compared to scanning electron microscopy. Marine Ecology Progress Series, 5: 103-106.

Fuhrman, J. & Suttle C.A. (1993). Viruses in marine planktonic systems. Oceanography, 6: 51-63.

Fujioka, R.S., Loh, P.C. & Lau, S.L. (1980). Survival of human enteroviruses in the Hawaiian ocean environment: evidence for virus inactivation by microorganisms. Applied

Environmental Microbiology, 39: 1105-1110.

Goldman, J.C. (1988). Spatial and temporal discontinuities of biological processes in pelagic surface waters. In: Toward a Theory on biological-Physical Interactions in the World Ocean, ed. B.J Rothschild, Kluwer Academic Publishers, pp 273-296.

González, J.M. & Suttle, C.A. (1993). Grazing by marine nanoflagellates on viruses and virus-sized particles: ingestion and digestion. Marine Ecology Prog. Ser., 94: 1-10.

Gowing, M.M. (1993). Large virus-like particles from vacuoles of phaeodarian radiolarians and from other marine samples. Marine Ecology Progress Series, 101: 33-43.

Hara, S., Terauchi, K. & Koike, I. (1991). Abundance of Viruses in marine waters: Assessment by epifluorescence and transmission electron microscopy. Applied and Environmental Microbiology, 57: 2731-2734.

Hedges, J. & Farrington, J. (1993). Measurement of dissolved organic carbon and nitrogen in natural waters: Workshop report. Marine Chemistry, 41: 5-10.

Hedges, J., Lee, C. & Wangersky, P.J. (1993). Comments from the editors on the Suzuki statement. Marine Chemistry, 41: 289-290.

Heissenberger, A. & Herndl, G. J. (1994). Formation of high molecular weight material by free-living marine bacteria. Mar. Ecol. Prog. Ser., 111: 129-135.

Heldal, M. & Bratbak, G. (1991). Production and decay of viruses in aquatic environments. Marine Ecology Progress Series, 72: 205-212.

Hennes, K.P. & Suttle, C.A. (1995). Direct counts of viruses in natural waters and laboratory cultures by epifluorescence microscopy. Limnology and Oceanography, 40(6): 1050-1055.

Hsu, Y.L., Engelking, H.M. & Leong, J.C. (1986). Occurrence of different types of infectious hematopoietic necrosis virus in fish. Applied and Environmental Microbiology, 52 (6): 1353-1361.

Jackson, G.A. (1988). Implication of high dissolved organic matter concentrations for organic properties and processes. Oceanography Magazine, 1(2): 28-33.

Jackson, G.A. (1990). A model of the formation of marine algal flocs by physical coagulation processes. Deep-sea Research Vol.37, 8: 1197-1211.

Jamart, B.M., Winter, D.F. & Banse, K. (1979). Sensitivity analysis of a mathematical model of phytoplankton growth and nutrient distribution in the Pacific Ocean off the northwestern U.S. coast. J. Plankton res., 1: 267-290.

Jiang, S.C. & Paul, J.H. (1994). Seasonal and diel abundance of viruses and occurrence of lysogeny/bacteriocinogeny in the marine environment. Marine Ecology Prog. Ser., 104: 163-172.

Johnson, B.D. & Kepkay, P.E. (1992). Colloid transport and bacterial utilization of oceanic DOC. Deep-Sea Research, Vol.39, No. 5: 855-869.

Jørgensen, N.O.G., Kroer, N., Coffin, R.B., Yang, X.H. & Lee, C. (1993). Dissolved free amino acids, combined amino acids, and DNA as sources of carbon and nitrogen to marine bacteria. Marine Ecology Progress Series, 98: 135-148.

Jumars, P.A., Penry, D.L., Baross, J.A., Perry, M.J., & Frost, B.W. (1989). Closing the microbial loop: dissolved carbon pathway to heterotrophic bacteria from incomplete

ingestion, digestion and absorption in animals. Deep-Sea Research, 36: 483-495.

Keil, R.G. & Kirchman, D.L. (1993). Dissolved combined amino acids in marine seawaters: chemical form and utilization by heterotrophic bacteria. Limnology and Oceanography, 38 (6): 1256-1270.

Keil, R.G. & Kirchman, D.L. (1994). Abiotic transformation of labile protein to refractory protein in sea water. Marine Chemistry, 45: 187-196.

Kellogg, C.A., Rose, J.B., Jiang, S.C., Thurmond, J.M. & Paul, J.H. (1995). Genetic diversity of related vibriophages isolated from marine environments around Florida and Hawaii, USA. Marine Ecology Progress Series, 120: 89-98.

Kepkay, P.E. (1994). Particle aggregation and the biological reactivity of colloids. Marine Ecology Progress Series, 109: 293-304.

Kermack, W. O. & Mckendrick, A. G. (1927). Contributions to the mathematical theory of epidemics.1. Proc. Royal Soc. 115A: 700-721.

Kermack, W. O. & Mckendrick, A. G. (1932). Contributions to the mathematical theory of epidemics.2. The problem of endemicity. Proc. Royal Soc. 138A: 55-83.

Kermack, W. O. & Mckendrick, A. G. (1933). Contributions to the mathematical theory of epidemics.3. Further studies of the problem of endemicity. Proc. Royal Soc. 141A: 94-122.

Kiefer, D.A. & Atkinson, C.A. (1984). Cycling of nitrogen by plankton: a hypothetical description based upon efficiency of energy conversion. Journal of Marine research, 42: 655-675.

Kirchman, D.L., Suzuki, Y., Garside, C. & Ducklow, H.O. (1991). High turnover rates of dissolved organic carbon during a spring phytoplankton bloom. Nature 352: 612-614.

Laskin, A. I. & Lechevalier, H. A. (1978). Handbook of medical microbiology, Vol. 2. Fungi, algae, protozoa and viruses. 2nd edition. CRC Press, Cleveland. ISBN-084937202X

Laskin, A. I. & Lechevalier, H. A. (1981). Handbook of medical microbiology, Vol. 3. Microbial composition: aminoacids, proteins and nucleic acids. 2nd edition. CRC Press, Cleveland.

Lee, C. & Henrichs, S.M. (1993). How the nature of dissolved organic matter might affect the analysis of dissolved organic carbon. Marine Chemistry, 41: 105-120.

Lohrenz, S.E., Knauer, G.A., Asper, V.L., Tuel, M., Michaels, A.F. & Knapp, A.H. (1992). Seasonal variability in primary production and particle flux in the northwestern Sargasso Sea: U.S. JGOFS Bermuda Atlantic Time-Series Study. Deep-Sea Res., 39: 1373-1391.

Longhurst, A.R. & Harrison, W.G. (1989). The biological pump: profiles of plankton production and consumption in the upper ocean. Prog. Ocanog. 22: 47-123.

Maranger, R., Bird, D.F. & Juniper, S.K. (1994). Viral and bacterial dynamics in Arctic sea ice during the spring algal bloom near Resolute, N.W.T., Canada. Marine Ecology Progress Series, 111: 121-127.

Marchant, H.J. & Scott, F.J. (1993). Uptake of sub-micrometre particles and dissolved organic material by Antarctic choanoflagellates. Marine Ecology Progress Series, 92: 59-64.

Mari, J. & Bonami, J.R. (1988). PC84, a parvo-like virus from the crab Carcinus mediterraneous: Pathological aspects,

ultrastructure of the agent, and first biochemical characterization. J. Invertebr. Pathol. 51(2): 145-156.

Martin, J. H. & Fitzwater, S. E. (1992). Dissolved organic carbon in the Atlantic, Southern and Pacific oceans. Nature 356: 699-700.

Martin, J. H. & Fitzwater, S. E. (1988). Iron deficiency limits phytoplankton growth in the north-east Pacific subarctic. Nature 331: 431-343.

Maruyama, A., Oda, M. & Higashihara, T. (1993). Abundance of virus-sized non-DNase-digestible DNA (coated DNA) in eutrophic seawater. Applied environmental Microbiology, 59: 712-717.

May, R. M. & Anderson, R. M. (1979). Population biology of infectious diseases: part II. Nature 280: 455-461.

Mayer, J. A. & Taylor, F. J. R. (1979). A virus which lyses the marine nanoflagellate *Micromonas pusilla*. Nature 281: 299-301.

Michaels, A.F., Bates, N.R., Buesseler, K.O., Carlson, C.A. & Knap, A.H. (1994). Carbon-cycle imbalances in the Sargasso Sea.

Michaels, A.F. (1994). BATS update: Interannual patterns are emerging from five years of data. U.S. JGOFS Newsletter vol. 5, number 3, pg. 8.

Miller, A.E.J., Mantoura, R.F.C. & Preston, M.R. (1993). Shipboard investigation of DOC in the N.E. Atlantic using platinum based catalysts in a Shimadzu TOC-500, HTCO analyzer. Mar. Chem., 41: 215-221.

Moloney, C.L. & Field, J.G. (1991). The size-based dynamics of plankton food webs. I. A simulation model of carbon and

nitrogen flows. Journal of Plankton research, Vol.13, 5:1003-1039.

Moloney, C.L., Field, J.L. & Lucas, M. (1991). The size-based dynamics of plankton food webs. II. Simulations of three contrasting southern Benguela food webs. Journal of Plankton Research, Vol.13, 5: 1039-1092.

Morales, C.E., Bedo, A., Harris, R.P. & Tranter, P.R.G. (1991). Grazing of copepod assemblages in the north-east Atlantic: the importance of the small size fraction. Journal of Plankton Research, Vol.13, 2: 455-472.

Morell, V. (1993). Dinossaur DNA: The hunt and the hype. Science, 261: 160-162.

Murray, A.G. & Jackson, G.A. (1992). Viral dynamics: a model of the effects of size, shape, motion and abundance of single-celled planktonic organisms and other particles. Mar. Ecol. Prog. Ser., 89: 103-116.

Murray, A.G. & Jackson, G.A. (1993). Viral dynamics II: a model of the interaction of ultraviolet light and mixing processes on virus survival in seawater. Mar. Ecol. Prog. Ser., 102: 105-114.

Nagasaki, K., Ando, M., Imai, I., Itakura, S. & Ishida, Y. (1993). Virus-like particles in an apochlorotic flagellate in Hiroshima Bay, Japan. Marine Ecology Progress Series, 96: 307-310.

Nagasaki, K., Ando, M., Itakura, S., Imai, I. & Ishida, Y. (1995). Viral mortality in the final stage of *Heterosigma akashiwo* (Raphidophyceae) red tide. Journal of Plankton Research, : 1449-

Najjar, R.M. (1990). Simulations of the phosphorous and oxygen cycles in the world ocean using a general circulation

model. PhD dissertation Princeton Univ., Princeton New Jersey

Nelson, D. E. (1991). A new method for carbon isotopic analysis of protein. Science, 251: 552-554.

Olsen, L.F. & Schaffer, W.M. (1990). Chaos versus noisy periodicity: Alternative hypotheses for childhood epidemics. Science, 249:499-504.

Pace, M.L., Glasser, J.E. & Pomeroy, L.R. (1984). A simulation analysis of continental shelf food webs. Marine Biology, 82:47-63.

Palenik, B. & Morel, F.M.M. (1991). Applied and Environmental Microbiology, 57: 2440-

Paul, J.H., Jiang, S.C. & Rose, J.B. (1991). Concentration of viruses and dissolved DNA from aquatic environments by vortex flow filtration. Applied and Environmental Microbiology Vol.57, 8: 2197-2204.

Peltzer, E.T. & Brewer, P.G. (1993). Some practical aspects of measuring DOC - sampling artifacts and analytical problems with marine samples. Mar. Chem., 41: 243-252.

Platt, T., Sathyendranath, S. & Ravindran, P. (1990). Primary production by phytoplankton: analytic solutions for daily rates per unit area of water surface. Proc. R. Soc. Lond. B 241 :101-111.

Platt, T., Jauhari, P. & Sathyendranath, S. (1992). The importance and measurement of new production. In *Primary Productivity and Biogeochemical Cycles in the Sea*, P.G. Falkowski & A.D. Woodhead, editors, Plenum Press, New York, pp 273-284.

Pomeroy, L.R. (1974). The ocean's food web, a changing paradigm. Bioscience, 24: 499-504.

Pool, R. (1989). Is it chaos or is it just noise? Science 243: 25-26.

Prezelin, B.B. & Glover, H.E. (1991). Variability in time/space estimates of phytoplankton, biomass and productivity in the Sargasso Sea. Journal of Plankton Research, 13: 45-67.

Proctor, L. M. & Fuhrman, J. A. (1990). Viral mortality of marine bacteria and cyanobacteria. Nature 343: 60-62.

Proctor, L. M. & Fuhrman, J. A. (1991). Roles of viral infection in organic particle flux. Mar. Ecol. Prog. Ser. 69: 133-142.

Quental-Mendes, R. (1992). Modelling of Marine Ecosystems: A viral solution to the DOC enigma. MPhil report. Department of Oceanography. University of Southampton.

Raymont, J.E.G. (1983). Plankton and Productivity in the Oceans, Pergamon Press, Oxford.

Rand, D.A. & Wilson, H. (1991). Chaotic Stochasticity: A ubiquitous source of unpredictability in epidemics. Proceedings of the Royal Society B246: 179-184.

Reinfelder, J. R. & Fisher, N. S. (1991). The assimilation of elements ingested by marine copepods. Science 251: 794-796.

Riebesell, U., Wolf-Gladrow, D.A. & Smetacek, V. (1993). Carbon dioxide limitation of marine phytoplankton growth rates. Nature 361: 249-251.

Rosenzweig, M.L. (1971). Paradox of enrichment. Science 171: 385-387.

Sarmiento, J.L. (1992). Ocean carbon cycle modelling: The euphotic zone. U.S. JGOFS Newsletter vol. 4, number 2: 1,8-9.

Sharp, J.H. (1973). Total organic carbon in seawater - comparison of measurements using persulfate oxidation and high temperature combustion. Marine Chemistry 1: 211-229.

Sidorowich, J. J. (1992). Chaos and epidemiology: Repellors attract attention. Nature 355: 584-585.

Sieracki, M.E., Johnson, P.W. & Sieburth, J. McN. (1985). Detection, enumeration and sizing of planktonic bacteria by image-analyzed epifluorescence microscopy. Applied and Environmental Microbiology, 49: 799-810.

Smith, D.C., Steward, G.F., Azam, F. & Hollibaugh (1992). Virus and bacteria abundances in the Drake Passage during January and August 1991. Antarctic Journal of the U.S., 27(5): 125-127.

Stallknecht, D. E., Shane, S. M., Kearney, M. T. & Zwank, P. J. (1990). Persistence of avian influenza viruses in water. Avian Dis. 34: 406-411.

Steele, J.H. & Henderson, E.W. (1992). The role of predation in plankton models. Journal of Plankton Research 14: 157-172.

Stent, G. S. (1963). Molecular Biology of Bacterial Viruses, Freeman, San Francisco.

Sugihara, G. & May, R. M. (1990). Nonlinear forecasting as a way of distinguishing chaos from measurement error in time series. Nature 344: 734-741.

Sugimura, Y. & Suzuki, Y. (1988). A high-temperature catalytic oxidation method for non-volatile dissolved organic carbon in seawater by direct injection of liquid samples. Mar. Chem. 24: 105-131.

Sundquist, E. T. in *The Carbon Cycle and Atmospheric CO_2: Natural Variations Archean to Present* (eds Sundquist, E. T. &

Broecker, W. S.) 5-59 (American Geophysical Union, Washington DC. 1985).

Suttle, C. A., Chan, A. M. & Cottrell, M. T. (1990). Infection of phytoplankton by viruses and reduction of primary productivity. Nature 347: 467-469.

Suttle, C. A., Chan, A. M. & Cottrell, M. T. (1991). Use of ultrafiltration to isolate viruses from seawater which are pathogens of marine phytoplankton. Apl. Environ. Microbiol. 57: 721-726.

Suttle, C. A., Chan, A. M. & Cottrell, M. T. (1991). Virus ecology. Nature 351: 612-613.

Suttle, C.A. & Chan, A.M. (1995). Viruses infecting the marine Prymnesiophyte *Chrysochromulina* spp.: isolation, preliminary characterization and natural abundance. Marine Ecology Progress Series, 118: 275-282.

Suttle, C.A. & Chen, F. (1992). Mechanisms and rates of decay of marine viruses in seawater. Apl. Environ. Microbiol. Vol. 58, 11: 3721-3729

Suzuki, Y., Sugimura, T. & Itoh, T. (1985). A catalytic oxidation method for the determination of total nitrogen dissolved in seawater. Mar. Chem. 16: 83-97.

Suzuki, Y. (1993). On the measurement of DOC and DON in seawater. Marine Chemistry, 41: 287-288.

Suzuki, Y., Tanoue, E. & Ito, T. (1992). A high temperature catalytic oxidation method for the determination of dissolved organic carbon in seawater: analysis and improvement. Deep-Sea Research, 39: 185-198.

Sverdrup, H. U., Johnson, M. W. & Fleming, R. H. *The Oceans* (Prentice-Hall, Englewood Cliffs, New Jersey, 1941).

Taylor, A.H., Joint, I. (1990). A steady-state analysis of the "microbial loop" in stratified systems. Marine Ecology progress series, 59: 1-17.

Thingstad, T.F., Heldal, M., Bratbak, G. & Dundas, I.(1993). Are viruses important partners in pelagic food webs ?. Trends in Ecology and Evolution, Vol.8, 6: 209-213.

Tobiesen, A. (1991). The succession of microheterotrophs and phytoplankton within the microbial loop in Oslofjorden, May-October 1984. Journal of Plankton Research, Vol.13, 1: 197-216.

Toggweiler, J.R. (1989). Is the downward dissolved organic matter (DOM) flux important in carbon transport? In: W.H. Berger, V.S. Smetacek and G. Wefer (Editors), Productivity of the Oceans: Present and Past. Wiley, New York, pp. 65-83.

Toggweiler, J.R. (1990a). Diving into the organic soup. Nature, 345:203-204.

Toggweiler, J.R. (1990b). Bombs and ocean carbon cycles. Nature, 347:122-123.

Toggweiler, J.R. (1994). Carbon cycle. Vanishing in Bermuda. Nature, 372:505-506.

Tranvik, L.J., Sherr, E.B. & Sherr, B.F. (1993). Uptake and utilization of 'colloidal DOM' by heterotrophic flagellates in seawater. Marine Ecology Progress Series, 92: 301-309.

VanEtten, J.L., Meints, R.H., Burbank, D.E., Kuczmarski, D., Cuppels, D.A. & Lane, L.C. (1981). Isolation and characterization of a virus from the intracellular green alga symbiotic with Hydra viridis. Virology, 113(2): 704-711.

Wangersky, P.G. (1993). Dissolved organic carbon methods: a critical review. Mar. Chem., 41: 61-74.

Waterbury, J.B. (1992). Viruses of marine bacteria. Oceanus, 35(3): 107-108.

Weisse, T. & Scheffel-Moeser, U. (1991). Uncoupling the microbial loop: growth and grazing loss rates of bacteria and heterotrophic nanoflagellates in the North Atlantic. Mar. ecol. Prog. ser., 71: 195-205.

Wheeler, P.A. & Kirchman, D.L. (1986). Utilisation of inorganic and organic nitrogen by bacteria in marine systems. Limnol. Oceanogr., 31: 998-1009.

Wheeler, P.A. & Kokkinakis, S.A. (1990). Ammonium recycling limits nitrate use in the Oceanic Subarctic Pacific. Limnol. Oceanogr., 35: 1267-1278.

Williams, P.M. & Druffel, E.R.M. (1988). Dissolved organic matter in the ocean: Comments on a controversy. Oceanography Magazine 1(1): 14-17.

Wilcox, R.M. & Fuhrman, J.A. (1994). Bacterial viruses in coastal seawater: lytic rather than lysogenic production. Marine Ecology Progress Series, 114: 35-45.

Yamada, T., Higashiyama, T. & Fukuda, T. (1991). Screening of natural waters for viruses which infect chlorella cells. Applied and Environmental Microbiology, Vol.57, 12: 3433-3437.